Analytical and numerical investigations of form-finding methods for tensegrity structures

Von der Fakultät Informatik, Elektrotechnik und
Informationstechnik der Universität Stuttgart
zur Erlangung der Würde eines
Doktors der Naturwissenschaften (Dr. rer. nat.)
genehmigte Abhandlung

Vorgelegt von
Giovani Gomez Estrada
aus Mexiko

Hauptberichter:	Prof. Dr. Hans-Joachim Bungartz
Mitberichter:	Prof. Dr. Manfred Bischoff
Mitberichter:	Prof. Dr. Thomas Ertl
Tag der Einreichung:	19.10.2006
Tag der mündlichen Prüfung:	12.07.2007

Max-Planck-Institut für Metallforschung
und Universität Stuttgart, 2007

Contents

List of Figures

List of Tables

List of Main Symbols and Functions

Scalars

b	Number of edges or members.
d	Number of geometric dimensions.
m	Number of mechanisms.
n	Number of vertices or nodes.
r	Rank of the equilibrium matrix.
s	Number of states of self-stress.

Vectors

$\mathbf{d}$	Displacements or mechanisms.
$\mathbf{q}^0$	Prototypes of member forces.
$\mathbf{t}$	Tension coefficients or force density coefficients.
$\mathbf{x}$	Cartesian coordinates in the x-axis.
$\mathbf{y}$	Cartesian coordinates in the y-axis.
$\mathbf{z}$	Cartesian coordinates in the z-axis.

Matrices

$\mathcal{A}$	Equilibrium matrix.
$\mathcal{C}$	Incidence matrix.
$\mathcal{D}$	Force density matrix.
$\mathcal{K}_t$	Tangent stiffness matrix.
$\mathcal{M}$	Basis of mechanisms.
$\mathcal{Q}$	Diagonal matrix of tension coefficients.
$\mathcal{T}$	Basis of tension coefficients.

Functions

$\underset{(\star)}{\arg\min}(\star\star)$	Argument $(\star)$ in which the function $(\star\star)$ is minimised.
$\text{eig}(\star)$	Eigenvalues of $(\star)$.
$\phi(\star)$	Euler's totient function of $(\star)$.
$\text{GCD}(\star, \star\star)$	Greatest common divisor of $(\star)$ and $(\star\star)$.
$\otimes$	Kronecker tensor product.
$\text{rank}(\star)$	Rank of matrix $(\star)$.
$\text{sgn}(\star)$	Sign of elements in vector $(\star)$.
$\text{diag}(\star)$	Square matrix with the vector $(\star)$ along its diagonal.
$(\star)^T$	Transpose of $(\star)$.
$\|(\star)\|$	Vector norm of $(\star)$.

Chapter 1

Introduction

Computational mechanics (CM) uses advanced computing methods, mechanics, physics, and mathematics in the study of modern engineering systems governed by the laws of mechanics. The scope of the research on this topic includes theoretical and computing methods used in many fields, such as solid and structural mechanics, fluid mechanics, fracture mechanics, transport phenomena, and heat transfer. Many of the mathematical models used in CM are based on fundamental laws of physics (e.g., the principles of motion, energy, and force) developed over centuries of research on the behaviour of mechanical systems under the action of natural forces.

CM is a fundamental part of computational science and engineering, from which it takes its strong interdisciplinary character. Computational science and engineering, along with theory and experiment, is used to develop conceptual and mathematical abstractions for simulation of a wide range of physical and engineering systems. Hence, research within CM emphasises a multidisciplinary approach in which mechanics and physics converge not only through analytical and computational methods, but also through novel numerical methods developed in their own right. The latter methods especially are of primary interest because general weighted residual methods, such as finite element, boundary element, and finite difference, can be applied to real-life problems.

CM encompasses design, analysis, and simulation of products that are used in every facet of modern life. It has a wide impact on automotive, aerospace, defence, chemical, communication, and biomedical fields; and in virtually any manufacturing industry, including power generation. A discipline that allows advances in modern science and technology, CM will continue to play an important role in future industrial developments also.

CM has been an integral component of scientific and industrial research for long because of its various uses. A striking feature common to most current large-scale research is the power, maturity, and sophistication reached by this branch of computational science and engineering. Some other areas, indeed, have conclusively demonstrated that large scale computer simulations are the only means by which key physical phenomena can be elucidated.

Both CM and its parent area, computational science and engineering, are by nature inter- and multi-disciplinary. Their foundations lie in mechanics, physics and mathematics, and they largely depends on computing methods, but nevertheless it is analytical and numerical modelling at their heart.

1.1 Statically indeterminate structures

One of the many fields in which CM plays an important role is in analysing complex elasticity and structural analysis problems found in the design of structures, such as hyperbolic paraboloids, cable grids, barrel vaults, membranes, domes, towers, tensegrity structures, prestressed assemblies, foldable structures, and many other cable arrangements. To do so, it brings together theories of mechanics, such as elasticity theory and strength of materials, and advanced computing algorithms to model structures of several degrees of freedom, large size, and complexity.

A common feature of many of those structures is that their static equilibrium equations are not sufficient for uniquely determining internal and reaction forces. Hence, such structures are called *statically indeterminate structures*. There are important areas of study in CM that deal with modelling, form-finding and displacement analysis of statically indeterminate structures. One statically indeterminate structure, which has attracted great attention recently, is the class of tensegrity structures. As found in other statically indeterminate structures, the geometry plays an important role for their analysis. Figure 1.1 shows a simple example that illustrates this problem of statics where the statical (in-)determinacy largely depends on the *geometry* and pre-stress the structure has adopted.

For instance, the central node in Fig. 1.1a can sustain and equilibrate a vertical load P by applying compressive axial forces to the bars. The structure is rigid up to certain level in which the "snap-through" phenomenon appears. It is a statically determinate structure. On the other hand, when the bars are arranged as shown in Fig. 1.1b, with no pre-stress, the two-bar structure has no initial resistance to vertical loads. It is called a "finite" mechanism. The situation is however different if pre-stress is present, see Fig. 1.1c. Here, the pre-stress is $t_0 \neq 0$, i.e. the bars are in tension so $t_0 > 0$, and the structure has an initial resistance against a vertical load P. Intuitively, if the bars behave as elastic springs, it is seen that a deflection Δ due to P is a function of the pre-stress level t_0. In this example, the relationship (e.g. see [117]) between the pre-stress t_0, load P and small displacement Δ, is:

$$\frac{EA}{L_0}\Delta^3 + 2t_0 L_0 \Delta - P L_0^2 = 0,$$

where EA is the axial stiffness of both bars. Thus, when the pre-stress is not present

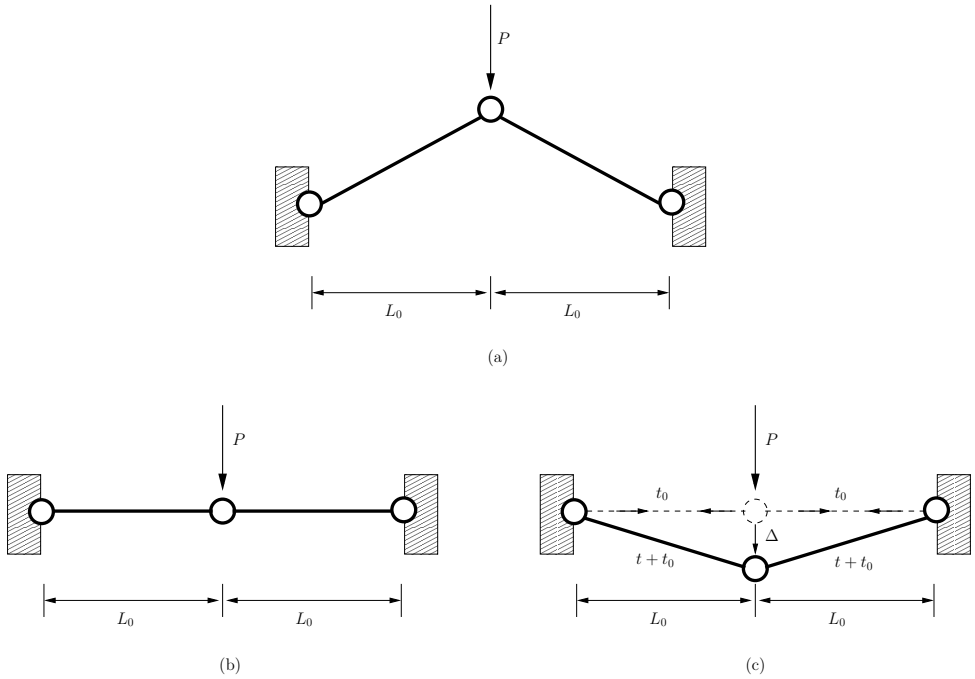

Fig. 1.1: Deformation of a two-bar planar structure : (a) the length of both bars is larger than L_0, here the central node is capable of sustaining a load P by introducing compressive axial forces in the two bars, until certain level in which the "snap-through" phenomenon is observed; (b) when the length of both bars is L_0 the central node is unable to resist a load P; (c) a pre-stress level $t_0 > 0$ appears when the initial bar lengths are shorter than L_0, here the central node undergoes a displacement Δ capable of equilibrating the vertical load P.

($t_0 = 0$ as in Fig. 1.1b) the load,

$$P = 2\,\frac{\Delta t_0}{L_0} + \frac{EA\,\Delta^3}{{L_0}^3},$$

is a third order function of the displacement Δ, meanwhile a resistance to load is proportional to t_0 in the pre-stressed example ($t_0 > 0$ as in Fig. 1.1c). In the latter, the structure is said to be stiffened by the pre-stress and called an "infinitesimal" mechanism. This mechanism of deformation is indicated with the solid lines in Fig. 1.1c. The linkage requires no external load for equilibrium, so it could rest in a "state of self-stress" for $P = 0$. This state is indicated with the dotted lines in Fig. 1.1c. Notice that an initial resistance to P is basically related to the pre-stress and not because of the axial stiffness, EA, of individual bars. Therefore, it is said the overall stiffness or flexibility of the structure does not depend of the axial stiffness of the elements but to the *geometry* of the linkage. That is why this load-carrying mode is called "geometric" stiffness. The structures studied in this dissertation, i.e. tensegrity structures, have pre-stress as one of their main features.

The analysis of pre-stressed structures requires to know to what extent and how the forces are transmitted to and throughout a structure. There are statically indeterminate structures, for instance cylindrical tensegrities, in which two or more configurations slightly differ in the pre-stress level; however, the response to load is diametrically differ-

ent from each other. Hence, for purpose of calculation, a more complete description of the problem should include information on the equilibrium geometry, pre-stress, supports, or member stiffnesses.

The modelling of statically indeterminate structures is particularly interesting when *no* loads are present. Geometric information is essential in the evaluation of any deflections when structures are subject to their *own* forces, due to existing pre-stress. For example, whether a statically indeterminate structure is strong enough to support itself is not known *a priori*. Hence, the first step toward the analysis of statically indeterminate structures is the calculation of the three-dimensional shape in the static equilibrium, prior to evaluation of any deflections. This raises two relevant questions that form the central focus of this dissertation: *how does one find the shape of statically indeterminate structures like tensegrity structures? how does one calculate their equilibrium geometry?*

The basic problem is that there is no unique solution for the forces or geometry that equilibrate a statically indeterminate structure. This is where *form-finding* comes into play. *Form-finding* is a branch of CM dedicated to computing the three-dimensional shape of a structure in static equilibrium, given a statically meaningful state of stress and load. Form-finding methods are useful in the search for geometries that minimise or favour certain shapes. CM has plenty of form-finding methods, with some of them being in use[1] since 1970s. Nonetheless, only a few form-finding methods are available for a certain class of statically indeterminate structures called "tensegrity" structures.

1.2 Tensegrity structures

Tensegrity structures are statically indeterminate structures in which form-finding and computer modelling play an important role in their development. A contraction of "tensional integrity", the term tensegrity was coined by R.B. Fuller in the 1950s to describe K. Snelson's structures [178, 142, 143].

In proper engineering terms, tensegrity is usually associated to pin-jointed structures that are mechanically stabilised by the action of prestress. Tensegrity structures are modelled with Hookean members that neither require anchorage points nor the application of external forces to maintain a static self-equilibrium. Another characteristic of these statically indeterminate structures lies in the arrangement of their structural members. According to the traditional definition [163], tensegrity structures are

> established when a set of discontinuous compression components interacts with a set of continuous tensile components to define a stable volume in space.

Hence, tensegrity structures have basically two components: discontinuous compressive members (e.g., struts) and continuous tensile members (e.g., cables). It is also pop-

[1]Earlier works did not employ "computational" but more "physical" methods, e.g., the minimal surfaces calculated with soap films by Frei Otto and Horst Berger in late 1950s.

ular to build up multiple modules of tensegrities in which the struts are connected (e.g. [141, 142]). Therefore, R. Motro [141] describes tensegrity structures as systems

> whose rigidity is the result of a state of self-stressed equilibrium between cables under tension and compression elements and independent of all fields of action.

This concept is illustrated with the small tensegrity structure shown in Fig. 1.2: Here, a continuous network of tension elements (Fig. 1.2a) interacts with a set of compression elements (Fig. 1.2b) in such a way that the resulting structure (Fig. 1.2c) has a state of self-stressed equilibrium. This is thus the "tensegrity" concept of self-equilibrating tension and compression forces.

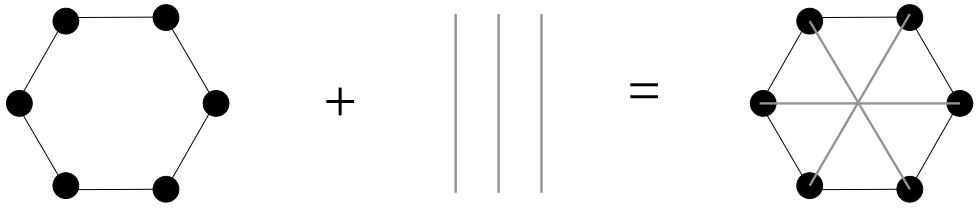

Fig. 1.2: A tensegrity hexagon : (a) six nodes interconnected by six cables, i.e. continuous network of tensile members; (b) a set of three compressive members (thick gray lines); (c) equilibrium geometry with the pairwise interactions of tensile and compressive members.

1.3 Applications and challenges of tensegrity structures

The concept of tensegrity is applied in a range of apparently far away areas[2]. While the treatment here is introductory, the application areas are discussed at length in Chapter 2.

Tensegrities are of interest in structural design studies because of their aesthetic value and lightweight property. The latter property favours their application in space and in deployable structures. There is also an interesting link between tensegrities and rigidity. For instance, the generalisation of the physical model of joints (e.g., atoms) and members (e.g., bonds) is exploited in the computation of rigidity of molecular structures [201, 200] and molecular conformations [94].

Furthermore, there is an ongoing debate on whether the tensegrity principle (self-stress and self-equilibrium) can be used as a general design principle in some biological materials (see e.g. [87] for a review), and to what extent and how this principle can be used in the construction of "smart materials" (e.g. [194, 127, 154, 177]).

[2]The reader should notice that sometimes the "tensegrity concept" is used in a rather arbitrary way when it comes to biology or medicine. This is explained in greater detail in Chapter 2.

There are a few fundamental problems associated to tensegrity structures standing alongside the many application areas. One essential problem is the initial geometry on which a tensegrity structure is based. The determination of the self-stressed equilibrium geometry is known as form-finding, and it is discussed at length in this dissertation. Other fundamental problems are about determining the mechanical behaviour of single tensegrity modules and their aggregation into larger structures. Together with this scalability issue, other problems arise like estimating the module's stability, tolerance to manufacturing imperfections, and their active control of tensegrity with actuators. In all these aspects, many ideas that are now applied to tensegrity structures evolved from related fields dealing with structures of a similar nonlinear geometrical behaviour.

The primary challenges related to tensegrity structures identified in this research are summarised in the following points:

1. development of analytical form-finding methods with application to high-order tensegrity structures;

2. form-finding of arbitrary tensegrity structures (spheres, cylinders and asymmetric structures) involving only minimal knowledge of the structure;

3. simultaneous form-finding and optimisation of system design parameters, for instance including constraints on member lengths and axial stiffnesses;

4. advancements in parameter identification and sensibility analysis to cope with material imperfections, as well as fabrication and assembly inaccuracies;

5. methods for faster form-finding of assemblies of known tensegrity units, e.g. capitalising on essentially known units which are pile-up for tensegrity masts and tensegrity grids;

6. dynamics and control of tensegrity structures including folding, unfolding, active members and additional constraints of non-smooth character.

The research presented here focuses on the first two items of the list. It is entirely related to form-finding issues, which without a proper treatment the remaining points cannot be satisfactorily addressed. Form-finding is the first problem that should be reasonably solved to move on in tensegrity structures. The other items, although important, are left for future work.

Based on the current progress in mathematical and related numerical methods for calculating tensegrity structures, the immediate future is likely to see important advances in the aforementioned points. It is hoped that the present dissertation adds *momentum* to this effort.

1.4 State of the art of form-finding methods for tensegrity structures

Form-finding is one of the basic problems in the design of any statically indeterminate structures, and tensegrity structures are no exception. Tensegrity structures are not only statically, but often kinematically, indeterminate structures and require an initial form-finding procedure (e.g. [142, 191]). The form-finding process of tensegrity structures poses extra constraints. Detailed three-dimensional information is needed to create a state of self-stressed self-equilibrium, that is, only pre-stress is considered.

Tensegrity structures only exist in a state of self-equilibrium, which requires the calculation of member forces in a particular spatial arrangement. To do so, mathematical models and associated numerical algorithms have to represent nontrivial (i.e., nonzero) solutions for the member forces (i.e., tension or compression) in such a way that the structure is stable. The resulting self-stressed self-equilibrium state is determined up to affine and projective transformations. The geometry is due to the stress distribution of the self-stressed structure, which in the case of tensegrities is without the application of external forces or anchorage points.

Form-finding methods for tensegrity structures typically compute a single critical parameter that turns the structure to self-stressed equilibrium. That is, the calculated structures are normally described by a single unknown, which, if correctly estimated, causes the structure to be in self-stressed equilibrium. Therefore, some assumptions are placed on the mathematical and mechanical models, e.g., a twisting angle, a strut-to-cable length ratio, or a force-to-length ratio. The latter ratio is also known as the *tension coefficient* or the *force density coefficient*, a specification formalism which has been adopted for this dissertation.

A twisting angle is perhaps the easiest form-finding method for tensegrity structures like the triplex and quadruplex, shown in Fig. 1.3. To shorten the names, the term *n-plex* is used for higher-order tensegrity cylinders. The triplex and quadruplex, 3-plex & 4-plex, have triangles and squares for constitutive polygons, shown in Fig. 1.3a and Fig. 1.3c, respectively. The equilibrium configuration can be attained by calculating a certain twisting angle among the parallel polygons such that it causes the structure to have a state of self-stressed self-equilibrium [51, 191, 185, 146, 145, 142, 96]. The height of these cylinders is not explicitly defined by twisting angles, but it can be easily included to get the final form in a subsequent step.

Other methods, however, predefine the length of all cables and iteratively elongate the struts until the state of self-stressed equilibrium is found. This assumption again left only one parameter to be determined, i.e., the ratio of cable-to-strut length. Dynamic relaxation [139] and nonlinear programming [157] approaches for the form-finding of tensegrity structures work in a similar manner. Interestingly, one analytical form-finding method [142] also exists, which also predefines cable lengths; however, it calculates the ratio directly without involving any iterative process.

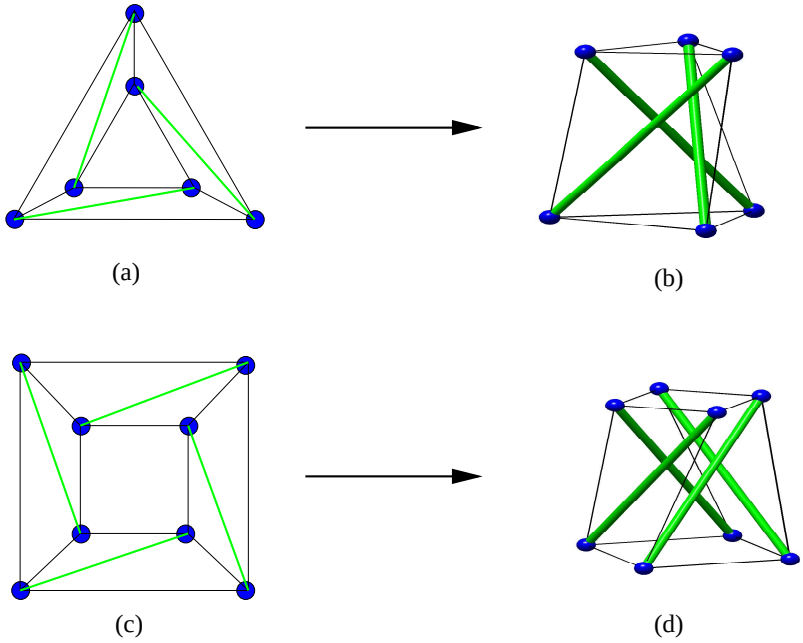

Fig. 1.3: Triplex and quadruplex : (a) connectivity of the triplex; (b) equilibrium geometry; (c) connectivity of the quadruplex; (d) equilibrium geometry; the connectivity of (a) and (c) shows a continuous network of tensile members (black segments) and a set of compressive members (thick green lines).

In general, form-finding methods using tension coefficients tend to be more flexible because they can describe single-parameter and multi-parameter self-stressed equilibrium geometries [195, 196, 191]. A procedure, called *force density method*, is employed to calculate the tension coefficients in the self-stressed state. It is typically analytical and calculated with symbolic software. The number of different tension coefficients that participates in the form-finding is defined beforehand. However, a selection of only two different tension coefficients is most popular: the first tension coefficient is normalised to be unitary, while the second one is unknown. Then, the force density method calculates the reduced row echelon form of a force density matrix created with the tension coefficients. An irreducible polynomial that produces a required rank deficiency is identified. The real roots of these polynomials provide the tension coefficients that cause the structure to be in self-stressed equilibrium. Chapter 2 elaborates on this procedure as it is not required in our brief discussion here.

It is thus seen that each form-finding method, be it analytical or numerical, has noteworthy limitations. Each method is designed to work under certain narrow assumptions or domain knowledge (see [142, 191] for a survey). Usually, to cope with a potentially large number of unknowns, one or more of the following assumptions is used: element lengths are predefined in dynamic relaxation and nonlinear programming procedures, a global symmetry is assumed in a group theory-based form-finding procedure, and/or a restricted number of different tension coefficients are imposed in symbolic analyses. The last constraint is used for the first part of the present dissertation.

Tensegrities like the 3-plex and 4-plex, shown in Fig. 1.3, have a characteristic equi-

librium configuration that appears in higher-order cylinders. A form-finding procedure starts with a node-to-node connectivity (e.g., Fig. 1.3a or Fig. 1.3c), as well as certain constraints, depending on the method employed, and calculate the equilibrium geometry (e.g., Fig. 1.3b or Fig. 1.3d). In the case of these two tensegrities, it is possible to do so by means of either twisting angles, strut-to-cable length ratios, or tension coefficients. All these approaches produce entirely equivalent solutions, i.e., the solution is basically the same self-stressed equilibrium geometry.

Analytical solutions for the form-finding of tensegrity structures are known for small systems. They give some insights into parameter dependencies ; however, in general, they do not extend to structures of both higher order and of difficult and generally multi-parameter forms. Modelling becomes worse for larger systems governed by assembly of tensegrity units. In spite of many fine mathematical developments, the combination of essentially known units is still extremely difficult, both theoretically and practically. The problems with respect to parameter dependencies and sensitivities concerning initial conditions include many open questions.

Numerical form-finding solutions, on the other hand, are generally achievable and, as computers become more powerful, they are less costly to obtain. Modelling and simulation are at the core of contemporary studies for tensegrity structures, not only for form-finding but also for the study of the mechanical behaviour and sensitivity problems related to tolerance to manufacturing imperfections. Capability in analysis will naturally lead to topology optimisation and later to shape finding. The investigations presented here are a step forward in the analysis of tensegrity structures, and it is expected that additional design information will be included in future form-finding methods.

1.5 Overview of the research

This dissertation presents analytical and numerical investigations of form-finding methods for tensegrity structures, with particular emphasis on cylindrical and spherical tensegrity structures.

The investigations cover triplex, quadruplex, truncated tetrahedron, expanded octahedron and truncated icosahedron structures, to name a few. The research is focused on two complementary form-finding methods, each with its own advantages and limitations. In the first one, the symmetry and a reduced number of different tension coefficients pose a certain constraint on the model that allows an analytical treatment of tensegrity cylinders. A versatile numerical procedure is developed in the second investigation. It alleviates many assumptions and is thus far more general. The numerical form-finding procedure is used to calculate both cylindrical and spherical tensegrities, as well as planar tensegrities.

The detailed scope and driving questions that motivate both studies are described as follows.

Analytical investigations

The first study presents a thorough analysis of tensegrity cylinders, e.g., the triplex, the quadruplex, and higher-order cylinders. The proposed form-finding procedure does indeed exploit the inherent symmetry of these cylinders. In the course of the research, certain tensegrities were found to have more than one possible configuration out of the same node-to-node connections. They are thus called *equivalent* or *structurally identical* configurations. For instance, there are no other possible geometrical configurations for the triplex or quadruplex, Fig. 1.3; however, there are two for pentaplex, as shown in Fig. 1.4a-c. Figure 1.4b and 1.4c shows the two equivalent configurations for the 5-plex generated out of the same nodal connectivity, Fig. 1.4a. Interestingly, the 6-plex has only one configuration while the 7-plex has three. It is not, however, immediately obvious why it is so.

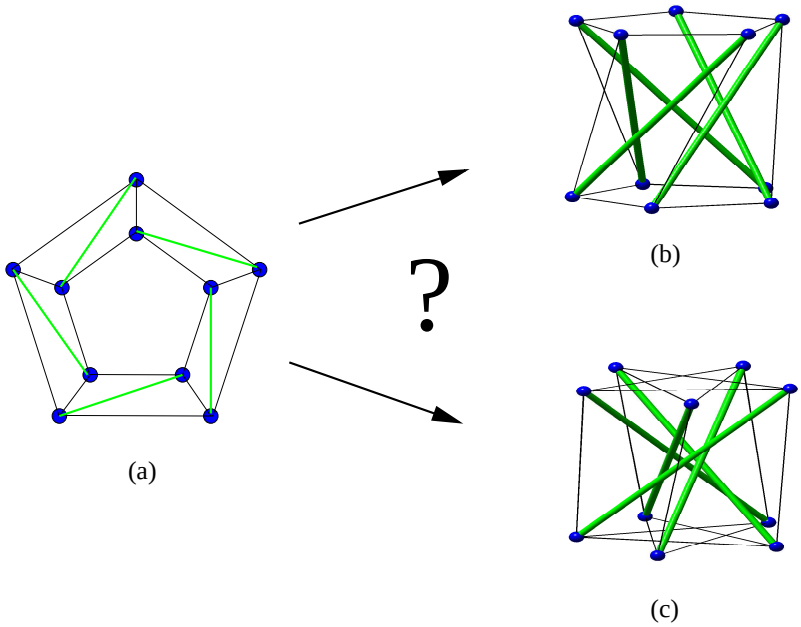

Fig. 1.4: Form-finding of the pentaplex : (a) the connectivity of a pentaplex. There are two geometrically different configurations out of the same connectivity, and both configurations are self-stressed; (b) first self-equilibrium geometry; (c) star-like arrangement of the second self-equilibrium geometry. The pentaplex (b) and (c) are said to be *equivalent* or *structurally identical* configurations. Thick green lines are struts.

As higher-order tensegrity cylinders are explored, several questions arise. For instance, it is possible to ask: **(i)** how many configurations exist for a certain cylinder? **(ii)** what sort of differences do they have? **(iii)** is it just possible to select the *best* among the range of equivalent configurations? **(iv)** is the 5-plex shown in Fig. 1.4b better than one in Fig. 1.4c? and **(iv)** in which sense is "best" or "better" defined?

Conventional assumptions on the form-finding procedures, e.g., the symmetry imposed on tensegrity cylinders, may not always be available or easy to estimate beforehand for other classes of tensegrities. There is a lack of reports describing general form-finding procedures, which, for instance, could solve both cylindrical and spherical tensegrities. This

gap in the literature hinders the general applicability of existing form-finding methods, and thus tensegrity structures altogether.

Numerical investigations

In the second study, a form-finding procedure that provides solutions to most traditional problems is proposed. As exact analytical solutions become unmanageable for more complex structures, a numerical procedure was developed. Tension coefficients seem to be more flexible and convenient for form-finding methods, in stark contrast to angles or ratios of member lengths. One problem in the path to numerical form-finding procedures is the initialisation. Where does one start? If the number of assumptions is to be reduced, it might be sensible to consider what "minimal" information one needs to start a form-finding method.

The lack of *a priori* information was identified and addressed by developing an unconventional numerical form-finding procedure that only uses: the node-to-node connections and the sign of individual members as either tension or compression. 2D and 3D structures, as well as symmetric and asymmetric cases for tensegrity cylinders, are discussed.

Tensegrity cylinders described in the analytical study study were re-calculated; however, a restricted number of tension coefficients for the form-finding was not assumed. This leads to the question: **(v)** how many different tension coefficients can be calculated for a tensegrity cylinder? It is also natural to compare some aspects of both analytical and numerical procedures. In particular, **(vi)** what is the accuracy of the numerical solution compared to the analytical one? Further, **(vii)** how does one search among equivalent configurations? Or, **(viii)** what are the (dis-)advantages of computing analytical and numerical solutions? Is it worth computing a numerical solution?

So far, the area of form-finding has plenty of methods that require specific knowledge of the final tensegrity structure. This introduces extra constraints to the user and hinders uncompromised designs. Never the less, as a result of the two investigations, previous and new tensegrity structures can easily be calculated and certainly opens the door to novel designs. It is expected that these investigations will help to discover new structures and provide starting points for future developments in the form-finding of statically indeterminate structures.

1.6 Outline of the dissertation

The dissertation is organised as follows. The terminology and equations used throughout the research are presented in Chapter 2. Some the many areas of application of tensegrity structures are briefly listed there. The overview in Chapter 2 is broad but self-contained to bridge the gap between apparently disconnected areas.

An analytical treatment for the form-finding of tensegrity cylinders is presented in

Chapter 3. Besides calculating the form-finding of tensegrity cylinders of non-equal circular faces, the number of equivalent solutions is also counted and enumerated. In doing so, points **(i)** and **(ii)** are addressed in a purely geometrical, exact way.

Discussions on the stability and non-uniqueness of the analytical form-finding treatment of tensegrity cylinders are provided in Chapter 4. Point **(ii)** is dealt with an energy criterion. Further, points **(iii)** and **(iv)** are carried out with the principle of minimum strain energy. The chapter also serves as an interface between the analytical and numerical form-finding studies by focusing on point **(v)**.

A numerical form-finding method is fully described in Chapter 5. The solutions of the novel iterative procedure were compared to other approaches. The chosen cases of study are cylindrical and spherical tensegrity structures. Close attention was paid to points **(vi)** and **(vii)**. Finally, conclusions drawn from both studies appear in Chapter 6. The advantages and disadvantages (point **(viii)**) of the analytical and numerical methods are discussed in the final chapter.

Chapter 2

Tensegrity structures

A general overview of tensegrities, including the most important application areas, is provided in this chapter. The terminology and equations used in this dissertation are also defined. It is important to remark that the nomenclature in the field of tensegrity structures is not unified; nevertheless, an effort is made to adhere to [142] and [191]. Besides a general introduction to tensegrity structures, the information necessary to proceed with the remaining chapters is presented here; for a larger overview, the reader is encouraged to consult [142].

The chapter is organised as follows. After presenting the basic hypotheses in Sections 2.1 and 2.2, an overview of application areas is shown in Section 2.3. Equilibrium equations of a general pin-jointed framework are provided in Section 2.4, and rank conditions for a structure having a state of self-stress are shown in Section 2.5. A calculation of the initial stiffness in statically indeterminate structures is provided in Section 2.6. A review of form-finding methods for tensegrity structures is presented in Section 2.7. The review focuses on the triplex as basic structure. Finally, a full example is presented in Section 2.8, with all main matrices, vectors, and calculations associated to the form-finding of the triplex.

2.1 Attraction and repulsion

Tensegrity structures are used to model a wide range of physical systems. What makes tensegrity structures so general is the concept of balancing tension and compression in a closed system. Because tensegrities are statically indeterminate structures[1], their internal forces are nonzero and it focuses the interest on how the members balance their forces. There are many physical systems where the particles interact in such a way, resulting in a

[1]The term "statically indeterminate" seems to be introduced into English literature in the early 20th century, e.g. in the discussion of arch bridges over the Niagara river [110]. However, the problem in which the bar tensions are not uniquely determined by the equations of nodal equilibrium was first presented and solved by Navier [148], and shortly afterwards by Moseley, Poncelet, Maxwell and Mohr [37, 38, 40, 42, 95]. The term itself, "statically indeterminate", is probably a direct translation from the German "statisch unbestimmt", which is used since the late 19th century, e.g. [144].

self-equilibrated system. However, as can be seen later on, many applications of tensegrity structures use this formalism for more qualitative rather than quantitative guidelines. Moreover, in general, the selection of tensegrity structures in the fields of biology and medicine seems to be based on empirical knowledge and very few measurements.

The key point in the tensegrity concept, i.e., balancing continuous tension and discontinuous compression, can represent different varieties of physical models. In a general setting, tension and compression are replaced by attraction and repulsion, respectively. Interactions between nodes are assumed to be perfectly pointwise, insofar as these interactions are modelled with massless joints (i.e. nodes).

Figure 2.1 illustrates the interacting forces in a tensegrity structure. The continuous network of attraction (Fig. 2.1a) and discontinuous repulsion (Fig. 2.1b) acts upon one another (Fig. 2.1c) to keep a self-stressed self-equilibrium (Fig. 2.1d) configuration. Compression elements are shown as thick gray lines. Figure 2.1c shows the assembly of tension and compression between the nodes with pointwise interactions of attraction and repulsion, respectively. The diagonal dotted lines in Fig. 2.1b or Fig. 2.1c do not touch or interfere with each other.

Figure 2.1d shows the wiring of this small tensegrity structure: tension forces are replaced by cables and repulsion by struts (thick gray lines). There is no intersection in the pair of struts shown in Fig. 2.1d. The scalar quantities for tension and compression forces that self-equilibrate the structure Fig. 2.1d are not unique[2], but a self-stressed self-equilibrium configuration is determined up to affine and projective transformations [59, 186]. The geometry of Fig. 2.1d is due to the balancing of forces, with no external loads nor anchorage points.

2.2 Basic hypotheses

A number of basic assumptions should be clarified before presenting the mathematical models and numerical algorithms used for the form-finding of tensegrity structures. It is convenient to discuss the mathematical model as well as the limitations of the current approach.

Research on tensegrity structures normally idealises tensegrities in which the structural members are held together by frictionless joints, and the self-weight of the structural members is neglected. Strictly speaking, the idealised condition of frictionless and massless joints is, of course, never satisfied, but it is a simplification that helps in calculations and gives meaningful reference points. The members, either in tension or compression, are assumed to be made of isotropic linear-elastic materials. This assumption focus to the extremely narrow limit within which, in the case of ordinary materials, Hooke's law is satisfied. A given member is either in tension or compression, i.e. a tension element cannot support compression and vice versa. While there is no buckling considered for

[2]The solution for the internal forces of Fig. 2.1d is a vector $\mathbf{t} = \alpha[1\ 1\ 1\ 1\ -1\ -1]$, with α for tension and $-\alpha$ for compression; α can be an arbitrary positive (real) constant.

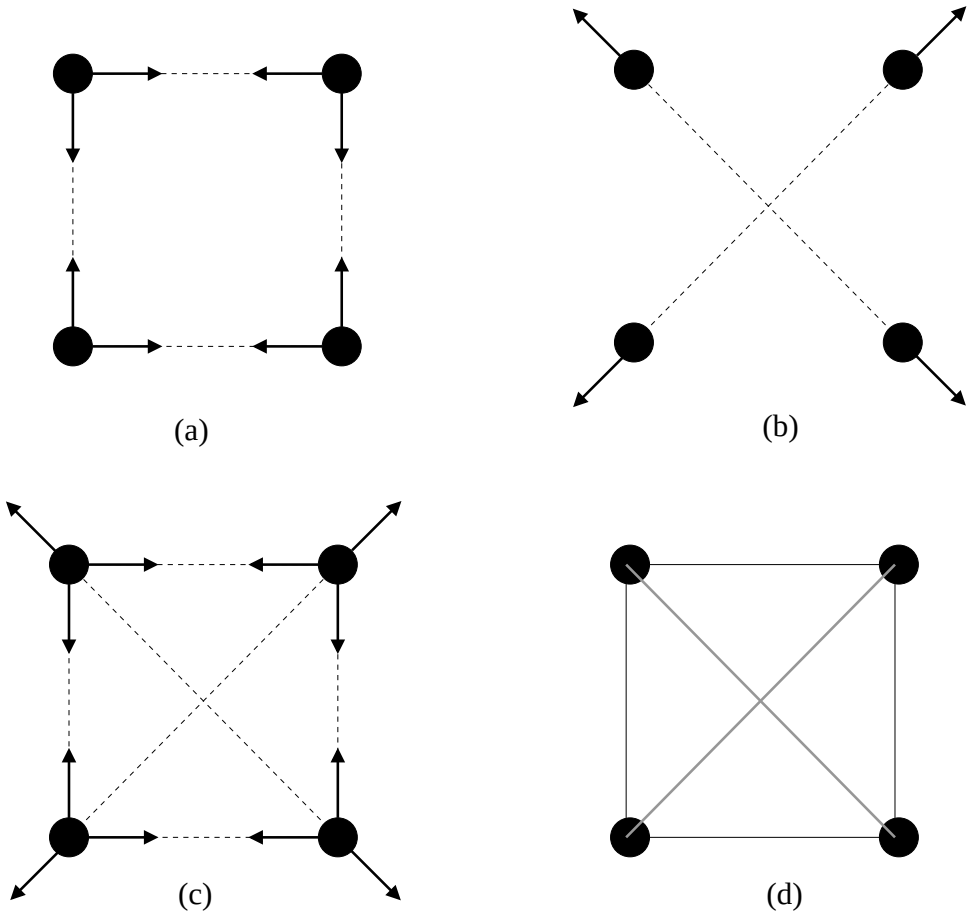

Fig. 2.1: Pointwise interaction in tensegrity structures : (a) continuous tension or attraction; (b) discontinuous compression or repulsion; (c) superposition of the forces; (d) pin-jointed structure in a self-stressed self-equilibrium state established by balancing cables in tension and struts in compression. The (unconnected) thick gray lines represent elements in compression.

compression elements, there is no slacking either for tensile members. Neither temperature nor gravity modify the equilibrium state.

Finally, small deflection theory is assumed in the equilibrium and compatibility equations. Infinitesimal displacements of the structure that preserve bar lengths, i.e., inextensional displacements, are used throughout the dissertation. Importantly, tensegrities are modelled in self-equilibrium, free of any external forces and without constraining any degree of freedom.

2.3 Applications

Tensegrities are applied in a range of apparently disconnected areas. PubMed[3] is a good source of articles on tensegrity in life sciences journals, or ISI Web of Science[4] for a broader search. The interplay and arrangement of tension and compression show some interesting characteristics common to many prestressed structures, including living organisms, which include:

- structures being able to fold and deploy,
- re-establishing geometry and stiffening due to the prestress, and
- lightweight structures because of the extensive use of tensile members.

While tensegrities are best known as space structures, there are little known areas in which the "tensegrity concept" is used as a guiding model. The quantitative and qualitative aspects of tensegrity structures are used in a broad class of problems. In many cases, interest is not on calculating an equilibrium geometry but in analysing structures that lose rigidity, or computing floppy modes. In the following, the main areas in which tensegrities, or closely related concepts, play an important role are briefly reviewed.

Architecture and civil engineering

Tensegrities are of interest in structural design studies because of their lightweight property, aesthetic and modern look. Usually, the structures are built in such a way that struts are connected, which might not be the original definition for tensegrity.

It is interesting to mention the following developments, starting of course with the many designs by K. Snelson [178], tensegrity domes [17, 24, 86, 85, 90, 112, 119, 122, 140, 149, 166, 173, 187, 189, 203], tensegrity bridges [44, 202], tensegrity towers [113, 64, 161, 172], tensegrity glass-tower [11], antennas [73, 114, 115, 190], deployable tents [23], and architectural designs [120, 121, 122, 36]. This is the classical field in which tensegrity structures are applied, see [142] for a longer list of references.

Biology and chemistry

The current trend of applying tensegrity structures in biomechanics of cells and molecules is helping researchers to qualitatively understand the structure-function relationship of cells. Such an application also provides quantitative discrete cell models to researchers of biomechanics and tissue engineering. Because of the complexity of the material properties

[3] http://www.ncbi.nlm.nih.gov/entrez
[4] http://isiknowledge.com

and the geometries encountered in applications, implementation of biomechanical models in numerical codes is vital. A common goal for those working in cell mechanics is to analyse the causal connections and to make predictions based on abstraction and general principles observed in adherent cells.

Ingber and co-workers, as well as a few other independent authors, have repeatedly published that some aspects of adherent cells can be qualitatively modelled with tensegrities, for instance cell spreading, motility and mechanotransduction [87, 97, 106, 107, 104, 103, 102]. Cellular tensegrity models are employed to explain the balance of forces, the movements of organelles and the changes in cytoskeletons that start biochemical reactions [87, 108, 43, 81, 88, 150, 155, 5]. It is known that cells are mechanically less stable, and show reduced motility and migration by disturbing the cytoskeleton [75], which is explained as a loss of rigidity in the cellular tensegrity model. Further, changes in cytoskeleton, due to controlled physical distortion, are also associated to changes in cell growth and function, and these phenomena are said to be somehow explained with the cellular tensegrity model [98, 105, 108, 101, 100, 99].

However, with over a hundred publications in the field, a quantitative model for the cellular mechanical behaviour is yet to be seen. The validation of mathematical models often requires careful laboratory experiments or testing; nevertheless, there are few quantitative validations of the cellular tensegrity hypothesis. Some steps taken forward in this direction are the investigations done by some researchers [25, 26, 27, 55, 57, 56, 54] for the modelling of cytoskeleton of adherent cells. The author of this dissertation is not aware of any development on models of cellular tensegrities for motility and spreading.

Other biological models with links to tensegrity structures are related to the Caspar-Klug theory of virus structure or virus as minimum energy structures [29, 111, 128]. Other authors created DNA "tensegrity" structures [124] - a claim that is very debatable.

Tensegrity structures are also used for the qualitative modelling of the muscular-skeletal system [118, 152], which balances the forces of muscles (tension) and bones (compression).

There is also a fascinating link between tensegrities and rigidity. For instance, generalisation of the physical model of joints (e.g., atoms) and members (e.g., bonds) is used in the computation of protein flexibility prediction [109, 164], and the rigidity of molecular structures [200, 201] and molecular conformations [94].

Smart structures

Unlike "traditional structures", the so called "smart structures" automatically react to loading activity. Smart structures use actuators and sensors to react and achieve a certain goal, for instance structural stability or locomotion.

Diverse characteristics of tensegrity structures are used in this domain. For instance, a number of structures [70, 71, 72, 82, 83, 65, 6] that can withstand the loads in an

active way have been reported. Tantalisingly, the analysis of tensegrity structures can be complemented with artificial intelligence methods to improve the accuracy of dynamic relaxation methods and active structural control. Hence, it is called an "active structure".

There is one interesting parameter study of "tensegrity fabric" [126, 127] for dampening the friction between this compliant surface and the fluid it moves through. The design space remains largely unexplored but their preliminary study gave promising research directions.

Other active structures concentrate more on the control of tension elements, making them actuators that improve the overall stiffness and folding of the structure [61, 62, 63, 138, 153, 156, 162, 175, 176, 181, 182, 183], one of which - a triplex with actuators - can lead to successful locomotor robots [154]. Other publications on the active control of tension and compression elements are [16, 69, 33, 34, 35, 129, 130, 131, 132]. Finally, there is considerable amount of literature on the characterisation and optimisation of parameters for the control and manoeuvring of tensegrity structures [2, 3, 4, 7, 1].

Other interesting applications

Tensegrities are guiding models for democratic collaboration and decision making [8, 9, 170, 10, 184, 160]. An icosahedron is chosen to model hierarchy-free interaction of people working toward a common goal. The model can allocate and distribute a number of participants. A limited number of skilled persons collaborate on a certain project (incident tensile member on nodes), while only a few can lead and peer review other projects (compression between two nodes). This model is said to be free of hierarchy because of the lack of a "top" or "bottom" in spherical tensegrities.

Tensegrity structures provide ideas for the folding and unfolding process of attachment pads in hornet's legs [84]. Other interesting applications are the modelling of multi-vehicle systems [151]; piezo-tensegrity, which is the coupling of tensegrity structures and electrically active devices [28]; rigidity percolation [74, 50, 134]; and "afunctional" abstract molecular architectures [68].

2.4 Geometry and tension coefficients

The terminology and equations used in this dissertation are presented here. It is important to remark that the nomenclature in the field of tensegrity structures is not unified. Some areas, such as mathematical rigidity, use similar matrices and vectors; nevertheless, the way they are related to engineering concepts is not obvious. Within tensegrity structures, there is no standard way of representing the main symbols and equations. An effort is made to adhere to [142] and [191].

Figure 2.2 is used to exemplify the equations of static equilibrium of an unconstrained reference node i connected to nodes j and k by members $\overline{i\,j}$ and $\overline{ik}$, respectively. The

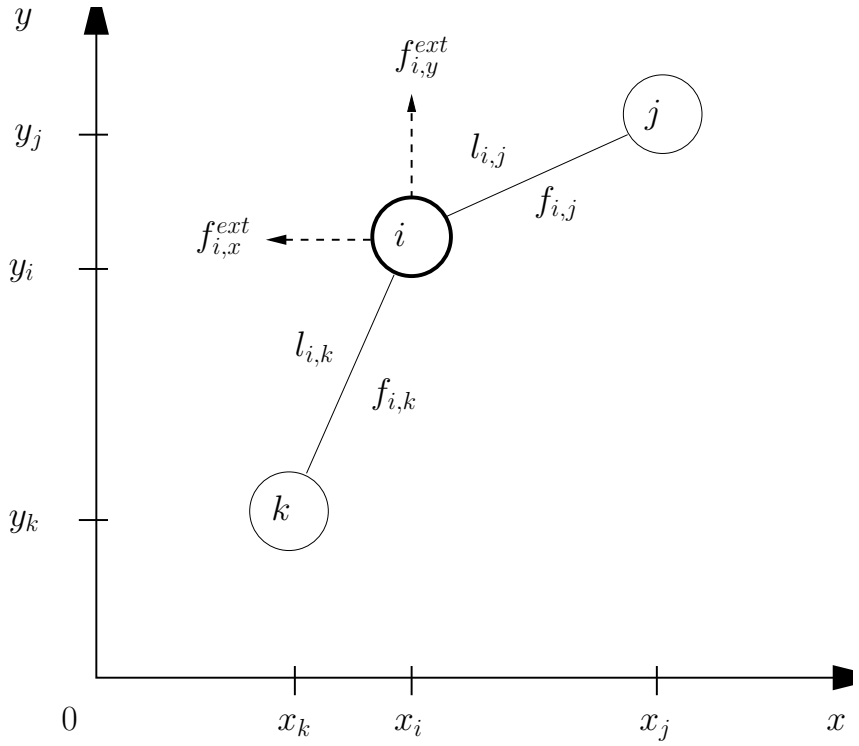

Fig. 2.2: Equilibrium of an unconstrained node : the unconstrained reference node i is connected to nodes j and k. The three nodes lie within a two-dimensional space, for clarity, but the equations are written for a three-dimensional space. Here $f_{A,B}$ is the force between nodes A and B and $l_{A,B}$ is the length of member $\overline{AB}$. The node i is in equilibrium with nodes j and k, and external forces $f^{ext}_{i,x}$ and $f^{ext}_{i,y}$.

equilibrium equations are given by:

$$\left.\begin{array}{rcrcl} (x_i - x_j) f_{i,j}/l_{i,j} & + & (x_i - x_k) f_{i,k}/l_{i,k} & = & f^{ext}_{i,x} \\ (y_i - y_j) f_{i,j}/l_{i,j} & + & (y_i - y_k) f_{i,k}/l_{i,k} & = & f^{ext}_{i,y} \\ (z_i - z_j) f_{i,j}/l_{i,j} & + & (z_i - z_k) f_{i,k}/l_{i,k} & = & f^{ext}_{i,z} \end{array}\right\} \tag{2.1}$$

where any member $\overline{AB}$ that connects any two nodes "A" and "B", in Fig. 2.2, has an internal force $f_{A,B}$ and a length $l_{A,B}$; and f^{ext} is the external force. A simplified linearised notation $q_{A,B} = f_{A,B}/l_{A,B}$ known as *tension coefficient*[5], or *force density* coefficient [123, 171] is often used. Equation (2.1) can thus either be written as:

$$\left.\begin{array}{rcrcl} (x_i - x_j) q_{i,j} & + & (x_i - x_k) q_{i,k} & = & f^{ext}_{i,x} \\ (y_i - y_j) q_{i,j} & + & (y_i - y_k) q_{i,k} & = & f^{ext}_{i,y} \\ (z_i - z_j) q_{i,j} & + & (z_i - z_k) q_{i,k} & = & f^{ext}_{i,z} \end{array}\right\} \tag{2.2}$$

[5]Credited to Müller-Breslau and Weyrauch, see [38] pp. 9, 69 and 156; but nevertheless the term was amply used and popularised by Southwell [179].

or as

$$\left.\begin{array}{rcrcrcl} (q_{i,j}+q_{i,k})x_i & - & q_{i,j}x_j & - & q_{i,k}x_k & = & f_{i,x}^{ext} \\ (q_{i,j}+q_{i,k})y_i & - & q_{i,j}y_j & - & q_{i,k}y_k & = & f_{i,y}^{ext} \\ (q_{i,j}+q_{i,k})z_i & - & q_{i,j}z_j & - & q_{i,k}z_k & = & f_{i,z}^{ext}. \end{array}\right\} \tag{2.3}$$

The tensegrity structures analysed in this dissertation have a state of self-stress with unconstrained nodes in $\Re^{\mathtt{d}}$, and zero external load in $\mathtt{d}$-dimensions. Let $\mathbf{x} = [x_1 \ \dots \ x_{\mathtt{n}}]^T$, $\mathbf{y} = [y_1 \ \dots \ y_{\mathtt{n}}]^T$, and $\mathbf{z} = [z_1 \ \dots \ z_{\mathtt{n}}]^T$ be the vectors of Cartesian coordinates for $\mathtt{n}$ nodes in the x-, y-, and z-axes, respectively. Here $(\star)^T$ represents a transpose operation. It is used an incidence matrix $\mathcal{C} \in \Re^{\mathtt{b}\times\mathtt{n}}$, which has one row per member $\overline{A\,B}$, and its columns A and B have entries $+1$ and -1, respectively. Equivalently, the incidence matrix $\mathcal{C} = (c_{i\,j})$ is the $\mathtt{b} \times \mathtt{n}$ matrix defined by

$$c_{i\,j} = \begin{cases} +1 & \text{if } j \text{ is the initial node of member } i, \\ -1 & \text{if } j \text{ is the terminal node of member } i, \\ \ \ 0 & \text{otherwise,} \end{cases}$$

for all $i = 1 \dots \mathtt{b}$ members composed by pairs of nodes $\overline{A\,B}$, in which $A \neq B$, see e.g. [14, 15]. Notice that the orientation $\overline{A\,B}$ or $\overline{B\,A}$ is irrelevant for the subsequent calculations. With the incidence matrix $\mathcal{C}$, the projected lengths, e.g. $(x_A - x_B)$, in the x-, y-, and z-axes are therefore written in vector form as $\mathcal{C}\mathbf{x}, \mathcal{C}\mathbf{y}$, and $\mathcal{C}\mathbf{z}$, respectively.

Let $\mathbf{t} \in \Re^{\mathtt{b}}$ be a vector of tension coefficients, with one entry for each of the $\mathtt{b}$ members. It is possible to write the matrix form of Eq. (2.2) by factorising the projected lengths in the equilibrium matrix $\mathcal{A} \in \Re^{\mathtt{dn}\times\mathtt{b}}$ and a vector $\mathbf{t}$ of tension coefficients:

$$\mathcal{A}\mathbf{t} = \underbrace{\begin{pmatrix} \mathcal{C}^T \ \mathrm{diag}(\mathcal{C}\mathbf{x}) \\ \mathcal{C}^T \ \mathrm{diag}(\mathcal{C}\mathbf{y}) \\ \mathcal{C}^T \ \mathrm{diag}(\mathcal{C}\mathbf{z}) \end{pmatrix}}_{\text{Equilibrium matrix}} \mathbf{t} = \mathbf{0}, \tag{2.4}$$

where $diag(\star)$ is a square matrix with the vector $(\star)$ along its diagonal, and $\mathtt{d} = 3$ for a three-dimensional structure. See [136] for more information on linear algebra.

Similarly, if tension coefficients of Eq. (2.3) are factorised, its matrix representation relates a symmetric matrix $\mathcal{D} \in \Re^{\mathtt{n}\times\mathtt{n}}$, known as the force density matrix (FDM), or stress matrix in mathematics [46], and the nodal coordinates:

$$\mathcal{D}[\mathbf{x}\,\mathbf{y}\,\mathbf{z}] = \underbrace{\left(\mathcal{C}^T \ \mathrm{diag}(\mathbf{t}) \ \mathcal{C}\right)}_{\text{FDM}}[\mathbf{x}\,\mathbf{y}\,\mathbf{z}] = [\mathbf{0}\,\mathbf{0}\,\mathbf{0}]. \tag{2.5}$$

Equation (2.4) relates the projected lengths to tension coefficients, whereas Eq. (2.5) relates tension coefficients to nodal coordinates. Equation (2.5) has quadratic form

$\mathbf{x}\mathcal{D}\mathbf{x}^t = \sum \mathbf{t}_{ij}(\mathbf{x}_i - \mathbf{x}_j)^2$, where the sum is over the pairs of connected nodes $\{i, j\}$. Notice that matrix $\mathcal{D} = (d_{i\,j})$ can be written as:

$$d_{i\,j} = \begin{cases} -q_{i\,j} & \text{if } i \neq j, \\ \sum_{k\neq i}^{\mathtt{n}} q_{i\,j} & \text{if } i = j, \\ 0 & \text{if nodes } i \text{ and } j \text{ are not connected,} \end{cases}$$

where $q_{i\,j}$ is a tension coefficient between nodes i and j. In Gaussian network models (e.g. [193]), a very similar matrix $\mathcal{D}$ is used to represent biological macromolecules with residues of proteins (nodes) and bonds (bars) by introducing a cut-off distance for spatial interactions.

A force density matrix $\mathcal{D}$ is also found in the literature as $\mathcal{D} = \mathcal{C}^T\mathcal{Q}\mathcal{C}$, where $\mathcal{Q}$ is the diagonal matrix of $\mathbf{t}$. When there is no risk of confusion the explicit representation, Eq. (2.5), is used in this dissertation.

The force density matrix $\mathcal{D}$ is symmetric, positive semi-definite. Notice $\mathcal{D}$ is the matrix of second order differences of the structure, known in other fields as discrete or combinatorial Laplacian matrix [14, 15, 135]; in this case, a Laplacian computed with negative and positive edge weights. The matrix $\mathcal{D}$ can be expressed, likewise in graph theory, by subtracting weighted versions of the vertex degree and adjacency matrices. Interestingly, $\mathcal{D}$ is conceptually a Kirchhoff matrix with positive and negative conductances. Equations like the force density matrix and equilibrium matrix are present in a variety of fields, and could be bridged by the Tellegen's theorem or similar formalisms [89]. Both equations can be combined, for a 3D structure, in the next relation:

$$\begin{pmatrix} \mathcal{D} & & \\ & \mathcal{D} & \\ & & \mathcal{D} \end{pmatrix} \begin{bmatrix} \mathbf{x} \\ \mathbf{y} \\ \mathbf{z} \end{bmatrix} - \begin{pmatrix} \mathcal{C}^T \operatorname{diag}(\mathcal{C}\mathbf{x}) \\ \mathcal{C}^T \operatorname{diag}(\mathcal{C}\mathbf{y}) \\ \mathcal{C}^T \operatorname{diag}(\mathcal{C}\mathbf{z}) \end{pmatrix} \mathbf{t} = \mathbf{0},$$

or, written in another way,

$$(\mathcal{I}_3 \otimes \mathcal{D}) \begin{bmatrix} \mathbf{x} \\ \mathbf{y} \\ \mathbf{z} \end{bmatrix} - \mathcal{A}\mathbf{t} = \mathbf{0},$$

where the Kronecker tensor product, $\otimes$, is used to shorthand the notation. It is important to stress that, in the following sections, it is assumed however that neither element lengths, coordinates, nor tension coefficients are known *a priori*.

2.5 Rank conditions and nullity

Two necessary but not sufficient rank conditions have to be satisfied in a `d`-dimensional structure that is in a state of self-stress, e.g. [142, 91, 46]. The first one ensures the existence of at least one state of self-stress, if

$$\mathtt{r} = \mathrm{rank}(\mathcal{A}) < \mathtt{b}, \tag{2.6}$$

which is necessary for a non trivial solution of Eq. (2.4). This rank deficiency provides the number of independent states of self-stress $\mathtt{s} = \mathtt{b} - \mathtt{r} \geq 1$ and the *total* number of infinitesimal mechanisms $\mathtt{m} = \mathtt{dn} - \mathtt{r}$ for a structure in $\mathtt{d}$-dimensions, as explained in [20].

The structural parameters, $\mathtt{s}$ and total $\mathtt{m}$, are related through the Maxwell's rule[6], which in 3D is:

$$3\mathtt{n} - \mathtt{b} - c = \mathtt{m} - \mathtt{s},$$

with constraints $c \geq 6$; recall that $\mathtt{n}$ is the number of joints and $\mathtt{b}$ the number of bars in the structure. However, the total number of mechanisms includes rigid-body motions, $c \geq 3$ for 2D, and $c \geq 6$ for 3D.

The values of $\mathtt{s}$ and $\mathtt{m}$ give us the common classification, e.g. [158], of structures according to their degree of static and kinematic indeterminacy:

$\mathtt{s} = 0, \mathtt{m} = 0$: Statically and kinematically determinate structure;

$\mathtt{s} > 0, \mathtt{m} = 0$: Statically indeterminate and kinematically determinate structure;

$\mathtt{s} = 0, \mathtt{m} > 0$: Statically determinate and kinematically indeterminate structure;

$\mathtt{s} > 0, \mathtt{m} > 0$: Statically and kinematically indeterminate structure.

Tensegrity structures are statically, and often kinematically, indeterminate structures. To put it explicitly, statically indeterminate structures have at least one state of self-stress, and kinematically indeterminate structures have at least one mode of deformation which is not a rigid-body motion, i.e. $\mathtt{s} > 0$ and $\mathtt{m} > 0$. For instance, the small tensegrity structure with four nodes and six bars, Fig. 2.1d, is a statically indeterminate and kinematically determinate structure with $\mathtt{s} = 1$ and $\mathtt{m} = 0$.

To clarify the terminology, henceforth, the symbol $\mathtt{m}$ will be associated to the total number of infinitesimal mechanisms *minus* the rigid-body motions, unless otherwise stated. Thus, the parameter $\mathtt{m}$ corresponds to internal mechanisms. The number of states of self-stress indicate the non-trivial solutions to the system of equilibrium equations. The second rank condition is related to the semi-definite matrix $\mathcal{D}$ of Eq. (2.5) as follows:

$$\mathrm{rank}(\mathcal{D}) < \mathtt{n} - \mathtt{d}, \tag{2.7}$$

for a geometric embedding into $\Re^{\mathtt{d}}$. For an embedding of maximal affine space [91, 46, 47, 48] the largest possible rank of $\mathcal{D}$ is $(\mathtt{n} - \mathtt{d} - 1)$ for a $\mathtt{d}$-dimensional structure. Basically,

[6]The rule, which relates the number of necessary bars to make a framework stiff, $\mathtt{b} = 3\mathtt{n} - 6$, was in fact presented by Möbius long before Maxwell [38]. The rule acquire its present form from the works of Buchholdt et al. [18] and Calladine [20].

the nullity of $\mathcal{D}$ is $(\mathtt{d}+1)$. The nullity of a matrix is the dimension of its nullspace: the nullity for a 2D structure is three, and the nullity for a 3D structure is four. The nullity of $\mathcal{D}$ is used in the form-finding procedure described in Chapter 5.

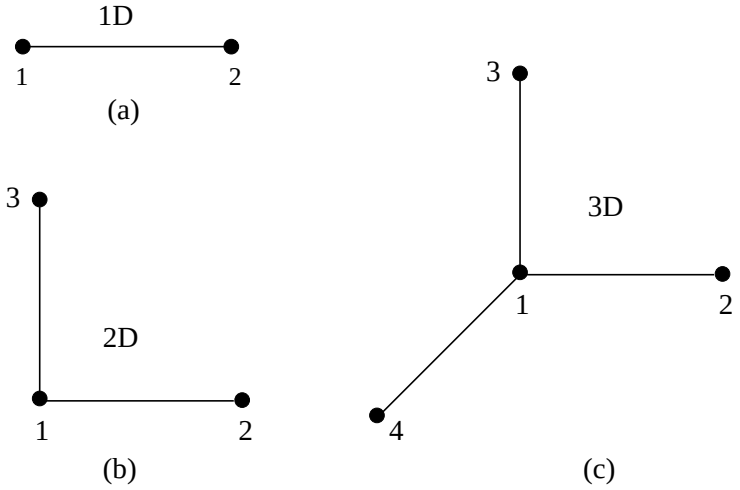

Fig. 2.3: Rank conditions for the force density matrix : (a) the affine space of a line has dimension two; (b) the affine space of a plane has dimension three; (c) the affine space of a solid has dimension four.

An intuitive explanation of this rank condition is shown in Fig. 2.3. For instance, the affine space spanned by a line has a dimension two (Fig. 2.3a), for a plane it is three (Fig. 2.3b) and for a geometric solid it is four (Fig. 2.3c).

From a graph-theoretical perspective, the form-finding problem basically consists in: computing edge weights such that the (weighted) Laplacian of the graph is positive semi-definite of certain nullity, and edge weights satisfy some pre-defined sign pattern for tension/compression elements. There are however some constraints on stability and nullity that should be taken into account.

A degenerate configuration may exist in which, for example, three or more points are placed on the same straight line for a planar figure. That is, a planar figure may degenerate in a line, which is of lower dimension. The numerical algorithms using this rank condition, Eq. (2.7), should verify whether the nullspace really spans the expected dimension without degeneracy. For instance, it could happen that the dimension of the nullspace of a 3D structure is four but one of the eigenvectors of this nullspace is the $\mathbf{1}$-vector, with which the solid degenerates in a planar figure. The proposed form-finding procedure discussed in Chapter 5 takes this maximal rank condition and nullity to find a tensegrity structure.

2.6 Initial stiffness

Once a tensegrity structure is found, it is convenient to assess the stability of its self-equilibrium configuration. This configurations involves at least one state of self-stress

and infinitesimal mechanisms. It amounts to verify that $[\mathbf{x}\,\mathbf{y}\,\mathbf{z}]$ and $\mathbf{t}$ create a *stable* self-equilibrated structure in a kinematically indeterminate assembly. Or, in other words, the state of self-stress should stiffens all the infinitesimal mechanisms. Both tension coefficients and total number mechanisms are involved in this calculation.

Let $[\mathbf{x}\,\mathbf{y}\,\mathbf{z}]$ be the nodal coordinates of a structure in a state of self-stress, $\mathtt{s} \geq 1$. It is known [159] that the basis of vector spaces of tension coefficients and mechanisms of a self-stressed structure are calculated from the null spaces of the equilibrium matrix. If equilibrium matrix is factorised,

$$\mathcal{A} = \begin{pmatrix} \mathcal{C}^T \operatorname{diag}(\mathcal{C}\mathbf{x}) \\ \mathcal{C}^T \operatorname{diag}(\mathcal{C}\mathbf{y}) \\ \mathcal{C}^T \operatorname{diag}(\mathcal{C}\mathbf{z}) \end{pmatrix} = \mathcal{U}\mathcal{V}\mathcal{W}^T, \tag{2.8}$$

the null spaces of Eq. (2.8) have the following structure,

$$\mathcal{U} = [\mathbf{u}_1\,\mathbf{u}_2\,\ldots\,|\,\mathbf{d}_1\,\ldots\,\mathbf{d}_{\mathtt{dn}-\mathtt{r}}], \tag{2.9}$$

and

$$\mathcal{W} = [\mathbf{w}_1\,\mathbf{w}_2\,\ldots\,|\,\mathbf{t}_1\,\ldots\,\mathbf{t}_{\mathtt{b}-\mathtt{r}}], \tag{2.10}$$

where $\mathtt{r}$ is the rank of the diagonal matrix V; the vectors $\mathbf{d} \in \Re^{\mathtt{dn}}$ denote the $\mathtt{m} = \mathtt{dn} - \mathtt{r}$ infinitesimal mechanisms; and the vectors $\mathbf{t} \in \Re^{\mathtt{b}}$ the states of self-stress, each of which solves the homogeneous Eq. (2.4). Let $\mathcal{M} \in \Re^{\mathtt{dn}\times\mathtt{dn}-\mathtt{r}}$ be a matrix of mechanisms, $\mathcal{M} = [\mathbf{d}_1\,\ldots\,\mathbf{d}_{\mathtt{dn}-\mathtt{r}}]$, directly from Eq. (2.9), and possibly including the rigid-body motions. By definition, the compatibility matrix ($\mathcal{A}^T$) shows that mechanisms do not elongate any member, i.e. $\mathcal{A}^T\mathcal{M} = \mathbf{0}$.

Having calculated $\mathcal{A}$ and tension coefficients, Eq. (2.10), the tangent stiffness matrix is easily calculated. It is known that a vector of tension coefficients contributes to the tangent stiffness matrix,

$$\begin{array}{rcccc} \mathcal{K}_t & = & \mathcal{K}_e & + & \mathcal{K}_g, \\ & = & \mathcal{A}\mathcal{G}\mathcal{A}^T & + & (\mathcal{A}\mathcal{Q}\mathcal{A}^T + \mathcal{I}_3 \otimes \mathcal{D}), \end{array} \tag{2.11}$$

of pre-stressed, kinematically indeterminate structures, see e.g. [93, 145]. Here $\mathcal{Q}$ is the $\mathtt{b} \times \mathtt{b}$ diagonal matrix of tension coefficients, $\mathcal{G}$ is the $\mathtt{b} \times \mathtt{b}$ diagonal matrix of axial stiffnesses, $\mathcal{I}_3$ is the 3x3 identity matrix, and $\otimes$ is the Kronecker tensor product.

If an infinitesimal and inextensional mechanism $\mathbf{d} \in \mathcal{M}, \mathcal{M} = [\mathbf{d}_1\,\ldots\,\mathbf{d}_{\mathtt{dn}-\mathtt{r}}]$ as described in Eq. (2.9), is applied to $\mathcal{K}_t$, two terms Eq. (2.11) vanish, i.e. $\mathcal{A}^T\mathbf{d} = \mathbf{0}$. The stability of this initial state, or initial stiffness, of a structure therefore only involves, e.g. [145, 93, 197, 199], a section of the geometric stiffness: $\mathcal{I}_3 \otimes \mathcal{D}$. Stability of tensegrity

structures has been discussed not only from a mechanical point of view ([76, 67, 195, 198]) but from a mathematical rigidity perspective ([48, 47, 46, 52, 51]). Other non-linear analysis of tensegrity structures and affine systems close to singularities have been analysed in [12, 19, 66].

The infinitesimal mechanisms can be stiffened by the state of self-stress and this stiffness does not depend on the axial stiffness of the bars. Thus, the structure has an initial stiffness against load, and it is controlled by the level[7] of pre-stress rather than the stiffness of individual structural members.

The stability of a statically indeterminate pin-jointed structure in $\mathtt{d} = 3$ dimensions, can be therefore tested with no other loads than its infinitesimal and inextensional mechanisms. This can be done with the quadratic form of $\mathcal{I}_3 \otimes \mathcal{D}$ and $\mathcal{M}$,

$$\Lambda = \mathcal{M}^T(\mathcal{I}_3 \otimes \mathcal{D})M, \tag{2.12}$$

which is positive semi-definite if and only if $\mathcal{D}$ is positive semi-definite, for all $\mathtt{m} \in \Re^{\mathtt{dn}}$. For a positive $\mathcal{D}$, it has to be verified whether or not $\mathcal{I}_3 \otimes \mathcal{D}$, i.e. the reduced form of Eq. (2.11), imparts positive stiffness to all directions defined by the inextensional displacements except for the six rigid body motions,

$$\mathrm{eig}(\Lambda) = [\underbrace{\lambda_1 = \lambda_2 = \ldots \lambda_6 = 0}_{\text{rigid body motions}} \quad \underbrace{\lambda_7 > 0 \ldots \lambda_{\mathtt{dn}-\mathtt{r}} > 0}_{\text{positive stiffness}}], \tag{2.13}$$

that appear in the analysis of free standing structures in $\mathtt{d} = 3$ dimensions. Equation 2.13 shows eigenvalues in increasing order and repeated according to their multiplicity. Here, it is assumed that there is a single state of self-stress, which is the typical example discussed in the related literature. In a general case, $\mathtt{s} \geq 2$, but nevertheless, is more problematic to verify whether or not the assembly possesses stiffness in all considered states of self-stress, e.g. [21, 22]. It is also possible that structures with $\mathtt{s} \geq 2$ have members that switch from tension to compression, depending of the state of self-stress. This fact introduces new design problems because a member is not uniquely assigned a tension or compression value. All structures presented in this dissertation avoid such a problem, each of them has a single state of self-stress.

2.7 Form-finding of tensegrity structures

Form-finding methods for tensegrity structures typically compute a single critical parameter that renders the structure to self-stressed equilibrium. That is, the structures being calculated are normally described by a single unknown which, if correctly estimated, cause the structure to be in self-stressed equilibrium. Therefore, some assumptions are placed

[7] A non-zero level of pre-stress that does not cause buckling in any member.

on the mathematical and mechanical models, for instance: a twisting angle, a strut-to-cable length ratio, or a force-to-length ratio. The latter ratio is also known as the tension coefficient or the force density coefficient, specification formalism which has been adopted for this dissertation.

A twisting angle is perhaps the easiest form-finding method for cylindrical tensegrity structures. The two triangles from which the triplex is composed are not aligned one over the other. The equilibrium configuration is found by calculating a certain angle between the parallel polygons such that it causes the structure to have a state of self-stressed self-equilibrium [51, 191, 185, 146, 145, 142, 96].

The twisting angle θ between the triangles of a 3-plex is $\theta = \pi/6$, and, in general, the angle is

$$\theta = \pi \left(\frac{1}{2} - \frac{j}{n} \right),$$

for any n-plex, e.g. [191, 142]; where $1 \leq j < n/2$, and $n \geq 3$. The angle θ, created between the parallel triangles of a triplex (Fig. 2.4a), is clearly seen in Fig. 2.4b. This parameter is normally assumed $j = 1$, however, the characteristics of n-plexes within the range $1 \leq j < n/2$ are largely unexplored. The relationship of j and n is not obvious, and it is clarified in the Chapters 3 and 4.

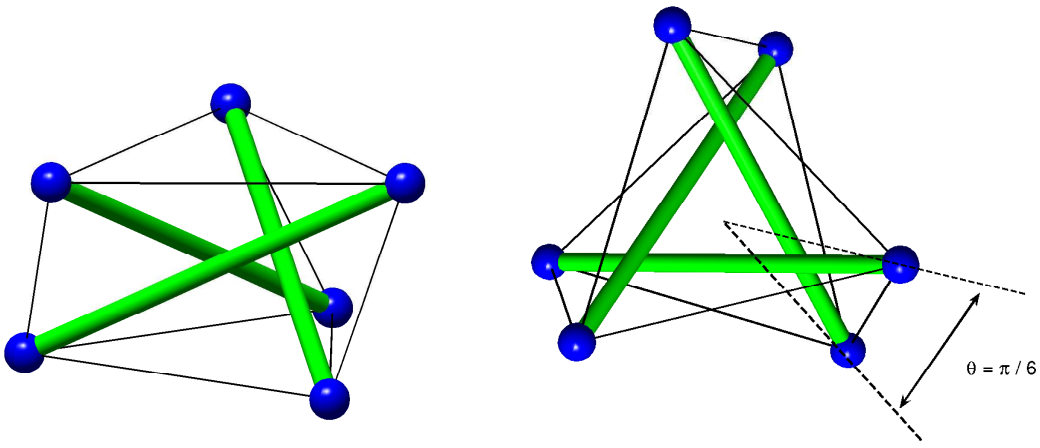

(a) (b)

Fig. 2.4: Form-finding with twisting angles : (a) equilibrium configuration of the triplex; (b) a top view shows the angle formed between both parallel triangles, adapted from [142], pp. 103.

Other form-finding methods, however, pre-define the length of all cables and iteratively elongate the struts until the state of self-stressed equilibrium is found. This assumption left, again, only one parameter to be determined, e.g. the ratio between cable and strut length. Dynamic relaxation [139] and non-linear programming [157] approaches for the form-finding of tensegrity structures work in such a manner[8]. Interestingly, there is also

[8]This form-finding method is closely related to the distance geometry formalism, with which current

one analytical form-finding method [142] that requires to pre-define the cable length but it calculates the ratio, directly, without involving any iterative process.

For instance, if the parallel triangles of a triplex are inscribed in circles of radii $r = \frac{\sqrt{3}}{3}$ (Fig. 2.5a) and separated by a height $h = \frac{\sqrt{3+3\sqrt{3}}}{3}$, all tensile components have unitary length, whilst all compression components have length $l_s = \sqrt{1 + \frac{2\sqrt{3}}{3}}$, see Fig. 2.5b. This result is essentially what other authors found for $l_s = 1.46788$, e.g. [191].

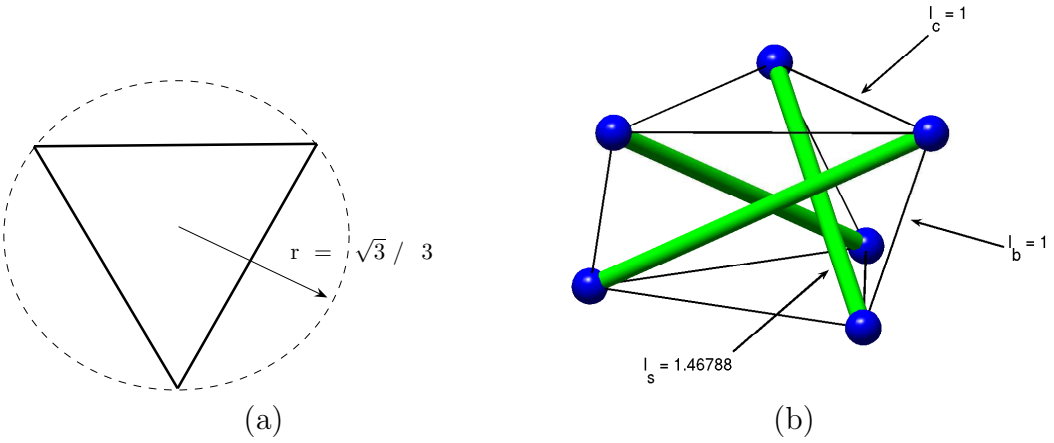

Fig. 2.5: Form-finding with length ratios : (a) unitary radius for the inscribed triangles of the triplex; (b) the length of compression components is calculated by keeping unitary lengths in all tensile components; l_c stands for cable length, l_b is bracing cable length, and l_s is strut length.

In general, form-finding methods using tension coefficients tend to be more flexible because they can describe single and multi-parameter self-stressed equilibrium geometries [195, 196, 191]. The procedure, called force density method, is typically analytical and employs symbolic software. The number of different tension coefficients that participates in the form-finding is defined beforehand. However, the selection of only two different tension coefficients is most popular: the first tension coefficient being normalised to the unity and the second one is the unknown. Then, the force density method calculates the reduced row echelon form of a matrix, which is created with the tension coefficients. In case of a triplex, the force density matrix $\mathcal{D}$,

molecular structures can be calculated from the distances between bonded atoms. The distances are found by experimental measurements and three-dimensional structures, consistent with them, have to be calculated. Moreover, the distances are written in matrix form, in the same way as the item-item distance matrix used in classical multidimensional scaling.

$$\mathcal{D} = \mathcal{C}^T Q \mathcal{C} = \begin{bmatrix} 2 & -1 & -1 & q & 0 & -q \\ -1 & 2 & -1 & -q & q & 0 \\ -1 & -1 & 2 & 0 & -q & q \\ q & -q & 0 & 2 & -1 & -1 \\ 0 & q & -q & -1 & 2 & -1 \\ -q & 0 & q & -1 & -1 & 2 \end{bmatrix},$$

has row echelon form,

$$\begin{bmatrix} 2 & -1 & -1 & q & 0 & -q \\ 0 & q & -q & -1 & 2 & -1 \\ 0 & 0 & 0 & 3/2 - 1/2\,q^2 & 0 & 1/2\,q^2 - 3/2 \\ 0 & 0 & 0 & 0 & \frac{q^2-3}{q} & -\frac{q^2-3}{q} \\ 0 & 0 & 0 & 0 & 0 & 0 \\ 0 & 0 & 0 & 0 & 0 & 0 \end{bmatrix};$$

where the diagonal matrix,

$$\mathcal{Q} = \begin{bmatrix} 1 & 0 & 0 & 0 & 0 & 0 & 0 & 0 & 0 & 0 & 0 & 0 \\ 0 & 1 & 0 & 0 & 0 & 0 & 0 & 0 & 0 & 0 & 0 & 0 \\ 0 & 0 & 1 & 0 & 0 & 0 & 0 & 0 & 0 & 0 & 0 & 0 \\ 0 & 0 & 0 & 1 & 0 & 0 & 0 & 0 & 0 & 0 & 0 & 0 \\ 0 & 0 & 0 & 0 & 1 & 0 & 0 & 0 & 0 & 0 & 0 & 0 \\ 0 & 0 & 0 & 0 & 0 & 1 & 0 & 0 & 0 & 0 & 0 & 0 \\ 0 & 0 & 0 & 0 & 0 & 0 & q & 0 & 0 & 0 & 0 & 0 \\ 0 & 0 & 0 & 0 & 0 & 0 & 0 & q & 0 & 0 & 0 & 0 \\ 0 & 0 & 0 & 0 & 0 & 0 & 0 & 0 & q & 0 & 0 & 0 \\ 0 & 0 & 0 & 0 & 0 & 0 & 0 & 0 & 0 & -q & 0 & 0 \\ 0 & 0 & 0 & 0 & 0 & 0 & 0 & 0 & 0 & 0 & -q & 0 \\ 0 & 0 & 0 & 0 & 0 & 0 & 0 & 0 & 0 & 0 & 0 & -q \end{bmatrix},$$

assigns unitary tension coefficients to tensile components in the parallel triangles of the triplex. Variables q and $-q$ are unknowns for bracing cables and struts, respectively. The incidence matrix $\mathcal{C}$ is explained in Section 2.8.

Irreducible polynomials that produce the required rank deficiency are identified from the row echelon form, shown previously. The real roots of these polynomials, e.g. $\frac{q^2-3}{q}$ for the triplex, provide the tension coefficients that cause the structure to be in self-stressed

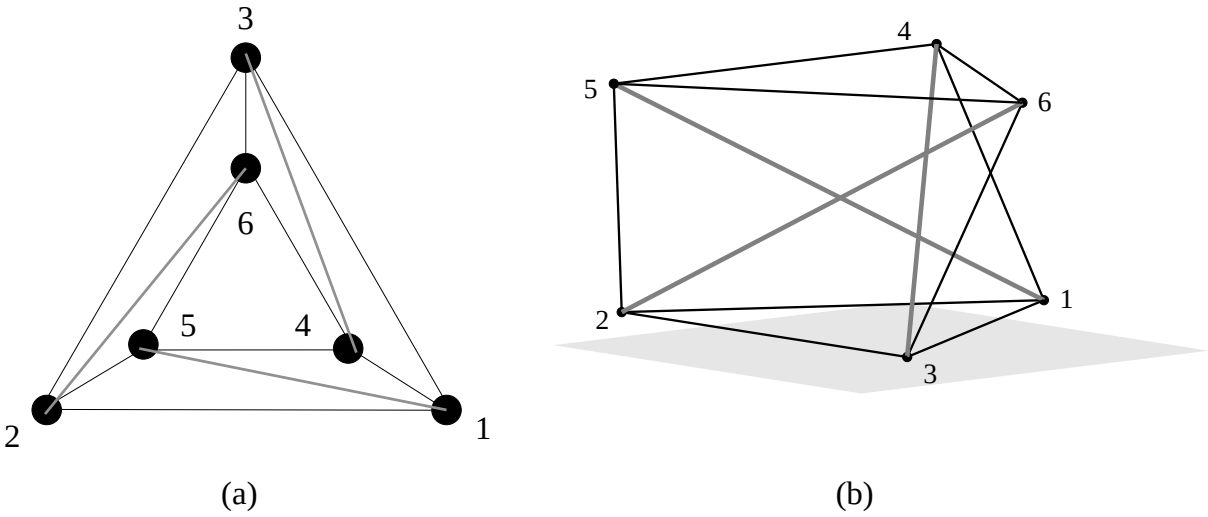

(a) (b)

Fig. 2.6: A triplex : (a) six nodes being interconnected by nine cables and three struts; (c) equilibrium geometry with one state of self-stress

equilibrium, i.e. $q = \sqrt{3}$. The correct nullity, four in this case, see Eq. (2.7), is found by looking for the positive real roots. Chapters 3 and 5 elaborates on this procedure which it is not need in our abbreviated discussion here.

2.8 Example: the triplex

Before moving on to the main part of this dissertation, it seems convenient to show one small example with all its main matrices and vectors. This section presents the tension coefficients, coordinates, force density and equilibrium matrices associated to the triplex. The coordinates and tension coefficients of the self-stressed solution are presented with no further explanation. They are derived in detail in Chapter 3.

The six nodes ($\mathtt{n} = 6$) and their connections ($\mathtt{b} = 12$) are shown in Fig. 2.6. This tensegrity, Fig. 2.6, is called triplex and it is perhaps the smallest three-dimensional tensegrity structure. It consists of two triangles, made of tensile components, connected by three bracing cables and three struts. It is a well-known tensegrity structure, which Motro [142] also calls "elementary equilibrium" or "simplex", and its equilibrium configuration can be found by numerous form-finding techniques.

From the figure Fig. 2.6 it can be seen that there are twelve members, listed as follows: $\overline{1\,2}$, $\overline{2\,3}$, $\overline{1\,3}$, $\overline{4\,5}$, $\overline{5\,6}$, $\overline{4\,6}$, $\overline{1\,4}$, $\overline{2\,5}$, $\overline{3\,6}$, $\overline{1\,5}$, $\overline{2\,6}$, and $\overline{3\,4}$; with no distinction for order $\overline{A\,B}$ or $\overline{B\,A}$. The vectors $\mathbf{x}, \mathbf{y}, \mathbf{z} \in \Re^{\mathtt{n}}$ of Cartesian coordinates of the six nodes are as follows:

$$\begin{aligned}
\mathbf{x} &= [1 \quad -1/2 \quad -1/2 \quad \tfrac{\sqrt{3}}{2} \quad -\tfrac{\sqrt{3}}{2} \quad 0]^T, \\
\mathbf{y} &= [0 \quad \tfrac{\sqrt{3}}{2} \quad -\tfrac{\sqrt{3}}{2} \quad 1/2 \quad 1/2 \quad -1]^T, \\
\mathbf{z} &= [0 \quad 0 \quad 0 \quad 1 \quad 1 \quad 1]^T.
\end{aligned}$$

The incidence matrix, $\mathcal{C} \in \Re^{\mathtt{b}\times\mathtt{n}}$, shown in Eq. (2.14), has one row for each of these twelve pairs of nodes:

$$\mathcal{C} = \begin{array}{c} \begin{array}{cccccc} 1 & 2 & 3 & 4 & 5 & 6 \end{array} \\ \left(\begin{array}{cccccc} 1 & -1 & 0 & 0 & 0 & 0 \\ 0 & 1 & -1 & 0 & 0 & 0 \\ 1 & 0 & -1 & 0 & 0 & 0 \\ 0 & 0 & 0 & 1 & -1 & 0 \\ 0 & 0 & 0 & 0 & 1 & -1 \\ 0 & 0 & 0 & 1 & 0 & -1 \\ 1 & 0 & 0 & -1 & 0 & 0 \\ 0 & 1 & 0 & 0 & -1 & 0 \\ 0 & 0 & 1 & 0 & 0 & -1 \\ 1 & 0 & 0 & 0 & -1 & 0 \\ 0 & 1 & 0 & 0 & 0 & -1 \\ 0 & 0 & 1 & -1 & 0 & 0 \end{array} \right) \end{array} . \tag{2.14}$$

For clarity, the nodes (1-6) are indicated with labels at the top of the incidence matrix $\mathcal{C}$, Eq. (2.14), in which the first row of $\mathcal{C}$ (from top to bottom) means a connection between nodes 1 and 2; and only the columns of these pair of entries, 1 and 2, are non-zero. The associated tension coefficients are $q = 1$ for the six horizontal cables: $\overline{1\,2}$, $\overline{2\,3}$, $\overline{1\,3}$, $\overline{4\,5}$, $\overline{5\,6}$, $\overline{4\,6}$; $q = \sqrt{3}$ for each bracing cable cables: $\overline{1\,4}$, $\overline{2\,5}$, $\overline{3\,6}$; and, finally, $q = -\sqrt{3}$ for the three struts: $\overline{1\,5}$, $\overline{2\,6}$, $\overline{3\,4}$. Therefore, the vector $\mathbf{t} \in \Re^{\mathtt{b}}$ of tension coefficients is

$$\mathbf{t} = \left[\begin{array}{cccccccccccc} 1 & 1 & 1 & 1 & 1 & 1 & \sqrt{3} & \sqrt{3} & \sqrt{3} & -\sqrt{3} & -\sqrt{3} & -\sqrt{3} \end{array} \right]^T .$$

Having calculated the incidence matrix $\mathcal{C}$ and the vector of tension coefficients $\mathbf{t}$, the force density matrix, or stress matrix in mathematics, is:

$$\mathcal{D} = \mathcal{C}^T \mathrm{diag}(\mathbf{t}) \mathcal{C} = \left[\begin{array}{cccccc} 2 & -1 & -1 & -\sqrt{3} & \sqrt{3} & 0 \\ -1 & 2 & -1 & 0 & -\sqrt{3} & \sqrt{3} \\ -1 & -1 & 2 & \sqrt{3} & 0 & -\sqrt{3} \\ -\sqrt{3} & 0 & \sqrt{3} & 2 & -1 & -1 \\ \sqrt{3} & -\sqrt{3} & 0 & -1 & 2 & -1 \\ 0 & \sqrt{3} & -\sqrt{3} & -1 & -1 & 2 \end{array} \right] .$$

It is possible to verify that the nullity of $\mathcal{D}$ is four, and it satisfies Eq. (2.7). From the equilibrium equations follows that $\mathcal{D}\mathbf{x} = \mathbf{f}_x^{ext} = \mathbf{0}$, $\mathcal{D}\mathbf{y} = \mathbf{f}_y^{ext} = \mathbf{0}$, $\mathcal{D}\mathbf{z} = \mathbf{f}_z^{ext} = \mathbf{0}$. Actually, the coordinates $[\mathbf{x}, \mathbf{y}, \mathbf{z}]$ can be calculated by factorising $\mathcal{D} = \mathcal{U}\mathcal{V}\mathcal{U}^T$, and looking into the leftmost eigenvectors in the unitary matrix $\mathcal{U}$; here the diagonal matrix $\mathcal{V}$ has eigenvalues $[\lambda_1 = \lambda_2 = \ldots \lambda_4 = 0 \;\; \lambda_5 = 6\,\lambda_6 = 6]$. With the coordinates of the self-equilibrated configuration, the infinitesimal mechanisms are calculated by decomposing the equilibrium matrix, $\mathcal{A} \in \Re^{3\mathtt{n}\times\mathtt{b}}$:

$$\mathcal{A} = \begin{bmatrix}
\frac{3}{2} & 0 & \frac{3}{2} & 0 & 0 & 0 & 1-\frac{\sqrt{3}}{2} & 0 & 0 & 1+\frac{\sqrt{3}}{2} & 0 & 0 \\
-\frac{3}{2} & 0 & 0 & 0 & 0 & 0 & 0 & \frac{\sqrt{3}-1}{2} & 0 & 0 & -\frac{1}{2} & 0 \\
0 & 0 & -\frac{3}{2} & 0 & 0 & 0 & 0 & 0 & -\frac{1}{2} & 0 & 0 & -\frac{\sqrt{3}-1}{2} \\
0 & 0 & 0 & \sqrt{3} & 0 & \frac{\sqrt{3}}{2} & -1+\frac{\sqrt{3}}{2} & 0 & 0 & 0 & 0 & \frac{\sqrt{3}+1}{2} \\
0 & 0 & 0 & -\sqrt{3} & -\frac{\sqrt{3}}{2} & 0 & 0 & \frac{1-\sqrt{3}}{2} & 0 & -1-\frac{\sqrt{3}}{2} & 0 & 0 \\
0 & 0 & 0 & 0 & \frac{\sqrt{3}}{2} & -\frac{\sqrt{3}}{2} & 0 & 0 & 1/2 & 0 & 1/2 & 0 \\
-\frac{\sqrt{3}}{2} & 0 & \frac{\sqrt{3}}{2} & 0 & 0 & 0 & -1/2 & 0 & 0 & -1/2 & 0 & 0 \\
\frac{\sqrt{3}}{2} & \sqrt{3} & 0 & 0 & 0 & 0 & 0 & \frac{\sqrt{3}-1}{2} & 0 & 0 & 1+\frac{\sqrt{3}}{2} & 0 \\
0 & -\sqrt{3} & -\frac{\sqrt{3}}{2} & 0 & 0 & 0 & 0 & 0 & 1-\frac{\sqrt{3}}{2} & 0 & 0 & -\frac{\sqrt{3}+1}{2} \\
0 & 0 & 0 & 0 & 0 & \frac{3}{2} & 1/2 & 0 & 0 & 0 & 0 & \frac{\sqrt{3}+1}{2} \\
0 & 0 & 0 & 0 & \frac{3}{2} & 0 & 0 & \frac{1-\sqrt{3}}{2} & 0 & 1/2 & 0 & 0 \\
0 & 0 & 0 & 0 & -\frac{3}{2} & -\frac{3}{2} & 0 & 0 & -1+\frac{\sqrt{3}}{2} & 0 & -1-\frac{\sqrt{3}}{2} & 0 \\
0 & 0 & 0 & 0 & 0 & 0 & -1 & 0 & 0 & -1 & 0 & 0 \\
0 & 0 & 0 & 0 & 0 & 0 & 0 & -1 & 0 & 0 & -1 & 0 \\
0 & 0 & 0 & 0 & 0 & 0 & 0 & 0 & -1 & 0 & 0 & -1 \\
0 & 0 & 0 & 0 & 0 & 0 & 1 & 0 & 0 & 0 & 0 & 1 \\
0 & 0 & 0 & 0 & 0 & 0 & 0 & 1 & 0 & 1 & 0 & 0 \\
0 & 0 & 0 & 0 & 0 & 0 & 0 & 0 & 1 & 0 & 1 & 0
\end{bmatrix},$$

in $\mathcal{A} = \mathcal{U}\mathcal{V}\mathcal{W}^T$. It follows that $\mathcal{A}\mathbf{t} = \mathbf{f}^{ext} = \mathbf{0}$. The rank of $\mathcal{A}$ is 11, so it fulfils the rank condition Eq. (2.6), i.e. it is rank deficient. The unitary matrices $\mathcal{U} \in \Re^{18\times18}$ and $\mathcal{W} \in \Re^{12\times12}$, see Eq. (2.8), contain the basis for mechanisms, Eq. (2.9) and tension coefficients, Eq. (2.10),respectively. For instance, the original vector of tension coefficients is found in the right null space of $\mathcal{W}$, i.e.

$$\mathcal{W} = [\,\mathbf{w}_1\,\mathbf{w}_2\,\ldots\,\mathbf{w}_{11}\,|\,\mathbf{t}],$$

meanwhile the left nullspace,

$$\mathcal{U} = [\,\mathbf{u}_1\,\mathbf{u}_2\,\ldots\,\mathbf{u}_{11}\,|\,\mathbf{d}_1\,\mathbf{d}_2\,\ldots\,\mathbf{d}_7],$$

contains the infinitesimal displacements that produce no bar elongation: $\mathcal{A}^T\mathbf{d}_i = \mathbf{0}$, moving along the mechanism. The eigenvalues of the quadratic form of mechanisms, $\mathcal{M} = [\mathbf{d}_1\,\mathbf{d}_2\,\ldots\,\mathbf{d}_7]$, and the reduced stiffness matrix, $\mathbf{I}_3 \otimes \mathcal{D}$, show that six out of these seven infinitesimal displacements exert no work,

$$eig(\mathcal{M}^T(\mathbf{I}_3 \otimes \mathcal{D})\mathcal{M}) = [\underbrace{0\,0\,0\,0\,0\,0}_{rigid-body}\,4.8\,],$$

and correspond to the six rigid-body motions, see Eq. (2.13). The seventh eigenvalue is positive ($\lambda_7 = 4.8$), Summarising, the structure has $\mathtt{n} = 6$, $\mathtt{b} = 12$, $\mathtt{s} = 1$ and $\mathtt{m} = 1$; the sign test Eq. (2.13) shows only one infinitesimal mechanism of deformation producing positive work: the state of self-stress stiffens the structure.

Chapter 3

Analytical form-finding of tensegrity cylinders

After having presented the basic definitions and terminology, in the previous Chapter, here it is shown an analytical investigation of tensegrity cylinders. This first investigation focuses on certain tensegrity structures that are quite well-known for long time, but nevertheless some basic features of these cylinders have not been investigated so far. Moreover, the set of tension coefficients that self-equilibrate a cylinder is analytically derived in a straightforward way, and it improves previous calculations in this field.

The current Chapter provides insights into three different aspects of these cylindrical structures. Firstly, an analytical form-finding process is presented for tensegrity cylinders of equal and non-equal circular faces. The novel solution is shown in terms of tension coefficients and covers cylinders consisting of either convex or star polygons. Secondly, asymptotic analyses of lengths and forces in the cylinders are calculated as the number of nodes used to discretise the circular faces tends to infinity. Thirdly, it is shown how to count and enumerate all possible equivalent solutions for a given n.

The Chapter is organised as follows. A brief introduction to tensegrity cylinders is presented in Sections 3.1 and 3.2. An analytical form-finding procedure is presented in Section 3.3. The asymptotic analysis of the tension coefficients and the enumeration of solutions are shown in Sections 3.5 and 3.4, respectively. A full example (Section 3.6) and a brief discussion of a possible implementation (Section 3.7) help to clarify the details in our form-finding method. Some conclusions of this Chapter are drawn in Section 3.8.

3.1 Tensegrity cylinders

As indicated in the previous Chapter, the form-finding process of cylindrical tensegrities, e.g. the triplex and the quadruplex [142], has been studied using several approaches. There are, basically, four major classes of solution procedures for the form-finding of

tensegrity cylinders: dynamic relaxation and cable-to-strut ratios [142], non-linear programming [157], twisting angles [185, 146, 145, 51, 191], and by calculating tension coefficients[1] [79, 195, 196].

In a previous work, [79], a form-finding procedure for tensegrity cylinders was presented in terms of tension coefficients, i.e. force divided by length. The solution, however, only considered equal circular faces, and there was no attempt to characterise the different configurations. Circular and non-circular faces are covered in the present analysis.

3.2 Geometric arrangement of tensegrity cylinders

Convex cylinders

A tensegrity cylinder, e.g. the triplex and quadruplex [142], consists of two polygons which are interconnected by a set of n bracing cables and n struts. Each polygon consists of $n \geq 3$ nodes, and each node is linked to three members in tension and one in compression. Two out of the three tensile members lie in the same polygon, and the third member, a bracing cable, joins both parallel polygons. Figures 3.1a and 3.1b show the triplex ($n = 3$) and the quadruplex ($n = 4$), respectively.

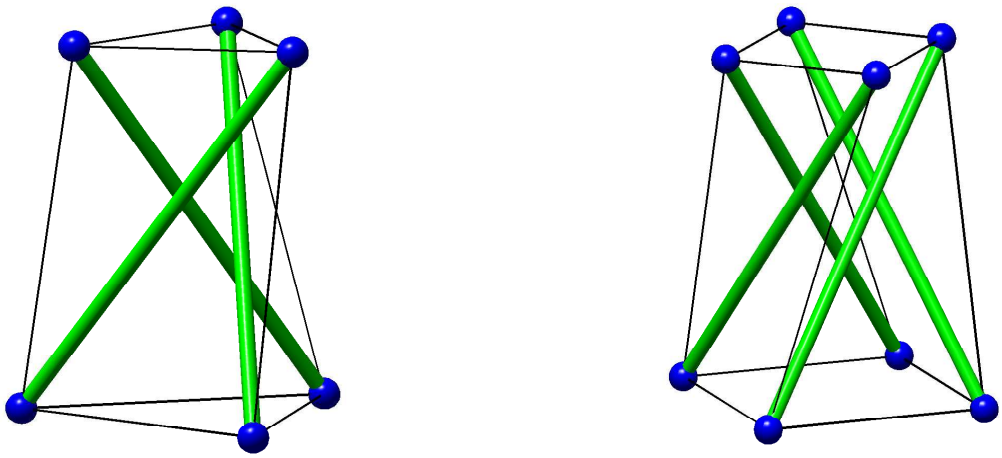

Fig. 3.1: Some examples of well-known tensegrity cylinders : Thick green lines represent elements in compression. (a) 3-plex; (b) 4-plex.

[1]The force-to-length ratio of a member, also known as force density coefficient, see the previous Chapter or [142, 191] for the standard terminology followed in this Chapter.

Star-like cylinders : equivalent configurations

However, the design of a pentaplex, or 5-plex for short, has an extra degree of freedom. It has two possible geometrical arrangements for the five nodes on the circular ends, see Fig. 3.2. It can be seen that the five nodes (Fig. 3.2a) can be joined with a continuous network of cables following the labels and arrows in Figs. 3.2b-c. It is possible to join the sequence of nodes from "A" to "E" without any cut in two different geometric arrangements.

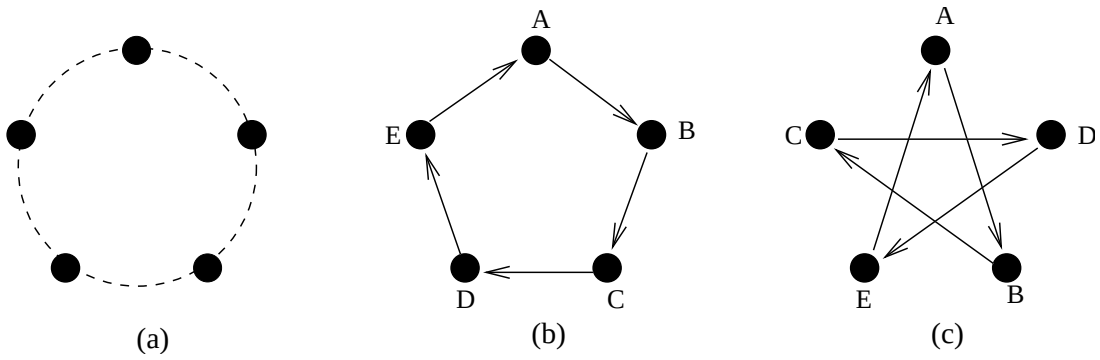

Fig. 3.2: Connecting five nodes in the plane with a single curve : (a) nodes lying on a circumference; (b) convex pentagon; (c) star pentagon, see e.g. [58].

The connections seen in Figs. 3.2b-c are effectively equivalent and can be exchanged from one to the other by a continuous re-arrangement of the nodes. They are therefore called "equivalent" configurations in the remaining Sections.

The corresponding tensegrity cylinders appear in Figs. 3.3a-b. These cylinders are in fact two equivalent configurations of the 5-plex, which can be seen from their labels. All nodes of Fig. 3.3a and their connections actually exist in Fig. 3.3b.

For instance, a node "A" is connected with cables to "B" and "E", while it is being connected with a bracing cable to "A'" and with a strut to "B'". Both cylinders, Fig. 3.3a and Fig. 3.3b, are wired in the same way.

However, those cylinders differ in their geometric arrangement. A closed figure with $n = 5$ nodes connected by n members can be either a convex (Figs. 3.3c and 3.2b) or a star polygon (Figs. 3.3d and 3.2c), e.g. [58]. It is generated by successively connecting by straight members every j-th of the n nodes lying on a circumference, in which $1 \leq j < n/2$. For instance, in the star polygon (Fig. 3.3d), a node "A" is connected to node "B" at $j = 2$ steps along the circumference (from "A" to "B" via "D" along the dotted line in anticlockwise direction), while in the convex polygon (Fig. 3.3c) these nodes are $j = 1$ steps apart, in clockwise direction.

Thus, it can be seen that both 5plex shown in Fig. 3.4a and Fig. 3.4b have the following connections:

- The first pentagon has $\overline{AB}$, $\overline{BC}$, $\overline{CD}$, $\overline{DE}$, and $\overline{EA}$.

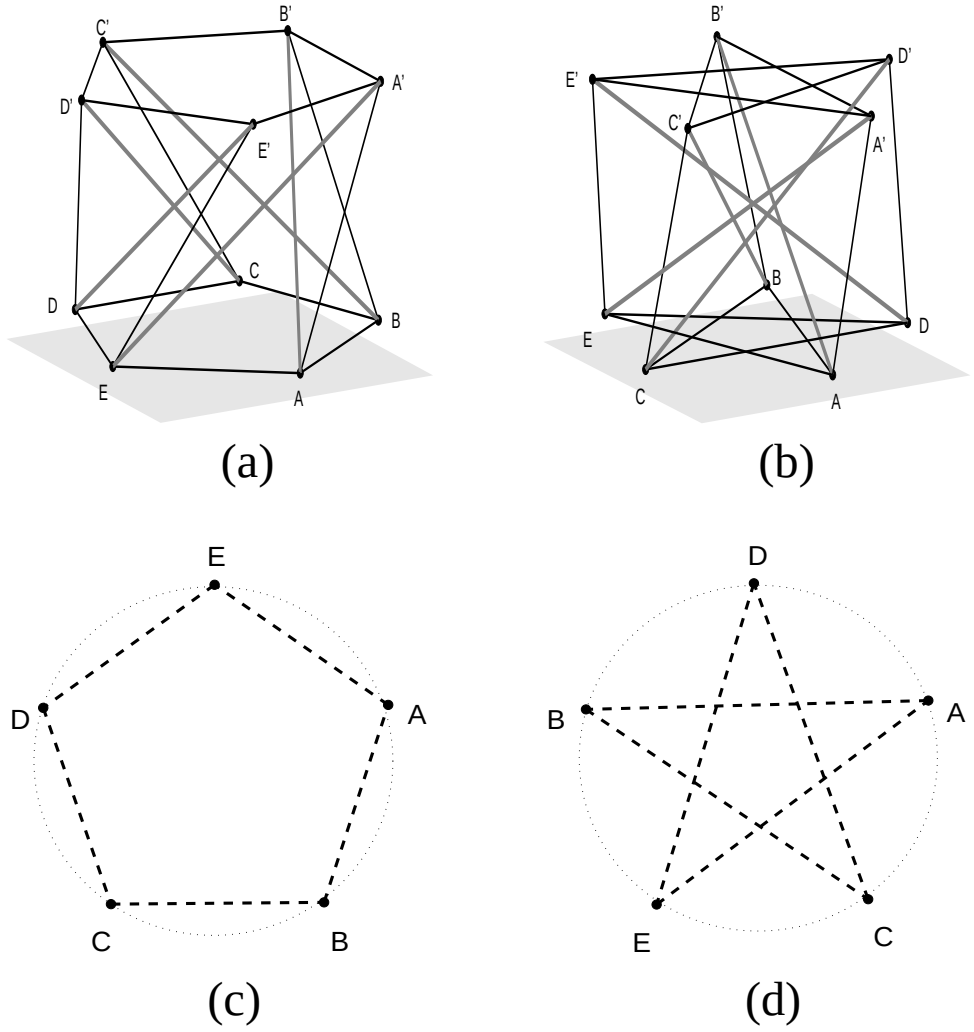

Fig. 3.3: Two configurations for the pentaplex : (a) 5-plex, $j = 1$; (b) 5-plex, $j = 2$; (c) convex polygon with $j = 1$ and its circumcircle; (d) star polygon with $j = 2$ and its circumcircle. The 5-plex with $j = 1$ and $j = 2$, (a) and (b), respectively, are equivalent configurations.

- The second pentagon has: $\overline{A'B'}$, $\overline{B'C'}$, $\overline{C'D'}$, $\overline{D'E'}$, and $\overline{E'A'}$.
- The bracing cables are: $\overline{AA'}$, $\overline{BB'}$, $\overline{CC'}$, $\overline{DD'}$, and $\overline{EE'}$.
- Finally, the struts are: $\overline{AB'}$, $\overline{BC'}$, $\overline{CD'}$, $\overline{DE'}$, and $\overline{EA'}$.

A top view of Fig. 3.3 can help to visualise the cylinder. Figure 3.4 has been created with different tapering so as to provide easier reading of their labels. The connections in both Fig. 3.4a and Fig. 3.4b are exactly the same. That is why it is said that both tensegrities are "equivalent" or "structurally identical" configurations.

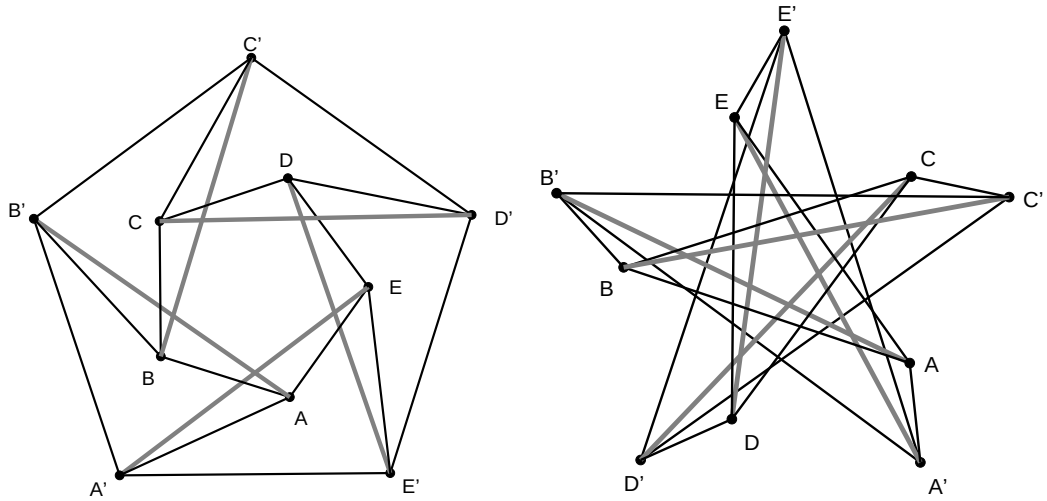

Fig. 3.4: Labels of two 5plex : top view of the only two *equivalent* configurations of the 5-plex. (a) with $j = 1$; (b) with $j = 2$.

Form-finding with tension coefficients

As explained in the previous Chapter, most form-finding studies of cylindrical tensegrity structures have concentrated on determining the twisting angle between the two polygonal faces. However, the analytical solutions of the form-finding of tensegrity cylinders can also be expressed in terms of tension coefficients. It has been shown [195, 196] how a symbolic analysis can be used to find the critical tension coefficients for struts and bracing cables that generate a state of self-stress. The procedure uses Gaussian elimination and root extraction.

A similar form-finding method that seeks the rank deficiency of the equilibrium matrix is presented in [181]. Other form-finding method also uses root extraction of polynomials [174], involving polynomials of hundred terms and 2^{n+1} roots for a given n-plex. Although their proposed symbolic form-finding seems sound and complete, their procedure is very time-consuming. cylinders. Moreover, it is not easy to write the general solution for an arbitrarily large cylinder or calculate cylinders with non-equal circular faces. An analytical form-finding procedure by which the tension coefficients are obtained in a straightforward way is introduced in the following Section.

3.3 Analytical form-finding procedure

Here it is described an analytical form-finding procedure for tensegrity cylinders in terms of tension coefficients that covers equal and non-equal circular faces. Similar geometrical models, like Fig. 3.5a, have been studied with other form-finding methods based on a twisting angle between the polygons, e.g. [51, 191, 185, 146, 145, 142, 96]. In a previous

work, an analytical form-finding procedure in terms of tension coefficients was derived for cylinders with equal-sized polygons [79]. This Section extends our study to cylinders consisting of circumscribed polygons with non-equal radii. It doing so, it is shown that tension coefficients are more appropriate than twisting angles to gain further insights into tensegrity cylinders.

A cylinder, Fig. 3.5, has two polygons, each one with $n \geq 3$ points placed on the circumferences of radii r_1 and r_2, separated at height h. The circumferences are identical up to a scale factor r_1/r_2. They consist of members connecting every j-th node lying on the circumference (Fig. 3.5b), where $1 \leq j < n/2$. The six nodes, from p_a to p_f, shown in Fig. 3.5a, have the following cylindrical coordinates:

$$\left.\begin{array}{rcl} p_a &=& [-r_2 \sin\left(\frac{\pi j}{n}\right), r_2 \cos\left(\frac{\pi j}{n}\right), 0] \\ p_b &=& [r_2 \sin\left(\frac{\pi j}{n}\right), r_2 \cos\left(\frac{\pi j}{n}\right), 0] \\ p_c &=& [r_1 \cos\left(2\frac{\pi j}{n}\right), r_1 \sin\left(2\frac{\pi j}{n}\right), h] \\ p_d &=& [r_1 \cos\left(2\frac{\pi j}{n}\right), -r_1 \sin\left(2\frac{\pi j}{n}\right), h] \\ p_e &=& [r_2 \sin\left(3\frac{\pi j}{n}\right), r_2 \cos\left(3\frac{\pi j}{n}\right), 0] \\ p_f &=& [r_1, 0, h]. \end{array}\right\} \quad (3.1)$$

The members in Fig. 3.5a have the following meaning throughout the Chapter: the segment $\overline{p_f p_a}$ is a strut of length l_s and tension coefficient q_s; $\overline{p_f p_b}$ is a bracing cable of length l_b and tension coefficient q_b; $\overline{p_f p_c}, \overline{p_f p_d}$ are cables of length l_{c_1} and tension coefficient q_{c_1}; $\overline{p_b p_e}, \overline{p_b p_a}$ are cables of length l_{c_2} and tension coefficient q_{c_2}. By convention, the sign of a tension coefficient is negative for compression members (i.e. struts) and positive for tension members (i.e. all types of cables).

Equal circular faces

The equations of static equilibrium for the point p_f, Eq. (3.1) and Fig. 3.5a, can be solved by assuming, for simplicity but without loss of generality, that tension coefficients in adjacent horizontal cables ($\overline{p_f p_d}$ and $\overline{p_f p_c}$) are unitary, i.e. $q_{c_1} = 1$. In this Section equal circular faces are assumed, i.e. $r_1 = r_2$, and it follows that $q_{c_2} = 1$. The ratio of tapering, r_1/r_2, is of course unitary but it is explicitly shown since it will make clear the transition from equal to non-equal circular faces. This normalisation, in q_{c_1} and q_{c_2}, means one can scale all the tension coefficients up to a nonzero positive constant without affecting the self-equilibrium. After the normalisation, the equilibrium equations may have only one unknown, say q, which is the tension coefficient that equilibrates both: strut and bracing cable at point p_f. Since the cylinder is fully symmetric, the solution found for point p_f applies to all other points within the same polygon with radius r_1. The simplification yields $q = q_b = -q_s$. This simplification is clarified in Section 4.3. It can be verified that the static equilibrium equations are satisfied in the $y-$ and $z-$ directions for a reference node p_f. The equilibrium equation in the x-direction is

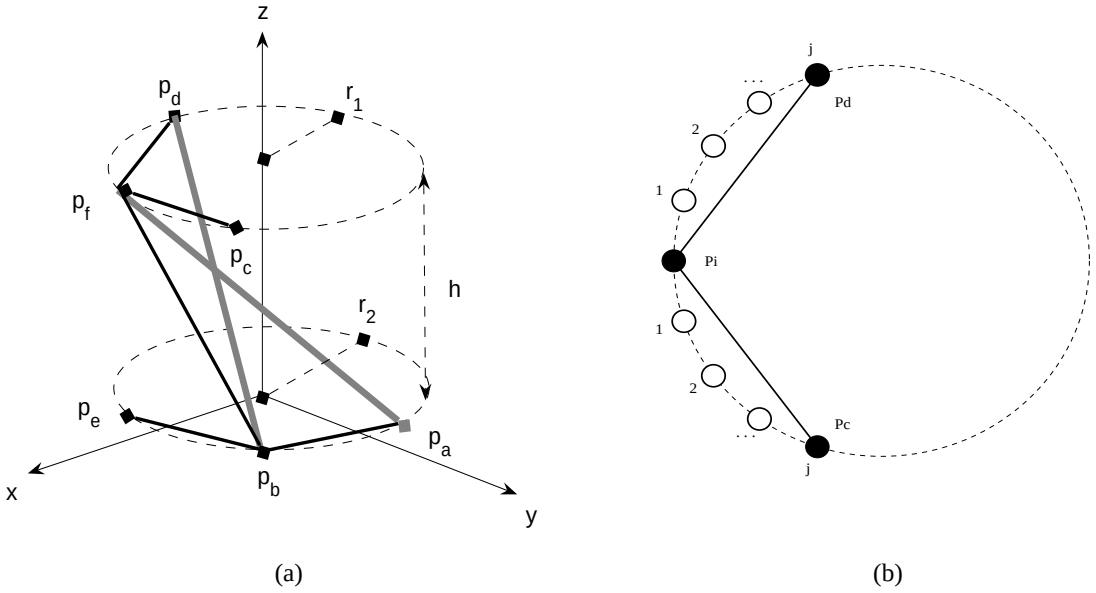

Fig. 3.5: Self-equilibrium state of a tensegrity cylinder : (a) members connecting two reference points, p_f and p_b. The thick gray lines represent members in compression; (b) cables connecting every j-th of the n nodes lying on the circumference (dashed line).

$$2\,qr_2\,\sin\left(\frac{\pi\,j}{n}\right)+2\,r_1\,\cos\left(2\,\frac{\pi\,j}{n}\right)-2\,r_1=0,$$

with q being the only unknown. By solving for q one gets,

$$q=-\frac{\left(2\,r_1\,\left(\cos\left(\frac{\pi\,j}{n}\right)\right)^2-2\,r_1\right)}{r_2\left(\sin\left(\frac{\pi\,j}{n}\right)\right)}=2\,\frac{r_1}{r_2}\,\sin\left(\frac{\pi\,j}{n}\right).$$

Thus, in order to self-equilibrate a tensegrity cylinder its horizontal cables must have $q_{c_1}=1$, for bracing cables

$$q_b=2\,\frac{r_1}{r_2}\,\sin\left(\frac{\pi\,j}{n}\right), \tag{3.2}$$

and for struts

$$q_s=-2\,\frac{r_1}{r_2}\,\sin\left(\frac{\pi\,j}{n}\right). \tag{3.3}$$

The tension coefficients are valid for cylinders with equal radii. It was mentioned that in this case $r_1/r_2=q_{c_1}=1$, and it follows from the equilibrium equations that $q_{c_2}=1$. This completes the set of tension coefficients necessary to self-equilibrate a tensegrity cylinder with equal-sized circular faces, and it is equivalent to the formulation presented in [79].

Two well-known results follow from Eq. (3.2) and Eq. (3.3): the 3-plex has $q_b = -q_s = 2\sin(\pi/3) = \sqrt{3}$, and the 4-plex has $q_b = -q_s = 2\sin(\pi/4) = \sqrt{2}$; as have been found by other authors using a symbolic form-finding procedure based on the force density method [142, 195, 196, 191]. The solution does not explicitly involve the height of the cylinder, but this is included in the definition of a tension coefficient (member force/actual length).

Non-equal circular faces

However, in a more general setting, $r_1 \neq r_2$, and the tension coefficient $q_{c_2} \neq 1$. It is thus needed to solve the equilibrium equations for both polygons in the case of non-equal circular faces. Using $q_{c_1} = 1$, as defined before, as well as Eq. (3.2) and Eq. (3.3), one can calculates q_{c_2} for $r_1 \neq r_2$. The equilibrium equation for a reference point p_b in the y-direction is,

$$\frac{({r_1}^2 - q_{c_2}{r_2}^2)}{r_2}\left(\cos\left(\frac{\pi\, j}{n}\right) - \cos\left(3\,\frac{\pi\, j}{n}\right)\right) = 0.$$

By solving for q_{c_2} one gets, $q_{c_2} = \frac{{r_1}^2}{{r_2}^2}$.

In summary, a general ($r_1 \neq r_2$) tensegrity cylinder consisting of $4n$ members has the following tension coefficients:

$$\left.\begin{array}{rcl} q_{c_1} & = & 1 \\ q_{c_2} & = & \frac{{r_1}^2}{{r_2}^2} \\ q_b & = & 2\,\frac{r_1}{r_2}\,\sin\left(\frac{\pi\, j}{n}\right) \\ q_s & = & -2\,\frac{r_1}{r_2}\,\sin\left(\frac{\pi\, j}{n}\right) \end{array}\right\} \text{ for } 1 \leq j < n/2, \tag{3.4}$$

for horizontal cables q_{c_1} and q_{c_2}, bracing cables q_b, and struts q_s. This set of tension coefficients, Eq. (3.4), is valid up to non-zero positive (real) constants.

3.4 Enumerating solutions: regular convex and star polygons

The meaning of the parameter j in Eq. (3.4) remains to be clarified. Depending on its value, the cylinders are made up of convex polygons ($j = 1$ in Fig. 3.3a) or star polygons ($j > 1$ in Fig. 3.3b). The parameter $1 \leq j < n/2$ is not arbitrary [79]. Consider for example the case $n = 6$ for which two values are within the range $1 \leq j < n/2$: $j = 1$ and $j = 2$, as shown in Figs. 3.6a-b.

The value $j = 2$ creates a hexagram, Fig. 3.6b, which is not a single network but the

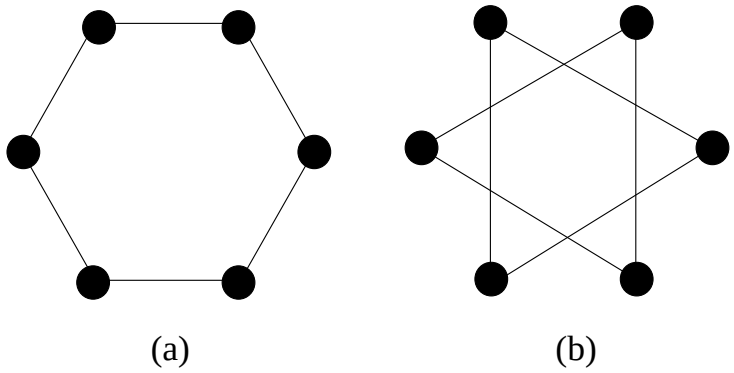

Fig. 3.6: Two different relationships of j for $n = 6$: (a) the single connected curve is generated with $j = 1$; (b) two superimposed triangles generated with $j = 2$

superposition of two triangles. However, if $j = 1$ one can see that all $n = 6$ nodes are interconnected and form a single network, Fig. 3.6a.

3.4.1 Possible configurations

In order to construct single connected networks, the relationship between n and j should be such that the trigonometric angles $(\pi j/n)$, in Eq. (3.4), generate single closed curves embedded in two dimensions, e.g. [58, 169]. This is the case if j and n are relative primes or co-primes, which can be checked with the greatest common divisor (GCD), i.e. when $\mathrm{GCD}(n, j) \equiv 1$. Enumerating the solutions can thus be done by finding any $1 \leq j < n/2$ being a co-prime to n. The following constraint is used in Eq. (3.4) to calculate the tension coefficients:

$$\left.\begin{array}{rcc} q_{c_1} & = & 1 \\ q_{c_2} & = & \frac{{r_1}^2}{{r_2}^2} \\ q_b & = & 2\,\frac{r_1}{r_2}\,\sin\left(\frac{\pi\, j}{n}\right) \\ q_s & = & -2\,\frac{r_1}{r_2}\,\sin\left(\frac{\pi\, j}{n}\right) \end{array}\right\} \text{ for all } 1 \leq j < n/2 \text{ s.t. } GCD(n, j) \equiv 1. \qquad (3.5)$$

Polygons satisfying this condition are visualised as single looped curves with $n(j-1)$ crossings, see Figs. 3.3c and 3.3d. The parameter j only affects the tension coefficients of bracing cables and struts.

3.4.2 Counting the equivalent configurations

There are several equivalent solutions for most cylinders with $n \geq 3$ and they are related to the aforementioned angle. For instance, the pentaplex has exactly two equivalent solutions, Fig. 3.3a and Fig. 3.3b, but in general it is not obvious the number of equivalent solutions for a larger n-plex.

It is possible to count the number of these equivalent solutions for each n from Eq. (3.5), without actually searching for all $1 \leq j < n/2$ that satisfy $\mathrm{GCD}(n, j) \equiv 1$. The number of real roots or algebraic order of the trigonometric function $\sin(\pi/n)$ that appears in Eq. (3.5) is given in terms of Euler's totient function, $\phi(n)/2$, see e.g. [169, 13, 167]. In our context, Euler's totient function counts the number of different ways to connect, with a single connected curve, a polygon of n nodes, and thus it yields the number of equivalent n-plexes.

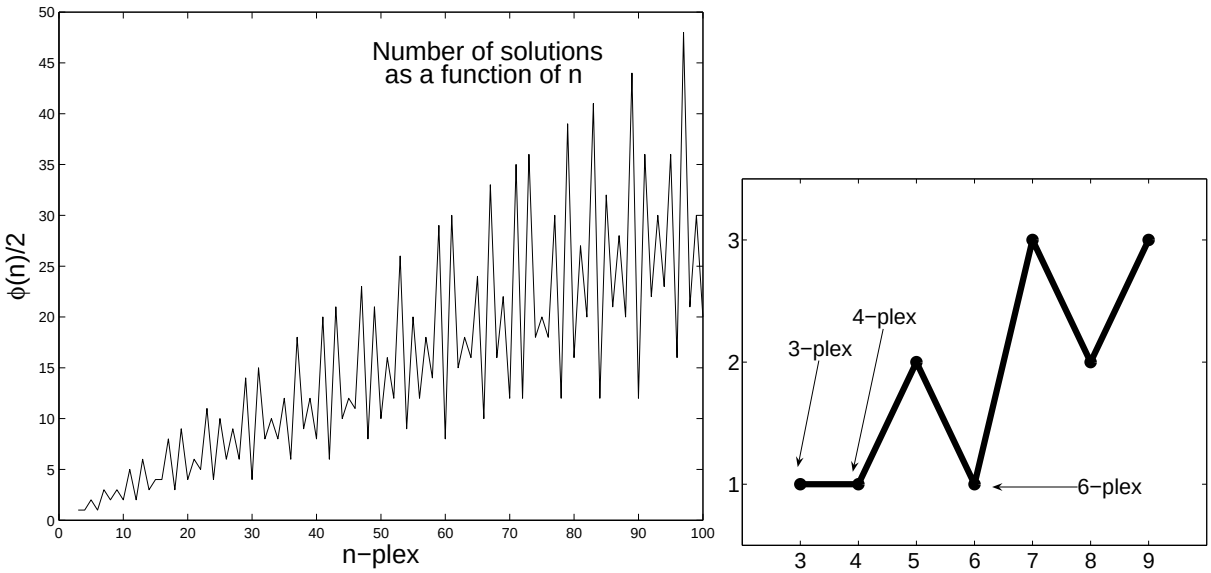

(a) (b)

Fig. 3.7: Number of equivalent configurations, $\phi(n)/2$, for a given n-plex : (a) There are $\phi(n)/2$ equivalent configurations for a given n. The Euler's totient function, $\phi(n)/2$, is not a monotonically increasing function. (b) Only three n-plexes have no star-like configuration, i.e. $j = 1$. The 5-plex has two equivalent solutions, while 7-plex and 9-plex have three equivalent solutions.

Figure 3.7a depicts the number of equivalent solutions for tensegrity cylinders. Notice that by definition $\mathrm{GCD}(n, 1) \equiv 1$, thus at least one cylinder exists ($j = 1$) for any n, i.e. the convex polygon. Interestingly, there are only three n-plexes ($n = 3, 4, 6$) with $\phi(n)/2 \equiv 1$, see the inset Fig. 3.7b and Table (3.1). They have no equivalent star-like cylinders thus $j = 1$ in Eq. (3.5) and appear in the first entry, from top to bottom, of Table (3.1). For a prime number n, the totient function is $\phi(n) = n - 1$. Hence, the number of solutions for those cylinders is $\frac{n-1}{2}$, and corresponds to local maxima points in Fig. 3.7a.

Moreover, it follows from Eq. (3.5) that the hexaplex is the only n-plex that can have unitary tension coefficients for all cables and struts, if $r_1 = r_2$, Eq. (3.5) gives $q_{c_1} = q_{c_2} = 1$ and $q_b = -q_s = 1$. Thus, in the 6-plex, every member length is equal to the absolute value of its member force. Other tensegrities falling into this category are the X-truss (Fig. 2.1) and the cube with struts connecting opposing "top" and "bottom" vertices.

Table (3.1) shows the n-plexes that have only a few number of equivalent solutions,

$\phi(n)/2$.

$\phi(n)/2$	n-plex
1	$3, 4, 6$
2	$5, 8, 10, 12$
3	$7, 9, 14, 18$
4	$15, 16, 20, 24, 30$
5	$11, 22$

Table 3.1: Number of equivalent solutions for some tensegrity structures : The first row shows that the 3-plex, 4-plex and 6-plex are tensegrity cylinders with only one possible equivalent configuration, i.e. $\phi(n)/2 \equiv 1$. The 5-plex, presented in Fig. 3.2 and Fig. 3.3, has two equivalent configurations. The 9-plex, analysed in Section 3.6 has three equivalent solutions.

In summary, for a given n, all solutions that satisfy $\text{GCD}(n, j) \equiv 1$ are equivalent solutions consisting of close looped curves with $n(j-1)$ crossings. A given n-plex has $\phi(n)/2 \geq 1$ equivalent solutions. For $j = 1$, there are no crossings and the polygons are convex. Any other solution not satisfying $GCD(n, j) \equiv 1$ corresponds to disconnected polygons.

3.5 Analysis of tension coefficients, forces and lengths

3.5.1 Tension coefficients

The analytical solution in terms of tension coefficients gives immediate access to forces and lengths. Hence, one can analyse these asymptotic values when n or j approach their limits. A reader should be aware of inherent limitations of the small displacement theory used in this work. The order of a tensegrity cylinder can be arbitrarily large, $n \to \infty$, while j can be arbitrarily close to $n/2$. These limits have to be handled carefully insofar certain forces and lengths tend to zero. The study of their asymptotic values is indeed important to understand the cylinders for large enough n.

The tension coefficients in the horizontal cables, q_{c_1} and q_{c_2} in Eq. (3.5), are unaffected by any change in n or j. However, tension coefficients of bracing cables and struts in Eq. (3.5) show an interesting limit value:

tension coefficient	limit $n \to \infty$	limit $j \to n/2$
$q_b = 2\,\frac{r_1}{r_2}\,\sin\left(\frac{\pi j}{n}\right)$	0	$2\,\frac{r_1}{r_2}$,
$q_s = -2\,\frac{r_1}{r_2}\,\sin\left(\frac{\pi j}{n}\right)$	0	$-2\,\frac{r_1}{r_2}$.

(3.6)

It is seen in Eq. (3.6) how tension coefficients in bracing cables and struts are zero

when n tend to infinity. Since the tension coefficients are defined as force divided by length, it is indeed possible to explore the value of both forces and lengths. A Taylor expansion of q_b and q_s in Eq. (3.6) shows that values of tension coefficients in bracing cables and struts decrease inversely proportional to n: $q_b = -q_s = 2\frac{r_1}{nr_2}\pi\, j + O\left(\frac{1}{n^3}\right)$. On the other hand, if one vary the parameter $j \to n/2$ the tension coefficients tend to a finite value, as a ratio of the tapering. There is however one drawback for $j \to n/2$: struts collide in the centre; the incircle is reduced with j, e.g. Fig. 4.6.

3.5.2 Lengths

The tension coefficients q_b and q_s in Eq. (3.4) have a graphical meaning. The value of $2\sin\left(\frac{\pi j}{n}\right)$ corresponds to the length of a horizontal cable formed by connecting any two consecutive nodes at j steps. This length is depicted in Fig. 3.5b and corresponds to the length, after defining j, of the segment $\overline{p_f p_c}$ or $\overline{p_f p_d}$. The lengths l_{c_1} and l_{c_2} grow monotonically for $1 \leq j < n/2$. The lengths for each member, calculated from the coordinates Eq. (3.1), are defined as follows:

$$\left.\begin{array}{rcl} l_{c_1} & = & 2\,r_1\,\sin\left(\frac{\pi j}{n}\right) \\ l_{c_2} & = & 2\,r_2\,\sin\left(\frac{\pi j}{n}\right) \\ l_b & = & \sqrt{r_1^2 + r_2^2 + h^2 - 2\,r_1 r_2\,\sin\left(\frac{\pi j}{n}\right)} \\ l_s & = & \sqrt{r_1^2 + r_2^2 + h^2 + 2\,r_1 r_2\,\sin\left(\frac{\pi j}{n}\right)} \end{array}\right\} \tag{3.7}$$

Notice that l_{c_1} and l_{c_2}, in Eq. (3.7), include a term $2\sin\left(\frac{\pi j}{n}\right)$, which tends to zero for large n, see Eq. (3.6). The length of horizontal cables is therefore zero when n tends to infinity, inasmuch as the unstressed bar length, $l_0 = EAl/(ql + EA)$, tends to zero for the same limit; here E is the elastic modulus in a bar with cross sectional area A and length $l = l_{c_1}$ or $l = l_{c_2}$. This limit, $n \to \infty$, has to be handled carefully since it is not physically meaningful to assume zero-length cables. The limit values are thus used to show the tendency of lengths, Eq. (3.7), and tension coefficients, Eq. (3.6). The behaviour is certainly a decreasing length as a function of the number of nodes used to discretise the circular faces.

3.5.3 Forces

Any member of the cylinder has bar force $f = EA(l - l_0)/l_0$, where E is the elastic modulus, A the cross sectional area, and l_0 the unstressed bar length. Member forces can be calculated with the tension coefficients and lengths, Eq. (3.4) and Eq. (3.7) respectively. The definition of tension coefficient is force divided by length, $q = f/l$, thus the member forces are:

$$\left.\begin{array}{rcccl} f_{c_1} & = & q_{c_1} l_{c_1} & = & 2\, r_1\, \sin\left(\frac{\pi\, j}{n}\right), \\ f_{c_2} & = & q_{c_2} l_{c_2} & = & 2\, \frac{r_1^2}{r_2} \sin\left(\frac{\pi\, j}{n}\right), \\ f_b & = & q_b l_b & = & 2\, \frac{r_1}{r_2}\, \sin\left(\frac{\pi\, j}{n}\right) \sqrt{r_1^2 + r_2^2 + h^2 - 2\, r_1 r_2\, \sin\left(\frac{\pi\, j}{n}\right)}, \\ f_s & = & q_s l_s & = & -\ 2\, \frac{r_1}{r_2}\, \sin\left(\frac{\pi\, j}{n}\right) \sqrt{r_1^2 + r_2^2 + h^2 + 2\, r_1 r_2\, \sin\left(\frac{\pi\, j}{n}\right)}, \end{array}\right\} \tag{3.8}$$

where f_c, f_b and f_s are forces in horizontal cables, bracing cables and struts, respectively. The terms like $2\, \sin\left(\frac{\pi\, j}{n}\right)$, in Eq. (3.8), tend to zero as n increases, see Eq. (3.6). Thus, the limit values for large n and large j of the member forces Eq. (3.8) are as follows:

force	limit $n \to \infty$	limit $j \to n/2$
f_{c_1}	0	$2r_1$
f_{c_2}	0	$2\frac{r_1^2}{r_2}$
f_b	0	$2\frac{r_1}{r_2}\sqrt{(r_1 - r_2)^2 + h^2}$
f_s	0	$-2\frac{r_1}{r_2}\sqrt{(r_1 + r_2)^2 + h^2}$

(3.9)

The decreasing trend for large n, i.e. zeros in Eq. (3.9), is due to the fact that terms like $2\, \sin\left(\frac{\pi\, j}{n}\right)$ decrease inversely proportional to n.

The tendency of these member forces is interesting, but the limit value (i.e. zero force) should be handled carefully : it implies zero-length horizontal cables. Figure 3.8 shows this decreasing trend of all member forces; here the y-axis has (logarithmic) arbitrary scale in newtons. A Taylor expansion of f_b and f_s, for $n \to \infty$, gives more details of this limit value:

$$f_b = -f_s = 2\, \frac{r_1\, \pi\, j}{r_2\, n} \sqrt{r_1^2 + r_2^2 + h^2} + O\left(\frac{1}{n^2}\right).$$

That is, member forces increase within the range $1 \leq j < n/2$, and higher-order terms decrease with n.

In summary, the tension coefficients (forces divided by lengths) in both struts and bracing cables have the same magnitude and decrease with the order of a cylinder. The tension coefficients in horizontal cables are unaffected by n or j. The force in any member (tension coefficient times length) rapidly decreases as n grows, but it increases with $1 \leq j < n/2$. The limit value of member forces, for $j \to n/2$, is a finite non-zero value. For the case $j = 1$, the larger n the better the circumference is approximated by a convex polygon, and the distance between any pair of adjacent nodes in the horizontal planes decreases as a function of n.

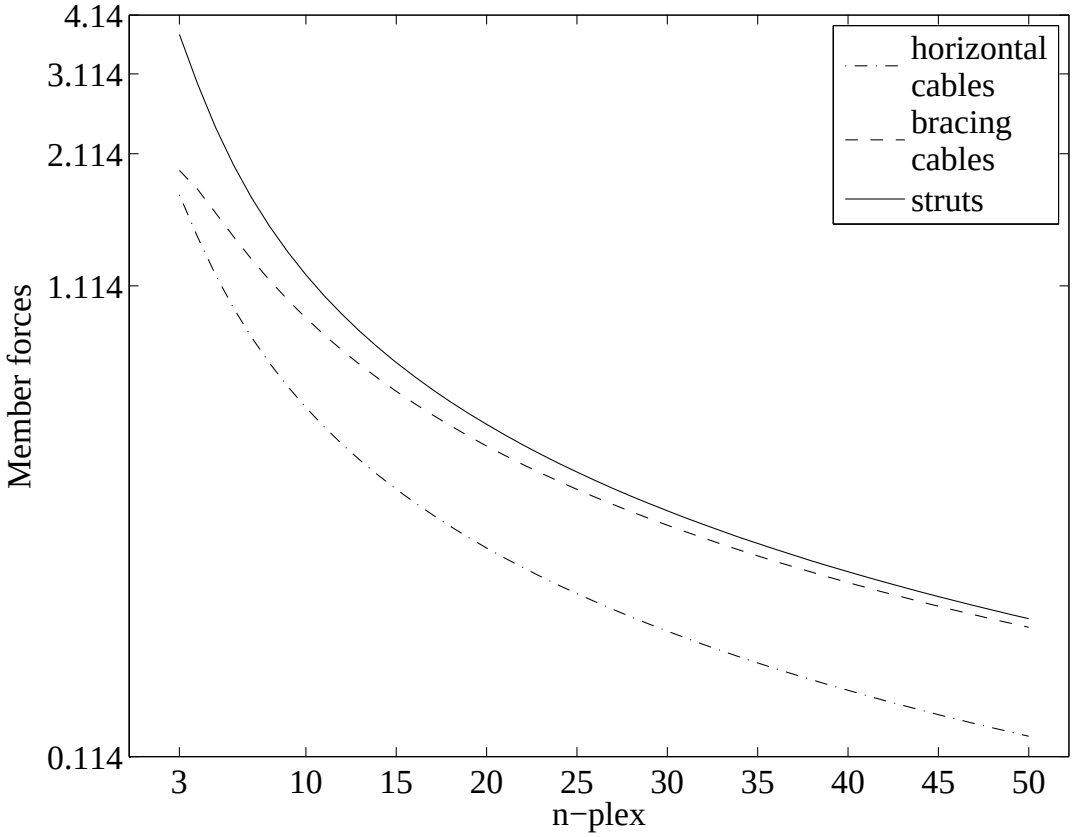

Fig. 3.8: Logarithmic plot of member forces versus n : Numerical calculation showing how the member forces decrease monotonically with n. All cylindrical tensegrity structures are calculated with $r_1 = r_2 = h = 1$.

3.6 A full example: the 9-plex

This Section develops the form-finding of a tensegrity cylinder, and illustrates the use of equations presented so far. It has been chosen the 9-plex. The 9-plex consists of two enneagons, i.e. 9-sided polygons, linked with nine bracing cables and nine struts. All examples of this cylinder have $r_1 = 1$ and $r_2 = 2$.

There are four possible, $1 \leq j < 9/2$, ways to wire the cylinders. A visual inspection of the four options, depicted in Fig. 3.9, confirms that there are only three valid polygons, i.e. $j = 1, 2, 4$. Table 3.1 shows that there are three valid cylinders associated to the 9-plex. The values of j can be calculated with the Euler's totient function, $\phi(9)/2 = 3$, directly without drawing the polygons.

The four polygons are listed as follows: $j = 1$ is the regular enneagon shown in Fig. 3.9a; $j = 2$ and $j = 4$ are star enneagons shown in Fig. 3.9b and Fig. 3.9d; and $j = 3$ is a nonagram composed of three equilateral triangles, shown in Fig. 3.9c.

A nonagram, $j = 3$, has no single curve connecting all nine points in the plane. It is straightforward to calculate which j, from the $1 \leq j < 9/2$, produces a valid,

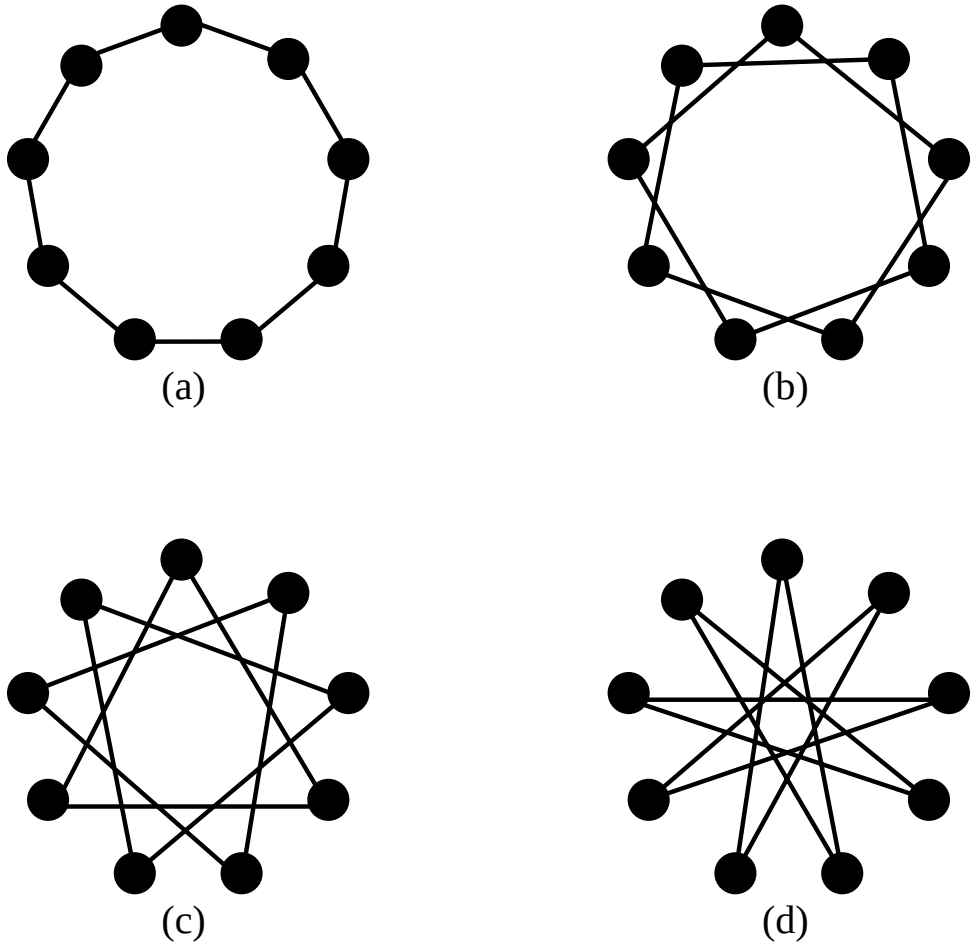

Fig. 3.9: Connecting nine nodes on the plane : (a) j=1; (b) j=2; (c) j=3; (d) j=4.

fully connected polygon. A quick calculation of the greatest common divisor shows that GCD(9,1) = GCD(9,2) = GCD(9,4) = 1, but GCD(9,3)=3. It is therefore clear that only $j = 1, 2, 4$ produce valid polygons and $j = 3$ produces a nonagram.

The form-finding of the three valid 9-plex is calculated with Eq. (3.5). All tension coefficients for the nine tensile elements in the circumference of radius r_1 are $q_{c_1} = 1$, and for radius r_2 are $q_{c_2} = 1^2/2^2 = 1/4$. The other tension coefficients, for bracing cables (q_b) and struts (q_s), are listed below:

$$\left.\begin{array}{llllll} \text{if } j=1, & q_b = -q_s = & 2\frac{1}{2}\sin(\frac{\pi j}{n}) = & \sin(\pi/9) & = 0.3420 \\ \text{if } j=2, & q_b = -q_s = & 2\frac{1}{2}\sin(\frac{\pi j}{n}) = & \sin(2\pi/9) & = 0.6427 \\ \text{if } j=4, & q_b = -q_s = & 2\frac{1}{2}\sin(\frac{\pi j}{n}) = & \sin(4\pi/9) & = 0.9848 \end{array}\right\} \qquad (3.10)$$

Figure 3.10 shows the three valid configurations for the 9-plex, all of them derived from the same node-to-node connectivity. That is why Figs. 3.10a-c are said to be equivalent configurations from a connectivity point of view. The tension coefficients are the ones listed in Eq. (3.10).

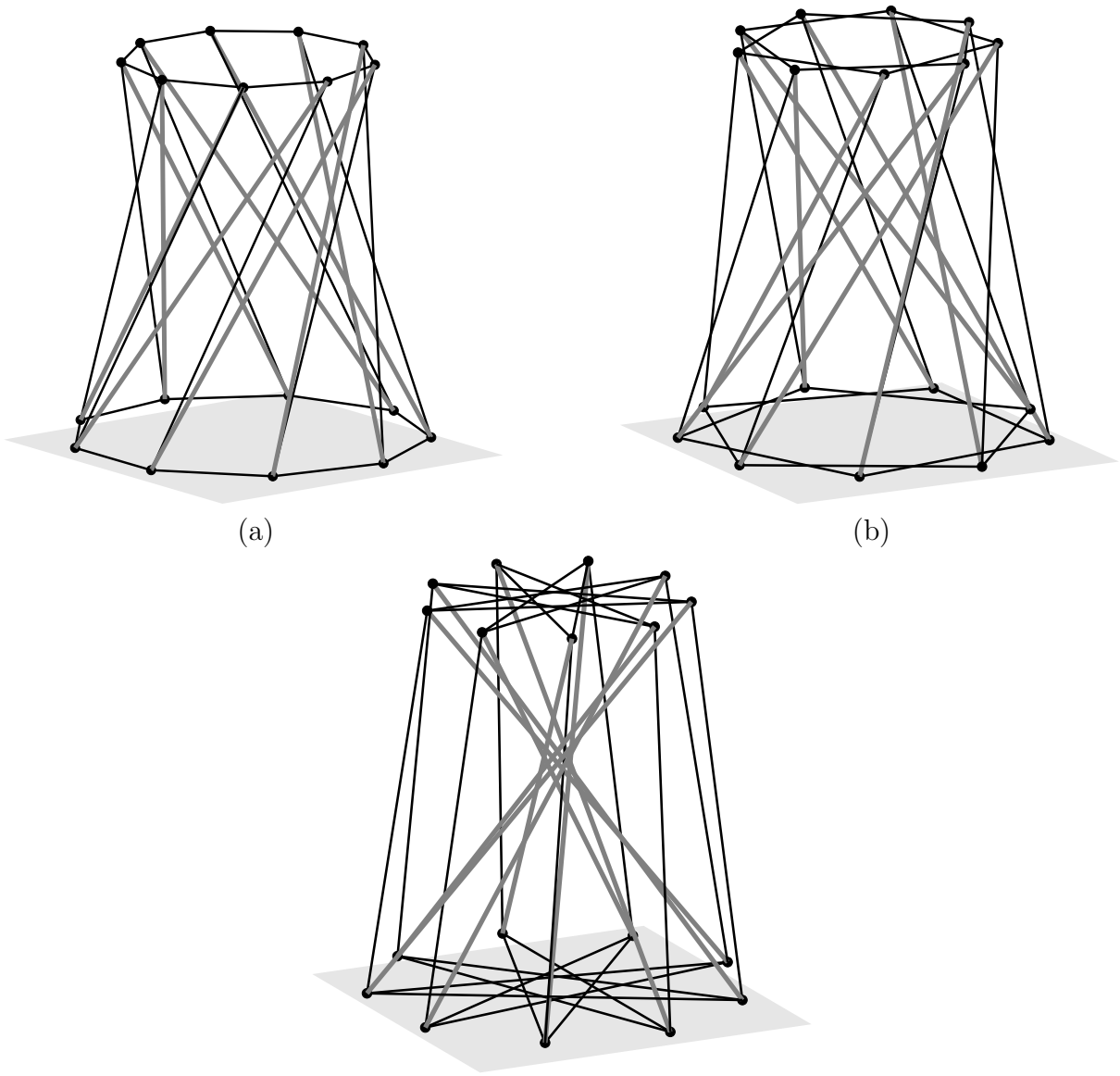

Fig. 3.10: Three possible solutions for the 9-plex : (a) j=1; (b) j=2; (c) j=4. All configurations are actually derived from the same nodal connectivity, i.e. equivalent, the only variation is the parameter j of Eq. (3.5). One state of self-stress is found in all cylinders.

Advantages of the presented form-finding method are better appreciated when a comparison with other methods based on tension coefficients is shown. A symbolic form-finding procedure based on the force density method is presented in [142, 195, 196]. In order to obtain the tension coefficients that self-equilibrate a cylindrical tensegrity structure, the authors look for the positive real roots of a minimal polynomial that annihilates a force density matrix, calculated with $q = q_b = -q_s$ which is the only unknown; here it is assumed $q_{c_1} = q_{c_2} = 1$. It implies $r_1 = r_2 = 1$, or in other words, a cylinder with equal circular ends.

A search of the abovementioned polynomials requires the solution of a system of linear equations: a force density matrix with dimensions $2n \times 2n$. To start with, the force density matrix $\mathcal{D} = \mathcal{C}^T \, \mathrm{diag}(\mathbf{t})\mathcal{C}$ has

$$\mathbf{t} = [1, \ldots, 1, q, \ldots, q, 1, \ldots, 1, -q, \ldots, -q], \tag{3.11}$$

and it is symbolically reduced to row echelon form. The procedure works with the assumption $q_b = -q_s$ and $q_{c_1} = q_{c_2} = 1$, that is why $\mathbf{t}$, Eq. (3.11), consists of four sections, with nine entries each one. From left to right, the vector $\mathbf{t}$ is:

$$\mathbf{t} = [q_{c_1}, \ldots q_{c_1}, q, \ldots, q, q_{c_2}, \ldots q_{c_2}, -q, \ldots, -q].$$

By determining the irreducible factors, one can see that the polynomial,

$$q^8 - 9\,q^6 + 27\,q^4 - 30\,q^2 + 9 = 0,$$

has positive real roots: 0.6840, 1.2855, 1.7320, 1.9696; which are the same values obtained by applying Eq. (3.5). However, Eq. (3.5) provides a direct way to calculate the tension coefficients. That is, if $r_1 = r_2$ it follows from Eq. (3.5), that: $q_b = -q_s = 2\,\sin(\pi/9) = 0.6840$, $q_b = -q_s = 2\,\sin(2\pi/9) = 1.2855$, $q_b = -q_s = 2\,\sin(4\pi/9) = 1.9696$. A set of values which can be seen in Table 3.2. The missing root, 1.7320, is in fact $2\sin(3\pi/9)$ with which comes from a non-valid cylindrical tensegrity structure, i.e. $j = 3$ and $n = 9$.

It is interesting to notice that Eq. (3.5) selects the valid cylinders, which in the symbolic form-finding method has to be verified after the echelon form and root extraction. It is also convenient to remark that our solution covers equal and non-equal circular faces: $q_{c_2} = r_1^2/r_2^2$. Further, solutions obtained with the symbolic form-finding method described above leave us with no clue about j, which influences the geometry, i.e. convex or star-like cylinders.

3.7 Implementation

This Section shows a piece of code that calculates the critical tension coefficient in struts and bracing cables that self-equilibrate a tensegrity cylinder. The code, written for Maple, has no intention to be a definite guide in how to implement Eq. (3.5) and has no claim of good coding style. It calculates q_b, which is equal to $-q_s$. Tension coefficients on the parallel, circular faces are not calculated since $q_{c_1} = 1$ for normalisation reasons, and q_{c_2} is straightforward, i.e. $q_{c_2} = r_1^2/r_2^2$. The code is shown in Fig. 3.11, and it uses the package of number theory (line 1).

The procedure accepts two parameters, the order of our tensegrity cylinder n and the ratio r of the circular faces r_1/r_2, see line 3. It basically searches for all $\phi(n)/2$ equivalent

```
 1  with(numtheory):
 2
 3  q := proc(n, r)
 4    local j, c, ans;
 5
 6    c   := 0;
 7    ans := [];
 8
 9    for j while c < phi(n)/2 do
10      if gcd(n, j) = 1 then
11        ans := [ op(ans) , [ j, evalf(2*r*sin(Pi*j/n))] ];
12        c := c+1;
13      fi;
14    od;
15
16    return ans;
17  end;
```

Fig. 3.11: Implementation of the form-finding method : this Maple code allow us to calculate the critical tension coefficient in bracing cables and struts that self-equilibrates a tensegrity cylinder of order n.

cylinders such that are composed of valid polygons, see lines 9-10. Line 11 pack the valid solutions in a list of pairs $[j, q_s]$. The two examples calculated in this Chapter, the 9-plex, with equal and non-equal circular faces, are shown in Table 3.2.

tapering	call: $(n,\, r_1/r_2)$	output: $[j, q_s]$
$r_1 = r_2 = 1$	$q(9, 1/1)$	$[[1, 0.6840], [2, 1.2855], [4, 1.9696]]$
$r_1 = 1,\, r_2 = 2$	$q(9, 1/2)$	$[[1, 0.3420], [2, 0.6427], [4, 0.9848]]$

Table 3.2: Calculation of the 9-plex : The 9-plex with equal circular faces ($r_1 = r_2$), and non-equal circular faces ($r_1 \neq r_2$). The resulting tension coefficients are presented in pairs $[j, q]$, with $q = q_b = -q_s$, for all $\phi(n)/2$ valid cylinders of a given n-plex.

The values for the first 9-plex, with equal circular faces correspond to the tension coefficients (q_b) found with the symbolic form-finding procedure, or Eq. (3.5) with $r_1 = r_2$ as described in the previous Section. The tension coefficients are: 0.6840, 1.2855 and 1.9696, for $j = 1, 2, 4$. For $r_1 \neq r_2$, see Eq. (3.10), the values are calculated with Eq. (3.5) for $r_1 = 1$ and $r_2 = 2$: 0.3420, 0.6427 and 0.9848, for $j = 1, 2, 4$, respectively. Both examples of the 9-plex, with equal and non-equal circular faces, appear in Table 3.2 and can easily be generated by Fig. 3.11.

3.8 Conclusions and final remarks

This Chapter presented a form-finding procedure and a comprehensive analysis of cylindrical tensegrity structures (n-plexes), in which the circular faces are composed of either convex or star polygons. The circular faces consists of polygons created by connecting every j-th node lying on their circumference. The analysis is done on the basis of tension coefficients, and allows to calculate them directly in analytical way. The analytical investigations permit to address the following issues at once:

Firstly, a solution for any n-plex, with equal and non-equal circular faces, is easily calculated in closed-form. Tension coefficients, i.e. force divided by length, were used instead of twisting angles. For cylinders with equal circular faces our solution agrees with previous studies. Tension coefficients that self-equilibrate the cylinders can be calculated for an arbitrarily large n-plex.

Interestingly, as a historical note, a tension coefficient like $2r\sin(\pi/n)$, can easily be deduced from a paper [180] that deals with tubular frameworks for aeroplane fuselages; here r is the radius of the framework. The paper, published in 1933, develops a procedure for the calculation of stresses in tubular frameworks and it is, to our best knowledge, the first use of tension coefficients similar to $2r\sin(\pi/n)$ in mechanics. In his analysis, however, Southwell assumed that every bar in the framework can sustain both tension or compression.

Secondly, it is possible to choose between convex ($j = 1$) and star-like ($j > 1$) cylinders. The equations developed for the form-finding introduce a parameter j with which a switch in the appearance of the n-plex is allowed. In fact, each circular face is visualised as single looped curves with $n(j-1)$ crossings

Thirdly, the enumeration of all valid j, coming from structurally identical n-plexes, generated out of the same n, is accomplished with the greatest common divisor. The configurations are indexed by a parameter j that changes the geometric arrangement of the nodes. All tensegrity cylinders have at least one valid j, in which $j = 1$ corresponds to convex cylinders.

Finally, it is also possible to count the total number of equivalent configurations. The number of these equivalent configurations is given by the Euler's totient function, which is not a monotonically increasing function with n, and its upper bound is a linear function of n. It is also possible to count and show solutions having exactly certain number of equivalent configurations. One interesting result of our analysis is that only three cylinders ($n = 3, 4, 6$) have no equivalent star polygons. The hexaplex deserves special attention because it is the only n-plex that can sustain unitary tension coefficients, i.e. the values of axial force and length per member are equal, in all members.

Chapter 4

Stability and non-uniqueness of the solution for tensegrity cylinders

The previous Chapter presented an analysis of cylindrical tensegrity structures. The form-finding of cylindrical tensegrity structures was analytically derived using tension coefficients. An analysis of these structures shows that a number of solutions exists for almost any n-plex. A number of geometrically different but equally valid cylinders produced with the same connectivity, nodes and members was calculated. There are actually $\phi(n)/2$ equivalent solutions for any n-plex. However, it is not clear *a priori* what the differences or properties are among all $\phi(n)/2$ equivalent configurations per n. There must be a difference other than geometry. This Chapter presents further analytical but also numerical studies that shed light into their differences.

The current Chapter provides insights into three different aspects of cylindrical tensegrity structures. Firstly, an analysis of their elastic strain energy is used to classify a number of equivalent configurations that are generated out of the same n-plex. It is shown that the strain energy attains its minimum at a state corresponding to convex cylinders, and show how this energy is related to mathematical concepts of rigidity. Secondly, it is shown how the analytical form-finding solution in terms of tension coefficients is non-unique. The typical assumption of having a reduced set of different tension coefficients is relaxed. In doing so, asymmetric cylinders are created in such a way that all tension coefficients are distinct from each other. Thirdly, the initial stiffness of these cylinders show that their single state of self-stress stiffens all internal mechanisms. A full example, the 30-plex, is presented to illustrate the concepts developed in this Chapter.

4.1 Introduction

In the previous Chapter $\phi(n)/2$ equivalent solutions of the form-finding procedure were shown for every n-plex. It is not clear a priori in which properties other than the geometric arrangement of their nodes, they differ. In order to investigate their differences, the elastic

potential energy of these equilibrium configurations is analysed. Global equilibrium is attained in the state of least energy. Therefore configurations with less potential energy are preferred to other local minima with higher value.

The analytical form-finding procedure, presented in the previous Chapter, introduced a typical but unnecessary simplification. A geometrical model was based on three different elements: horizontal cables, bracing cables and struts. Since the tension coefficient in bracing cables and struts are identical scalar quantities, the set of tension coefficients is reduced by symmetry to horizontal and vertical members.

Moreover, if equal-sized faces are requested, the tension coefficients of all horizontal members are unitary. It leaves only one unknown to be calculated. However, all these simplifications are not necessarily. Tensegrity cylinders can be calculated in such a way that all members have a different tension coefficient from each other. The inherent symmetry of the tension coefficients can be eliminated: no more parallel polygons, the equilibrium for a single node does not copy to all other nodes by symmetry, member lengths are no longer equal, &c.

Henceforth, the term "asymmetric" will refer to configurations having as many different tension coefficients as members, i.e. there are no discernible groups of tension coefficients. The cylinders lose their symmetry in the tension coefficients, geometry and lengths. The non-uniqueness of the analytical form-finding procedure for tensegrity cylinders is thus discussed by presenting examples of asymmetric configurations.

Other authors have shown that tensegrity cylinders have a single state of self-stress [185, 142, 191]. However little is known on whether or not asymmetric star-like cylinders have a state of self-stress at all or if their self-equilibrium is stable. An analysis of the initial stiffness allow us to to classify the equilibrium of cylinders. Finally, the relationship between initial stiffness and related mathematical concepts is briefly discussed. For example, what does a concept like "global rigidity" mean in engineering terms, and to what extent and how this concept relates to structural stability. The present analytical study contributes to fill this conceptual gap.

This Chapter is organised as follows. The calculation of the state of global equilibrium is shown in Section 4.2. Asymmetric configurations and their initial stiffnesses are discussed in Section 4.3 and 4.4, respectively. A full example, the 30-plex, is presented in Section 4.5. Finally, some conclusions of this work appear in Section 4.6.

4.2 Stability and global equilibrium

As previously shown in Section 3.4.2, there are $\phi(n)/2$ structurally identical solutions out of the same n-plex, and it is not clear whether or not their equilibrium is similar. To address this question, an elastic strain energy is assigned to each of these solutions. The energy is based on the pre-strain level in the members. This strain energy corresponds to the total elastic energy that is stored in the pre-stressed members of a tensegrity

cylinder. Assuming that all members, in all $\phi(n)/2$ equivalent solutions for the same n, are made of the same material and have the same cross sectional area: a comparison of their elastic strain energy allows to distinguish the structures on the ground of the principle of minimum strain energy, which is a particular case of the principle of least action. A derivation of the elastic strain energy follows.

Elastic strain energy

The elastic strain energy of a (cylindrical) tensegrity structure is calculated by describing its members as Hookean springs that store elastic energy upon experiencing a pre-strain ε. Let e_i, ε_i and a_i be the Young's modulus, the strain and the cross-sectional area of the i-th member, respectively. Then, if the stress and length of the i-th member are described as $\sigma_i = e_i\varepsilon_i$ and l_i, respectively, the strain energy per unit volume of a structure is given by:

$$U = \frac{1}{2}\sum_{i=1}^{4n}\sigma_i\varepsilon_i = \frac{1}{2}\sum_{i=1}^{4n}e_i\varepsilon_i^2 = \frac{1}{2}\sum_{i=1}^{4n}e_i(\frac{f_i}{e_i a_i})^2 = \frac{1}{2}\sum_{i=1}^{4n}\frac{f_i^2}{e_i a_i^2} = \frac{1}{2}\sum_{i=1}^{4n}\frac{l_i^2 q_i^2}{e_i a_i^2}. \tag{4.1}$$

Here, each sum is taken over all $4n$ members of any cylindrical tensegrity structure, and f_i is the axial force of the i-th member. If the elastic strain energy of two or more structures is compared, with the same Young's modulus and cross-sectional area per member, the strain energy Eq. (4.1) is just $U \propto \sum_{i=1}^{4n} l_i^2 q_i^2$. For clarity, the strain energy for a given n-plex at configuration j, with member lengths ($l^{n,j}$) and tension coefficients ($q^{n,j}$), is written as follows:

$$U^{n,j} \propto \underbrace{n(l_{c_1}^{n,j})^2 q_{c_1}^2 + n(l_{c_2}^{n,j})^2 q_{c_2}^2}_{\text{horizontal cables}} + \underbrace{n(l_b^{n,j})^2(q_b^{n,j})^2}_{\text{bracing cables}} + \underbrace{n(l_s^{n,j})^2(q_s^{n,j})^2}_{\text{struts}}. \tag{4.2}$$

Please recall that tension coefficients in horizontal cables, i.e. q_{c_1} and q_{c_2}, are not affected by the parameter j. The components of the analytical expression Eq. (4.2), involving squared tension coefficients and lengths for any n and j, are listed as follows:

$$\left.\begin{array}{lcl}
q_{c_1}^2 & = & 1 \\
q_{c_2}^2 & = & \frac{{r_1}^4}{{r_2}^4} \\
(q_b^{n,j})^2 = (q_s^{n,j})^2 & = & 4\,\frac{{r_1}^2}{{r_2}^2}\left(\sin\left(\frac{\pi\, j}{n}\right)\right)^2 \\
(l_{c_1}^{n,j})^2 & = & 4\,{r_1}^2\left(\sin\left(\frac{\pi\, j}{n}\right)\right)^2 \\
(l_{c_2}^{n,j})^2 & = & 4\,{r_2}^2\left(\sin\left(\frac{\pi\, j}{n}\right)\right)^2 \\
(l_s^{n,j})^2 & = & {r_1}^2 + {r_2}^2 + 2\,r_1 r_2\,\sin\left(\frac{\pi\, j}{n}\right) + h^2 \\
(l_b^{n,j})^2 & = & {r_1}^2 + {r_2}^2 - 2\,r_1 r_2\,\sin\left(\frac{\pi\, j}{n}\right) + h^2.
\end{array}\right\} \tag{4.3}$$

Then, for structurally identical tensegrities, i.e. all $\phi(n)/2$ possible configurations out of the same n-plex, the expression Eq. (4.2) with squared lengths and tension coefficients Eq. (4.3), is the elastic energy absorbed by the springs as a result of their deformation at configuration j. This strain energy is written as follows:

$$\begin{aligned} U^{n,j} &\propto -2\,n\tfrac{{r_1}^2}{{r_2}^2}\left(3\,{r_1}^2+3\,{r_2}^2+2\,h^2\right)\left(\cos\left(2\,\tfrac{\pi\,j}{n}\right)-1\right), \\ &\approx 4\pi^2 j^2\,\tfrac{{r_1}^2}{n{r_2}^2}\left(3\,{r_1}^2+3\,{r_2}^2+2\,h^2\right)+O\left(\tfrac{1}{n^2}\right). \end{aligned} \tag{4.4}$$

It can be seen from Eq. (4.4) that the strain energy $U^{n,j}$ decreases with the number n of nodes used to discretise each circular face. But the strain energy, and hence the work done by self-stressing the cylinder, increases with j for a given n. This result shows that the equilibrium state, and therefore $U^{n,j}$, is different for each of the $\phi(n)/2$ equivalent configurations of a tensegrity cylinder of order n: the larger the j the larger also the elastic strain energy that is stored in the deformed members of the cylinder. This can be seen in Fig. 3.5b, where the length $\overline{p_f p_c}$ or $\overline{p_f p_d}$ and thus the member stress increases monotonically within the range $1 \leq j < n/2$.

Minimum strain energy

Following either Castigliano's theorem of least work[1] or Rayleigh's principle, the configuration j for which the elastic strain energy, Eq. (4.4), assumes its least value is the true state of equilibrium. This is exactly the case for $j = 1$ in Eq. (4.4). That is, the state of minimal strain energy or ground state corresponds to convex cylinders, $j = 1$, for any n-plex.

That is, for a given n, the strain energy $U^{n,j}$ is monotonically increasing for $1 \leq j < n/2$: $U^{n,1} < U^{n,2} < \ldots < U^{n,n/2-1}$. This information can be of interest to algorithm designers because a number of solutions, exactly $\phi(n)/2 - 1$, are known to be non-global minima in closed-form. Thus, for any n-plex, the minimum of the strain energy is at configuration $j = 1$, i.e. convex polygonal faces. Figure 4.1 depicts the strain energy, Eq. (4.4), of a unitary 100-plex for all the $\phi(100)/2 = 20$ possible configurations.

The energy distribution, Fig. 4.1, shows for simplicity a cylinder with $r_1 = r_2 = 1$. After a quick calculation one could get,

$$U^{n,j} \propto -4\,n\left(3+h^2\right)\left(\cos\left(2\,\frac{\pi\,j}{n}\right)-1\right) \approx \frac{4\,(6+2\,h^2)\,\pi^2 j^2}{n}+O(\frac{1}{n^2}), \tag{4.5}$$

[1]The theorem, introduced in Castigliano's thesis [31] and later on in [32], was considered plagiarised [39, 45, 188, 30] from an earlier paper by Menabrea [133]. Professor Luigi Cremona, then president of the Accademia delle Scienze di Torino, ended the controversy by supporting his colleague Menabrea and declaring [188], basically, that Mr. Castigliano did a good work but Mr. Menabrea has the merit of enunciating a general principle. Actually, Menabrea and Cotterill [53] were around the same idea of least work, however, neither of them had a correct and rigorous proof of the theorem before Castigliano's publications. Finally, other authors, e.g. Bertrand and Jenkins cited by [37, 38, 39], made original but little known contributions prior Castigliano's thesis.

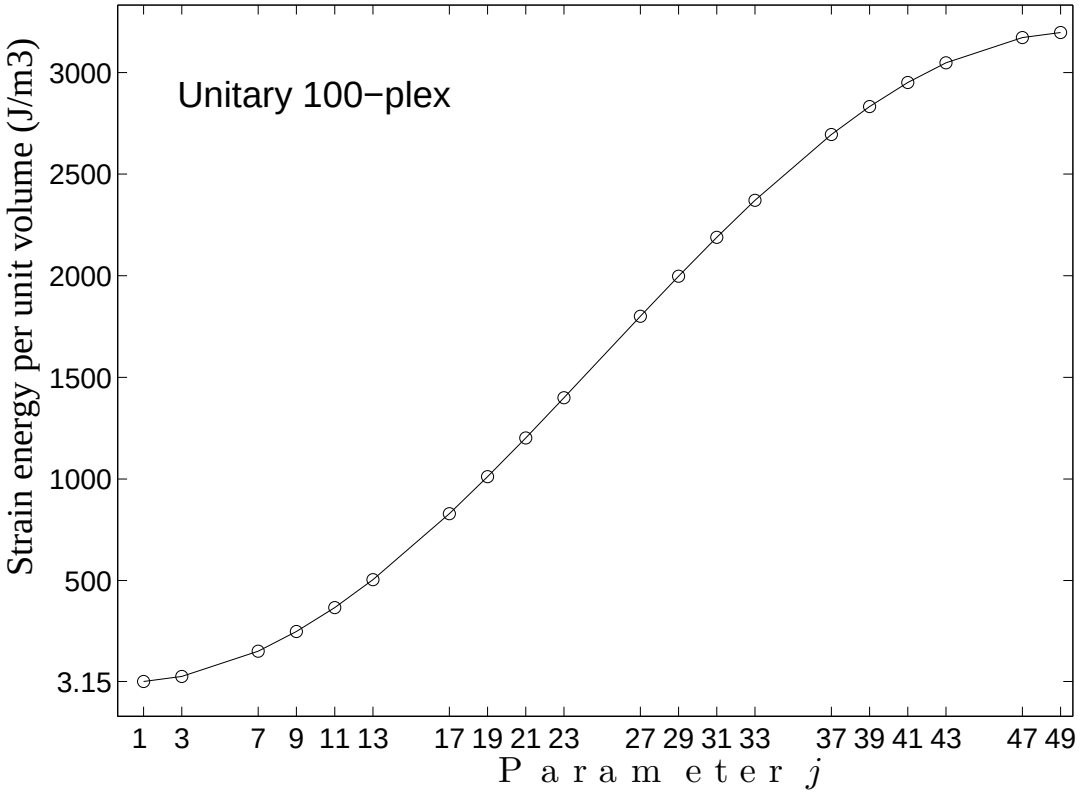

Fig. 4.1: Elastic strain energy : possible configurations j of a unitary 100-plex, i.e. $r_1 = r_2 = h = 1$. A minimum strain energy is attained at $j = 1$, which is the tensegrity cylinder with convex faces.

which shows the energy Eq. (4.5) proportional to j, for a fixed n and h. The shape of Fig. 4.1 is a half sine function insofar as all tension coefficients like $2\sin(\pi j/n)$ are evaluated within $1 \leq j < n/2$. The lower bound is thus $j = 1$ and upper bound is at configuration $j \to n/2$.

In summary, the energy is thus inversely proportional to the number of nodes used to discretise the cylinder, see e.g. Eq. (4.5). For a given n, the strain energy $U^{n,j}$ of all the $\phi(n)/2$ structurally identical tensegrities out of the same n-plex increases proportionally to j. The energy of a tensegrity cylinder of order n is thus minimised for $j = 1$, i.e. the convex cylinder.

4.3 Non-uniqueness of the analytical solution for tensegrity cylinders

A very relevant aspect of the form-finding of tensegrity cylinders, the non-uniqueness of the analytical solution, is discussed in this Section. It might be convenient to ask whether or not a unique set of tension coefficients is completely specified after fixing n, j, r_1 and r_2 in Eq. (3.5). Is it a solution, or *only* one possible solution for a tensegrity cylinder of order

n? Several solutions might exist by multiplying Eq. (3.5), but that is not a satisfactory answer. So, that is why the concept of "uniqueness" comes into play.

Uniqueness is, in turn, a very interesting question which is solely based on the geometrical model adopted in Eq. (3.1) and Fig. 3.5. A highly symmetric geometrical model was derived from which only two unknowns have to be determined: q_{c_2} for the horizontal cables, and $q = q_b = -q_s$ for the bracing cables and struts. The solution is indeed very symmetric in the tension coefficients and lengths.

In one hand, the tension coefficients are valid up to (non-zero) positive multiplicative constants. That is, all tension coefficients can be multiplied by a positive constant and reach the same self-equilibrium state. On the other hand, a fundamental assumption in the presented analytical form-finding procedure, however, is the distinction of three groups of tension coefficients in Eq. (3.5). These groups are:

1. cables in a circumferences of radius r_1 with q_{c_1};
2. cables in a circumference of radius r_2 with q_{c_2};
3. bracing cables and struts with $q = q_b = -q_s$.

In the following, the assumption of having a reduced number of different tension coefficients is revised.

4.3.1 How many different groups of tension coefficients?

One may wonder why only three and no more groups of tension coefficients were defined. The difficulty lies in the analytical model which is easily handled because it has few unknowns. The model is over simplified. This is of course not the only possible solution, but none the less one has to rely on numerical form-finding algorithms.

In geometrical terms, the number of different configurations and tension coefficients is infinite, but the number of states of self-stress does not change under affine or projective transformations [59, 186]. More importantly, the solution, in terms of tension coefficients, is not unique even after fixing a (non-zero) positive real constant. It is certainty possible to define more groups of tension coefficients other than q_{c_1}, q_{c_2}, q_b and q_s.

In an extreme case, asymmetric equilibrium configurations can be calculated in which the vector of tension coefficients, $\mathbf{t}$,

$$\mathbf{t} = [q_1\, q_2\, \ldots\, q_{4n}],$$

that self-equilibrate the tensegrity cylinder is has different entries for all $4n$ members,

$$\mathbf{t} = [q_1 \neq q_2 \neq \ldots \neq q_{4n}].$$

This is particularly important in the context of practical constructions of tensegrity structures. In such a case, the analytical solution might not be easily achieved in practice due to assembly and manufacturing inaccuracies. In a realistic scenario, none of the actual tension coefficients may match its analytical value. This immediately rises questions about the tolerance of those tension coefficients. The question is briefly discussed in the present Chapter.

A rough approximation of tolerance values can be obtained by calculating the tensegrity cylinders with asymmetric tension coefficients, where $q_1 \neq q_2 \neq \ldots \neq q_{4n}$. Thus, asymmetric tension coefficients are allowed in each member. A numerical form-finding procedure, developed earlier on [80] and discussed in full length in Chapter 5, was adapted to generate asymmetric tension coefficients.

In our calculations, the tension coefficients and lengths are indeed very different from the analytically calculated values in this and previous Chapter. It is known that self-stressed configurations are determined up to affine and projective transformations [59, 186]. Little is known, however, on how do tension coefficients vary. The comparison of the two sets of tension coefficients, symmetric and asymmetric, might give a clue of the confidence intervals and manufacturing tolerances relevant to the design of tensegrity structures. Next section shows a small example with the discrepancies between cylinders with symmetric and asymmetric tension coefficients.

4.3.2 Examples of asymmetric tensegrity cylinders

Two examples, a symmetric n-plex and its asymmetric counterpart are discussed here in more detail. In this example the unitary symmetric 3-plex, for simplicity, it is set $r_1 = r_2 = h = j = q_{c_1} = q_{c_2} = 1$. With these values Eq. (3.5) thus gives bracing cables with $q_b = 2\sin(\pi/3) = \sqrt{3}$ and struts with $q_s = -2\sin(\pi/3) = -\sqrt{3}$. This is the reference configuration that appears in the first column from the left of Table (4.1).

For clarity, the twelve tension coefficients, which appear as rows in Table (4.1), are grouped in three sections: six horizontal cables, three bracing cables and three struts. The symmetry introduced in the geometrical model for the analytical form-finding method of cylindrical tensegrity structures can be seen in the tension coefficients.

Certainly, only two groups are observed if the absolute value of tension coefficients is employed: horizontal cables with $q_{c_1} = q_{c_2} = 1$ and vertical members with $q_b = -q_s = \sqrt{3} = 1.73$, e.g. first column from the left of Table (4.1). Symmetry which is also reflected in member lengths, shown again in the first column from the left of Table (4.2). The height of this symmetric cylinder, as described in Section 2.7, is $h = \frac{\sqrt{3+3\sqrt{3}}}{3}$ and radii $r = \frac{\sqrt{3}}{3}$ for both r_1 and r_2. It gives a fully symmetric 3-plex with unitary cable lengths.

Three asymmetric cases can be generated with the form-finding procedure to be presented in the next Chapter. That procedure requires one "prototype" of member forces: either tension (+1) or compression (−1). A variation in these ±1 values generate asym-

	Ref.	Test1a	Test1b	Test1c	Test2a	Test2b	Test2c	Test3a	Test3b	Test3c
	1.0000	1.0000	1.0000	1.0000	1.0000	1.0000	1.0000	1.0000	1.0000	1.0000
top	1.0000	1.4216	0.7547	1.4308	1.2745	1.9010	0.9054	11.3882	3.0829	0.4849
and	1.0000	1.1376	0.8749	1.7781	0.7371	0.4554	0.1260	1.4055	1.9359	3.1765
bottom	1.0000	1.4325	0.7403	1.7150	0.8803	1.3378	1.3780	4.2455	4.2341	0.4273
cables	1.0000	1.0165	0.9548	1.5038	0.4402	0.5314	0.2263	0.7460	13.0897	2.3559
	1.0000	1.1110	0.9335	0.9839	0.5473	1.0757	1.5508	1.4234	1.7253	1.7646
	1.7321	2.2604	1.3937	3.1377	1.4658	1.1825	1.1515	5.0844	1.9912	2.2293
bracing	1.7321	1.7151	1.7093	2.1637	1.4561	1.9014	1.5449	1.5226	16.4382	1.1710
cables	1.7321	2.2232	1.4618	2.0766	1.1243	2.3348	1.3414	13.2279	4.7463	4.1729
	-1.7321	-2.0164	-1.5360	-2.5299	-1.4188	-1.5274	-1.3165	-3.4644	-3.7782	-2.0842
struts	-1.7321	-2.0044	-1.5506	-2.2139	-1.2675	-1.9609	-1.3593	-7.2391	-9.8029	-1.8760
	-1.7321	-2.1324	-1.4621	-2.5170	-1.3344	-1.7528	-1.3335	-4.0832	-4.1945	-2.7860

Table 4.1: Tension coefficients of 3-plexes found with random prototypes : the first column from the left shows the reference tension coefficients of a symmetric 3-plex calculated with Eq. (3.5) and $n = 3$. The first test with positive random values assigned to cables appears in columns Test1x; the second test, shown in columns Test2x, consists of negative random values assigned to struts; finally, columns Test3x show the third test which assigned positive random values to cables and negative random values to struts.

	Ref.	Test1a	Test1b	Test1c	Test2a	Test2b	Test2c	Test3a	Test3b	Test3c
	1.0000	1.0430	0.9657	1.0970	0.7824	1.0540	0.9934	1.3010	1.7020	1.1159
top	1.0000	0.9312	1.0510	0.9643	0.5955	0.7131	1.0218	0.5786	1.0696	1.4389
and	1.0000	1.0327	0.9862	0.9508	0.9319	1.1938	1.5861	1.0138	1.2278	0.4917
bottom	1.0000	0.9315	1.0521	0.9682	1.0547	0.7731	0.6304	0.7085	0.6303	1.4794
cables	1.0000	1.0371	0.9869	0.9454	1.3939	1.2269	1.1893	1.4555	0.5981	0.6094
	1.0000	1.0381	0.9640	1.0992	1.2523	1.0993	0.5902	1.3190	1.0528	1.0261
	1.0000	0.7002	0.7991	0.6265	0.7101	1.0432	0.8860	0.5405	1.3933	0.9019
bracing	1.0000	0.8572	0.6956	0.8037	0.6835	0.5993	0.6029	1.3583	0.4300	1.3812
cables	1.0000	0.7080	0.7719	0.8298	0.9654	0.6741	0.9547	0.4564	0.7346	0.3456
	2.1547	1.9328	1.8983	1.8544	1.9350	1.9546	1.9680	1.9933	1.4989	1.8263
struts	2.1547	1.9368	1.8805	1.9679	1.8494	1.8374	1.7873	1.9811	1.9471	1.7057
	2.1547	1.8434	1.9438	1.8715	1.8644	1.8147	1.7872	1.1984	1.9714	1.9087

Table 4.2: Member lengths of a 3-plex found with random prototypes : the first column from the left is the reference length of a symmetric 3-plex with unitary member lengths in cables and bracing cables. Columns Test1x, show the member lengths calculated by assigning positive random values to cables; the second test, Test2x, shows the member lengths calculated with negative random prototypes for struts; finally, columns Test3x show the member lengths of our third test which assigned positive random values to cables and negative random values to struts.

metric solutions for the tension coefficients that self-equilibrate a tensegrity structure. The three cases in which the prototypes can be initialised are as follows:

1. assign positive random numbers to prototype cables,
2. assign negative random numbers to prototype struts,
3. assign positive random numbers to prototype cables *and* negative random numbers to prototype struts.

Details of the numerical form-finding procedure are left for the next Chapter and are not necessary for the purposes of this Section. Figures 4.2a-c show one example of each

type of random prototypes. Three examples are shown in Table (4.1) for each of the three different ways to assign the random prototypes of member forces. The examples are denoted "Test1x" for prototypes with positive random numbers to cables, "Test2x" for prototypes with negative random numbers to struts, and "Test3x" for prototypes with positive random numbers to cables and negative random numbers to struts.

Actually, tension coefficients that appear under columns "Test1x" in Table (4.1) correspond to member lengths "Test1x", Table (4.2), and so on. All tension coefficients calculated with the numerical procedure appear normalised such that the first tension coefficient is 1. The normalisation makes both symmetric and asymmetric tension coefficients comparable to what was followed in Section 3.3.

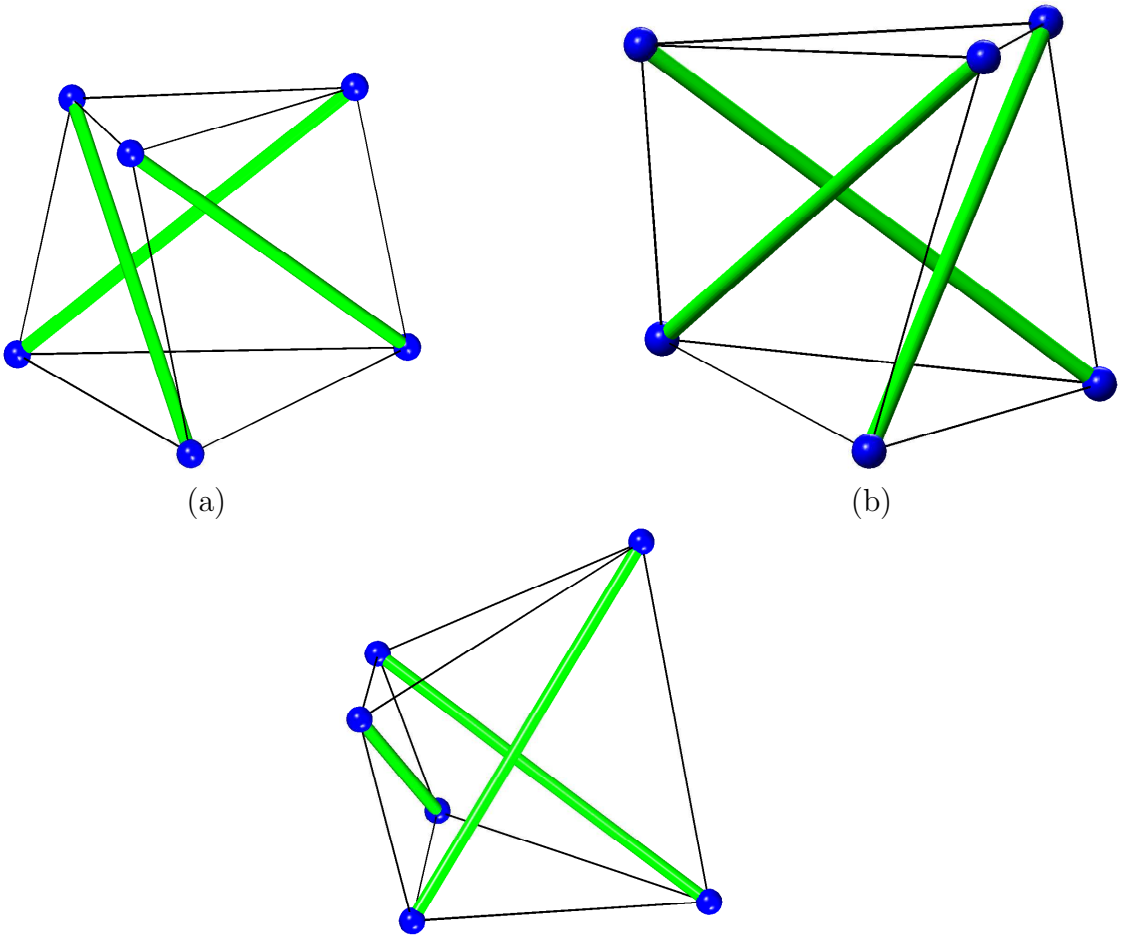

Fig. 4.2: Example of asymmetric tensegrity structures : (a) 3-plex calculated by assigning positive random numbers to cables; (b) 3-plex calculated by assigning negative random numbers to struts; (c) 3-plex calculated by assigning positive random numbers to cables *and* negative random numbers to struts.

Table (4.1) contrasts the large differences between each symmetric and asymmetric examples. For instance, the average value for tension coefficients q_{c_1} and q_{c_2} are 1.6971 (instead of 1.0), q_b has average value 3.0455 (instead of 1.73), and q_s is -2.6127 (instead

of -1.73); compare other columns to the reference configuration shown in the first column from the left of Table (4.1).

Similarly, member lengths in Table (4.2) are quite different to the reference 3-plex. It is shown that not only the tension coefficients are different but also the member lengths follow this asymmetric pattern. It is no longer possible to group tension coefficients or lengths into a few classes. The average member lengths are as follows: l_{c_1} and l_{c_2} are 1.0175 (instead of 1.0), l_b has average value 0.794 (instead of 1.0), and l_s is 1.85 (instead of 2.15). There is no attempt to calculate which test introduces the largest deviation from the reference tension coefficient or member lengths.

4.4 Initial stiffness

The number of independent states of self-stress is found to be $s = 1$, regardless of j or n. The number of inextensional modes of deformation (mechanisms) is $m = 2n + 1$. The number of states of self-stress and mechanisms are known, e.g. [185, 146, 145], for n-plexes with $j = 1$. Our study shows, however, that this result also holds for n-plexes with $j > 1$.

Here, the initial response of a structure in its pre-stressed geometry is calculated. The usual analysis of pre-stressed, kinematically indeterminate structures, see e.g. [93, 145, 197], is employed to verify the stability of these structures. This is a test in which the tangent stiffness matrix is subjected to inextensional displacements at zero external load, i.e. the initial stiffness of a free standing structure.

It is known that a vector of tension coefficients contributes to the tangent stiffness matrix,

$$\begin{array}{rcccc} \mathcal{K}_t & = & \mathcal{K}_e & + & \mathcal{K}_g, \\ & = & \mathcal{A}\mathcal{G}\mathcal{A}^T & + & (\mathcal{A}\mathcal{Q}\mathcal{A}^T + \mathcal{I}_3 \otimes \mathcal{D}), \end{array} \tag{4.6}$$

of pre-stressed, kinematically indeterminate structures, see e.g. [93, 145]. Here $\mathcal{A}$ is the equilibrium matrix, e.g. [159], as defined in Eq. (2.4), as

$$\mathcal{A} = \begin{pmatrix} \mathcal{C}^T \ \mathrm{diag}(\mathcal{C}\mathbf{x}) \\ \mathcal{C}^T \ \mathrm{diag}(\mathcal{C}\mathbf{y}) \\ \mathcal{C}^T \ \mathrm{diag}(\mathcal{C}\mathbf{z}) \end{pmatrix},$$

calculated with the Cartesian coordinates in the x-, y-, and z-axis, of the pin-jointed structure; incidence matrix $\mathcal{C} \in \Re^{4n \times n}$; force density matrix $\mathcal{D} = \mathcal{C}^T \mathcal{Q} \mathcal{C}$, in which $\mathcal{Q}$ is the $(4n \times 4n)$ diagonal matrix of tension coefficients; $\mathcal{G}$ is the $(4n \times 4n)$ matrix of axial stiffnesses, $\mathcal{I}$ is the 3x3 identity matrix; and $(\star)^T$ denotes the transpose operation. The matrix $\mathcal{D}$ is called stress matrix in mathematics, e.g. [47, 48].

4.4.1 Sign test

A free standing tensegrity cylinder has an initial state of equilibrium in which it is subject to inextensional mechanisms of deformation, $\mathcal{M} = [\mathbf{d}_1\, \mathbf{d}_2\, \ldots\, \mathbf{d}_{2n+1}]$; here vectors of mechanisms, $\mathbf{d} \in \Re^{3n}$, can be calculated, e.g. [159] or Eq. (2.9), from the left null space of $\mathcal{A}$ using a singular value decomposition. The stability of this initial state, or initial stiffness of a structure, only involves a section of the geometric stiffness, e.g. [145, 93, 197], i.e. two terms in Eq. (4.6) vanish with mechanisms: $\mathcal{A}^T\mathbf{d} = \mathbf{0}$. Therefore, infinitesimal mechanisms applied to Eq. (4.6) reduce the tangent stiffness matrix to $\mathcal{I}_3 \otimes \mathcal{D}$.

The reduced tangent stiffness matrix can be used to check whether or not a structure has stiffness against its inextensional modes of deformation at once, as opposed to calculate $\mathcal{K}_t\mathbf{d} = \mathbf{f} = \mathbf{0}$, [22, 93]. So, it is possible to write

$$\Lambda = \mathcal{M}^T(\mathcal{I}_3 \otimes \mathcal{D})\mathcal{M},$$

as quadratic form of $\mathcal{M}$ and the main part of the geometric stiffness matrix, $\mathcal{I}_3 \otimes \mathcal{D}$. The quadratic form Λ, i.e. linearised work [22], is positive semi-definite if and only if $\mathcal{D}$ is also positive semi-definite.

Interestingly, it is found $2(j-1)$ negative eigenvalues in the force density matrix $\mathcal{D}$, for any n-plex with parameter j. If $\mathcal{D}$ is positive, it has to be verified whether or not its state of self-stress imparts positive stiffness to the $2n-5$ internal mechanisms of a given n-plex. If it does, the eigenvalues of Λ should indicate that only six directions have no stiffness,

$$\begin{aligned} \text{eig}(\Lambda) &= eig(\mathcal{M}^T(\mathbf{I}_3 \otimes \mathcal{D})\mathcal{M}) \\ &= [\underbrace{\lambda_1 = \lambda_2 = \ldots \lambda_6 = 0}_{\text{rigid body motions}} \quad \underbrace{\lambda_7 > 0 \ldots \lambda_{2n+1} > 0}_{\text{positive stiffness}}], \end{aligned} \tag{4.7}$$

insofar as they are mechanisms corresponding to rigid body motions that appear in the analysis of free standing structures in three dimensions. There are not constrained degrees of freedom in our analysis, that is why six rigid body motions should appear in Eq. (4.7). There should not be any negative eigenvalue in the signed test Eq. (4.7). All other $2n-5$ infinitesimal mechanisms are stiffened by the state of self-stress for $j = 1$. The signed test Eq. (4.7) shows a number of negative eigenvalues when $j > 1$. In summary, the geometric stiffness matrix, of any n-plex with $j = 1$, is positive semi-definite and its single state of self-stress stiffens all inextensional mechanisms. The convex cylinders are therefore mechanically stable structures.

It is also possible to stack g cylinders on the top of each other so as to create g-stage masts. Here, the number of states of self-stress and mechanisms are $\mathtt{s} = g$ and $m = g + 2(n-3)$, respectively. In this g-stage masts the struts of one module are pin-jointed to the ones of the next stage. It is a well-known fact, i.e. needle tower by K. Snelson, that by modifying the connectivity and allow only discontinuous struts, a single state of self-stress for an arbitrary number of stages can be calculated, e.g. the analysis in [146].

4.4.2 Initial stiffness of asymmetric and star-like cylinders

Asymmetric cylinders generated with $j = 1$ have one state of self-stress, $s = 1$, and are mechanically stable. Conversely, the star-like cylinders, symmetric or asymmetric with $j > 1$ were found associated to configurations which are not mechanically stable. For instance, the 5-plex composed of star polygons (Fig. 3.3b) has a state of self-stress but its momentary equilibrium configuration is unstable.

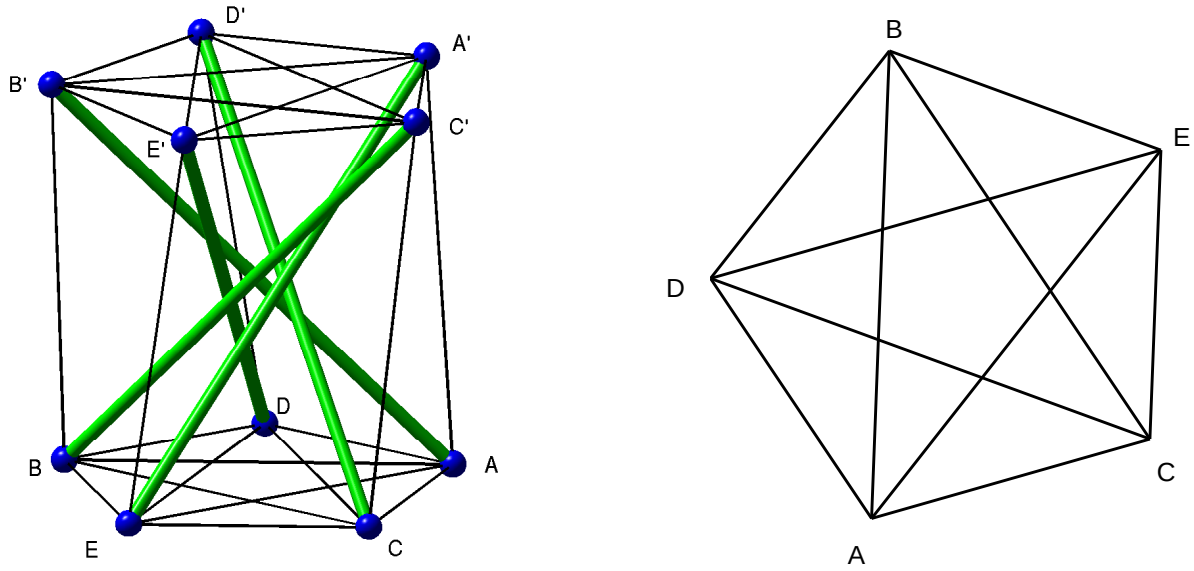

(a) (b)

Fig. 4.3: Extra tensile elements in a star-like cylinder : (a) a 5-plex with five extra cables in each star polygon; (b) five extra connections join the arms of this star.

Although star-like cylinders were unstable, they could be the starting configuration to more complex designs, e.g. Fig. 4.3, Fig. 4.4d, or Fig. 4.4f. Their negative eigenvalues are removed from the force density matrix by adding a few horizontal cables. An extreme case is found by joining all arms of the the star polygons, in both circular faces, e.g. Fig. 4.3a-b.

However, by adding only two horizontal cables to the 5-plex in one circular face, i.e. by connecting $\overline{AC}$ and $\overline{AD}$ in Fig. 3.3d, the resulting star-like cylinder is stable. This is shown Fig. 4.4c-d, it has $\mathtt{s} = 1$. Other connectivities can be tried, for instance Figures 4.4e-f show the 5-plex with five extra cables connecting the star polygon of one circular face.

Struts in any of the abovementioned examples remain discontinuous and produce conceptually valid tensegrity structures. Table (4.3) shows the tension coefficients of a star-like cylinder, the 5-plex with $j = 2$, as well as two other configurations that stabilise the structure. The form-finding is done with a numerical procedure, shown in the next Chapter. The negative eigenvalues in $\mathcal{D}$ are removed from the 5-plex with $j = 2$ by adding (i) two horizontal cables or (ii) more cables (e.g. five) in one circular face, see the last two columns of Table (4.3). The 5-plex with five extra cables in one circular face has $\mathtt{s} = 4$, and the linear combination of the states of self-stress allows a correct combination

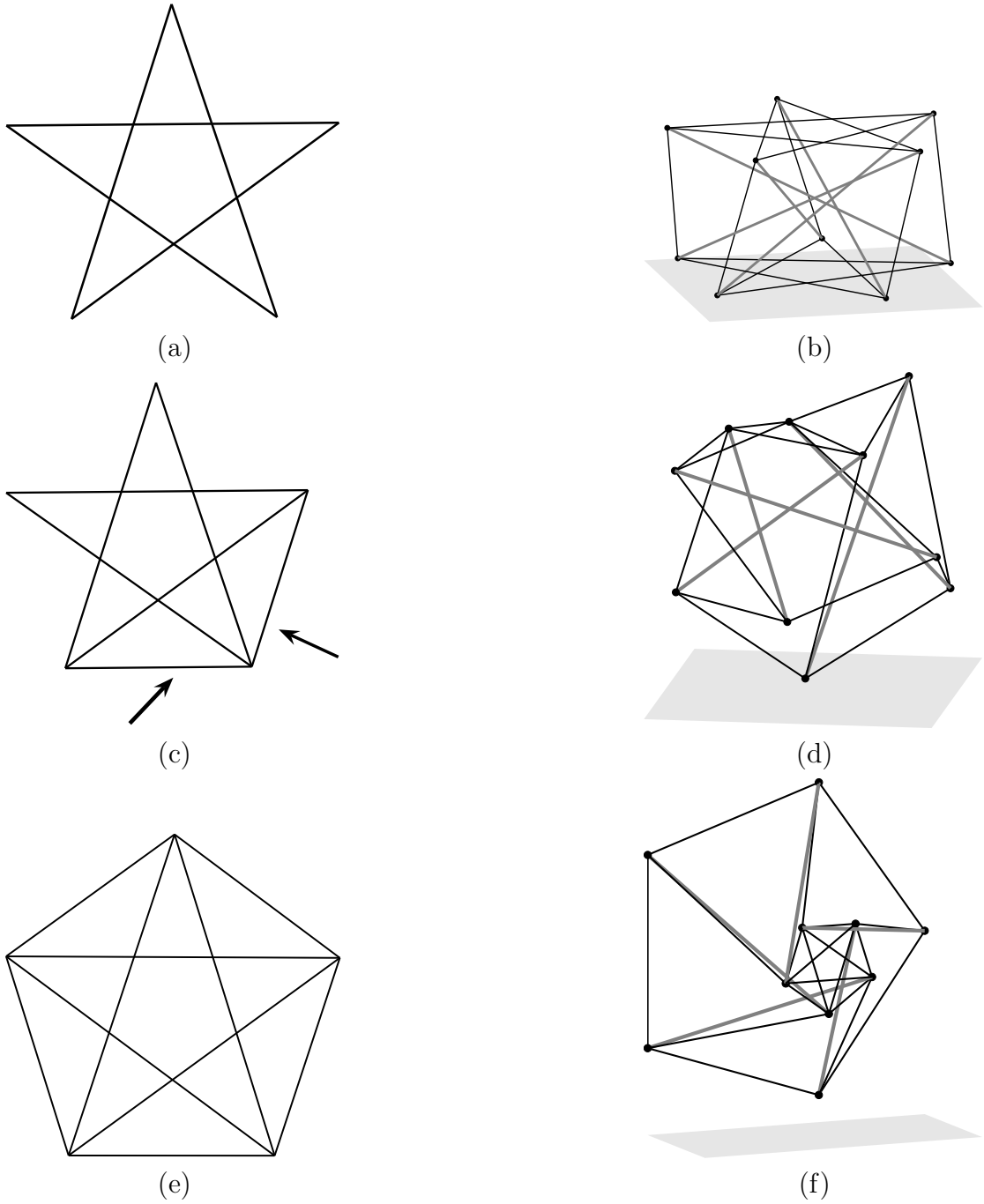

Fig. 4.4: Stabilisation of star-like cylinders : (a) both faces with $j = 2$; (b) unstable 5-plex; (c) one face with two extra cables; (d) stable cylinder; (e) one face with five extra cables joining all arms of the star polygon; (f) stable cylinder.

of tension and compression in the members that match our initial design: the five extra members are set in tension.

members	5-plex	5-plex + 2 cables	5-plex + 5 cables
	1.0000	1.0000	1.0000
	1.0000	0.6532	1.0000
horizontal	1.0000	0.6842	1.0000
cables, r_1	1.0000	0.6080	1.0000
	1.0000	0.8774	1.0000
	1.0000	0.2925	0.3019
	1.0000	0.7308	0.3019
horizontal	1.0000	0.4148	0.3019
cables, r_2	1.0000	0.4735	0.3019
	1.0000	0.6758	0.3019
	1.9021	0.9752	1.1975
	1.9021	1.0045	1.1975
bracing	1.9021	0.9413	1.1975
cables	1.9021	1.0210	1.1975
	1.9021	0.9732	1.1975
	-1.9021	-0.9442	-1.1975
	-1.9021	-1.0269	-1.1975
struts	-1.9021	-0.8712	-1.1975
	-1.9021	-1.0554	-1.1975
	-1.9021	-0.9216	-1.1975
		0.6434	0.9308
extra		0.9602	0.9308
horizontal			0.9308
cables, r_1			0.9308
			0.9308

Table 4.3: Tension coefficients of one extended 5-plex with $j = 2$: It is shown here the tension coefficients of one 5-plex with $j = 2$, as well as the result of adding two or five horizontal cables to one circular face. The negative eigenvalues in the matrix $\mathcal{D}$, created for star-like 5-plex with $j = 2$, can be removed by adding a couple of horizontal cables. The resulting structure is a conceptually valid tensegrity structure, with a continuous network of tension and discontinuous elements in compression.

4.4.3 Rigidity

Interestingly, other authors [51] found tensegrity cylinders with $j = 1$ to be "special", so called "globally rigid", and this concept is related to global strain energy minima. Authors in [51] proved the positive semi-definitiveness of a force density matrix $\mathcal{D}$ of maximal rank for configurations with $j = 1$. All cylinders, for any n and all valid j, see Eq. (3.5), fulfil the mentioned maximal rank condition. Therefore, the "globally rigid" only refers to the positive semi-definitiveness of $\mathcal{D}$, for a given n and $j = 1$. Positive semi-definiteness of quadratic forms like $\mathcal{D}$ is equivalent to positiveness of the eigenvalues of Λ not associated

to rigid body motions, see Eq. (4.7). In fact, all these eigenvalues,

$$\lambda_7 > 0 \ldots \lambda_{2n+1} > 0,$$

are positive, i.e. the function has a minimum for $j = 1$. The global minima is attained when all eigenvalues associated to non-trivial mechanisms are positive ($j = 1$), otherwise the configuration ($j > 1$) is a stationary point but not an extremum. Thus, "globally rigid" seems to be a consequence of the principle of minimum strain energy.

Moreover, Eq. (4.7) provides the link to other concepts in the hierarchy of mathematical rigidity, namely "pre-stress stable" and "second-order rigidity" [52]. It turns out that "pre-stress stable" is equivalent to the following sign test in the quadratic form the tangent stiffness matrix: $\mathcal{M}^T\mathcal{K}_t\mathcal{M} > 0$, for all non-trivial infinitesimal mechanisms; and $\mathcal{M}^T\mathcal{K}_t\mathcal{M} = 0$, for the rigid body motions. Further, the term "second-order rigidity" is equivalent to Eq. (4.7): $\mathcal{M}^T(\mathcal{I}_3 \otimes \mathcal{D})\mathcal{M} > 0$, for every non-trivial infinitesimal mechanism. In this case, concepts "pre-stress stable" and "second-order rigidity", have equivalent sign tests since the material stiffness matrix vanishes for infinitesimal mechanisms. Therefore it comes to no surprise [52] that if a tensegrity is "pre-stress stable" then it is said to be "second-order rigid" as well.

However, the simplicity of Eq. (4.7) has the additional advantage that identifies the six rigid body motions,

$$\lambda_1 = \lambda_2 = \ldots \lambda_6 = 0,$$

from the left null space of the equilibrium matrix $\mathcal{A}$. Therefore a sign and maximal rank condition on $\mathcal{D}$ are superseded in this context by a more clear definition in terms of initial stiffness. In engineering terms, a positive semi-definite force density matrix and sign test Eq. (4.7) check whether or not a structure has positive stiffness in its self-equilibrium state.

Since the maximum and minimum of a quadratic form can be expressed in terms of eigenvalues, it can be concluded that all star-like cylinders, with $j > 1$ and thus with mixed signs among their eigenvalues, are not extremal values but saddle points in the quadratic function.

4.5 A full example: the 30-plex

It is shown an example of the formalism developed in this Chapter. The cylinder to be calculated is the 30-plex. The best way to understand the equations is by presenting a full example.

The 30-plex has $n = 30$ nodes in each circular face and $4 * 30 = 120$ members. It is set $r_1 = 1$, $r_2 = 2$ and $h = 3$ for all the $\phi(30)/2 = 4$ possible solutions. The structurally identical configurations are found to be $j = \{1, 7, 11, 13\}$, e.g. using Eq. (3.5). All other values of j produce disconnected cylinders.

Figures 4.5a-d show the four equivalent solutions for a 30-plex. The noticeable difference is the way tensile members are arranged on the circular faces. The struts, shown in thick gray lines, do not touch or intersect. However, if n is sufficiently large all struts will collide in the cylinder's centre. The theoretical limit is when $j \to n/2$ but struts may hit each other for much smaller j. The graphical model from which Eq. (3.5) was derived did not consider cross-sectional areas of struts. So, there is no hint about a maximum strut thickness allowed in cylinders.

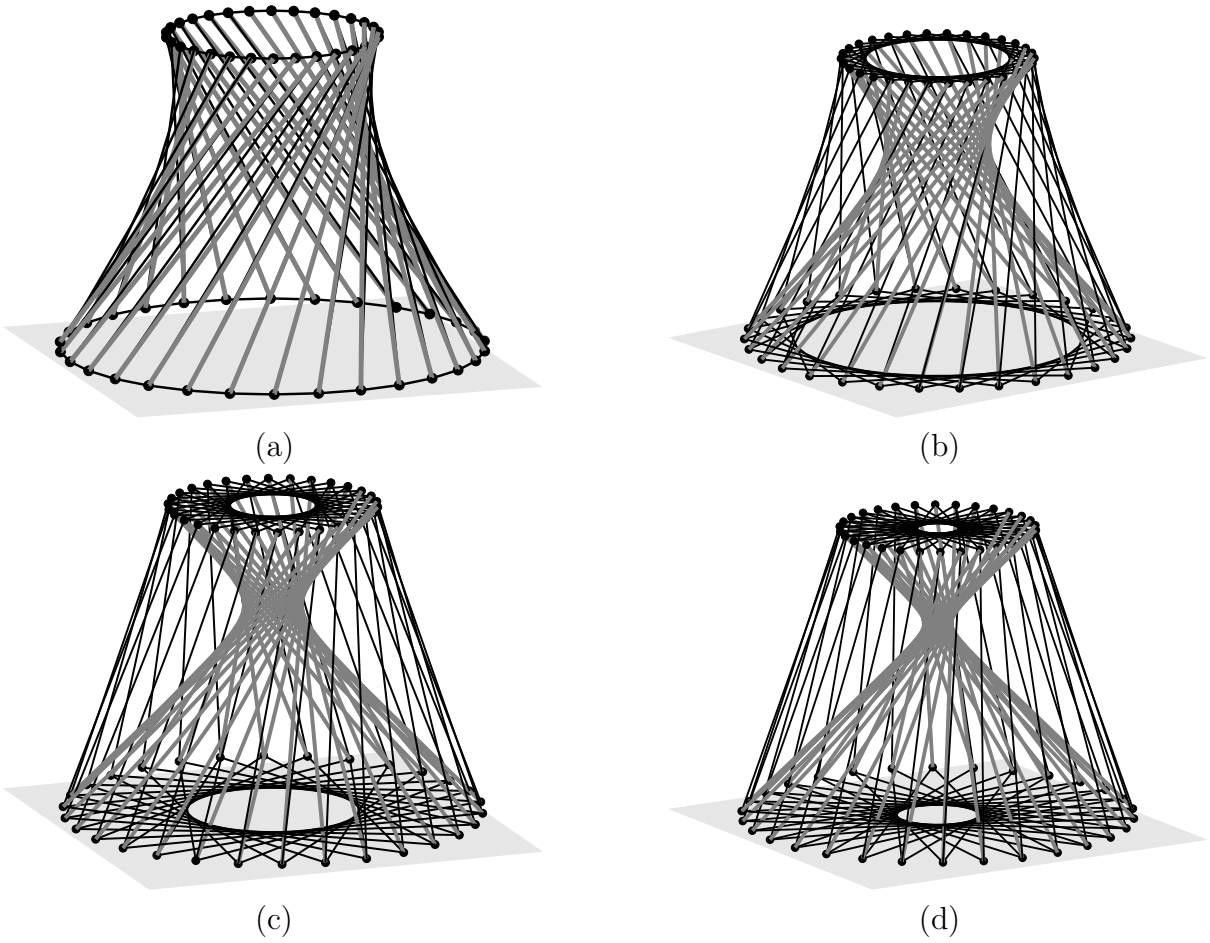

Fig. 4.5: Four possible solutions for a 30-plex : (a) j=1; (b) j=7; (c) j=11; (d) j=13.

Table (4.4) shows analytical solutions of tension coefficients, calculated with Eq. (3.5), for a 30-plex. Tension coefficients are represented as follows: horizontal cables are q_{c_1} and q_{c_2}, bracing cables are $q_b^{30,j}$ and struts are $q_s^{30,j}$. Here j can take values {1,7,11,13}.

Member lengths can be calculated from Eq. (3.1). Table (4.5) shows member lengths of a 30-plex organised in: horizontal cables ($l_{c_1}^{30,j}$) and ($l_{c_2}^{30,j}$), bracing cables ($l_b^{30,j}$) and struts ($l_s^{30,j}$).

A tension coefficient is defined as a member force divided by its length. Therefore, member forces are directly calculated from Table (4.4) and Table (4.5). The member forces for a 30-plex are shown in Table (4.6): $f_{c_1}^{30,j}$ and $f_{c_2}^{30,j}$ for horizontal cables, $f_b^{30,j}$ for bracing cables, and $f_s^{30,j}$ for struts.

$j=1$	$j=7$	$j=11$	$j=13$
$q_{c_1}=1$	$q_{c_1}=1$	$q_{c_1}=1$	$q_{c_1}=1$
$q_{c_2}=1/4$	$q_{c_2}=1/4$	$q_{c_2}=1/4$	$q_{c_2}=1/4$
$q_b^{30,1}=\sin(1/30\,\pi)$	$q_b^{30,7}=\sin\left(\frac{7}{30}\,\pi\right)$	$q_b^{30,11}=\sin\left(\frac{11}{30}\,\pi\right)$	$q_b^{30,13}=\sin\left(\frac{13}{30}\,\pi\right)$
$q_s^{30,1}=-\sin(1/30\,\pi)$	$q_s^{30,7}=-\sin\left(\frac{7}{30}\,\pi\right)$	$q_s^{30,11}=-\sin\left(\frac{11}{30}\,\pi\right)$	$q_s^{30,13}=-\sin\left(\frac{13}{30}\,\pi\right)$

Table 4.4: Example of tension coefficients : four configuration of a 30-plex.

$j=1$	$j=7$	$j=11$	$j=13$
$l_{c_1}^{30,1}=0.2090$	$l_{c_1}^{30,7}=1.3382$	$l_{c_1}^{30,11}=1.8270$	$l_{c_1}^{30,13}=1.9562$
$l_{c_2}^{30,1}=0.4181$	$l_{c_2}^{30,7}=2.6765$	$l_{c_2}^{30,11}=3.6541$	$l_{c_2}^{30,13}=3.9125$
$l_b^{30,1}=3.6853$	$l_b^{30,7}=3.3650$	$l_b^{30,11}=3.2164$	$l_b^{30,13}=3.1760$
$l_s^{30,1}=3.7971$	$l_s^{30,7}=4.0836$	$l_s^{30,11}=4.2016$	$l_s^{30,13}=4.2323$

Table 4.5: Example of lengths : a 30-plex

$j=1$	$j=7$	$j=11$	$j=13$
$f_{c_1}^{30,1}=0.2090$	$f_{c_1}^{30,7}=1.3382$	$f_{c_1}^{30,11}=1.8270$	$f_{c_1}^{30,13}=1.9562$
$f_{c_2}^{30,1}=0.1045$	$f_{c_2}^{30,7}=0.66913$	$f_{c_2}^{30,11}=0.9135$	$f_{c_2}^{30,13}=0.9781$
$f_b^{30,1}=0.3852$	$f_b^{30,7}=2.2516$	$f_b^{30,11}=2.9384$	$f_b^{30,13}=3.1066$
$f_s^{30,1}=-0.3969$	$f_s^{30,7}=-2.7325$	$f_s^{30,11}=-3.8384$	$f_s^{30,13}=-4.1398$

Table 4.6: Example of forces : the 30-plex

Finally, the elastic strain energy corresponding to our four configurations arising from the same 30-plex is easily calculated with Eq. (4.4). The values of this energy are as follows:

$$\begin{aligned} U^{30,1} &= 10.8169 \\ U^{30,7} &= 443.2584 \\ U^{30,11} &= 826.2196 \\ U^{30,13} &= 947.2050 \end{aligned}$$

It is seen that configuration $j=1$ corresponds to the minimum strain energy. In fact,

the strain energy is best described with the parameter j, from which it is observed: $U^{30,1} < U^{30,7} < U^{30,11} < U^{30,13}$. This behaviour was previously described and exemplified with a 100-plex, Fig. 4.1, but holds for any n-plex.

Table (4.7) shows how the force density matrix with $j = 1$ has zero negative eigenvalues. It has a maximal rank condition in 3D, i.e. nullity four. The quadratic form $\mathcal{D}$ has a minimum when $j = 1$, and all other configurations are not extremal values. These mixture of eigenvalues, for $j > 1$, affects the reduced form of the stiffness matrix Λ, see Eq. (4.7). Only the configuration $j = 1$ stiffens all inextensional mechanisms, except for six rigid-body motions.

matrix	eigenvalues	$j = 1$	$j = 7$	$j = 11$	$j = 13$
$\mathcal{D}$	$\lambda < 0$	$\boxed{0}$	12	20	24
	$\lambda = 0$	4	4	4	4
	$\lambda > 0$	56	44	36	32
Λ	$\lambda < 0$	$\boxed{0}$	14	24	26
	$\lambda = 0$	6	6	6	6
	$\lambda > 0$	55	41	31	29

Table 4.7: Eigenvalues and initial stiffness : number of positive, zero and negative eigenvalues in the force density matrix and reduced stiffness matrix. Small boxes highlight the configuration $j = 1$ which has zero negative eigenvalues in both $\mathcal{D}$ and sign test Λ, see Eq. (4.7).

Finally, it was described that star polygons have $n(j-1)$ self-crossings in the horizontal planes, but little was said about the space inside a cylinder. The previous Chapter did not include a "top view" of the cylinders in which their incircle is seen. This is shown in Fig. 4.6. Obviously, the inradius decreases monotonically as a function of j. The Fig. 4.6 shows a top view of the four possible configurations of the 30-plex and $r_1 = r_2$ was selected as to maximise the view inside those cylinder. Struts in the first configurations, e.g. up to $j = 7$ or $j = 11$, seem not touching each other. However, every single step from $j = 1$ to $j \to n/2$ narrows the gap between any two struts, till eventually they struts intersect each other.

4.6 Conclusions and final remarks

An analysis of the stability and non-uniqueness of the analytical form-finding solution for tensegrity cylinders is presented. Our analysis is based on tension coefficients. The following four issues were discussed:

Firstly, structurally equivalent configurations were compared by means of their elastic strain energy. This energy was analytically derived. An energetic argument was used to classify the tensegrity cylinders into groups according to their global minima. In fact,

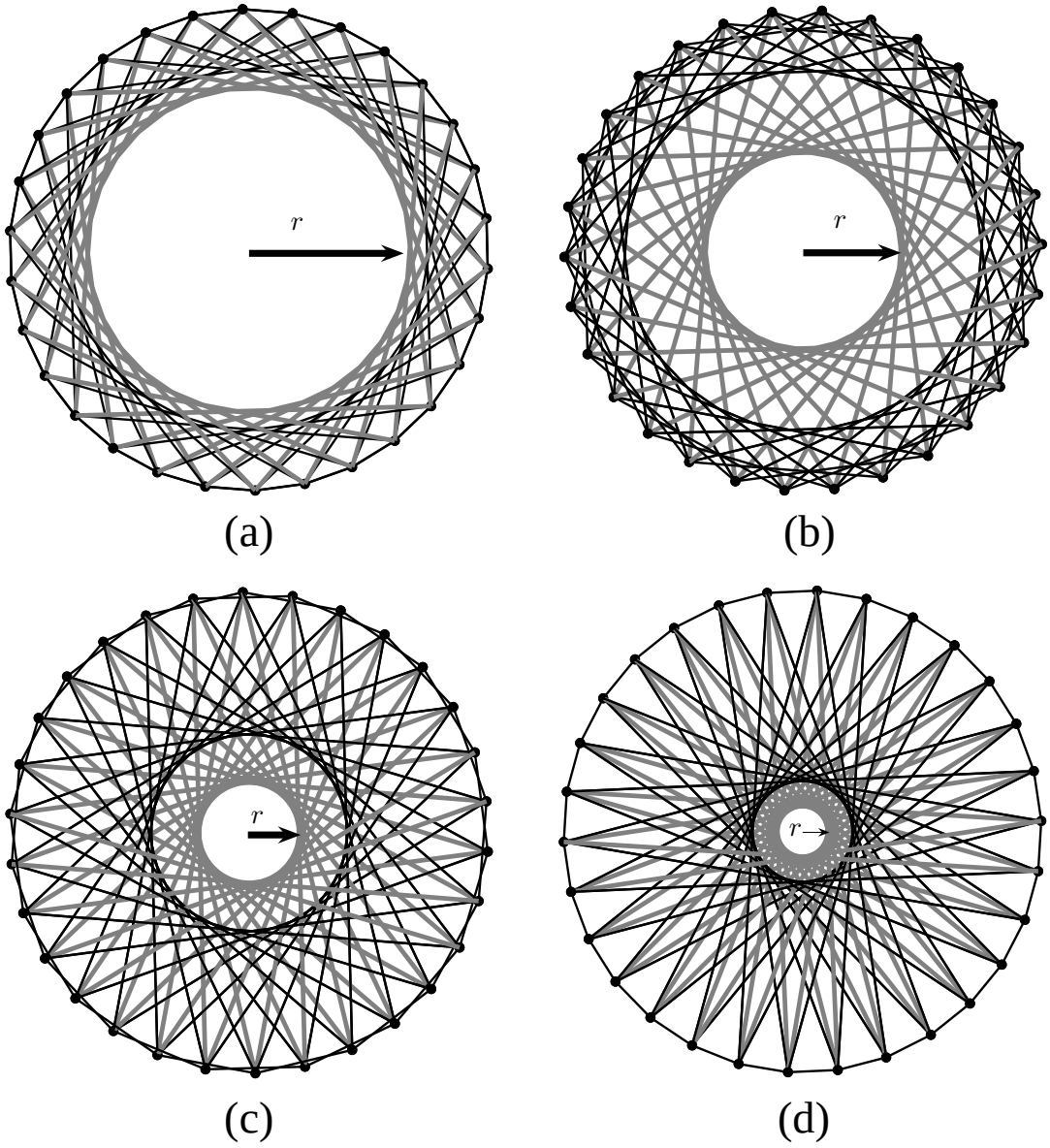

Fig. 4.6: Influence of j to the incircle of a 30-plex : top view of a 30-plex with (a) $j = 1$; (b) $j = 7$; (c) $j = 11$; (d) $j = 13$. The parameters $r_1 = r_2 = h = 1$ are selected in all cases.

the geometrical change of equivalent configurations, i.e. $1 \leq j < n/2$, was related to their strain energy. Actually, it follows from their elastic strain energy that the global equilibrium configuration is the cylinder with convex polygons, i.e. the energy function attains its minimum at $j = 1$, for any n-plex.

Secondly, even though all $\phi(n)/2$ equivalent configurations have one state of self-stress for any n and j, the stability of this state of self-stress depends of j. There are $2(j-1)$ negative eigenvalues in the force density matrix. Further analyses of the stiffness matrix confirmed that configurations with $j = 1$ are indeed in a minimum energetic state. Moreover, this result is closely related to the concept of global rigidity [51], which in our context is basically the application of the principle of least action or Castigliano's theorem

of least work: the strain energy $U^{n,j}$ takes its least value in the ground state $j = 1$, for any n-plex.

Other configurations with $j > 1$, which all satisfy the equilibrium equations, would require additional force or constraints in their degrees of freedom to maintain their momentary equilibrium. That is why the quadratic form has a stationary point but not an extremum, i.e. it has positive and negative eigenvalues for $j > 1$. Therefore, the mathematical concept of global rigidity, in the context of tensegrity cylinders, can be directly related to the mechanical concept of stable equilibrium: favour a configuration that brings the elastic strain energy at its least value. Closing the gap between mathematical rigidity, e.g. [47, 48, 91], and mechanical stability is an interesting research direction for future work.

Thirdly, while the cylinders with $j = 1$ are mechanically stable, the other structures ($j > 1$) should not be immediately discarded. Unstable tensegrity cylinders can be stabilised by adding cables or elastic membranes [168] to produce conceptually valid tensegrity cylinders. An interesting research direction is the stabilisation of tensegrity cylinders by a low pressurised fluid, like in Tensairity© [125]. This pressure-induced stability might produce interesting, light and deployable pneumatic tensegrity structures.

Examples of asymmetric tensegrity cylinders were presented in which all tension coefficients were allowed to take a different value. It is shown that the analytic solution based on reduced number of different tension coefficients is not unique. However, the corresponding asymmetric structures with $j = 1$ were also mechanically stable. The analysis of asymmetric tension coefficients helps to understand the capabilities and limitations of the form-finding procedure developed in the previous Chapter. Moreover, the difference between symmetric and asymmetric tension coefficients might give confidence intervals to cope with assembly and manufacturing inaccuracies. The form-finding process of asymmetric tensegrities and the analysis of their confidence intervals is also an interesting direction for future work.

Finally, as a historical note, the lengths and squared lengths of polygons and star polygons were studied as early as the 17th century by Kepler, e.g. cited in [169, 192]. It is said Kepler observed that the sides of a heptagon of unit circumradius are the positive real roots of:

$$x^6 - 7x^4 + 14x^2 - 7 = 0,$$

which in turn are: 0.8677, 1.5636 and 1.9498. The same roots or lengths can be obtained in closed-form with Eq. (3.5) and $n = 7$. It has $j = \{1, 2, 3\}$ and solutions: $2\sin(\pi/7) = 0.8677$, $2\sin(2\pi/7) = 1.5636$, and $2\sin(3\pi/7) = 1.9498$.

Likewise, the squared length of any side of the same heptagon are the roots of:

$$x^3 - 7x^2 + 14x - 7 = 0,$$

for the three possible configurations: $j = 1, 2, 3$. The three roots are: 0.7530, 2.4450, 3.8019; for $j = \{1, 2, 3\}$ respectively. Interestingly, these roots or squared lengths can also be calculated in closed-form with Eq. (4.3). Following the terminology of this dissertation,

the squared lengths of polygons and star polygons, l_{c_1} and l_{c_2} in Eq. (4.3), can be written

$$(l_r^{n,j})^2 = 4\,r^2\left(\sin\left(\frac{\pi\,j}{n}\right)\right)^2,$$

or

$$(l^{n,j})^2 = 4\,\left(\sin\left(\frac{\pi\,j}{n}\right)\right)^2,$$

for unitary circumradius, i.e. $r = 1$. Now, by applying $n = 7$ and $j = 1, 2, 3$ to this squared length, it follows that: $(l^{7,1})^2 = 4\sin(\pi/7)^2 = 0.7530$, $(l^{7,2})^2 = 4\sin(2\pi/7)^2 = 2.4450$, and $(l^{7,3})^2 = 4\sin(3\pi/7)^2 = 3.8019$. This is again the same result obtained by Kepler, but our procedure required no root extraction.

Chapter 5

Numerical form-finding of tensegrity structures

The two previous Chapters presented a detailed analysis of tensegrity cylinders. This class of highly symmetrical tensegrities allowed an analytical treatment. However, like any other analytical form-finding method it has its shortcomings. Analytical solutions for the form-finding of tensegrity structures, even in an approximate sense, are only possible for small symmetric systems, mostly restricted to few parameters like a single twisting angle or just a pair of critical tension coefficients. However, in general, analytical solutions do not extend to structures of multi-parametered forms, for instance with more than two groups of tension coefficients, as seen in the asymmetric solutions for cylindrical tensegrity structures.

A novel and versatile numerical form-finding procedure that alleviates many of these shortcomings is presented. It requires only a "minimal" knowledge of the structure, where "minimal" is defined as follows: the type of each member (i.e. either compression or tension) and the connectivity among the nodes to be known. Equilibrium geometry and force densities are iteratively calculated. The condition of maximal rank in the force density matrix and minimal member lengths were included in the form-finding procedure to guide the search to states of self-stress with minimal elastic potential energy. Since there are no assumptions upon cable lengths or cable-to-strut ratios, the numerical procedure is indeed able to calculate novel configurations. Notwithstanding the simplicity of the proposed approach, it compares favourably with all the leading techniques in the field. This is clearly exemplified through a series of examples.

5.1 Introduction

The analytical form-finding investigation presented in Chapter 3 required basically two critical tension coefficients: q_{c_2} for the second circular face and $q = q_b = -q_s$ for the bracing cables and struts. An analytical form-finding procedure is possible in so far the

cylindrical tensegrity structures were derived from a highly symmetrical model. More complex structures, i.e. asymmetric or spheres, can be computed however only through numerical procedures. There is no analytical treatment anymore in this Chapter. Symmetry is no longer part of the solution procedure. The formalism of tension coefficients is however employed here as well.

Other tensegrity structures beyond cylinders are more difficult to describe with one or two critical tension coefficients. A satisfactory form-finding of more complex tensegrities, for instance governed by assembly of tensegrity units, is far from current capabilities. Moreover, in spite of many advanced form-finding procedures the form-finding of aggregation of essentially known units is still extremely difficult. As explained in Chapter 2, most of the existing form-finding procedures compute a single critical parameter in an partially known structure. A form-finding procedure could typically compute a critical parameter such as (i) a twisting angle, (ii) a cable-to-strut ratio or (iii) a force-to-length ratio.

In most existing form-finding procedures assumptions on either the tension coefficients, the element lengths or the symmetry of the whole structure must be imposed *a priori*, see [142] or [191] for a survey. For instance, (i) few different types of tension coefficients are imposed in a symbolic analysis, (ii) element lengths have to be predefined in a dynamic relaxation procedure and non-linear programming, (iii) a global symmetry is assumed in a group-theory based form-finding procedure, and (iv) initial forces or force densities have to be arbitrarily initialised in numerical form-finding methods for tensegrity structures [204, 205].

Form-finding techniques have left a number of open questions because these data may not always be available or easy to estimate beforehand. The calculation of complex tensegrity structures therefore remains difficult. The general setting in form-finding should rely on minimal assumptions, because a design might not specify any member lengths, the number of different groups of lengths or tension coefficients.

The current Chapter presents a numerical form-finding procedure for statically indeterminate structures in self-equilibrium. A strategy of least assumptions was chosen and the procedure described here only requires: the type of each member (i.e. either compression or tension) and the connectivity (i.e. incidence matrix) between the nodes to be known. With this knowledge the proposed matrix algorithm approximates the self-equilibrium geometry and the tension coefficients. The procedure iteratively adjusts the tension coefficients and geometry until a state of self-stress is found.

This Chapter is organised as follows: The overall form-finding approach appears in Section 5.2, and it is based on the relevant definitions and rank conditions for tensegrity structures previously described in Sections 2.4 and 2.5. The core of our form-finding procedure is presented in Sections 5.3 and 5.4. Examples of two-dimensional (2D) and three-dimensional (3D) structures are presented in Section 5.5. A brief discussion about implementation details in Matlab is presented in Section 5.6, as well as the complexity and convergence of the algorithm in Section 5.7. The form-finding of the expanded octahedron is exemplified in Section 5.8. Finally, conclusions drawn from this Chapter appear in

Section 5.9.

5.2 Form-finding with prototypes

Contrary to most form-finding procedures, e.g. [142, 191] for a review, the numerical procedure shown here requires no initial assumptions about member lengths, geometry or symmetry of the structure. Instead, our procedure only requires to know the dimensions ($\mathtt{d}$) of the structure, the incidence matrix $\mathcal{C}$, and initial information about the type of each member. This information is contained in a vector $\mathbf{q}^0 \in \Re^b$ that is seen as a "prototype" of the tension coefficient for each member. Since the tension coefficient is defined as member force divided by its length, the signed prototypes like $+1$ and -1 can be seen as unitary compression and tensile components, respectively. That is, any entry in the vector $\mathbf{q}^0$ assigns the tension coefficient $+1$ or -1 to members that are chosen to be in tension or in compression, respectively:

$$\mathbf{q}^0 = [\underbrace{+1 \quad +1 \quad +1 \quad \ldots}_{\text{tension}} \quad \underbrace{-1 \quad -1 \quad -1 \quad \ldots}_{\text{compression}}]^T. \tag{5.1}$$

Subsequently, the matrix $\mathcal{D}$ is calculated from $\mathbf{q}^0$, i.e. $\mathcal{D} = \mathcal{C}^T \text{diag}(\mathbf{q}^0)\mathcal{C}$, and iteratively modified as to satisfy the rank conditions Eq. (2.7). In the course of these iterations, the numerical procedure tries to deviate as little as possible from the signs of the initial prototypes defined in Eq. (5.1).

An outline of the form-finding process is shown in Fig. 5.1. The incidence matrix ($\mathcal{C}$), the number of dimensions ($\mathtt{d}$) and a prototype of tension coefficients ($\mathbf{q}^0$) are initialised in Fig. 5.1a. At this stage, the vector of tension coefficients $\mathbf{q}^0$ need not produce a state of self-stress ($\mathtt{s} = 0$) in the structure.

Then, the nodal coordinates are approximated as a function of the tension coefficients (Fig. 5.1b); from these coordinates a new vector of tension coefficients is approximated (Fig. 5.1c). These two steps represent the core of the proposed form-finding procedure. They are repeated until a solution is found (Fig. 5.1d). At this point, at least one state of self-stress, $\mathtt{s} \geq 1$, is found and it is the end of our numerical procedure (Fig. 5.1e). The procedure shown in Fig. 5.1b and Fig. 5.1c will be described in detail in Sections 5.3.2 and 5.4.2, respectively.

Finally, a structure with $\mathtt{s} \geq 1$ must have tension coefficients such that $\mathcal{A}\mathbf{t} = \mathbf{0}$ and coordinates $\mathcal{D}[\mathbf{x}\,\mathbf{y}\,\mathbf{z}] = [\mathbf{0}\,\mathbf{0}\,\mathbf{0}]$. Implicitly, both rank conditions given in Eq. (2.6) and Eq. (2.7) are satisfied. If the calculated structure is in a stable self-equilibrium, see Section 4.4, one can say that a signed vector of tension coefficients $\mathbf{q}^0$ provided *enough* information to compute $[\mathbf{x}, \mathbf{y}, \mathbf{z}]$ and $\mathbf{t}$, a stable self-equilibrium state.

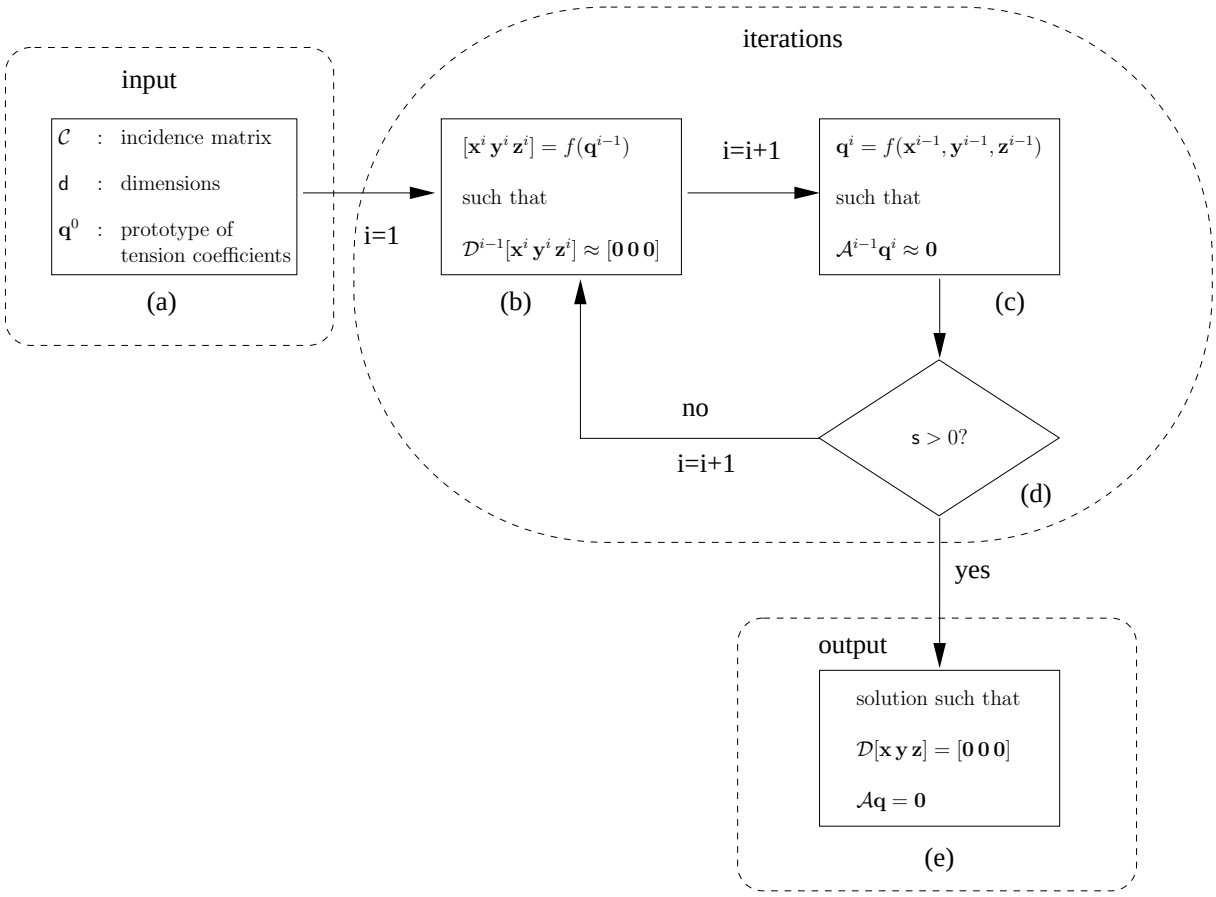

Fig. 5.1: Outline of the numerical form-finding procedure : (a) initialisation, no state of self-stress. Only a vector of prototypes of tension coefficients, the number of dimensions and the incidence matrix are required; (b) Approximated coordinates as a function of tension coefficients. Coordinates are calculated from the decomposition of a force density matrix with the current tension coefficients; (c) Approximated tension coefficients as a function of coordinates. Tension coefficients are calculated from the decomposition of an equilibrium matrix with the current coordinates; (d) The previous decomposition is used to test whether or not the structure has a state of self-stress; (e) Final coordinates and tension coefficients that create at least one state of self-stress.

5.3 From tension coefficients to coordinates

5.3.1 Equilibrium

Let $\mathbf{t}$ be a (non-zero) vector of tension coefficients and $\mathcal{C}$ be an incidence matrix for a $(\mathtt{d} = 3)$-dimensional tensegrity structure in a self-stressed state. The force density matrix is then given by $\mathcal{D} = \mathcal{C}^T \mathrm{diag}(\mathbf{t})\mathcal{C}$. If the matrix $\mathcal{D}$ is positive semi-definite of maximal rank [48], i.e. satisfies the rank condition Eq. (2.7) or equivalently it has a nullity $\mathtt{d}+1$, one can perform a Schur decomposition:

$$\mathcal{D} = \mathcal{C}^T\ \mathrm{diag}(\mathbf{t})\ \mathcal{C} = \mathcal{U}\mathcal{V}\mathcal{U}^T,$$

where the first $(\mathtt{d}+1)$ columns of the matrix $\mathcal{U} = [\,\mathbf{u}_1\,\mathbf{u}_2\,\ldots\,\mathbf{u}_{\mathtt{n}}\,]$, contain the basis of the nodal coordinates; and the diagonal matrix $\mathcal{V}$ has $\mathtt{d}+1 = 4$ zero eigenvalues for a 3D structure. That is, if the positive semi-definite matrix $\mathcal{V}$ has eigenvalues $[0\,0\,0\,0\,\lambda_5\,\ldots\,\lambda_{max}]$, the candidate eigenvectors are situated in the leftmost columns of $\mathcal{U}$. In this context, the matrix $\mathcal{U}$ has the basis for the nodal coordinates as column vectors in the nullspace, each of which solves the homogeneous Eq. (2.5).

It follows from the definition of $\mathcal{D}$ that the **1**-vector, $[1\,1\,1\,\ldots]^T$, solves the homogeneous Eq. (2.5). This **1**-vector, however, provides little information for the nodal coordinates and it should be avoided in subsequent calculations. See [136] for particular information on nullspaces and decompositions. The general solution,

$$[\,\mathbf{x}\,\mathbf{y}\,\mathbf{z}\,] = [\,\mathbf{u}_1\,\mathbf{u}_2\,\ldots\,\mathbf{u}_{\mathtt{d}+1}\,]\mathcal{T},$$

requires a transformation matrix $\mathcal{T} \in \Re^{(\mathtt{d}+1)\times\mathtt{d}}$. One can use $\mathcal{T}$ to change the geometry of the structure. Infinite number of geometrically different self-stressed configurations can thus be found for a single vector $\mathbf{t}$. Since the tension coefficients do not change under affine transformations [186], the numerical procedure can directly use the eigenvectors in the nullspace. Thus, for simplicity and without loss of generality the transformation matrix $\mathcal{T}$ is set to

$$\mathcal{T} = \begin{pmatrix} 1 & 0 & 0 \\ 0 & 1 & 0 \\ 0 & 0 & 1 \\ 0 & 0 & 0 \end{pmatrix}.$$

It is convenient to remark that static and kinematic properties of this kind of pin-jointed structures are invariant to projective transformations [165, 59]. That is, the values of $\mathtt{s}$ and $\mathtt{m}$ do not change under projective transformations. The vector $\mathbf{t}$ may however change its value under projective transformations. Conversely, a vector $\mathbf{t}$ remains unchanged under affine transformations, which also implies that $\mathtt{s}$ and $\mathtt{m}$ remain unchanged.

5.3.2 Non-equilibrium

Tensegrity structures generated by a vector of tension coefficients $\mathbf{q}^0$, Eq. (5.1), unlikely satisfy Eq. (2.7) and therefore the structures are not in self-equilibrium. In this case it is necessary to circumvent the lack of a useful nullspace in $\mathcal{D}$, from which the basis of the nodal coordinates can be computed. Here is show how an approximation of the nodal coordinates can be computed if the rank condition Eq. (2.7) is not satisfied. A matrix operation of a nonlinear map $f : \Re^{\mathtt{b}} \to \Re^{\mathtt{n}\times\mathtt{d}}$ of vector to matrix is presented. It takes $\mathbf{t}$ to compute an approximation of $[\mathbf{x}\,\mathbf{y}\,\mathbf{z}]$.

Let $\mathbf{t}$ be a vector of tension coefficients such that a force density matrix $\mathcal{D}$ factorised as

$$\mathcal{D} = \mathcal{C}^T \text{ diag}(\mathbf{t}) \, \mathcal{C} = \mathcal{U}\mathcal{V}\mathcal{U}^T, \tag{5.2}$$

does not satisfy Eq. (2.7), and may not be positive semi-definite. In general, a force density matrix with prototypes of tension coefficients $\mathbf{q}^0$ falls within this definition. The nullspace is therefore useless and other techniques need to be applied to identify a triplet, $\{\mathbf{u}_i, \mathbf{u}_j, \mathbf{u}_k\} \in \mathcal{U}$, of column vectors that approximates the equation of static equilibrium,

$$\mathcal{D}[\, \mathbf{u}_i \, \mathbf{u}_j \, \mathbf{u}_k \,] \approx [\mathbf{0}\, \mathbf{0}\, \mathbf{0}].$$

This is an approximated solution of static equilibrium in which the column vectors $\{\mathbf{u}_i, \mathbf{u}_j, \mathbf{u}_k\}$ do *not* correspond to the zero eigenvalues of Eq. (5.2). In fact, the approximated solution can be found with a mixture eigenvectors associated to eigenvalues in zero *and* negative eigenvalues.

A possible choice of these column vectors is to favour the triplet that produces a dominating structure, e.g. [47, 51], in which struts are of non-zero length but as short as possible. This minimal length condition has some advantages, for instance with respect to Euler buckling and globally rigid tensegrities [51, 48]. It is easy to choose the triplet $\{\mathbf{u}_i, \mathbf{u}_j, \mathbf{u}_k\}$ if one considers the problem in terms of lengths, in which the total squared length of the entire structure is minimised,

$$\sum_{p=1}^{\mathtt{b}} l_p^2 = ||\mathcal{C}\mathbf{u}_i + \mathcal{C}\mathbf{u}_j + \mathcal{C}\mathbf{u}_k||^2 . \tag{5.3}$$

To this end, the unitary matrix $\mathcal{U} = [\, \mathbf{u}_1 \, \mathbf{u}_2 \, \mathbf{u}_3 \, \ldots \, \mathbf{u}_{\mathtt{n}} \,]$ computed in Eq. (5.2), is used in the calculation of all projected lengths,

$$\mathcal{L} = \mathcal{C}\mathcal{U} = [\, (\mathbf{u}_1^A - \mathbf{u}_1^B) \, (\mathbf{u}_2^A - \mathbf{u}_2^B) \, \ldots \, (\mathbf{u}_{\mathtt{n}}^A - \mathbf{u}_{\mathtt{n}}^B) \,], \tag{5.4}$$

over all $1 \ldots \mathtt{n}$ axes for each pair (A, B) of connected nodes. It is convenient to remove the column vectors $\mathbf{u}_i$ for which $\mathcal{C}\mathbf{u}_i = \mathbf{0}$ in Eq. (5.4). In order to find the $\{\mathbf{u}_i, \mathbf{u}_j, \mathbf{u}_k\}$, Eq. (5.3), the columns of $\mathcal{L}$, Eq. (5.4), are identified according to their 2-norm,

$$[\, c_1 \, c_2 \, \ldots \,] = \arg\min_i ||\mathcal{L}_i|| , \tag{5.5}$$

where the elements of the sorted list $[\, c_1 \, c_2 \, \ldots \,]$ returned by the minimal argument function, $arg\,min(\star)$, correspond to the indices (i) in which the vector norm $||\mathcal{L}_i||$ is minimised. Notice that there may be multiple indices that correspond to the minimal 2-norm. Therefore, the minimal indices as well as their multiplicity are taken to have a pool of at least $\mathtt{d}$ candidate columns. Equation (5.5) helps to narrow the search space to

only a few column vectors of Eq. (5.4). The reduced matrix $\tilde{\mathcal{U}} = [\mathbf{u}_{c_1}\, \mathbf{u}_{c_2}\, \ldots\, \mathbf{u}_{\mathtt{d}+1}]$ is then used to factorise the projected lengths by means of a QR (or LU) decomposition,

$$\mathcal{Q}\mathcal{R} = (\mathcal{C}\tilde{\mathcal{U}})^T\, (\mathcal{C}\tilde{\mathcal{U}}), \tag{5.6}$$

and get access to the upper triangular matrix $\mathcal{R}$. In such a case, the lengths along each axis are handled columnwise, i.e. $\mathcal{C}\mathbf{u}_i = \mathcal{Q}\mathcal{R}_i$, and linearly dependent projected lengths have their pivot set to zero. To remark it explicitly, a unitary matrix $\mathcal{Q}$ in the orthogonal-triangular decomposition is not the diagonal matrix of tension coefficients defined in a force density matrix $\mathcal{D}$. Finally, smaller but non-zero pivots in the triangular matrix $\mathcal{R}$ help to choose the $\mathtt{d}$ linearly independent columns as nodal coordinates $[\mathbf{x}\,\mathbf{y}\,\mathbf{z}]$; here $\mathtt{d} = 3$.

This selection procedure, Eq. (5.5) and Eq. (5.6), helps to find configurations with minimal but non-zero projections, Eq. (5.3), with a maximal rank condition of $\mathcal{D}$, Eq. (2.7), and which have linearly independent projections $\mathcal{C}\mathbf{x}$, $\mathcal{C}\mathbf{y}$ and $\mathcal{C}\mathbf{z}$. In other words, the procedure picks a configuration that dominates all other equivalent ones, see [47, 51, 48]. At this point our form-finding procedure has calculated an approximated equilibrium configuration, such that $\mathcal{D}[\mathbf{x}\,\mathbf{y}\,\mathbf{z}] \approx \mathbf{0}$.

5.4 From coordinates to tension coefficients

5.4.1 Equilibrium

Let $[\mathbf{x}\,\mathbf{y}\,\mathbf{z}]$ be the nodal coordinates of a structure in a state of self-stress, $\mathtt{s} \geq 1$. It is known [159] that the basis of vector spaces of tension coefficients and mechanisms of a self-stressed structure are calculated from the nullspaces of the equilibrium matrix, see Eq. (2.8). To make this Chapter easier to follow, the decomposition Eq. (2.8) is written here again. The singular value decomposition of the equilibrium matrix is:

$$\mathcal{A} = \begin{pmatrix} \mathcal{C}^T\, \mathrm{diag}(\mathcal{C}\mathbf{x}) \\ \mathcal{C}^T\, \mathrm{diag}(\mathcal{C}\mathbf{y}) \\ \mathcal{C}^T\, \mathrm{diag}(\mathcal{C}\mathbf{z}) \end{pmatrix} = \mathcal{U}\mathcal{V}\mathcal{W}^T. \tag{5.7}$$

In this context the unitary matrix $\mathcal{U}$ has the following left nullspace,

$$\mathcal{U} = [\mathbf{u}_1\, \mathbf{u}_2\, \ldots\, |\, \mathbf{d}_1\, \ldots\, \mathbf{d}_{\mathtt{dn}-\mathtt{r}}],$$

and the matrix $\mathcal{W}$ has the following right nullspace,

$$\mathcal{W} = [\mathbf{w}_1\, \mathbf{w}_2\, \ldots\, |\, \mathbf{t}_1\, \ldots\, \mathbf{t}_{\mathtt{b}-\mathtt{r}}],$$

where $\mathtt{r}$ is the rank of the diagonal matrix $\mathcal{V}$; the singular vectors $\mathbf{d} \in \Re^{\mathtt{dn}}$ denote the $\mathtt{m} = \mathtt{dn} - \mathtt{r}$ infinitesimal mechanisms; and the singular vectors $\mathbf{t} \in \Re^{\mathtt{b}}$ the states of

self-stress, each of which solves the homogeneous equation Eq. (2.4). For a valid set of coordinates $[\mathbf{x}\,\mathbf{y}\,\mathbf{z}]$ if the rank of $\mathcal{A}$ is $\mathtt{r} = \text{rank}(\mathcal{A}) < \mathtt{b}$, it follows that matrix $\mathcal{A}$ comes from a statically indeterminate structure, or equivalently $\mathtt{s} \geq 1$.

5.4.2 Non-equilibrium

However, if the structure is not in a state of self-stress, the right nullspace of $\mathcal{A}$, as defined in Eq. (5.7), is not immediately available. That is the case when the matrix $\mathcal{A}$ is calculated with an approximation of the nodal coordinates (see Section 5.3.2). It is possible, however, to modify $\mathcal{A}$ in such a way that it is rank deficient. It is shown a matrix operation of a nonlinear map $f : \Re^{\mathtt{n}\times\mathtt{d}} \rightarrow \Re^{\mathtt{b}}$ of matrix to vector: from $[\mathbf{x}\,\mathbf{y}\,\mathbf{z}]$ to compute an approximation of $\mathbf{t}$.

Let $[\mathbf{x}\,\mathbf{y}\,\mathbf{z}]$ be a matrix of estimated nodal coordinates and $\mathtt{d} = 3$. By calculating the singular value decomposition of $\mathcal{A}$, $\mathcal{A} = \mathcal{U}\mathcal{V}\mathcal{W}^T$, one gets the matrix $\mathcal{W} = [\mathbf{w}_1\,\mathbf{w}_2\,\ldots\,\mathbf{w}_{\mathtt{b}}]$, from which the tension coefficients can be obtained. It is take for granted that $\mathcal{V}$ has singular values in decreasing order $[\sigma_{max}\,\ldots\,\sigma_{min}]$. Basically, if a single state of self-stress is assumed, $\mathtt{s} = 1$, the signs of the rightmost singular vector of $\mathcal{W}$ and the prototypes in $\mathbf{q}^0$ may not match, i.e. $sgn(\mathbf{w}_{\mathtt{b}}) \neq sgn(\mathbf{q}^0)$. So it is necessary to take more than one colum vector from the right of $\mathcal{W}$ to compute a vector $\mathbf{t}$ that best matches $\mathbf{q}^0$. For instance, by using a least square fit, the procedure can calculate the vector of coefficients $\tilde{\mathbf{t}}$ that minimises the quantity

$$\left|\left|[\mathbf{w}_j\,\ldots\,\mathbf{w}_{\mathtt{b}}]\tilde{\mathbf{t}} - \mathbf{q}^0\right|\right|^2, \tag{5.8}$$

for a block of column vectors $[\mathbf{w}_j\,\ldots\,\mathbf{w}_{\mathtt{b}}]$, such that

$$\mathbf{t} = [\mathbf{w}_j\,\ldots\,\mathbf{w}_{\mathtt{b}}]\tilde{\mathbf{t}}.$$

The procedure starts by setting $j = \mathtt{b} - 1$ and verify if the signs match, $sgn(\mathbf{t}) = sgn(\mathbf{q}^0)$. If it does, the procedure stops, otherwise it decreases j by one, and repeats it. This procedure imposes the existence of at least one state of self-stress that matches in signs with $\mathbf{q}^0$.

At the end, the vector $\tilde{\mathbf{t}}$ is the unique least square solution for the system

$$[\mathbf{w}_j\,\ldots\,\mathbf{w}_{\mathtt{b}}]\tilde{\mathbf{t}} = \mathbf{q}^0,$$

such that the product of the equilibrium matrix and the new vector of approximated tension coefficients,

$$\mathbf{t} = [\mathbf{w}_j\,\ldots\,\mathbf{w}_{\mathtt{b}}]\tilde{\mathbf{t}}, \tag{5.9}$$

gives an approximation solution to the equilibrium state,

$$\mathcal{A}\mathbf{t} = \begin{pmatrix} \mathcal{C}^T \text{ diag}(\mathcal{C}\mathbf{x}) \\ \mathcal{C}^T \text{ diag}(\mathcal{C}\mathbf{y}) \\ \mathcal{C}^T \text{ diag}(\mathcal{C}\mathbf{z}) \end{pmatrix} \mathbf{t} \approx \mathbf{0}. \tag{5.10}$$

The numerical form-finding procedure therefore approximates a state of equilibrium, Eq. (5.10), and preserves $sgn(\mathbf{q}^0)$, in the new vector $\mathbf{t}$, as defined in Eq. (5.9). The pseudocode is shown in Fig. 5.2.

$\mathbf{q}^0 = [+1, +1, \ldots, +1, -1, -1, \ldots, -1]$
$\mathbf{t} = \mathbf{q}^0$
$\mathtt{s} = 0$
do
  $\mathcal{U}\mathcal{V}\mathcal{U}^T = \mathcal{C}^T \text{diag}(\mathbf{t})\mathcal{C}$
  $[\mathbf{x}, \mathbf{y}, \mathbf{z}] = \text{select\_coordinates}(\mathcal{U})$
  $\mathcal{A} = \begin{pmatrix} \mathcal{C}^T \text{ diag}(\mathcal{C}\mathbf{x}) \\ \mathcal{C}^T \text{ diag}(\mathcal{C}\mathbf{y}) \\ \mathcal{C}^T \text{ diag}(\mathcal{C}\mathbf{z}) \end{pmatrix}$
  $\mathcal{U}\mathcal{V}\mathcal{W}^T = \mathcal{A}$
  $\mathbf{t} = \text{select\_tension\_coefficients}(\mathcal{W}, \mathbf{q}^0)$
  $\mathtt{s} = \text{count\_states\_selfstress}(\mathcal{V})$
while $\mathtt{s} = 0$

Fig. 5.2: Pseudocode : a numerical form-finding procedure approximates equilibrium coordinates from the current vector of tension coefficients (initialised as prototypes), and approximates tension coefficients from the current coordinates.

As the pseudocode indicates, Fig. 5.2, the approximations of coordinates and tension coefficients are the main calculations in the numerical procedure. This closes the loop in the form-finding procedure because with the vector $\mathbf{t}$, Eq. (5.9), the procedure calculates a new set $[\mathbf{x}\,\mathbf{y}\,\mathbf{z}]$, as described in Section 5.3.2. The procedure iteratively approximates a vector of tension coefficients and set of coordinates that self-equilibrate the statically indeterminate structure defined by $\mathcal{C}$ and $\mathbf{q}^0$.

5.5 Examples of 2D and 3D tensegrity structures

The usefulness of our procedure is demonstrated by presenting a few examples of 2D and 3D tensegrity units. The procedure works remarkably well for globally rigid tensegrities [46, 48], in which the matrix $\mathcal{D}$ is (i) positive semi-definite of (ii) maximal rank $\mathtt{n} - \mathtt{d} - 1$. This maximal rank condition means nullity three for 2D structures and nullity four for

3D structures. All examples presented in this paper fulfil these two conditions. Notice that no struts intersect in any tensegrity structure.

Examples in 2D

Figure 5.3a depicts a tensegrity hexagon. This hexagon was studied in 1878 by Crofton [60] as an example of a structure that satisfies the Maxwell's rule ($\mathtt{b} = 2\mathtt{n} - 3$) but it is statically indeterminate; see also [41, 40] for more information on Crofton's work. His graphical solution was generalised to $2k$-sided polygons, $k > 2$, by Kötter [116] in 1912. One can analyse this small tensegrity in exact symbolic form, e.g. as in [191]. The solution is a force density of $q_c = 1$ and $q_s = -1/2$ in cables and struts, respectively. The numerical form-finding procedure calculates exactly this solution. Here the struts, which are the elements in compression, are depicted by thick grey lines.

Another example of early 2D tensegrity structures is shown in Fig. 5.3b. This hexagonal tensegrity was studied by Mohr [137] in 1885. An example found in [91] is shown in Fig. 5.3c. Each one of these three tensegrities (Figs. 5.3a-c) has six nodes and nine members, and each tensegrity structure has $\mathtt{s} = 1$ and $\mathtt{m} = 1$. Here $\mathtt{m}$ excludes the three rigid body motions of a planar structure. It goes without saying that the complete enumeration of valid tensegrities with $\mathtt{n}$ nodes and $\mathtt{b}$ members remains an open problem.

Figure 5.3d is a compound of a square and a hexagon, in which the struts are placed such that there is no nodal symmetry, and two nodes lack incident struts. The numerical form-finding procedure can calculate the equilibrium configuration of nodes with no incident struts. Finally, Fig. 5.3e shows an example found in [49]. The tensegrities Figs. 5.3d-e have a single state of self-stress, $\mathtt{s} = 1$ and $\mathtt{m} = 2$, and they have eight nodes and twelve members.

5.5.1 Examples in 3D

5.5.2 Expanded octahedron

Using a symbolic analysis based on the force density matrix, Tibert and Pellegrino [191] calculated two solutions for the expanded octahedron, of which only one produces a positive semi-definite matrix $\mathcal{D}$. Applying our form-finding procedure, it is found that the expanded octahedron has indeed $\mathtt{s} = \mathtt{m} = 1$. The stable structure is shown in Fig. 5.4a. The 2-norm of $\mathcal{A}\mathbf{t}$ as a function of the number of iterations is plotted in a logarithmic scale in Fig. 5.4b. It can be seen that the iterative procedure converges in 14 iterations to one state of self-stress.

The ratio between strut and cable lengths is $l_s/l_c \approx 1.63299$, which is in agreement with other studies [142]. By normalising $\mathbf{t}$ with respect to the tension coefficient in the cables, a value ($q_c = 1$) and ($q_s = -3/2$) is found for 24 cables and 6 struts, respectively.

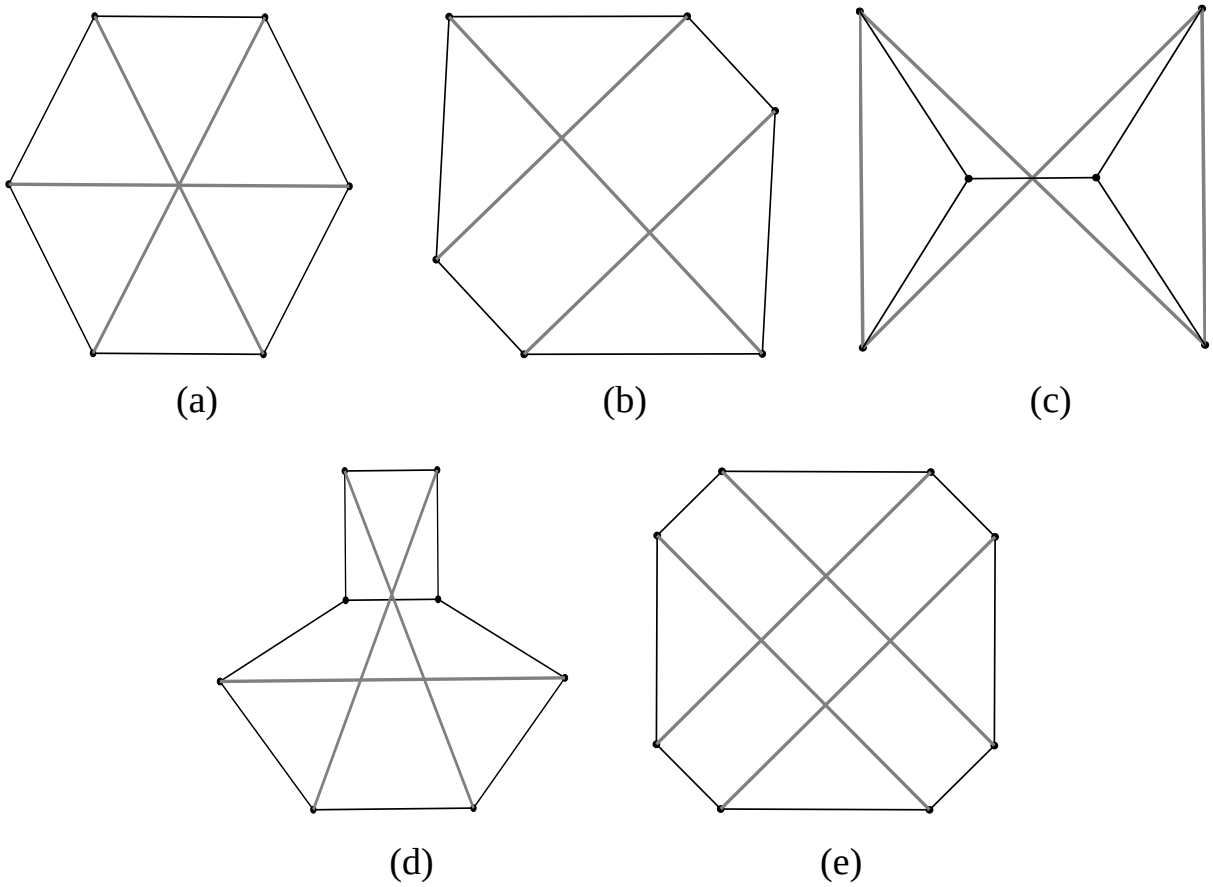

Fig. 5.3: Examples of planar tensegrities : The (unconnected) thick gray lines represent struts.

These values correspond to the ones found by [191] using a symbolic analysis. Notice that the form-finding procedure changes the lengths of all members at each iteration. The total length is plotted in Fig. 5.4c. In this case the members are elongated in every iteration until the self-equilibrium is found.

Moreover, the initial stiffness criterion, Eq. (4.7), shows that the state of self-stress imparts a positive stiffness to all but six directions, i.e. rigid body motions. This example demonstrates that the proposed form-finding procedure is able to efficiently calculate the solution that produces a positive semi-definite matrix $\mathcal{D}$.

5.5.3 Truncated tetrahedron

The truncated tetrahedron analysed by several authors [191, 157, 142] has *one* cable length as well as a single length for all struts. This structure is calculated by imposing these conditions *a priori*, e.g. in a dynamic relaxation [140] or in non-linear programming [157]. However, there is no such constraint in our proposed form-finding procedure. The numerical form-finding procedure found a solution with *two* different cable lengths and all struts being of equal length, see Fig. 5.5a. What is the difference between these solutions?

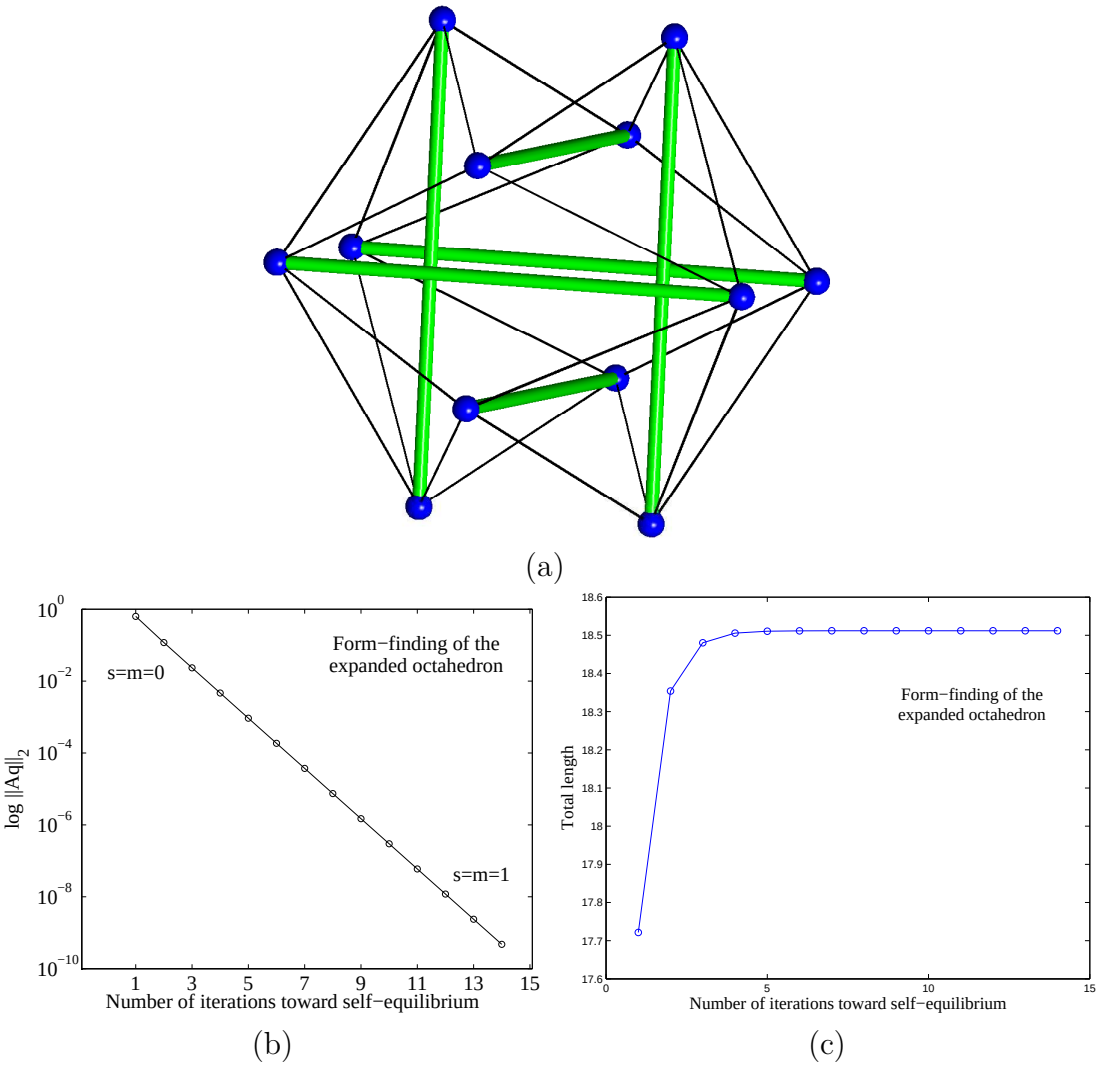

Fig. 5.4: Form-finding of the expanded octahedron : (a) expanded octahedron; (b) convergence to self-equilibrium; (c) net change of member lengths. Thick green lines represent elements in compression.

A comparison is here described by looking at their elastic potential energy. This is essentially the same approach followed in Section 4.2. As described in the previous Chapter, global equilibrium is attained in the state of least energy. Therefore configurations with less potential energy are preferred to other local minima with higher energy.

Similarly to the approach shown in Section 4.2, the elastic potential energy of a tensegrity structure is calculated by describing its members as Hookean springs that store energy upon experiencing a strain. Let $\mathbf{e}_i$, $\boldsymbol{\varepsilon}_i$ and $\mathbf{a}_i$ be the Young's modulus, the strain and the cross-sectional area of member i, respectively. Then, if the stress and length per member are defined as $\sigma_i = e_i\varepsilon_i$ and l_i, respectively, the elastic energy per unit volume of the structure is given by:

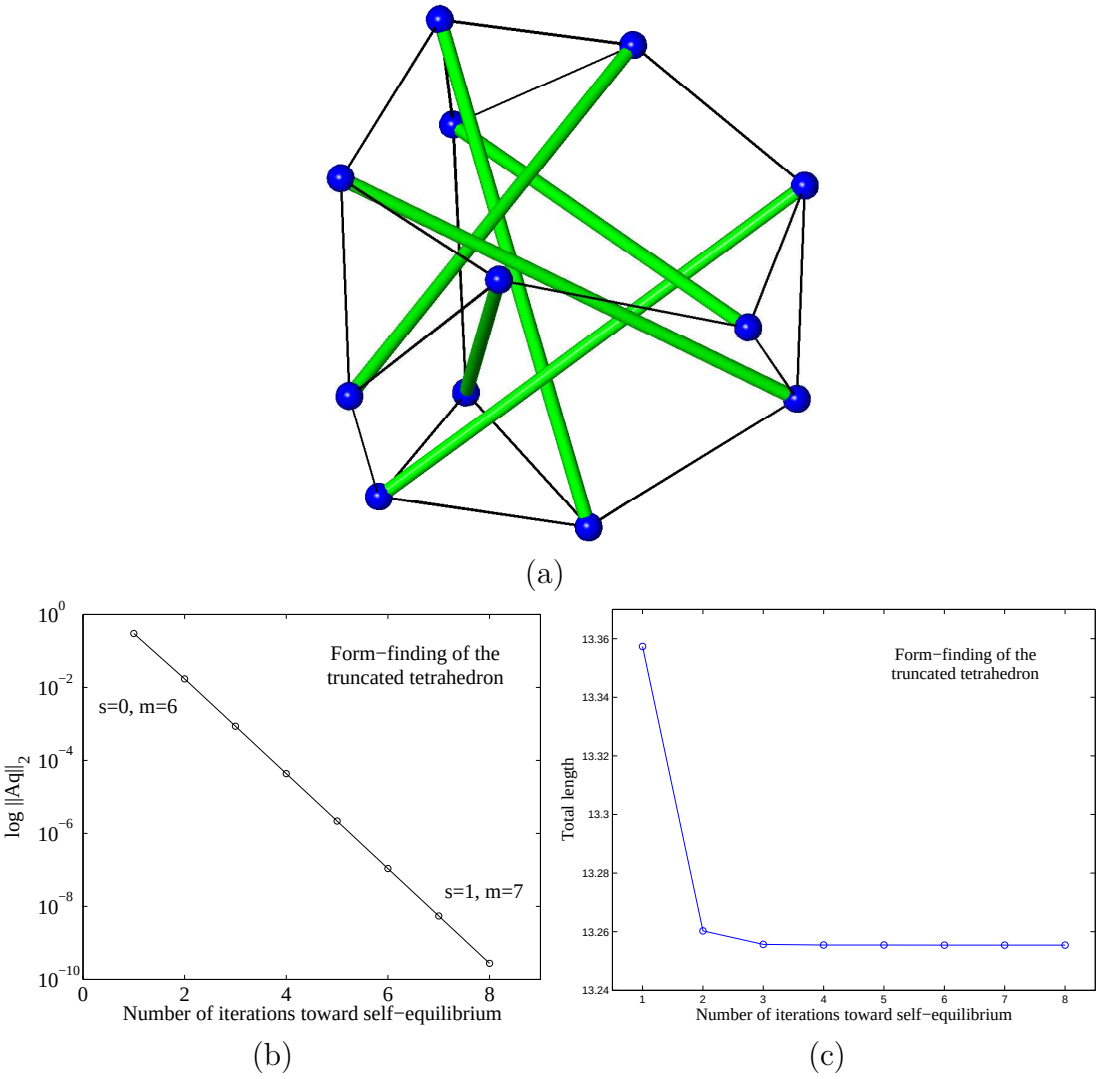

Fig. 5.5: Form-finding of the truncated tetrahedron : (a) truncated tetrahedron; (b) convergence to self-equilibrium; (c) net change of member lengths. Thick green lines represent elements in compression.

$$U = \frac{1}{2}\sum_{i=1}^{\mathtt{b}} \sigma_i \varepsilon_i \; = \frac{1}{2}\sum_{i=1}^{\mathtt{b}} e_i \varepsilon_i^2 \; = \frac{1}{2}\sum_{i=1}^{\mathtt{b}} e_i (\frac{f_i}{e_i a_i})^2 \; = \frac{1}{2}\sum_{i=1}^{\mathtt{b}} \frac{f_i^2}{e_i a_i^2} \; = \frac{1}{2}\sum_{i=1}^{\mathtt{b}} \frac{l_i^2 q_i^2}{e_i a_i^2}.$$

By comparing two or more structures with the same value of $\mathbf{e}_i\mathbf{a}_i$, as shown in Eq. (4.1), the difference in the elastic potential energy density is $U \propto \sum_{i=1}^{\mathtt{b}} l_i^2 q_i^2$.

The truncated tetrahedron calculated by [191, 157, 142] was compared to the solution found by us. The solution with a single cable length was calculated with the non-linear programming approach [157], provided by Gunnar Tibert. For the comparison, it was assumed that both structures have the same value for $\mathbf{e}_i\mathbf{a}_i$. The structures were rescaled to fit inside a box of unitary lengths, and their tension coefficients normalised so the

tension coefficient of a reference cable is unitary in both structures. Our calculations show:

- 12 cables with $q = 1$, 6 cables with $q = 1.3794$ and 6 struts with $q = -0.66714$ in the structure calculated by [191, 48].
- 12 cables with $q = 1$, 6 cables with $q = 1.1546$ and 6 struts with $q = -0.6170$ in our structure.

The calculation of the elastic energy density shows that the truncated tetrahedron calculated with a single cable length has an energy 20% **higher** than the solution with two cable lengths. In terms of equilibrium and stability the configuration with *two* cable lengths is therefore advantageous. The structure with only *one* cable length, possessing longer struts and larger tension coefficients, is suppressed by our form-finding procedure in favour of a low-energy structure with two different cable lengths.

The form-finding procedure takes 8 iterations to start from a configuration with $\mathtt{s} = 0$ and $\mathtt{m} = 6$ to converge towards the equilibrium configuration with $\mathtt{s} = 1$ and $\mathtt{m} = 7$, see Fig. 5.5b. Figure 5.5c shows the total length as a function of the number of iterations required to converge to self-equilibrium. The procedure finds an initial configuration and subsequently reduces its total length.

Moreover, the state of self-stress imparts positive stiffness to every infinitesimal mechanism of this structure, except for the six rigid-body displacements, e.g. Eq. (4.7). This demonstrates that the proposed form-finding procedure is capable of selecting a configuration with minimal elastic potential energy.

5.5.4 Truncated icosahedron

Murakami and Nishimura [147] have analysed the truncated icosahedron, Fig. 5.6a, with a rather complicated form-finding procedure based on group theory. Their form-finding takes advantage of the symmetry and is developed for the truncated versions of the five Platonic solids. It is unclear whether their group theory approach can be extended to handle other structures.

After 45 iterations our form-finding procedure calculates $\mathtt{s} = 1$ and $\mathtt{m} = 55$, which is in agreement with their assumptions [147]. Figure 5.6b show a truncated icosahedron and its convergence to $\mathtt{s} = 1$. The total length is initially over-estimated but it is reduced at each iteration, see Fig. 5.6c, till convergence is found.

By normalising the tension coefficients with respect to a reference cable, it was found: 60 cables with $q = 1$, 30 cables with $q = 0.6775$ and 30 struts with $q = -0.3285$. This solution provides positive stiffness to all mechanisms, see initial stiffness criterion Eq. (4.7), except for the six rigid-body displacements.

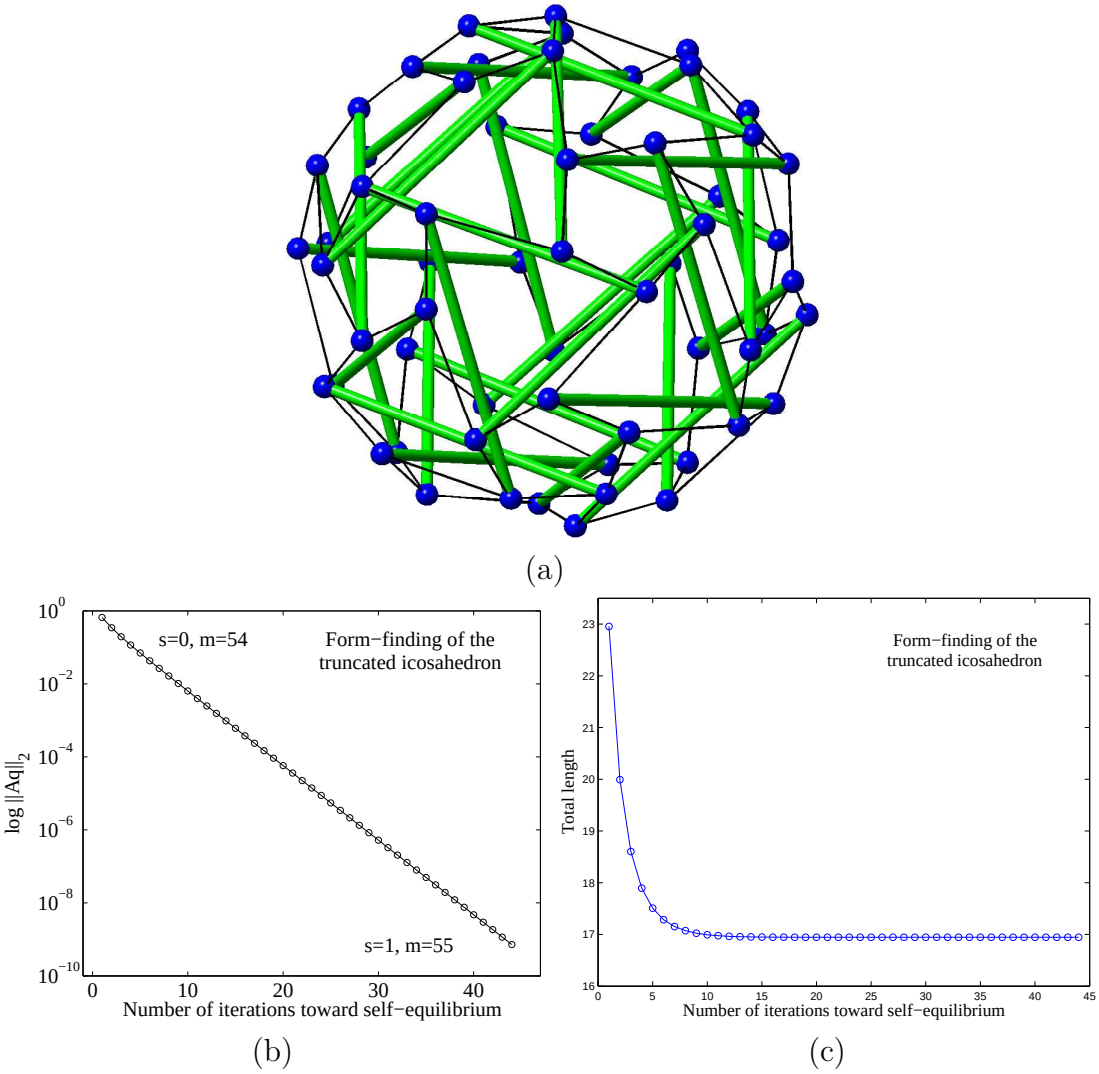

Fig. 5.6: Form-finding of the truncated icosahedron : (a) truncated tetrahedron; (b) convergence to self-equilibrium; (c) net change of member lengths. Thick green lines represent elements in compression.

5.5.5 Cylindrical tensegrities

Finally, the ability of the proposed procedure to find structures that correspond to global energy minima is further exemplified with cylindrical tensegrities. As seen in previous Chapters, two well known examples of cylindrical tensegrity structures are the triplex and the quadruplex for which $n = 3$ and $n = 4$, respectively.

The geometry of this class of tensegrity structure is described by a set of two parallel planes, "top" and "bottom" so to say, see [79] or Section 3.2. Here, each plane consists of n nodal points, and both planes are connected by n brace cables and n struts. An interesting feature of these cylinders is the number of equivalent or structurally identical configurations that exist for a given n. There are in fact $\phi(n)/2$ equally valid configura-

tions for any n-plex, see Section 3.4.2 for details.

The form-finding of cylindrical tensegrities has been studied using several approaches, for instance, the dynamic relaxation procedure by [142] and non-linear programming by [157]. But these approaches impose the condition of a unique cable length.

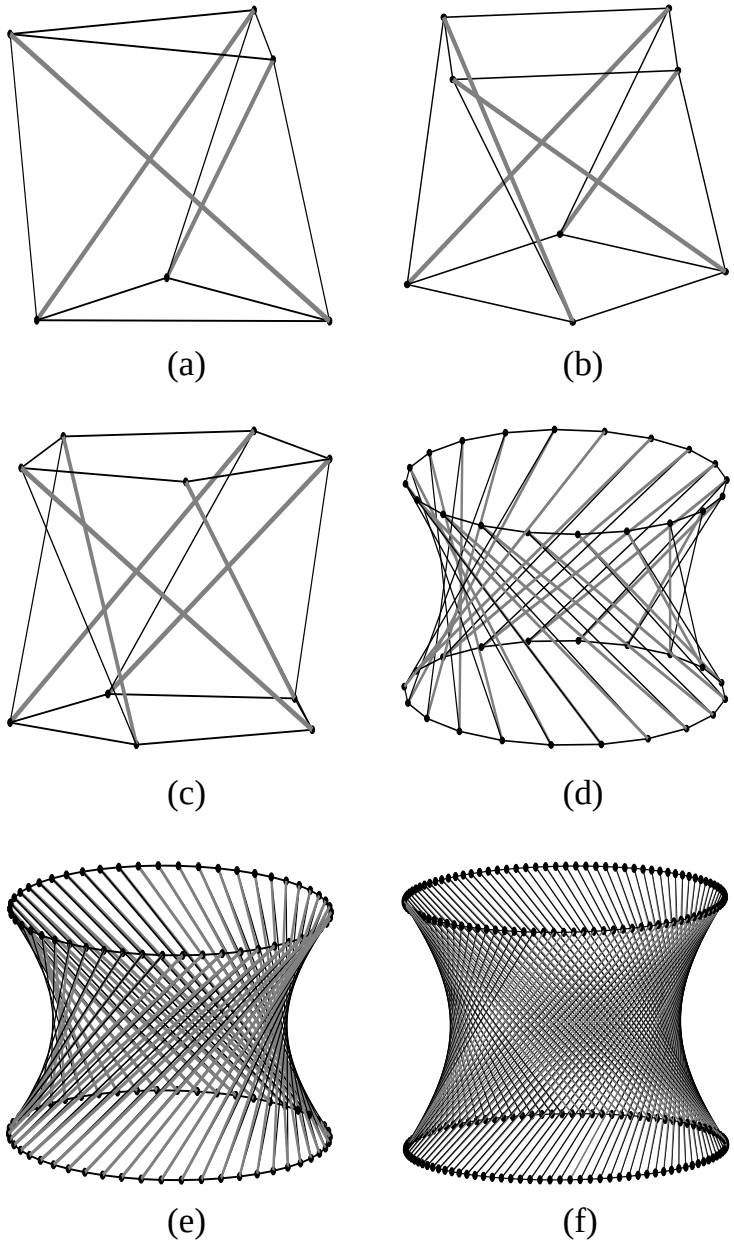

Fig. 5.7: Examples of cylindrical tensegrities of order n : (a) n=3, the triplex; (b) n=4, the quadruplex; (c) n=5; (d) n=20; (e) n=50; (f) n=100. Thick gray lines represent elements in compression.

Cylindrical tensegrities were re-calculated with the proposed form-finding procedure. For instance, the triplex and the quadruplex are shown in Figs. 5.7a and 5.7b, respectively. The (convex) pentaplex, or 5-plex for short, is shown in Fig. 5.7c: the numerical form-finding procedure converges to convex cylinders and discard the star-like configurations;

see Sections 4.2 and 4.4 for the implications of either convex or star-like cylinders. Finally, three examples (Figs. 5.7d-f) of (convex) tensegrity cylinders are shown. The examples have a large number of elements, such as the 20-plex, 50-plex, and 100-plex.

As expected, an analysis of their initial stability shows that the structures possess positive stiffness with the given state of self-stress. Moreover, the solutions have $l_{c_1} = l_{c_2}$ different from l_b and l_s. Coordinates derived from the eigenvectors of $\mathcal{D}$ did not produce unitary cylinders like $l_{c_1} = l_{c_2} = l_b$. Interestingly, the form-finding procedure is indeed able to selectively calculate the stable configuration among the $\phi(n)/2 - 1$ sub-optimal configurations, see Section 3.4.2 for the derivation of this number of equivalent but unstable configurations.

5.6 Implementation

In summary, the form-finding procedure iterates Eq. (5.5), Eq. (5.6) and Eq. (5.8) until the rank condition Eq. (2.6) is satisfied. The potential nullspaces in $\mathcal{D}$ and $\mathcal{A}$ are exploited as to impose the existence of at least one solution.

The number of geometrically different configurations and tension coefficients is infinite, but the structural parameter $\mathtt{s}$ does not change under affine or projective transformations [59, 186]. That is why the numerical procedure focuses on certain eigenvectors in $\mathcal{D}$ and $\mathcal{A}$. From these matrices, suitable eigenvectors are selected as the bases of vector spaces for both coordinates and tension coefficients.

In fact, it is Eq. (5.8) the one that forces the current equilibrium matrix to be rank deficient, i.e. having at least one state of self-stress or equivalently $\mathtt{r} = \text{rank}(\mathcal{A}) < \mathtt{b}$. The auxiliary equations Eq. (5.5) and Eq. (5.6) update the coordinates of the next equilibrium matrix, and so on till $\mathtt{s} > 0$. At the end, a vector $\mathbf{t}$ is found such that $\mathcal{A}\mathbf{t} = \mathbf{0}$, and this single vector $\mathbf{t}$ is our solution. The rest of the states of self-stress, in case $\mathtt{s} \geq 2$, can be calculated from the right nullspace of $\mathcal{A}$.

Matlab code

The numerical form-finding method for tensegrity structures in 3D is implemented in a few lines of Matlab code. The code appears in Fig. 5.8. All thresholds for rank conditions were set to 1e-10. The code, written for Matlab 7.0, has no intention to be a definite guide in implementing Eq. (5.5), Eq. (5.6) and Eq. (5.8). Moreover, Fig. 5.8 has no claim of good coding style.

The procedure, Fig. 5.8, guides both matrices $\mathcal{D}$ and $\mathcal{A}$ to be rank deficient, i.e. a proper rank, by selecting the appropriate eigenvector(s) in each decomposition and imposing the existence of at least one state of self-stress.

```
 1  tol   = 1e-10;                          % for zero tests
 2  sigma = 1;
 3
 4  while sigma > tol                       % until a state of self-stress is found
 5    [U,V] = schur(C'*diag(t)*C);          % basis for coordinates, D=UVU^T
 6    N = sum(diag(V)<tol);                 % potential nullity
 7    if N < 4, N=1:4; else N=1:N; end;     % get enough nullspace any way,
 8    U = U(:, N);                          % reduced search space
 9
10    [Q,R] = qr((C*U)'*(C*U));             % lengths projected in all directions
11    n = []; for i=1:size(R,2),            % norm_2
12      n(i)=norm(R(:,i)); end;             % n_i >= 0
13    [val,ind] = sort(n);
14    ind = ind(find(val > tol));           % ignore 1-vector, i.e. n_i=0
15
16    if length(ind) > 3                    % two possible triplets?
17      for i=1:length(ind)-2               % 1-2-3 or 2-3-4
18        l = C*U(:,ind(i:i+2));
19        if det(l'*l)>tol                  % linearly independent columns
20          ind = ind(i:end);
21          break;
22        end;
23      end;
24    end;
25
26    % take the approximate coordinates and approximate the tension coefficients
27    x = U(:,ind(1)); y = U(:,ind(2)); z = U(:,ind(3));
28    A = [ C'*diag(C*x) ; C'*diag(C*y) ; C'*diag(C*z) ];
29    [U,V,W] = svd(A,0);                   % SVD of the equilibrium matrix
30
31    % select the tension coefficients that match the prototypes
32    for i=0:size(A,2)-1
33      t = W(:,(end-i):end) * (W(:,(end-i):end) \ proto);
34      if sum(sign(t) - sign(proto) ~= 0) == 0
35        break;
36      end;
37    end;
38
39    sigma = V(end,end);                   % for the test of states of self-stress
40  end;
```

Fig. 5.8: An implementation of the form-finding method : sample code, in Matlab, as a proof of concept that calculates a vector of tension coefficients to self-equilibrate a tensegrity structure in 3D. The input parameters are the vector of prototypes, $\mathbf{q}^0$, which in the code is called "proto", and the incidence matrix $\mathcal{C}$. At the end, the vector "t" has the vector of tension coefficients that self-equilibrate the structure, $\mathcal{A}\mathbf{t} = \mathbf{0}$, and provides a state of self-stress, $\mathtt{s} > 0$.

From tension coefficients to coordinates

The very first iteration of code Fig. 5.8 requires the initialisation of prototypes (vector $\mathbf{q}^0$ is "proto" in line 33) and vector "t", i.e. $\mathbf{t} = \mathbf{q}^0$. Schur decomposition in line 5 requires this assignment of $\mathbf{t} = \mathbf{q}^0$ for the very first approximation of equilibrium coordinates. What it does is $\mathcal{D} = \mathcal{U}\mathcal{V}\mathcal{U}^T$, in which a force density matrix is calculated with the current vector of tension coefficients. Notice that a force density matrix, Eq. (5.2), requires an incidence matrix $\mathcal{C}$; e.g. Section 2.4 for a definition of incidence matrix. A schematic representation of these first steps appears in Fig. 5.9.

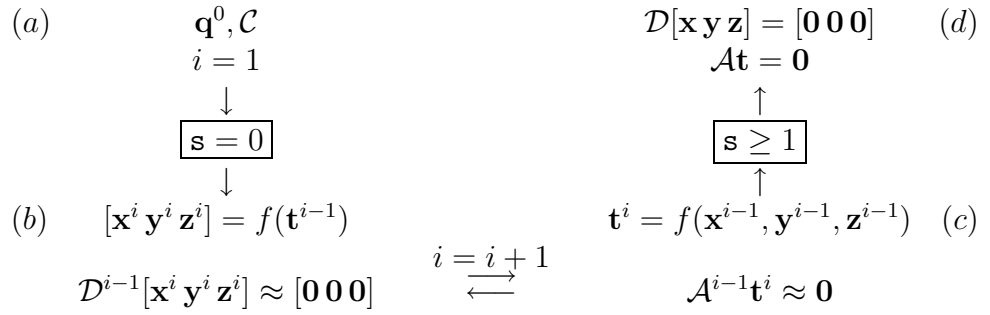

Fig. 5.9: Main equations of the proposed form-finding procedure : (a) Eq. (5.1), the first vector of tension coefficients $\mathbf{t}^0$ is a vector of prototypes $\mathbf{q}^0 = [\pm 1 \ldots \pm 1]^T$; (b) Eq. (5.5) and Eq. (5.6) approximate the coordinates as a function of tension coefficients; (c) Eq. (5.8) and Eq. (5.10) approximate the tension coefficients as a function of coordinates; (d) coordinates and tension coefficients that create at least one state of self-stress, see Eq. (2.4), Eq. (2.5) and Eq. (2.6)

Most of the lines, from 5 to 27, are employed to approximate the coordinates as a function of a vector of tension coefficients. Coordinates which approximate a state of self-equilibrium. After the Schur decomposition, in line 5, eigenvectors are accessible but only a few of them are used for the rest of calculations, see lines 6-8. This pre-selection narrows the search[1] space for the selection of potential coordinates. Both zero and negative eigenvalues are selected, i.e. line 6, for the potential coordinates. This reduced set, $\tilde{\mathcal{U}}$, has the potential nullspace for the basis of nodal coordinates. The procedure takes at least $\mathtt{d} + 1 = 4$ columns, independently on whether or not the current nullity is four; here this nullity refers to 3D structures.

Projected lengths, $\mathcal{C}\tilde{\mathcal{U}}$, are factorised as $\mathcal{QR}$ in line 10, see Eq. (5.4). A norm-2 is then calculated for every column vector, see lines 11-12, and indices minimising this norm are calculated in line 13, see Eq. (5.5). Indices corresponding to norm zero, i.e. the $\mathbf{1}$-vector, are discarded. Using this list of valid indices, the first triplet of linearly independent, consecutive eigenvectors in $\tilde{\mathcal{U}}$, is chosen, see lines 16-24.

From coordinates to tension coefficients

A set of approximated coordinates, line 27, is used to compute the equilibrium matrix $\mathcal{A}$ in line 28, see Eq. (2.4). A singular value decomposition of $\mathcal{A}$ gives access to the singular vectors of mechanisms and tension coefficients, Eq. (5.7). If the singular values of $\mathcal{V}$ follow the sequence $[\sigma_{max} \ldots \sigma_{min}]$, the rightmost singular vector from matrix $\mathcal{W}$ approximate a vector of tension coefficients such that $\mathcal{A}\mathbf{t} \approx \mathbf{0}$. This vector, however, might not match our selected signs, $sgn(\mathbf{t}) \neq sgn(\mathbf{q}^0)$. The procedure does therefore calculate a least square

[1] A reader might notice that indices $\{i, j, k\}$ of selected eigenvectors $\{\mathbf{u}_i, \mathbf{u}_j, \mathbf{u}_k\} \in \mathcal{U}$, see Eq. (5.2), could be used to get $\mathbf{t}$ without computing the sigular value decomposition of the equilibrium matrix $\mathcal{A}$. It is sufficient to force a rank reduction in $\mathcal{D}$ as follows: $\mathcal{V}_{ii} = 0$,$\mathcal{V}_{jj} = 0$, $\mathcal{V}_{kk} = 0$, and re-calculate $\hat{\mathcal{D}} = \mathcal{U}\mathcal{V}\mathcal{U}^T$. Then, the entries $\mathbf{t}_{AB} = \hat{\mathcal{D}}_{AB}$ are the tension coefficients that self-equilibrate the structure; here AB is any of the $\mathtt{b}$ segments in the structure connecting nodes A and B.

solution, Eq. (5.8), with a block of columns from the right of $\mathcal{W}$, and the prototypes $\mathbf{q}^0$, see lines 32-37.

A new vector of tension coefficients that approximates self-equilibrium is calculated in line 33, see Eq. (5.9), such that $\mathcal{A}\mathbf{t} \approx \mathbf{0}$ and $sgn(\mathbf{t}) = sgn(\mathbf{q}^0)$, in the least square sense. Finally, the procedure closes its loop, i.e. lines 39 and 4, by checking whether or not the smallest singular value of $\mathcal{A}$ is zero, which indicates a state of self-stress is found.

It is convenient to remark, however, that the final vector of tension coefficients $\mathbf{t}$ is not unique for the given structure. Other vectors $\mathbf{t}$, equally valid, may exist for the same $\mathcal{C}$ and the same signs of $\mathbf{q}^0$. In a broad context, the problem itself is ill-posed in the sense of Hadamard because: (i) a solution may not exists for $\mathcal{C}$ and $\mathbf{q}^0$, (ii) a solution is definitively not unique, several other solutions may exist with the same sign pattern $\mathbf{q}^0$, and (iii) experience gained in this dissertation is not conclusive as to assert whether or not the solution depends continuously on $\mathcal{C}$ and $\mathbf{q}^0$. For instance, Section 5.5.3 presented a truncated tetrahedron in which calculated tension coefficients are different from previously published research. A truncated tetrahedron could include extra cable elements and solutions are still found; however, including extra struts complicates the form-finding, which might not return a 3D result. Random assignments to $\mathbf{q}^0$, however preserving its same sign patter, can solve the truncated tetrahedron and result in asymmetric solutions. Thus, one could tentatively conclude that the solution depends continuously on $\mathcal{C}$ and $|\mathbf{q}^0|$, but not on $\text{sgn}(\mathbf{q}^0)$.

5.7 Complexity and convergence

The numerical form-finding procedure does compute three costly operations in each iteration: (i) a Schur decomposition for the calculation of coordinates from tension coefficients, (ii) a QR factorisation used to identify linearly-independent projected lengths, and (iii) a singular value decomposition for the calculation of tension coefficients from coordinates. The complexity of each section is shown for each operation.

Firstly, a Schur decomposition of the force density matrix $\mathcal{D} \in \Re^{\mathtt{n}\times\mathtt{n}}$ takes $O(\mathtt{n}^3)$ operations. Secondly, a QR factorisation of the set of projected lengths, $\mathcal{C}\tilde{\mathcal{U}}$, Eq. (5.4), takes $O(2\mathtt{n}^3/3)$ operations with a Householder reduction. Finally, the third operation is a singular value decomposition of the equilibrium matrix $\mathcal{A} \in \Re^{3\mathtt{n}\times\mathtt{b}}$. This third operation is the most costly because a singular value decomposition takes $O(\min(3\mathtt{nb}^2, 9\mathtt{bn}^2))$.

However, for the tensegrities analysed in this dissertation $3\mathtt{nb}^2 < 9\mathtt{bn}^2$. The number of bars easily exceeds nodes. The complexity of this step is therefore: $O(3\mathtt{nb}^2)$. Finally, since the computational effort of either Schur decomposition or QR factorisation is $O(\mathtt{n}^3) \ll O(3\mathtt{nb}^2)$, it is safe to say that the complexity of a single iteration of the numerical form-finding procedure is of order $O(3\mathtt{nb}^2)$.

This $O(3\mathtt{nb}^2)$ is the asymptotic upper bound, worst case scenario that could be reduced should sparse matrix operations be used, or in practical terms, by calculating only

the singular vector associated to the smallest singular value. The full singular value decomposition of the equilibrium matrix, $\mathcal{A} = \mathcal{U}\mathcal{V}\mathcal{W}^T$, is not useful unless the infinitesimal mechanisms, in $\mathcal{U}$, are analysed at each iteration. The singular value decomposition was selected, however, because of its stability in computing the approximation of tension coefficients.

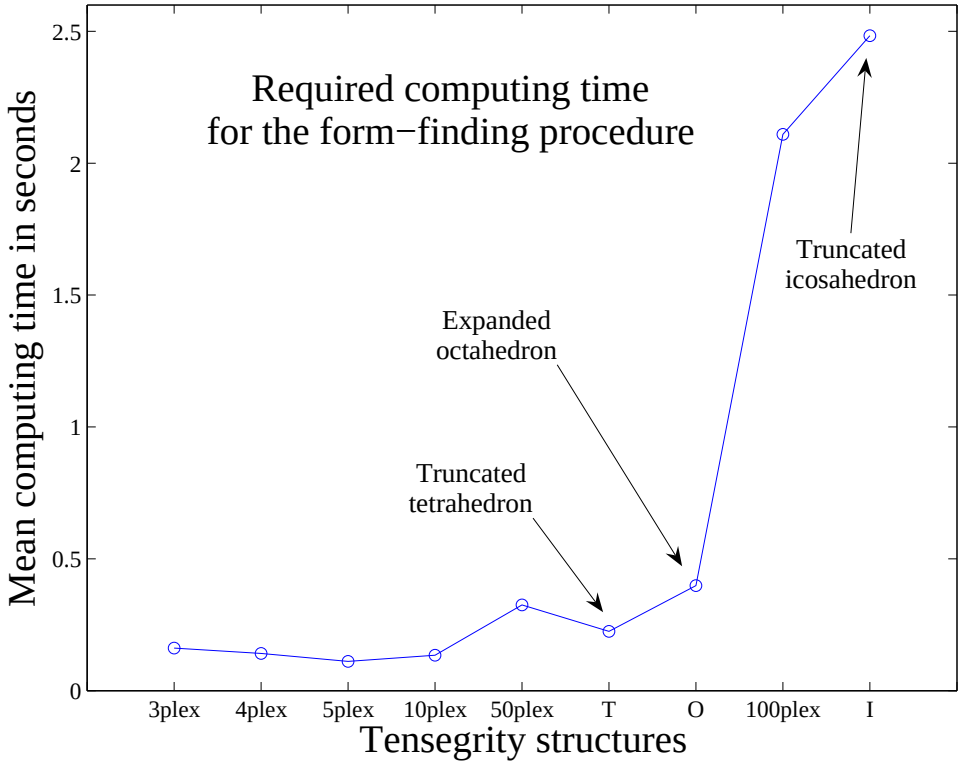

Fig. 5.10: Computing time : computing time required for the numerical form-finding procedure in a standard PC, Intel(R) XEON(TM) CPU 2.20GHz, running Matlab 7.0. Stopwatch timer functions tic and toc were used to measure the amount of time Matlab takes to complete the form-finding procedure.

The computational effort per iteration, $O(3\mathtt{n}\mathtt{b}^2)$, should be considered in view of how many iterations does the numerical procedure need to converge. The number of iterations, and hence the total computing time, may vary between 10 and 20 folds with the type of tensegrity structure, see Fig. 5.10. This figure shows the average computing time, in seconds, for ten runs of the numerical form-finding procedure over some representative tensegrity structures.

For instance, the numerical form-finding procedure requires only one iteration to solve any n-plex or 2D tensegrities. Even a larger cylinder, e.g. 50-plex with 100 nodes and 200 members, takes less computing time than the expanded octahedron with 12 nodes and 30 members. For comparable tensegrities in the number of nodes $\mathtt{n}$, the numerical procedure requires more iterations for the structures with larger number of members $\mathtt{b}$. The number of iterations for spherical tensegrities is about $O(\log(\mathtt{b}))$.

Random prototypes

It is convenient to mention complexity and $\mathbf{q}^0$, i.e. the vector of prototypes. The inclusion of some random entries in the vector of prototypes *increases* the number of iterations several folds. A simple structure, the triplex for instance, is calculated in only one iteration when the vector $\mathbf{q}^0$ consists of ± 1. However, it takes a dozen iterations to solve a triplex with a random vector $\mathbf{q}^0$; random values which however keep positive sign for cables and negative for struts. The results of this numerical experiments with random prototypes were described in Section 4.3.2. In that section only ten runs of the form-finding procedure were computed. The resulting tensegrity structures have asymmetric, i.e. all different, tension coefficients and lengths, see Table 4.1 and Table 4.2, respectively. Figure 4.2 presented examples of these geometries.

The random prototypes in $\mathbf{q}^0$ are uniformly distributed, pseudo-random numbers on the unit interval. Initial calculations have shown that randomness can be successfully included in the form-finding. As discussed in Section 4.3.2, the randomness added to vectors $\mathbf{q}^0$ produced asymmetric solutions for the tension coefficients of tensegrity cylinders. There are basically three arrangements of random numbers r for c cables and s struts in a vector of prototypes $\mathbf{q}^0$:

$$
\begin{aligned}
\mathbf{q}^0{}_1 &= [\underbrace{r_1\, r_2\, \ldots\, r_c}_{random}\, -1\, -1\, \ldots\, -1], \\
\mathbf{q}^0{}_2 &= [+1\, +1\, \ldots\, +1\, \underbrace{-r_1\, -r_2\, \ldots\, -r_s}_{random}], \\
\mathbf{q}^0{}_3 &= [\underbrace{r_1\, r_2\, \ldots\, r_c}_{random}\, \underbrace{-r_{c+1}\, -r_{c+2}\, \ldots\, -r_{c+s}}_{random}].
\end{aligned}
$$

Larger calculations, 1000 runs for each of the three assignments, of a tripex with random prototypes give the following median values:

1. $q = 1$ for cables, $q = 1.781$ for bracing cables, and $q = -1.79$ for struts when $\mathbf{q}^0{}_1$ is used; convergence in 12 iterations;
2. $q = 1$ for cables, $q = 1.725$ for bracing cables, and $q = -1.735$ for struts when $\mathbf{q}^0{}_2$ is used; convervence in 10 iterations; in about 11-12 iterations; and
3. $q = 1$ for cables, $q = 1.894$ for bracing cables, and $q = -1.869$ for struts when $\mathbf{q}^0{}_3$ is used; convergence in 13 iterations.

Notice *median* and not mean values are reported. Median values are the 50% percentile of sample, or 2nd quartile, and are good estimations of the center of sample data. The median is robust to outliers. Recall the exact solution: $q = 1$ for cables, and $q = \sqrt{3} = 1.732$ for bracing cables and struts. A larger calculation (100000 runs) with $\mathbf{q}^0{}_3$, the one

which has higher deviation from the theoretical value, shows: $q = 1$ for cables, $q = 1.787$ for bracing cables, and $q = -1.761$ for struts; values which are closer to $\sqrt{3}$ but exhibit the same pattern $q_b > |q_s|$.

The numerical form-finding procedure takes slighly more time to calculate a triplex with ${\mathbf{q}^0}_3$. That is, the more random entries in $\mathbf{q}^0$ the longer the convergence. The difference between 10 to 13 iterations is not so dramatic in this example, but more complicated structures might not converge at all with such a random prototypes.

New configurations can be created with the numerical procedure and random entries in $\mathbf{q}^0$. The numerical simulation of lengths and forces in novel asymmetric tensegrity structures might give a clue of the confidence intervals and manufacturing tolerances relevant to the design of tensegrity structures. This class of numerical form-finding is new and opens several research directions. However, new opportunities also bring new challenges: the current form-finding procedure shows that randomness in $\mathbf{q}^0$ increases the computing time and hampers the convergence. Notice that the numerical procedure might not converge to valid 3D structures when random assignments of signs are placed. Other tensegrity structures might not follow the same pattern, and sections of the numerical algorithm may need to be revised to improve the convergence in presence of random vectors $\mathbf{q}^0$, and avoid collisions between segments. This extension is however left for future work.

5.8 Numerical example

This section shows a numerical example in which the main matrices and vectors are calculated for a small tensegrity structure. The principal calculations are presented as outputs from Matlab 7.0. The example chosen is the expanded octahedron, discussed in Section 5.5. Its form-finding is rather simple and consists of two different tension coefficients: $q_c = 1$ and $q_s = -3/2$ for 24 cables and 6 struts, respectively. To start with, the vector $\mathbf{q}^0 \in \Re^{30}$ of prototypes is, $\mathbf{q}^0 = [+1\,,\,\ldots\,,\,+1\,,\,-1\,,\,-1\,,\,-1\,,\,-1\,,\,-1\,,\,-1\,]^T$, for the $\mathtt{b} = 30$ members of this structure. The example shows, for simplicity, prototypes ordered in a continuous way such that $\mathbf{q}^0$ has 24 cables $(+1)$ and then 6 struts (-1). It is important to remark one feature of $\mathbf{q}^0$ for the expanded octahedron. The tension coefficients in cables are actually solved, by coincidence in this small example, with the vector of prototypes. The solution $q_c = 1$ is already set in the vector $\mathbf{q}^0$ of prototypes. Therefore, only six tension coefficients, struts q_s, have to be determined.

Next, the incidence matrix, $\mathcal{C} \in \Re^{30\times 12}$, of the expanded octahedron relates the $\mathtt{b} = 30$ members to $\mathtt{n} = 12$ nodes:

$$\mathcal{C} = \begin{bmatrix}
1 & 0 & 0 & 0 & 0 & -1 & 0 & 0 & 0 & 0 & 0 & 0 \\
1 & 0 & 0 & 0 & 0 & 0 & -1 & 0 & 0 & 0 & 0 & 0 \\
1 & 0 & 0 & 0 & 0 & 0 & 0 & 0 & -1 & 0 & 0 & 0 \\
1 & -1 & 0 & 0 & 0 & 0 & 0 & 0 & 0 & 0 & 0 & 0 \\
0 & 1 & 0 & 0 & 0 & 0 & 0 & 0 & -1 & 0 & 0 & 0 \\
0 & 1 & 0 & 0 & 0 & 0 & 0 & -1 & 0 & 0 & 0 & 0 \\
0 & 1 & -1 & 0 & 0 & 0 & 0 & 0 & 0 & 0 & 0 & 0 \\
0 & 0 & 1 & 0 & 0 & 0 & 0 & -1 & 0 & 0 & 0 & 0 \\
0 & 0 & 1 & 0 & 0 & 0 & 0 & 0 & 0 & -1 & 0 & 0 \\
0 & 0 & 1 & -1 & 0 & 0 & 0 & 0 & 0 & 0 & 0 & 0 \\
0 & 0 & 0 & 1 & 0 & 0 & 0 & 0 & 0 & -1 & 0 & 0 \\
0 & 0 & 0 & 1 & 0 & 0 & 0 & 0 & 0 & 0 & -1 & 0 \\
0 & 0 & 0 & 1 & -1 & 0 & 0 & 0 & 0 & 0 & 0 & 0 \\
0 & 0 & 0 & 0 & 1 & 0 & 0 & 0 & 0 & 0 & -1 & 0 \\
0 & 0 & 0 & 0 & 1 & 0 & 0 & 0 & 0 & 0 & 0 & -1 \\
0 & 0 & 0 & 0 & 1 & -1 & 0 & 0 & 0 & 0 & 0 & 0 \\
0 & 0 & 0 & 0 & 0 & 1 & 0 & 0 & 0 & 0 & 0 & -1 \\
0 & 0 & 0 & 0 & 0 & 1 & -1 & 0 & 0 & 0 & 0 & 0 \\
0 & 0 & 0 & 0 & 0 & 0 & 1 & -1 & 0 & 0 & 0 & 0 \\
0 & 0 & 0 & 0 & 0 & 0 & 1 & 0 & 0 & 0 & -1 & 0 \\
0 & 0 & 0 & 0 & 0 & 0 & 0 & 1 & 0 & 0 & -1 & 0 \\
0 & 0 & 0 & 0 & 0 & 0 & 0 & 0 & 1 & -1 & 0 & 0 \\
0 & 0 & 0 & 0 & 0 & 0 & 0 & 0 & 1 & 0 & 0 & -1 \\
0 & 0 & 0 & 0 & 0 & 0 & 0 & 0 & 0 & 1 & 0 & -1 \\
1 & 0 & 0 & 0 & 0 & 0 & 0 & 0 & 0 & 0 & 0 & -1 \\
0 & 1 & 0 & 0 & 0 & 0 & -1 & 0 & 0 & 0 & 0 & 0 \\
0 & 0 & 1 & 0 & 0 & 0 & 0 & 0 & -1 & 0 & 0 & 0 \\
0 & 0 & 0 & 1 & 0 & 0 & 0 & -1 & 0 & 0 & 0 & 0 \\
0 & 0 & 0 & 0 & 1 & 0 & 0 & 0 & 0 & -1 & 0 & 0 \\
0 & 0 & 0 & 0 & 0 & 1 & 0 & 0 & 0 & 0 & -1 & 0
\end{bmatrix}.$$

Firstly, a Schur decomposition of $\mathcal{D} = \mathcal{U}\mathcal{V}\mathcal{U}^T$, Eq. (5.2), is employed to obtain the basis of coordinates. Matrix $\mathcal{D}$ has nullity one, and as such it does not fulfil Eq. (2.7). The valid nullity for a solid or 3D structure is four. It is therefore necessary to take at least $\mathtt{d}+1 = 4$ eigenvectors of $\mathcal{U}$. If the diagonal matrix $\mathcal{V}$ has eigenvalues $[-\lambda_{min} \ldots 0 \ldots \lambda_{max}]$, the candidate eigenvectors are situated in the leftmost columns of $\mathcal{U}$.

In this example, these eigenvectors correspond to the first four smallest eigenvalues: 0.0, 0.7639, 0.7639 and 0.7639. This will be the tentative nullspace $\tilde{\mathcal{U}}$ from which the coordinates are selected. A more detailed exploration of the four column vectors shows that one, i.e. corresponding to the zero eigenvalue, is the $\mathbf{1}$-vector. Thus, its entry is removed from the tentative nullspace with which it remains only three eigenvectors,

$$[\mathbf{x}\,\mathbf{y}\,\mathbf{z}] = \begin{pmatrix} -0.3482 & -0.0906 & -0.3472 \\ -0.2042 & 0.3991 & -0.2214 \\ 0.3029 & 0.3890 & -0.0833 \\ 0.3482 & 0.0906 & 0.3472 \\ 0.2042 & -0.3991 & 0.2214 \\ -0.3029 & -0.3890 & 0.0833 \\ 0.0701 & -0.4034 & -0.2869 \\ 0.1310 & 0.0836 & -0.4752 \\ -0.4725 & 0.1070 & 0.1238 \\ -0.0701 & 0.4034 & 0.2869 \\ 0.4725 & -0.1070 & -0.1238 \\ -0.1310 & -0.0836 & 0.4752 \end{pmatrix},$$

which are the approximated coordinates so far. The eigenvectors are linearly independent and can be plotted, see Fig. 5.11a. They give a very good visual approximation of the final shape. However, it is not in self-equilibrium, and therefore has no state of self-stress, i.e. $\mathbf{s} = 0$.

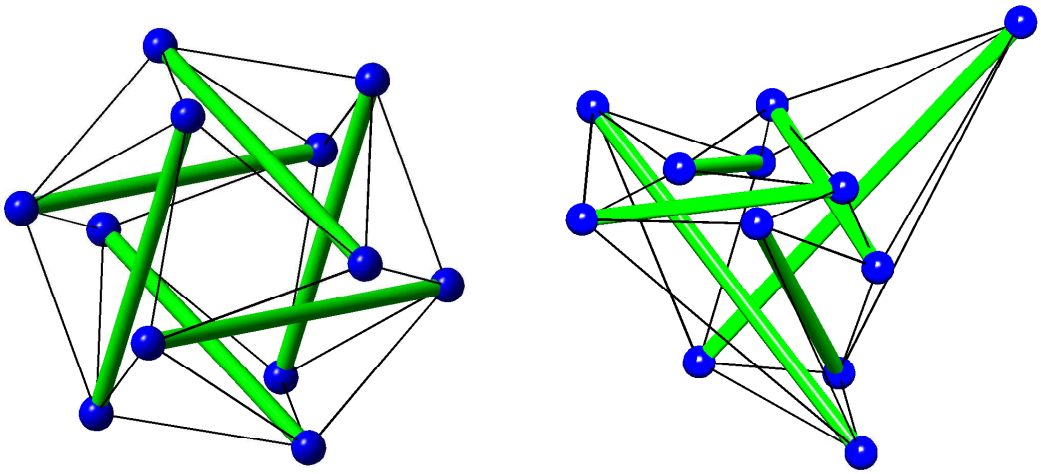

(a) (b)

Fig. 5.11: Numerical example : (a) shape of the expanded octahedron after the first iteration of the proposed numerical form-finding procedure. It has no state of self-stress yet, $\mathbf{s} = 0$, and $\mathcal{A}\mathbf{t} \neq \mathbf{0}$; (b) asymmetric expanded octahedron calculated from a random vector of prototypes $\mathbf{q}^0$.

Then, the approximated coordinates are used to calculate the equilibrium matrix, $\mathcal{A}$, see Eq. (5.7), from which the mechanisms and tension coefficients can be obtained by calculating its singular value decomposition, e.g. $\mathcal{A} = \mathcal{U}\mathcal{V}\mathcal{W}^T$. By looking at the least square solution that best fit $\mathbf{q}^0$, the block of columns has to be multiplied by $\tilde{\mathbf{t}} = -5.4194$, see Eq. (5.8). The approximated solution is found in the rightmost singular vector of $\mathcal{W}$. The approximated vector of tension coefficients, normalised such that the first element is unitary, is therefore:

Iteration	q_s	$\|\|\mathcal{A}\mathbf{t}\|\|$
1	-1.395081024	$6.321250e-01$
2	-1.478744228	$1.180807e-01$
3	-1.495737355	$2.333034e-02$
4	-1.499147007	$4.654919e-03$
5	-1.499829383	$9.305399e-04$
6	-1.499965876	$1.860902e-04$
7	-1.499993175	$3.721734e-05$
8	-1.499998635	$7.443439e-06$
9	-1.499999727	$1.488687e-06$
10	-1.499999945	$2.977373e-07$
11	-1.499999989	$5.954746e-08$
12	-1.499999998	$1.190949e-08$
13	-1.5	$2.381898e-09$
14	-1.5	$4.763800e-10$

Table 5.1: Iterations of the numerical form-finding procedure : The procedure takes 14 iterations to calculate a self-equilibrated structure with a cut-off value of 1e-10 in $||\mathcal{A}\mathbf{t}||$, and approximates q_s to its final value -3/2.

$$\mathbf{t} = [1\,,\, 1\,,\, 1\,\ldots\,,\, 1\,,\, -1.3951\,,\, -1.3951\,,\, -1.3951\,,\, -1.3951\,,\, -1.3951\,,\, -1.3951\,].$$

This vector $\mathbf{t}$ is not a valid solution. Here, the value of tension coefficients in struts is $q_s = -1.395$. It was shown in Section 5.5 that the correct solution has $q_s = -3/2$, but it is however an approximated solution such that $\mathcal{A}\mathbf{t} \approx \mathbf{0}$. In fact, the vector norm shows that is not near self-equilibrium, $||\mathcal{A}\mathbf{t}|| \approx 0.6321$.

Next iterations follow the same pattern back and forward: once an approximated vector of tension coefficients is found, approximated coordinates are then calculated. Table 5.1 shows how the tension coefficients in the six struts approximate $q_s = -3/2$, and the vector norm $||\mathcal{A}\mathbf{t}||$ approximates 1e-10 (i.e. zero).

A cut-off value for zero is set to 1e-10, which in this case means self-equilibrium: $\mathcal{A}\mathbf{t} = \mathbf{0}$. At this point, line 14 in Table 5.1, the matrix $\mathcal{A}$ is rank deficient and its right nullspace, see Eq. (5.7), contains the vector of tension coefficients that self-equilibrate the structure. Its right nullspace consists of one singular vector, assigned to $\mathbf{t}$, that creates one state of self-stress, $\mathtt{s} = 1$, up to 1e-10. In a standard PC, the numerical procedure is seen to run out of precision should this threshold be moved beyond 1e-10. If, for instance, a random vector $\mathbf{q}^0$ is assigned one could probably arrive to asymmetric shapes like Fig. 5.11b. This example ($\mathtt{s} = \mathtt{m} = 1$) shows the numerical procedure could converge to solutions in the event of random initial conditions (e.g. $\mathbf{q}^0$); however, it remains unclear whether or not asymmetric solutions can give useful confidence bounds for tension coefficients.

5.9 Conclusions and final remarks

A multi-parameter form-finding procedure for tensegrity structures is presented. Geometry and tension coefficients are iteratively computed from an incidence matrix and a vector of prototypes of member forces. The elements of this vector, $\mathbf{q}^0$, consist of unitary entries $+1$ and -1 for members in tension and compression, respectively. The conditions of a maximal rank of the force density matrix and minimal member lengths, were included in the form-finding procedure as to guide the search to one state of self-stress.

As opposed to most existing form-finding procedures, the novel procedure requires neither nodal coordinates, symmetry, element lengths, nor tension coefficients to be imposed *a priori*. This lack of assumptions leads to a versatile form-finding procedure that can calculate, for instance, (i) the expanded octahedron without assuming any tension coefficients, (ii) the truncated tetrahedron without assuming any cable lengths, (iii) the truncated icosahedron without assuming any global symmetry, and (iv) the cylindrical tensegrities without assuming any cable lengths. The numerical procedure is indeed able to calculate novel configurations.

Actually, the numerical form-finding procedure, (i) reproduces solutions obtained with techniques based on symbolic calculations, non-linear programming, dynamic relaxation and group theory, (ii) selects configurations of minimal elastic potential energy, as well as (iii) reduces the knowledge required in the design process to ± 1 depending on whether the member is in tension or compression. Previous and new structures are therefore easily handled with our proposed numerical procedure.

Moreover, the proposed form-finding procedure does not require tuning variables nor thresholds. However, it remains to study in greater detail structures with multiple state of self-stress. It seems to be possible the application of the proposed form-finding procedure to topology optimisation problems in which not only $+1$ and -1 entries are allowed but also 0. The form-finding procedure could be adapted to support zero entries in the vector of prototypes, Eq. (5.1). A zero could identify a member which is neither in tension nor compression and it could be eliminated from the design. Finally, it has been observed that other configurations can be found by using non-unitary (but still signed) entries in the vector of prototypes $\mathbf{q}^0$. The extension to fully exploit, i.e. asymmetric solutions, such a vectors is however largely unexplored and it is regarded as an interesting research direction for future work.

Chapter 6

Conclusions and final remarks

6.1 Analytical form-finding

A form-finding procedure and a comprehensive analysis of cylindrical tensegrity structures (n-plexes), in which the circular faces are composed of either convex or star polygons, have been presented. The circular faces consist of polygons created by connecting every j-th node lying on their circumference. The analysis is done based on tension coefficients, and enables, for the first time, to address the following issues at once:

(i) express the solution for an arbitrarily large n-plex;

(ii) calculate symmetric, asymmetric, and star-like cylinders;

(iii) count and enumerate equivalent configurations for an arbitrarily large n-plex;

(iv) relate geometrical change of equivalent configurations to strain energy;

(v) explore the asymptotic behaviour of member forces and lengths for large n.

For cylinders with equal circular faces, our solution agrees with previous studies. It was found that global rigidity is basically the principle of least action or Castigliano's theorem of least work: in the analysis of a tensegrity cylinder of order n, the strain energy $U^{n,j}$ takes its least value in the ground state $j = 1$. The other configurations $1 < j < n/2$, which all satisfy the equilibrium equations, would require additional force to maintain their momentary equilibrium. That is why the quadratic form has a stationary point but not an extremum, i.e., it has positive and negative eigenvalues for $j > 1$. Therefore, the mathematical concept of global rigidity, in the context of tensegrity cylinders, can be directly related to the mechanical concept of stable equilibrium: favour a configuration that takes its least value in the elastic strain energy.

The analytical form-finding investigation leads to novel results because of the flexibility that tension coefficients give to the equilibrium equations. However, the form-finding

of cylinders with non-equal circular faces is not new because it can be calculated with twisting angles. The benefits of studying cylindrical tensegrity structures with tension coefficients outweigh the difficulties in calculating them, for they help to:

(i) characterise the geometry as star-like cylinders or hollow cylinders because of the use of star and convex polygons;

(ii) count all equivalent solutions for an arbitrary n-plex;

(iii) enumerate all valid star-like cylinders;

(iv) count the crossings that tensile members create in the circular faces of star-like cylinders;

(v) count the negative eigenvalues that appear in force density matrices obtained from star-like cylinders.

Tension coefficients also allow the calculation of both forces and lengths per member, which are important components for the elastic strain energy. Global equilibrium can be therefore analytically calculated. The key factor is the form-finding under the formalism of tension coefficients. All these results would not be easy to calculate from solutions expressed as twisting angles or strut-to-cable length ratios. On the other hand, since the force density matrix is basically the Laplacian matrix of a weighted graph, a graph-theoretical study of its eigenvalues is of utmost interest. Thus, spectral graph theory for tensegrity structures is regarded as an interesting research direction.

6.2 Numerical form-finding

As opposed to existing form-finding procedures, our procedure requires neither nodal coordinates, symmetry, element lengths, nor tension coefficients to be imposed *a priori*. This lack of assumptions leads to a versatile form-finding procedure that can calculate, for instance:

(i) two-dimensional and three-dimensional tensegrity structures;

(ii) cylindrical tensegrities without assuming any cable lengths or a reduced number of different tension coefficients;

(iii) asymmetric cylindrical tensegrity structures;

(iv) a truncated tetrahedron without assuming any cable lengths;

(v) a expanded octahedron without assuming any number of different tension coefficients;

(vi) a truncated icosahedron without assuming any global symmetry.

It has been shown that the proposed matrix algorithm supports and confirms our initial hypothesis on the possible reduction of assumptions on form-finding methods. The form-finding procedure was used to verify some well-known results on tensegrity structures and also to refute the assumptions found on the truncated tetrahedron. In particular, the numerical investigations produced a form-finding method that is able to:

(i) reproduce solutions obtained with techniques based on time-consuming symbolic calculations, twisting angles, nonlinear programming, dynamic relaxation, and group theory;

(ii) select configurations of minimal elastic potential energy;

(iii) reduce the knowledge required in the design process to ± 1 depending on whether the member is in tension or compression.

After interpreting the results of both analytical and numerical form-finding methods, the results seem encouraging. The results have been validated with the existing literature and our calculations reproduce or improve well-known tensegrity structures. The numerical results are quite favourable and invalidate some time-consuming and constrained form-finding methods. Previous and new structures, in two dimensions and three dimensions, are therefore easily handled with our proposed numerical procedure.

The key point, from which the numerical form-finding method was devised, is the approximated solution found within the unitary matrices obtained from the factorisation of equilibrium matrices and force density matrices. The iterative process is a stepwise refinement that approximates a solution till a state of self-stress is found. Approximated solutions are calculated by introducing a tool, a vector of prototypes of tension coefficients, which only assigns the sign of member forces. The force density matrix is thus uncommitted on the final form with which the geometry converges.

6.3 Limitations and opportunities

There are drawbacks and limitations involved in any form-finding methods, and our analytical and numerical ones are no exception. First of all, the help received by using tension coefficients is paid with no control on member lengths or axial stiffnesses.

This is undoubtedly a drawback that can be remedied in post processing steps, which unfortunately were not covered in this dissertation. Our form-finding investigations used the basic equations of tension coefficients, in which a designer has no control on lengths and stiffnesses, and neglect dead loads. However, there are extensions that overcome these limitations, e.g. [92], and other techniques can use an initial geometry calculated with our form-finding methods to obtain fine details in subsequent analysis of geometric non-linear structures, e.g. [117].

The analytical form-finding method cannot easily be re-formulated to obtain solutions in which all tension coefficients are different from each other. This fact leads us to rely on numerical approximations. It would be interesting to have a procedure that calculates, either analytically or numerically, the bounds for this tolerance or sensitivity to flaws of tension coefficients. Also, the numerical form-finding method heavily relies on the "correctness" of the nodal connectivity, which might not be always right. The numerical procedure does not force an arbitrary structure to have a *meaningful* state of self-stress. Normally, if a random connectivity matrix is introduced, the form-finding process ends in two dimensions when three dimensions were required, or maps all nodes to a single point if two dimensions was requested. This is the principle of Garbage In, Garbage Out in action; but nevertheless a good starting point for random networks.

This is of course a problem of input data. In many designs, however, a topology optimisation step that deletes or adds structural members might be required; hence, it might guide the form-finding procedure to interesting structures. There are many ideas about coupling topology optimisation with the numerical form-finding method, which, however, have not been studied so far. The numerical form-finding method can be a starting point to the above-mentioned topology optimisation loop. It has the potential to free the designer from another parameter.

Finally, in a general setting, the basis of the numerical form-finding method could help other researchers in diverse fields. The numerical procedure searches for a geometry and tension coefficients that self-equilibrate a closed system subject to pointwise attractions and repulsions. Basic equations like the force density matrix, equilibrium matrix, and rank conditions are present in a variety of fields. It is therefore expected that the research presented here sheds light on numerical procedures devised for similar problems in other fields, such as rigidity percolation, molecular conformation, protein flexibility, or the determination of filament forces in cellular tensegrity models.

Bibliography

[1] S. Adriaenssens and M. Barnes. Tensegrity spline beam and grid shell structures. *Engineering Structures*, 23(1):29–36, 2001.

[2] J. B. Aldrich. *Control synthesis for a class of light and agile robotic tensegrity structures*. PhD thesis, University of California, San Diego, 2004.

[3] J. B. Aldrich and R. E. Skelton. Control/structure optimization approach for minimum-time reconfiguration of tensegrity systems. In R. C. Smith, editor, *Smart Structures and Materials 2003*, volume 5049, pages 448–459, San Diego, 2003. SPIE.

[4] J. B. Aldrich, R. E. Skelton, and K. Kreutz-Delgado. Control synthesis for a class of light and agile robotic tensegrity structures. In *Proceedings Of The 2003 American Control Conference*, pages 5245–5251, 2003.

[5] F. J. Alenghat, S. M. Nauli, R. Kolb, J. Zhou, and D. E. Ingber. Global cytoskeletal control of mechanotransduction in kidney epithelial cells. *Experimental Cell Research*, 301(1):23–30, 2004.

[6] M. Arsenault and C. Gosselin. Dynamic simulation of a spatial 3-DOF tensegrity mechanism. *Transactions of the Canadian Society for Mechanical Engineering*, 29(4):491–505, 2005.

[7] M. Arsenault and C. M. Gosselin. Kinematic, static, and dynamic analysis of a planar one-degree-of-freedom tensegrity mechanism. *Journal of Mechanical Design*, 127(6):1152–1160, 2005.

[8] S. Beer. On suicidal rabbits: A relativity of systems. *Systemic Practice and Action Research*, 3(2):115 – 124, 1990.

[9] S. Beer. *Team Tensegrity*. Wiley, New York, 1991.

[10] S. Beer. Origins of team syntegrity. In R. Espejo and M. Schwaninger, editors, *Corporate Effectiveness through Management Cybernetics*. Campus Verlag, Frankfurt, 1993.

[11] S. Behling, D. Braun, A. Fuchs, P. Seger, T. Stark, and T. Volz. Neue Baumaterialien der Zukunft. *Wechsel Wirkungen : Jahrbuch aus Lehre und Forschung der Universität Stuttgart*, 2004:16–28, 2004.

[12] N. Ben Kahla and K. Kebiche. Nonlinear elastoplastic analysis of tensegrity systems. *Engineering Structures*, 22(11):1552–1566, 2000.

[13] S. Beslin and V. de Angelis. The minimal polynomials of $sin(2\pi/p)$ and $cos(2\pi/p)$. *Mathematics magazine*, 77:146–149, 2004.

[14] N. Biggs. *Algebraic graph theory.* Cambridge Mathematical Library. Cambridge University Press, 1993.

[15] B. Bollobás. *Modern graph theory*, volume 184 of *Graduate texts in Mathematics.* Springer-Verlag, New York, 1998.

[16] M. Bouderbala and R. Motro. Folding tensegrity systems: Six strut modules and their assemblies. In S. Pellegrino and S. Guest, editors, *IUTAM-IASS Symposium On Deployable Structures: Theory And Applications*, volume 80, pages 27–36. Kluwer Academic Publishers, 2000.

[17] R. Bradshaw, D. Campbell, M. Gargari, A. Mirmiran, and P. Tripeny. Special structures: Past, present, and future. *Journal of Structural Engineering-ASCE*, 128(6):691–709, 2002.

[18] H. A. Buchholdt, M. Davies, and M. J. L. Hussey. The analysis of cable nets. *Journal of Applied Mathematics*, 4(4):339–358, 1968.

[19] J. Cabrera. Controlling instability with delayed antagonistic stochastic dynamics. *Physica A-Statistical Mechanics & its Applications*, 356(1):25–30, 2005.

[20] C. Calladine. Buckminster Fuller's 'tensegrity' structures and Clerk Maxwell's rules for the construction of stiff frames. *International Journal of Solids and Structures*, 14(2):161–172, 1978.

[21] C. Calladine and S. Pellegrino. Further remarks on first-order infinitesimal mechanisms. *International Journal of Solids and Structures*, 29(17):2119–2122, 1992.

[22] C. R. Calladine and S. Pellegrino. First-order infinitesimal mechanisms. *International Journal of Solids and Structures*, 27(4):505–515, 1991.

[23] D. M. Campbell, D. Chen, and P. Gossen. Design experience with nonlinear tension based systems: tents, trusses and tensegrity. Technical report, Geiger Engineers, 2005.

[24] D. M. Campbell, D. Chen, P. A. Gossen, and K. P. Hamilton. Tensioned fabric membrane roofs for "tensegrity" domes. In M. Sanayei, editor, *13th Structures Congress. Restructuring: America And Beyond*, pages 302–305, New York, 1995. ASCE.

[25] P. Cañadas, D. Isabey, C. Oddou, and S. Wendling. Time response of a viscoelastic tensegrity model to approach cell dynamical response. *Archives Of Physiology And Biochemistry*, 108:170–170, 2000.

[26] P. Cañadas, V. M. Laurent, P. Chabrand, D. Isabey, and S. Wendling-Mansuy. Mechanisms governing the visco-elastic responses of living cells assessed by foam and tensegrity models. *Medical Biological Engineering and Computing*, 41(6):733–739, 2003.

[27] P. Cañadas, V. M. Laurent, C. Oddou, D. Isabey, and S. Wendling. A cellular tensegrity model to analyse the structural viscoelasticity of the cytoskeleton. *J Theor Biol*, 218(2):155–173, Sep 2002.

[28] W. B. Carlson, D. Williams, and R. E. Newnham. Piezotensegritic structures for transducer applications. *Materials Research Innovations*, 3(3):175–178, 1999.

[29] D. L. D. Caspar and A. Klug. Physical principles in the construction of regular viruses. In *Cold Spring Harbor Symposia on Quantitative Biology*, volume XXVII, pages 1–24, 1962.

[30] C. A. Castigliano. Accademia delle scienze di torino. http://www.torinoscienza.it.

[31] C. A. Castigliano. Intorno al sistemi elastici. Master's thesis, Dissertazione presentata alla R. Scuola di Applicazione per gli Ingegneri in Torino per ottenere il diploma di laurea in ingegneria, 1873.

[32] C. A. Castigliano. Nuova teoria intorno all'equilibrio dei sistemi elastici. *Atti della R. Accademia delle Scienze di Torino*, 11:127–286, 1875.

[33] W. Chan. *Tensegrity minimal mass design, control and experiments*. PhD thesis, University Of California, San Diego, 2005.

[34] W. L. Chan, D. Arbelaez, F. Bossens, and R. E. Skelton. Active vibration control of a three-stage tensegrity structure. In *Smart Structures and Materials 2004*, volume 5386, pages 340–346. SPIE, 2004.

[35] W. L. Chan, S. Solari, and R. E. Skelton. Shape control of tensegrity plate: an experimental study. In *Proceedings of the ASME Aerospace Division 2004*, pages 63–68, 2004.

[36] J. E. Charalambides. *Computer method for the generation of the geometry of tensegrity structures*. PhD thesis, University of Texas at Austin, 2004.

[37] T. M. Charlton. Maxwell, jenkin and cotterill and the theory of statically-indeterminate structures. *Notes and Records of the Royal Society of London*, 26(2):233–246, 1971.

[38] T. M. Charlton. *A history of theory o f structures in the nineteenth century*. Cambridge University Press, Cambridge, 1982.

[39] T. M. Charlton. Least work theory according to menabrea, castigliano, and fränkel. *The Structural Engineer*, 62(11):345–347, 1984.

[40] T. M. Charlton. Contributions to the theory of frameworks by o. henrici and m. w. crofton. *Engineering Structures*, 11:199–201, 1989.

[41] T. M. Charlton. An extension of maxwell's theory of pin-jointed frameworks by m. w. crofton, f.r.s. *Notes and Records of the Royal Society of London*, 43(1):53–56, 1989.

[42] K. Chatzis. Mécanique physique, expérimentation et tradition dans la science des constructions de j.-v. poncelet (1788-1867). In A. Becchi, M. Corradi, F. Foce, and O. Pedemonte, editors, *Towards a History of Construction*, pages 343–354. Birkhäuser Verlag, Basel, 2002.

[43] C. S. Chen and D. E. Ingber. Tensegrity and mechanoregulation: from skeleton to cytoskeleton. *Osteoarthritis & Cartilage*, 7(1):81–94, 1999.

[44] R. Chow. Structural form as morphogenetic event. Master's thesis, Carleton University, 2002.

[45] P. Cicala. Castigliano's contribution in structural analysis and the equation of virtual works. *Meccanica*, 19:15–18, 1984.

[46] R. Connelly. Rigidity and energy. *Inventiones Mathematicae*, 66(1):11–33, 1982.

[47] R. Connelly. Rigidity. In P. M. Gruber and J. M. Wills, editors, *Handbook of convex geometry*, pages 223–271. Elsevier Science Publishers, 1993.

[48] R. Connelly. Tensegrity structures: why are they stable? In M. F. Thorpe and P. M. Duxbury, editors, *Rigidity theory and applications*, pages 47–54. Kluwer Academic/Plenum Publishers, 1999.

[49] R. Connelly and A. Back. Mathematics and tensegrity. *American Scientist*, 86:142–151, 1998.

[50] R. Connelly, K. Rybnikov, and S. Volkov. Percolation of the loss of tension in an infinite triangular lattice. *Journal of Statistical Physics*, 105(1-2):143–171, 2001.

[51] R. Connelly and M. Terrell. Globally rigid symmetric tensegrities. *Topologie structurale*, 21:59–77, 1995.

[52] R. Connelly and W. Whiteley. Second-order rigidity and prestress stability for tensegrity frameworks. *SIAM Journal on Discrete Mathematics*, 9(3):453–491, 1996.

[53] J. H. Cotterill. On the equilibrium of arched ribs of uniform section. *London, Edinburgh and Dublin Philosophical Magazine, Ser. 4*, 29:380, 1865.

[54] M. Coughlin and D. Stamenovic. A tensegrity structure with buckling compression elements - application to cell mechanics. *Journal Of Applied Mechanics-Transactions Of The Asme*, 64(3):480–486, 1997.

[55] M. F. Coughlin. *The microstructural basis of cellular deformability.* PhD thesis, Boston University, 2000.

[56] M. F. Coughlin and D. Stamenovic. A tensegrity model of the cytoskeleton in spread and round cells. *Journal of Biomechanical Engineering*, 120(6):770–777, 1998.

[57] M. F. Coughlin and D. Stamenovic. A prestressed cable network model of the adherent cell cytoskeleton. *Biophysical Journal*, 84(2 Part 1):1328–1336, 2003.

[58] H. Coxeter. *Regular complex polytopes*. Cambridge University Press, 1991.

[59] H. Crapo and W. Whiteley. Statics of frameworks and motions of panel structures, a projective geometric introduction. *Topologie structurale*, 6:43–82, 1982.

[60] M. W. Crofton. On self-strained frames of six joints. *Proceedings of the London Mathematical Society*, 10:13–16, 1878.

[61] B. de Jager and R. Skelton. Input/output selection for planar tensegrity models. In *Proceedings Of The 40th IEEE Conference On Decision And Control*, pages 4280–4285. IEEE Press, 2001.

[62] B. de Jager and R. E. Skelton. Input-output selection for planar tensegrity models. *IEEE Transactions on Control Systems Technology*, 13(5):778–785, 2005.

[63] B. de Jager, R. E. Skelton, and M. Masic. Integrated control/structure design for planar tensegrity models. In *Proceedings Of The 2002 IEEE International Conference On Control Applications*, pages 862–867. IEEE Press, 2002.

[64] M. de Oliveira and R. Skelton. A new topology of tensegrity towers with uniform force distribution. In R. C. Smith, editor, *Smart structures and materials 2005*, volume 5757, pages 198–208. SPIE, May 2005.

[65] M. Defossez. Shape memory effect in tensegrity structures. *Mechanics Research Communications*, 30(4):311–316, 2003.

[66] M. Defossez. Mechanical response of a tensegrity structure close to its integrity limit submitted to external constraints. *Mechanics Research Communications*, 31(5):569–575, 2004.

[67] H. Deng and A. S. K. Kwan. Unified classification of stability of pin-jointed bar assemblies. *International Journal of Solids and Structures*, 42(15):4393–4413, 2005.

[68] M. J. Denton, P. K. Dearden, and S. J. Sowerby. Physical law not natural selection as the major determinant of biological complexity in the subcellular realm: new support for the pre-Darwinian conception of evolution by natural law. *Biosystems*, 71(3):297–303, Oct 2003.

[69] S. Djouadi, R. Motro, J. S. Pons, and B. Crosnier. Active control of tensegrity systems. *Journal of Aerospace Engineering*, 11(2):37–44, 1998.

[70] B. Domer, E. Fest, V. Lalit, and I. F. C. Smith. Combining dynamic relaxation method with artificial neural networks to enhance simulation of tensegrity structures. *Journal of Structural Engineering-ASCE*, 129(5):672–681, 2003.

[71] B. Domer, B. Raphael, K. Shea, and I. F. C. Smith. A study of two stochastic search methods for structural control. *Journal of Computing in Civil Engineering*, 17(3):132–141, 2003.

[72] B. Domer and I. Smith. An active structure that learns. *Journal of Computing in Civil Engineering*, 19(1):16–24, 2005.

[73] J. Duffy, J. Rooney, B. Knight, and C. Crane. Review of a family of self-deploying tensegrity structures with elastic ties. *Shock and Vibration Digest*, 32(2):100–106, 2000.

[74] P. M. Duxbury, D. J. Jacobs, M. F. Thorpe, and C. Moukarzel. Floppy modes and the free energy: Rigidity and connectivity percolation on bethe lattices. *Phys. Rev. E*, 59(2):2084–2092, 1999.

[75] B. Eckes, D. Dogic, E. Colucci-Guyon, N. Wang, A. Maniotis, D. Ingber, A. Merckling, F. Langa, M. Aumailley, A. Delouvee, V. Koteliansky, C. Babinet, and T. Krieg. Impaired mechanical stability, migration and contractile capacity in vimentin-deficient fibroblasts. *Journal of Cell Science*, 111(Part 13):1897–1907, 1998.

[76] S. El-Lishani and H. Nooshin. Investigating the statical stability of pin-jointed structures using genetic algorithm. *International Journal of Space Structures*, 20:53–68, 2005.

[77] G. G. Estrada and H.-J. Bungartz. Duality between global rigidity and minimum strain energy. In *7th World Congress on Computational Mechanics*, Los Angeles, July 2006.

[78] G. G. Estrada, H.-J. Bungartz, and C. Mohrdieck. Numerical form-finding of 2D tensegrity structures. In E. Ramm, W. A. Wall, K.-U. Bletzinger, and M. Bischoff, editors, *Proc. of the Int. Conf. on Computation of Shell and Spatial Structures*, page 278, Salzburg, June 2005. IASS/IACM.

[79] G. G. Estrada, H.-J. Bungartz, and C. Mohrdieck. On cylindrical tensegrity structures. In E. Ramm, W. A. Wall, K.-U. Bletzinger, and M. Bischoff, editors, *Proc. of the Int. Conf. on Computation of Shell and Spatial Structures*, page 281, Salzburg, June 2005. IASS/IACM.

[80] G. G. Estrada, H.-J. Bungartz, and C. Mohrdieck. Numerical form-finding of tensegrity structures. *International Journal of Solids and Structures*, 43(22-23):6855–6868, November 2006.

[81] C. M. Ewing, R. Paul, E. Chang, A. W. Partin, D. J. Krovich, D. S. Coffey, and W. B. Isaacs. Re-establishment of the cadherin-catenin pathway in the prostatic cancer cell line PC3 leads to non-tumorigenic phenotype, and reorganization of the cytoskeletal filaments: A biological model of tensegrity. *Journal of Urology*, 157:368–368, 1997.

[82] E. Fest, K. Shea, D. Domer, and I. Smith. Adjustable tensegrity structures. *Journal of Structural Engineering-ASCE*, 129(4):515–526, 2003.

[83] E. Fest, K. Shea, and I. F. C. Smith. Active tensegrity structure. *Journal of Structural Engineering-ASCE*, 130(10):1454–1465, 2004.

[84] L. Frantsevich and S. Gorb. Arcus as a tensegrity structure in the arolium of wasps (Hymenoptera : Vespidae). *Zoology*, 105(3):225–237, 2002.

[85] F. Fu. Study on the new prestressed tensegrity structure. Master's thesis, Beijing University of Technology, 2000.

[86] F. Fu. Structural behavior and design methods of tensegrity domes. *Journal of Constructional Steel Research*, 61(1):23–35, 2005.

[87] C. Galli, S. Guizzardi, G. Passeri, G. M. Macaluso, and R. Scandroglio. Life on the wire: on tensegrity and force balance in cells. *Acta Biomed Ateneo Parmense*, 76(1):5–12, Apr 2005.

[88] A. Geitmann, W. McConnaughey, I. Lang-Pauluzzi, V. Franklin-Tong, and A. Emons. Cytomechanical properties of papaver pollen tubes are altered after self-incompatibility challenge. *Biophysical Journal*, 86(5):3314–3323, 2004.

[89] A. S. P. George Oster and A. Katchalsky. Network thermodynamics. *Nature*, 234(5329):393–399, 1971.

[90] P. Gossen, D. Chen, and E. Mikhlin. The first rigidly clad "tensegrity" type dome: the Crown Coliseum, Fayetteville, North Carolina. Technical report, Geiger Engineers, 2005.

[91] J. Graver, B. Servatius, and H. Servatius. *Combinatorial rigidity*, volume 2 of *Graduate Studies in Mathematics*. American Mathematical Society, 1993.

[92] L. Gründig, E. Moncrieff, P. Singer, and D. Ströbel. A history of the principal developments and applications of the force density method in germany 1970-1999. In *Fourth International Colloquium on Computation of Shell & Spatial Structures*, Chania-Crete, Greece, June 2000. IASS-IACM.

[93] S. Guest. The stiffness of prestressed frameworks: A unifying approach. *International Journal of Solids & Structures*, 43(3-4):842–854, 2006.

[94] T. Havel. Distance geometry: theory, algorithms and chemical applications. In P. von Ragué Schleyer, editor, *Encyclopedia of computational chemistry*, pages 723–742. John Wiley & Sons, 1998.

[95] J. Heyman. Truesdell and the history of the theory of structures. In A. Becchi, M. Corradi, F. Foce, and O. Pedemonte, editors, *Essays on the history of mechanics*, pages 9–19. Birkhäuser Verlag, Basel, 2003.

[96] L. A. Hinrichs. Prismic tensigrids. *Topologie structurale*, 9:3–14, 1984.

[97] D. Ingber. Cellular tensegrity: defining new rules of biological design that govern the cytoskeleton. *Journal Of Cell Science*, 104:613–627, 1993.

[98] D. Ingber. In search of cellular control: Signal transduction in context. *Journal of Cellular Biochemistry (Suppl.)*, 30-31(Suppl 30-31):232–237, 1998.

[99] D. E. Ingber. Integrin signaling, cellular tensegrity, and control of angiogenesis. *FASEB Journal*, 11:A1288–A1288, 1997.

[100] D. E. Ingber. Integrins, tensegrity, and mechanotransduction. *Gravit Space Biol Bull*, 10(2):49–55, Jun 1997.

[101] D. E. Ingber. Tensegrity: the architectural basis of cellular mechanotransduction. *Annual Review of Physiology*, 59:575–599, 1997.

[102] D. E. Ingber. The architecture of life. *Sci Am*, 278(1):48–57, Jan 1998.

[103] D. E. Ingber. Biological design principles that guide self-organization, emergence, and hierarchical assembly: From complexity to tensegrity. In Y. Bar-Yam, editor, *2nd International Conference on Complex Systems. Unifying Themes In Complex Systems*, pages 269–280, 2000.

[104] D. E. Ingber. The origin of cellular life. *Bioessays*, 22(12):1160–1170, Dec 2000.

[105] D. E. Ingber. Mechanical signalling and the cellular response to extracellular matrix in angiogenesis and cardiovascular physiology. *Circulation Research*, 91(10):877–887, 2002.

[106] D. E. Ingber. Tensegrity I. Cell structure and hierarchical systems biology. *Journal of Cell Science*, 116(7):1157–1173, 2003.

[107] D. E. Ingber. Tensegrity II. How structural networks influence cellular information processing networks. *Journal of Cell Science*, 116(8):1397–1408, 2003.

[108] D. E. Ingber. Mechanical control of tissue morphogenesis during embryological development. *Int J Dev Biol*, 50(2-3):255–266, 2006.

[109] D. J. Jacobs, A. J. Rader, L. A. Kuhn, and M. F. Thorpe. Protein flexibility predictions using graph theory. *Proteins: Structure, Function, and Genetics*, 44:150–165, 2001.

[110] H. S. Jacoby. Recent progress in american bridge construction. *Science*, 16(392):12–22, 1902.

[111] J. E. Johnson. Functional implications of protein-protein interactions in icosahedral viruses. *PNAS*, 93(1):27–33, 1996.

[112] M. Kawaguchi, I. Tatemichi, and P. Chen. Optimum shapes of a cable dome structure. *Engineering Structures*, 21(8):719–725, 1999.

[113] H. Klimke and S. Stephan. The making of a tensegrity tower. http://www.mero.de/uploads/tx_cwtcartoongallery/tens_tower_e.pdf, 2003. MERO GmbH.

[114] B. Knight, J. Duffy, C. Crane, and J. Rooney. Innovative deployable antenna developments using tensegrity design. In *Collection Of The 41st AIAA/ASME/ASCE/AHS/ASC Structures, Structural Dynamics, And Materials Conference And Exhibit*, volume 1, pages 984–994, 2000.

[115] B. F. Knight. *Deployable antenna kinematics using tensegrity structure design*. PhD thesis, University of Florida, 2000.

[116] E. Kötter. Über die Möglichkeit, n Punkte in der Ebene oder im Raume durch weniger als $2n-3$ oder $3n-6$ Stäbe von ganz unveränderlicher Länge unverschieblich miteinander zu verbinden. In *Festschrift Heinrich Müller-Breslau*, pages 61–80. Alfred Kröner Verlag, Leipzig, 1912.

[117] A. S. K. Kwan. A new approach to geometric nonlinearity of cable structures. *Computers & Structures*, 67(4):243–252, 1998.

[118] S. M. Levin. The tensegrity-truss as a model for spine mechanics: biotensegrity. *Journal of Mechanics in Medicine and Biology*, 2(3-4):375–388, 2002.

[119] M. Levy, W. Terry, and T. F. Jing. Hypar tensegrity dome construction methodology. In *International Congress on Innovative Large Span Structures : Concept, Design, Construction*, pages A148–A156, Montréal, 1992. Canadian Society of Civil Engineering.

[120] K. Liapi. A visualization method for the morphological exploration of tensegrity structures. In *International Conference on Information Visualisation*, pages 523–528, 2001.

[121] K. A. Liapi. Geometry in architectural engineering education revisited. *Journal of Architectural Engineering*, 8(3):80–88, 2002.

[122] K. A. Liapi and J. Kim. A parametric approach to the design of vaulted tensegrity networks. *International Journal of Architectural Computing*, 2:245–262, 2004.

[123] K. Linkwitz and H.-J. Schek. Einige bemerkungen zur berechnung von vorgespannten seilnetzkonstruktionen. *Ingenieur-Archiv*, 40:145–158, 1971.

[124] D. Liu, M. S. Wang, Z. X. Deng, R. Walulu, and C. D. Mao. Tensegrity: Construction of rigid DNA triangles with flexible four-arm DNA junctions. *Journal of the American Chemical Society*, 126(8):2324–2325, 2004.

[125] R. H. Luchsinger, M. Pedretti, and A. Reinhard. Pressure induced stability: from pneumatic structures to Tensairity©. *Journal of Bionics Engineering*, 1(3):141–148, 2004.

[126] H. Luo and T. R. Bewley. Design, modeling, and optimization of compliant tensegrity fabrics for the reduction of turbulent skin friction. In R. C. Smith, editor, *Smart Structures and Materials 2003*, volume 5049, pages 460–470, San Diego, 2003. SPIE.

[127] H. X. Luo and T. R. Bewley. Accurate simulation of near-wall turbulence over a compliant tensegrity fabric. In R. C. Smith, editor, *Smart Structures and Materials 2005*, volume 5757, pages 184–197. SPIE, 2005.

[128] I. Martinez-Ramos, A. Maya-Mendoza, P. Gariglio, and A. Aranda-Anzaldo. A global but stable change in HeLa cell morphology induces reorganization of DNA structural loop domains within the cell nucleus. *Journal of Cellular Biochemistry*, 96(1):79–88, 2005.

[129] M. Masic. *Design, optimization, and control of tensegrity structures*. PhD thesis, University of California, San Diego, 2004.

[130] M. Masic and R. Skelton. Path planning and open-loop shape control of modular tensegrity structures. *Journal of Guidance Control & Dynamics*, 28(3):421–430, 2005.

[131] M. Masic and R. E. Skelton. Open-loop control of class-2 tensegrity towers. In R. C. Smith, editor, *Smart Structures And Materials 2004*, volume 5383, pages 298–308, San Diego, 2004. SPIE.

[132] M. Masic and R. E. Skelton. Optimization of class 2 tensegrity towers. In A. B. Flatau, editor, *Smart Structures and Materials 2004*, volume 5390, pages 163–174, San Diego, 2004. SPIE.

[133] L. F. Menabrea. Nouveau principe sur la distribution des tensions dans les systèmes élastiques. *Comptes Rendus hebdomadaires des séances de l'Académie de Sciences de Paris*, 46:1056–1060, 1858.

[134] M. V. Menshikov, K. A. Rybnikov, and S. E. Volkov. The loss of tension in an infinite membrane with holes distributed according to a poisson law. *Advances in Applied Probabability*, 34(2):292–312, 2002.

[135] R. Merris. Laplacian matrices of graphs : a survey. *Linear Algebra and its Applications*, 197/198:143–176, 1994.

[136] C. D. Meyer. *Matrix analysis and applied linear algebra*. SIAM, 2000.

[137] O. C. Mohr. Beitrag zur theorie des fachwerkes. *Der Civilingenieur*, 31:289–310, 1885.

[138] K. W. Moored, S. A. Taylor, and H. Bart-Smith. Optimization of a tensegrity wing for biomimetic applications. In Y. Matsuzaki, editor, *Smart Structures and Materials 2006*, volume 6173, page 617313, San Diego, 2006. SPIE.

[139] R. Motro. Forms and forces in tensegrity systems. In H. Nooshin, editor, *Proceedings of the 3rd International Conference on Space Structures,*, pages 180–185. Elsevier, 1984.

[140] R. Motro. Tensegrity systems and geodesic domes. *International Journal of Space Structures*, 5(3/4):341–351, 1990.

[141] R. Motro. Tensegrity systems: the state of the art. *International Journal of Space Structures*, 7(2):75–82, 1992.

[142] R. Motro. *Tensegrity: Structural systems for the future*. Kogan Page Science, London, 2003.

[143] R. Motro and V. Raducanu. Tensegrity systems. *International Journal of Space Structures*, 18:77–84, 2003.

[144] H. F. B. Müller-Breslau. Zur frage der kennzeichen statisch bestimmter, stabiler fachwerke. *Schweizerische Bauzeitung*, V(4):19, 1885.

[145] H. Murakami. Static and dynamic analyses of tensegrity structures. II. Quasi-static analysis. *International Journal of Solids and Structures*, 38(20):3615–3629, 2001.

[146] H. Murakami and Y. Nishimura. Initial shape finding and modal analyses of cyclic right-cylindrical tensegrity modules. *Computers & Structures*, 79(9):891–917, 2001.

[147] H. Murakami and Y. Nishimura. Static and dynamic characterization of regular truncated icosahedral and dodecahedral tensegrity modules. *International Journal of Solids & Structures*, 38(50-51):9359–9381, 2001.

[148] C. L. M. H. Navier. *Résumé des leçons données a l'École Royale des Ponts et Chaussées, sur l'application de la mécanique a l'etablissement des constructions et des machines. Première partie.* Firmin Didot, Paris, 1826.

[149] M. Nestorovic. Analysis of the properties of integrally tensioned tensegrity domes. *Space Structures*, 1(4):1008–1016, 1993.

[150] K. Obara, K. Nobe, H. Nobe, M. S. Kolodney, P. De Lanerolle, and R. J. Paul. Effects of microtubules and microfilaments on [Ca2+](i) and contractility in a reconstituted fibroblast fiber. *American Journal of Physiology - Cell Physiology*, 279(3):C785–C796, 2000.

[151] R. Olfati-Saber and R. Murray. Graph rigidity and distributed formation stabilization of multi-vehicle systems. In *Conference on Decision and Control*. IEEE, 2002.

[152] C. Paul, M. Bellotti, S. Jezernik, and A. Curt. Development of a human neuromusculo-skeletal model for investigation of spinal cord injury. *Biological Cybernetics*, 93(3):153–170, 2005.

[153] C. Paul, H. Lipson, and F. Valero-Cuevas. Redundancy in the control of robots with highly coupled mechanical structures. In *International Conference on Intelligent Robots and Systems*, pages 802–808, 2005.

[154] C. Paul, J. W. Roberts, H. Lipson, and F. J. Valero-Cuevas. Gait production in a tensegrity based robot. In *International Conference on Advanced Robotics*, pages 216–222, 2005.

[155] R. J. Paul, P. S. Bowman, and M. S. Kolodney. Effects of microtubule disruption on force, velocity, stiffness and [Ca2+](i) in porcine coronary arteries. *American Journal of Physiology - Heart & Circulatory Physiology*, 279(5):H2493–H2501, 2000.

[156] M. Pedretti. Smart tensegrity structures for the Swiss Expo 2001. In R. O. Claus and W. B. Spillman, editors, *Smart Structures and Materials 1998*, volume 3330, pages 378–386, San Diego, 1998. SPIE.

[157] S. Pellegrino. *Mechanics of kinematically indeterminate structures.* PhD thesis, University of Cambridge, 1986.

[158] S. Pellegrino. Analysis of prestressed mechanisms. *International Journal of Solids and Structures*, 26(12):1329–1350, 1990.

[159] S. Pellegrino. Structural computations with the singular value decomposition of the equilibrium matrix. *International Journal of Solids and Structures*, 30(21):3025–3035, 1993.

[160] A. Pickering. The science of the unknowable: Stafford beer's cybernetic informatics. *Kybernetes: The International Journal of Systems & Cybernetics*, 33(3-4):499–521, 2004.

[161] J.-P. Pinaud. *Deployable tensegrity towers*. PhD thesis, University of California, San Diego, 2005.

[162] J.-P. Pinaud, M. Masic, and R. E. Skelton. Path planning for the deployment of tensegrity structures. In R. C. Smith, editor, *Smart Structures and Materials 2003*, volume 5049, pages 436–447, San Diego, 2003. SPIE.

[163] A. Pugh. *An introduction to tensegrity*. University of California Press, 1976.

[164] A. J. Rader, B. M. Hespenheide, L. A. Kuhn, and M. F. Thorpe. Protein unfolding: Rigidity lost. *PNAS*, 99:3540–3545, 2002.

[165] W. J. M. Rankine. On the mathematical theory of the stability of earth-work and masonry. *Proceedings of the Royal Society of London*, 8:60–61, 1856.

[166] D. Rastorfer. Structural gymnastics for the olympics + 2 tensegrity domes designed by geiger,david,h. *Architectural Record*, 176:128–135, 1988.

[167] P. Ribenboim. *Algebraic numbers*. John Wiley & Sons, 1972.

[168] K. Sakantamis and O. P. Larsen. The Cocoon method: a physical modelling tool for designing tensegrity systems. *International Journal of Space Structures*, 19(1):11–20, 2004.

[169] D. Y. Savio and E. R. Suryanarayan. Chebychev polynomials and regular polygons. *Amererican Mathematical Monthly*, 100:657–661, 1993.

[170] D. Schecter. Beer's "organizational tensegrity" and the challenge of democratic management. *Systemic Practice and Action Research*, 4(4):303 – 317, 1991.

[171] H.-J. Schek. The force density method for form finding and computation of general networks. *Computer Methods in Applied Mechanics and Engineering*, 3:115–134, 1974.

[172] M. Schlaich. Der Messeturm in Rostock - ein Tensegrityrekord. *Stahlbau*, 72(10):697–701, 2003.

[173] H. C. Schulitz. Das Niedersachsenstadion - die AWD-Arena. *Stahlbau*, 73(4):218 – –223, 2004.

[174] R. G. Selfridge. About some tensegrity structures. *International Journal of Space Structures*, 16(4):231–235, 2001.

[175] R. E. Skelton, R. Adhikari, J. P. Pinaud, W. L. Chan, and J. W. Helton. An introduction to the mechanics of tensegrity structures. In *Proceedings Of The 40th IEEE Conference On Decision And Control*, pages 4254–4259. IEEE Press, 2001.

[176] R. E. Skelton and F. Li. Economic sensor/actuator selection and its application to flexible structure control. In R. C. Smith, editor, *Smart Structures and Materials 2004*, volume 5383, pages 194–201, San Diego, 2004. SPIE.

[177] R. T. Skelton and C. Sultan. Controllable tensegrity: a new class of smart structures. In V. V. Varadan and J. Chandra, editors, *Smart Structures and Materials 1997*, volume 3039, pages 166–177, San Diego, 1997. SPIE.

[178] K. Snelson. Sculptures. http://www.kennethsnelson.net/.

[179] R. V. Southwell. Primary stress-determination in space frames. *Engineering*, CIX:165–168, 1920.

[180] R. V. Southwell. On the calculation of stresses in braced frameworks. *Proceedings of the Royal Society of London. Series A*, 139(839):475–507, 1933.

[181] C. Sultan. *Modeling, design, and control of tensegrity structures with applications*. PhD thesis, Purdue University, 1999.

[182] C. Sultan and R. E. Skelton. Integrated design of controllable tensegrity structures. In *ASME International Mechanical Engineering Congress and Exposition*, volume 54, pages 27–35. ASME, Fairfield, NJ, (USA), 1997.

[183] D. D. Symons, R. G. Hutchinson, and N. A. Fleck. Actuation of the kagome double-layer grid. part 1: prediction of performance of the perfect structure. *Journal of Mechanics and Physics of Solids*, 53(8):1855–1874, 2005.

[184] Syntegration©. Team syntegrity. http://www.team-syntegrity.com/.

[185] T. Tarnai. Simultaneous static and kinematic indeterminacy of space trusses with cyclic symmetry. *International Journal of Solids and Structures*, 16(4):347–359, 1980.

[186] T. Tarnai. Duality between plane trusses and grillages. *International Journal of Solids and Structures*, 25(12):1395–1409, 1989.

[187] T. Tarnai. Geodesic domes and fullerenes. *Philosophical Transactions: Physical Sciences and Engineering*, 343(1667):145–153, 1993.

[188] R. Tazzioli. Per una storia della fisica matematica italiana (1860-1880). In *Atti del XIX Congresso di Storia della Fisica e dell'Astronomia*, pages 97–107, Milano, 2000.

[189] W. R. Terry, G. A. Storm, K. M. Houghton, and W. S. Hofmeister. Building tension in buffalo. *Civil Engineering*, 67(5):40–43, 1997.

[190] A. G. Tibert. *Deployable tensegrity structures for space applications*. PhD thesis, KTH, 2002.

[191] A. G. Tibert and S. Pellegrino. Review of form-finding methods for tensegrity structures. *International Journal of Space Structures*, 18(4):209–223, 2003.

[192] L. F. Tóth. *Regular figures*, volume 48 of *International series of monographs on pure and applied mathematics*. Pergamon Press, Oxford, 1964.

[193] I. B. Turkan Haliloglu and B. Erman. Gaussian dynamics of folded proteins. *Physical Review Letters*, 79(16):3090–3093, 1997.

[194] J. J. M. van de Wijdeven and A. G. de Jager. Shape change of tensegrity structures: design and control. In *American Control Conference*, volume 4, pages 2522–2527, 2005.

[195] N. Vassart. *Recherche de forme et stabilité des systèmes réticulés autocontraints - application aux systèmes de tenségrité*. PhD thesis, l'Université Montpellier II - Sciences et Techniques du Languedoc, 1997.

[196] N. Vassart and R. Motro. Multiparametered formfinding method: Application to tensegrity systems. *International Journal of Space Structures*, 14(2):147–154, 1999.

[197] K. Volokh and O. Vilnay. Why pre-tensioning stiffens cable systems. *International Journal of Solids and Structures*, 37(13):1809–1816, 2000.

[198] K. Y. Volokh. Stability conjecture in the theory of tensegrity structures. *International Journal of Structural Stability and Dynamics*, 3(1):1–16, 2003.

[199] K. Y. Volokh and O. Vilnay. "natural", "kinematic" and "elastic" displacements of underconstrained structures. *International Journal of Solids and Structures*, 34(8):911–930, 1997.

[200] W. Whiteley. Rigidity of molecular structures: generic and geometric analysis. In M. F. Thorpe and P. M. Duxbury, editors, *Rigidity theory and applications*, pages 21–46. Kluwer Academic/Plenum Publishers, 1999.

[201] W. Whiteley. Counting out to the flexibility of molecules. *Physical Biology*, 2(4):S116–S126, 2005.

[202] Wilkinson Eyre Architects. Tensegrity bridge, National Building Museum - Washington D.C., USA. *A + U-Architecture & Urbanism*, (1):140–143, Dec 2005.

[203] X. F. Yuan and S. L. Dong. Nonlinear analysis and optimum design of cable domes. *Engineering Structures*, 24(7):965–977, 2002.

[204] J. Zhang and M. Ohsaki. Adaptive force density method for form-finding problem of tensegrity structures. *International Journal of Solids and Structures*, 43(18-19):5658–5673, 2006.

[205] J. Zhang, M. Ohsaki, and Y. Kanno. A direct approach to design of geometry and forces of tensegrity systems. *International Journal of Solids and Structures*, 43(7-8):2260–2278, 2006.

Summary

The analysis of statically indeterminate structures requires the calculation of an initial equilibrium geometry. Tensegrity structures are one of such statically indeterminate structures, with the additional constraint of holding their equilibrium configuration with the action of internal forces and without any anchorage point or external forces. The only source of balance is the state of self-stress held among tensile and compression forces. Tensegrity structures are thus statically indeterminate structures in a stable state of self-stressed self-equilibrium.

The basic problem with the modelling of statically indeterminate structures is that there is no unique solution for the forces or geometry that equilibrate a structure. This is where *form-finding* comes into play. The process of determining their three-dimensional equilibrium shape is commonly called form-finding. *Form-finding* is a branch of computational mechanics dedicated to computing the three-dimensional shape of a structure in static equilibrium, given a statically meaningful state of stress and load. Form-finding methods are useful in the search for geometries that minimise or favour certain shapes.

The form-finding process of tensegrity structures models linear elastic structural members held together by frictionless joints, and the self-weight of the structural members is neglected. Strictly speaking, the idealised condition of frictionless and massless joints is never satisfied, but it is a simplification that helps for the calculations and gives meaningful reference points. The members, either in tension or compression, are made of isotropic linear-elastic materials. There is no buckling considered for compression elements, and there is no slacking for tensile members either. There is no contribution from temperature or gravity.

Therefore, any equilibrium geometry considered in this dissertation is entirely defined by the interplay of its structural members, i.e. stand-alone tensegrity structures. Dead and live loads can be subsequently introduced, with another techniques, i.e. force density method or finite element methods, upon an initial equilibrium geometry calculated in this dissertation.

The key point in the tensegrity concept, i.e., balancing continuous tension and discontinuous compression, can represent a variety of physical models. In a general setting, tension and compression are replaced by attraction and repulsion, respectively. Tensegrity structures and related areas such as rigidity have applications in lightweight and foldable structures, domes, masts, models of cytoskeleton, muscular-skeletal systems, protein flex-

ibility prediction, and molecular conformation, just to name a few. The calculation of form and forces by means of form-finding methods is an essential step for the design of these prestressed structures.

This dissertation presents two investigations, one analytical and one numerical, on the form-finding of tensegrity structures. Both are in fact complementary. The main results from these investigations appear in [77, 78, 79, 80].

The analytical form-finding for a class of highly symmetric structures with cylindrical shape is first presented, while the numerical procedure for general structures is given in the second part. The numerical procedure especially is able to reproduce the results obtained with other form-finding methods with great accuracy. The versatility of the novel numerical form-finding procedure is none the less demonstrated by solving not only cylindrical but *also* spherical tensegrity structures. The details of both studies are listed below.

Analytical investigation

A thorough analysis of tensegrity cylinders, e.g., the triplex and the quadruplex, is presented in analytical form. The triplex, also known as three-strut tensegrity module or simplex [142], is shown in Fig. 6.1a. The term n-plex is used as a shortened term for higher-order tensegrity cylinders. Tensegrity cylinders have been extensively studied in different branches of mathematics and engineering (e.g. [195, 196, 157, 174, 185, 146, 145, 51, 191]). Many solutions for the form-finding of these structures exist, and though they are essentially equivalent they are expressed in terms of angles, strut-to-cable length ratios, or tension coefficients[1]. There is, however, no solution in terms of tension coefficients for cylinders with non-equal circular faces. The formalism of tension coefficients is helpful to gain insights into, for instance, counting and enumerating the equivalent solutions, as well as characterising the differences among them.

The proposed form-finding procedure does indeed exploit the inherent symmetry of cylindrical tensegrity structures (see Fig. 6.1b for the geometrical construction used to derive the equations of static self-equilibrium). The form-finding is presented in terms of tension coefficients for an arbitrarily large n-plex. In the course of the research, certain tensegrities were observed to have more than one possible geometrical configuration out of the same node-to-node connections. They are called *equivalent* or *structurally identical* configurations. Figures 6.1c-d show the two possible configurations for the 5-plex, with $j = 1$ and $j = 2$, where $1 \leq j < n/2$ is an integer parameter that affects the overall aspect of a cylinder.

[1]Force divided by length, also called *force density coefficients*.

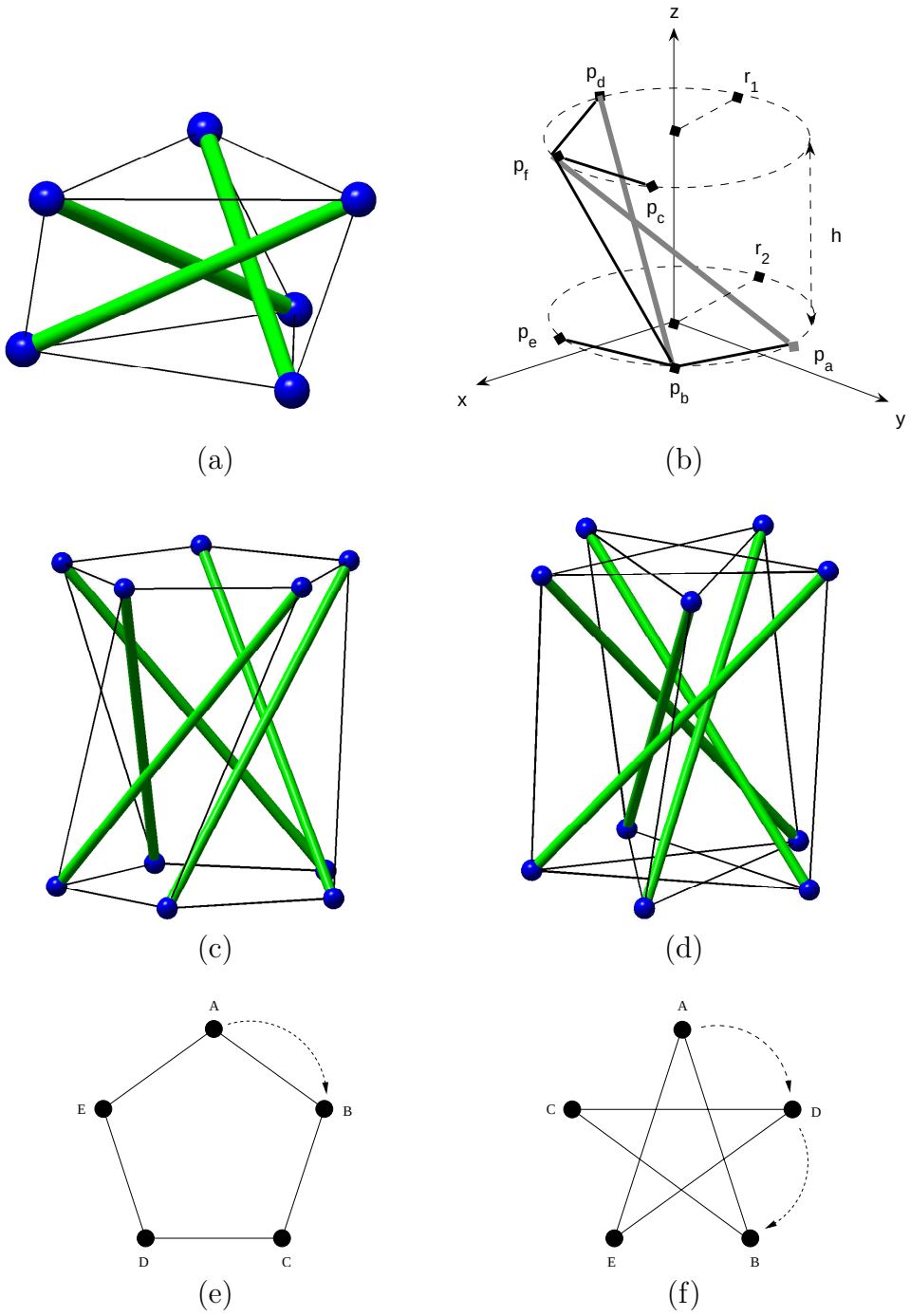

Fig. 6.1: Analytical investigations of cylindrical tensegrity structures : (a) the 3-plex in its stable self-equilibrium geometry; (b) geometrical model for a cylinder with radii r_1 and r_2, composed of two identical polygons with n nodes each one. The nodes are connected every j steps apart along the circumference; (c) first geometry of the 5-plex, $j = 1$; (d) second geometry of the 5-plex, $j = 2$; (e) constitutive polygon of the 5-plex with $j = 1$, i.e. each vertex is connected to the immediate neighbour on the circumcircle; (f) constitutive polygon of the 5-plex with $j = 2$, i.e. each vertex is connected to consecutive neighbours at two steps along the circumcircle. The example of consecutive nodes in (e) and (f) is the connection between nodes A and B. Thick green lines represent members in compression.

By solving the equations of static self-equilibrium for a cylindrical tensegrity structure, Fig. 6.1b, the closed-form solution for an arbitrary cylinder of order n, with radii r_1 and r_2, is:

$$\left.\begin{array}{rcl} q_{c_1} & = & 1 \\ q_{c_2} & = & \frac{{r_1}^2}{{r_2}^2} \\ q_b & = & 2\,\frac{r_1}{r_2}\,\sin\left(\frac{\pi j}{n}\right) \\ q_s & = & -2\,\frac{r_1}{r_2}\,\sin\left(\frac{\pi j}{n}\right) \end{array}\right\} \text{ for all } 1 \leq j < n/2 \text{ s.t. } GCD(n,j) \equiv 1. \qquad (6.1)$$

where q_{c_1} and q_{c_2} are the tension coefficients of tensile components (e.g. $\overline{p_f p_c}$ and $\overline{p_a p_b}$) connecting n nodes lying upon circumferences of radii r_1 and r_2, respectively; q_b is the tension coefficient assigned to each of the n bracing cables (e.g. $\overline{p_f p_b}$) that connects the circular faces; q_s is the tension coefficient assigned to each of the n struts (e.g. $\overline{p_f p_a}$) that keep the circular faces apart.

The closed-form solution, Eq. (6.1), agrees with previous works with equal circular faces, i.e. $r_1 = r_2$. For instance, the triplex shown in Fig. 6.1b has a critical tension coefficient of $q_b = -q_s = 2\sin(\pi/3)$ which is effectively $\sqrt{3}$, as reported in the literature, e.g. [142, 191, 195].

The tensile components are visualised as single closed, non-self-intersecting curves, embedded in two-dimensions with $n(j-1)$ crossings. If $j = 1$ the convex shape is obtained. This geometrical difference can be seen from the constitutive polygons of the 5-plex, Fig. 6.1e-f, with $j = 1$ and $j = 2$. For instance, Fig. 6.1f shows a star polygon, $j = 2$, with five crossings: $n(j-1) = 5(2-1) = 5$. It is important to remark that the height h of the cylinder is immerse in the tension coefficients, because they are defined as member force divided by length. There is one obvious constraint on the way the cables are placed on the circular faces. The arrangement of cables, of any circular face, must produce a fully connected network. This is easily checked with the greatest common divisor (GCD) of n and j: GCD(n,j)=1, for all $1 \leq j < n/2$.

The equivalent configurations have neither been counted nor characterised so far. The number of equivalent configurations is given by $\phi(n)/2$, where $\phi(\star)$ is the Euler's totient function. This function counts the number of positive real roots of the above-mentioned trigonometric function, $\sin(\pi/n)$, which appears in Eq. (6.1). The other roots, i.e. negative, reverse the sign of bracing cables and struts, which, although valid solutions, are inadmissible with the original design that sets tension to bracing cables and compression to struts. It turns out that there are only three cylindrical tensegrity structure that have no equivalent configurations, they are $n = 3, 4, 6$.

For $n = 5$ and $n > 6$, there is a number of different configurations per n and it is not clear *a priori* what sort of characteristics they have other than being geometrical. An energy argument was followed to analyse the range of equivalent configurations. The elastic strain energy is associated to each of the $\phi(n)/2$ structurally identical configurations coming out of the same n. Naturally, the state of least energy is favoured by principles like Castigliano's theorem of least work in mechanics or Rayleigh's principle on the theory

of vibrations. The elastic strain energy associated to the n-plex at configuration j is:

$$U^{n,j} \approx 4\pi^2 j^2 \frac{{r_1}^2}{n{r_2}^2}\left(3\,{r_1}^2 + 3\,{r_2}^2 + 2\,h^2\right) + O\left(\frac{1}{n^2}\right).$$

The comparison of the $\phi(n)/2$ equivalent tensegrity cylinders out of the same n-plex, all with the same radii and height, lead to $j = 1$ as the state of least energy. That is, the strain energy $U^{n,j}$, of a n-plex at configuration $1 \leq j < n/2$, increases with j: $U^{n,1} < U^{n,2} < \ldots < U^{n,n/2-1}$. Interestingly, a similar result was obtained, by other authors [51], for tensegrity cylinders analysed with mathematical rigidity. Tensegrity cylinders were called "globally rigid" [51] for $j = 1$, a result that, however, was left with no physical interpretation.

For instance, the 5-plex with $j = 1$, see Fig. 6.1c, is globally rigid and it is energetically better than the star-like cylinder shown in Fig. 6.1d with $j = 2$. The link established between mathematical rigidity and elastic strain energy concluded that global rigidity is itself a particular case of the Principle of Least Action in the form of adopting a configuration that minimises the strain energy. Thus, global rigidity is conceptually similar to Castigliano's theorem of least work and Rayleigh's principle on the theory of vibrations.

Numerical investigation

Analytical solution for the form-finding of tensegrity structures is possible only for smaller systems and does not easily extend to multi-parameter structures. For cylindrical tensegrity structures, the analytical solution has one crucial assumption: it classifies two groups of tension coefficients. The first is devoted to horizontal members ($q_{c_1} = 1$ and $q_{c_2} = r_1^2/r_2^2$), and the second for vertical members ($q = q_b = -q_s$). This simplification is included in the highly geometrical model used to describe the state of self-stress. It leaves only one unknown (q) to be determined. Therefore, a vector of tension coefficients that self-equilibrates a cylindrical tensegrity structure is:

$$\mathbf{t} = [\underbrace{1, 1, \ldots, 1, q_{c_2}, q_{c_2}, \ldots, q_{c_2}}_{\text{for horizontal cables}}, \underbrace{q, q, \ldots, q, -q, -q, \ldots, -q}_{\text{for bracing cables/struts}}].$$

Suppose for a moment that a cylinder has three or four groups of tension coefficients, instead of only two. In the extreme case, it could be possible for all tension coefficients to take a different value. That is, a different value for all tension coefficients from q_1 to q_{4n} in a cylinder:

$$\mathbf{t} = [q_1 \neq q_2 \neq \ldots \neq q_{4n}].$$

The inherent symmetry of our geometric model, Fig. 6.1b, is no longer valid. The geometrical model from which the analytical form-finding was devised cannot cope with

this number of extra groups of tension coefficients. Due to the rise in complexity, all previous works on tensegrity cylinders considered only two groups.

The literature of form-finding methods for tensegrity structures is plagued with such simplifications that assume important parts of the structure (see e.g. [142, 191] for a survey). Each form-finding method, be it analytical or numerical, has noteworthy limitations. That is why the form-finding procedures are designed to work under certain assumptions or domain knowledge. This hinders the applicability of form-finding methods to partially known structures. In general terms, it is not possible to anticipate the number of different tension coefficients or the member lengths beforehand.

In the second study, a form-finding procedure that provides solution to many traditional problems is proposed. Because exact analytical solutions become unmanageable for more complex structures, a numerical procedure was chosen. The identified method addressed the lack of *a priori* information by developing an unconventional form-finding procedure that only uses the node-to-node connections and the sign of individual members as either tension or compression. That is, the numerical form-finding procedure uses the incidence matrix and a vector of prototypes of tension coefficients. The latter vector has one entry per member in which the sign defines the force as either tension or compression, e.g.

$$\mathbf{q}^0 = [\underbrace{+1 \quad +1 \quad +1 \quad \ldots}_{\text{tension}} \quad \underbrace{-1 \quad -1 \quad -1 \quad \ldots}_{\text{compression}}].$$

Tensegrity structures are thus calculated by designing an incidence matrix ($\mathcal{C}$) and a vector of prototypes, $\mathbf{q}^0$. This decision influences the convergence. Other values, e.g. positive or negative random entries in $\mathbf{q}^0$, affect the convergence and the procedure might not converge at all.

A designer has the responsibility of selecting a meaningful $\mathbf{q}^0$ vector of prototypes for the incidence matrix $\mathcal{C}$. Figure 6.2 shows the pseudocode of the proposed form-finding procedure.

The numerical procedure, Fig. 6.2, basically computes a set of nodal coordinates that approximate the equilibrium configuration, then, the approximated coordinates are used to calculate the tension coefficients that approximate a self-stressed tensegrity structure. The numerical procedure is deterministic and has complexity $O(3\mathtt{nb}^2)$ per iteration; for a structure of `n` nodes and `b` members. The number of iterations vary greatly with the type of tensegrity. A solution for any cylindrical tensegrity structures is found in only one iteration. However, the number of iterations for spherical tensegrities is roughly a logarithmic function of `b`.

The main components of Fig. 6.2 are described as follows. A prototype of tension coefficients, $\mathbf{q}^0$, is used as design variable. The numerical procedure computes an approximation of the nodal coordinates from the current vector of tension coefficients,$\mathbf{t}$. This vector is initialised to $\mathbf{t} = \mathbf{q}^0$. The calculation involves a Schur decomposition of the

$\mathbf{q}^0 = [+1, +1, \ldots, +1, -1, -1, \ldots, -1]$
$\mathbf{t} = \mathbf{q}^0$
$\mathtt{s} = 0$
do
$\mathcal{U}\mathcal{V}\mathcal{U}^T = \mathcal{C}^T \mathrm{diag}(\mathbf{t})\mathcal{C}$
$[\mathbf{x}\,,\,\mathbf{y}\,,\,\mathbf{z}] = \mathrm{select\_coordinates}(\mathcal{U})$
$\mathcal{A} = \begin{pmatrix} \mathcal{C}^T\ \mathrm{diag}(\mathcal{C}\mathbf{x}) \\ \mathcal{C}^T\ \mathrm{diag}(\mathcal{C}\mathbf{y}) \\ \mathcal{C}^T\ \mathrm{diag}(\mathcal{C}\mathbf{z}) \end{pmatrix}$
$\mathcal{U}\mathcal{V}\mathcal{W}^T = \mathcal{A}$
$\mathbf{t} = \mathrm{select\_tension\_coefficients}(\mathcal{W}\,,\,\mathbf{q}^0)$
$\mathtt{s} = \mathrm{count\_states\_selfstress}(\mathcal{V})$
while $\mathtt{s} = 0$

Fig. 6.2: Pseudocode : the numerical form-finding procedure approximates the equilibrium coordinates from the current vector of tension coefficients (initialised as prototypes), and approximates the tension coefficients from the approximated coordinates.

current force density matrix, $\mathcal{D} = \mathcal{C}^T \mathrm{diag}\ (\mathbf{t})\mathcal{C}$. A selection procedure takes the potential coordinates by eliminating the **1**-vector and choosing linearly independent coordinates. The coordinates are then used to calculate an approximation of tension coefficients that self-equilibrate the structure. This is done by computing the right nullspace of the equilibrium matrix with singular value decomposition. A vector of tension coefficients is selected by taking the least square solution that best matches the signs defined in $\mathbf{q}^0$. The procedure iterates till a state of self-stress is found, $\mathtt{s} \neq 0$.

Three-dimensional and two-dimensional tensegrity structures, including cylindrical and spherical tensegrity structures, can be calculated with the new numerical form-finding method. Figure 6.3a shows a two-dimensional structure, while Fig. 6.3b-f shows three-dimensional tensegrity structures.

Tensegrity cylinders were recalculated, and the numerical procedure converging to structures with equal radii was found. That is, in the absence of constraints, the numerical form-finding procedure converges to structures that could be generated with $r_1 = r_2$. For instance, Fig. 6.3b shows the 50-plex calculated with the numerical procedure, and it has $r_1 = r_2$. On the other hand, the equilibrium geometry was calculated for cylindrical tensegrities with an unrestricted number of different tension coefficients. The numerical results show that it is indeed possible to set all tension coefficients differently. Moreover, their deviation from the analytical solution (with two groups) can give interesting clues for the tolerance, sensitivity to flaws, of tension coefficients in tensegrity cylinders. Figure 6.3c shows the 3-plex in which all tension coefficients were allowed to take different absolute values.

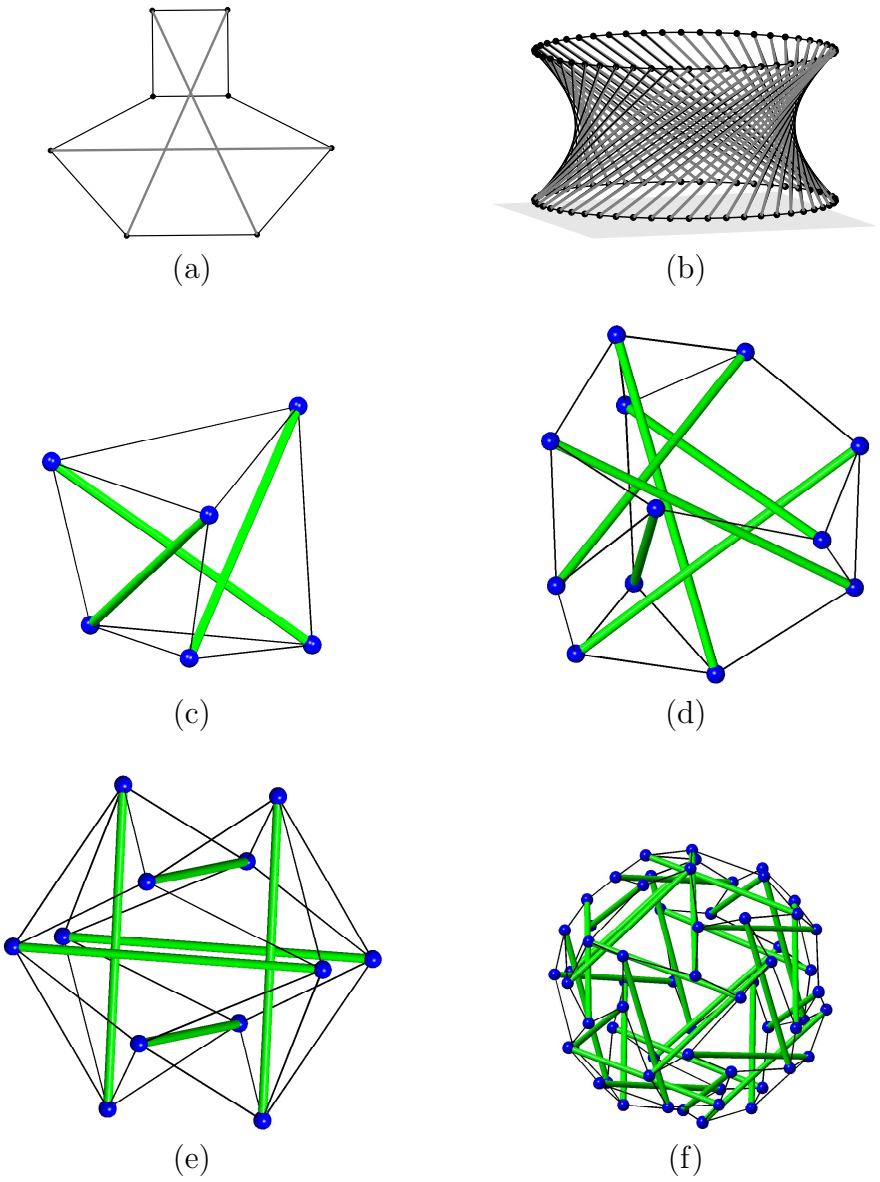

Fig. 6.3: Numerical investigations of tensegrity structures : (a) tensegrity structure in two-dimensions; (b) stable equilibrium geometry of the 50-plex; (c) asymmetric 3-plex in which all tension coefficients are different from each other; (d) equilibrium geometry of the truncated tetrahedron; (e) equilibrium geometry of the expanded octahedron; (f) equilibrium geometry of the truncated icosahedron. Thick green lines represent members in compression.

The truncated tetrahedron (Fig. 6.3d) is a spherical tensegrity structures that has been studied since the late 1970s. The basic assumption of these studies is that all cables have *one* common length, and that there is also a single length for all struts (e.g. [191, 157, 140, 142]). The two constraints on member lengths are imposed *a priori*.

However, because member lengths automatically emerge from our form-finding, the truncated tetrahedron was calculated to confirm or reject the assumption. A solution with

two different cable lengths and one strut length was found. The same energy argument was followed to distinguish between two equally valid configurations. It can be shown that the structure calculated with the proposed numerical form-finding method has a lower strain structure, while the structure calculated with the proposed analytical form-finding method has more energy than the configuration forced to have a single cable length. Based on strain energy considerations, the structure with two cable lengths should be preferred to the one with a single cable length.

To sum up, the novel procedure requires neither the nodal coordinates, the symmetry, the element lengths, nor the tension coefficients to be imposed *a priori*. This lack of assumptions leads to a versatile form-finding procedure that can calculate, for instance,

- two-dimensional tensegrity structures (e.g. Fig. 6.3a);
- the cylindrical tensegrities without assuming any cable lengths or a number of different tension coefficients (e.g. Fig. 6.3b);
- asymmetric cylindrical tensegrity structures (e.g. Fig. 6.3c);
- the truncated tetrahedron without assuming any cable lengths (e.g. Fig. 6.3d);
- the expanded octahedron without assuming any number of different tension coefficients (e.g. Fig. 6.3e);
- the truncated icosahedron without assuming any global symmetry (e.g. Fig. 6.3f).

The numerical procedure is indeed able to calculate novel configurations in three-dimensional as well as two-dimensional structures. Finally, it is worth mentioning that the numerical form-finding procedure: (i) reproduces solutions obtained with techniques based on symbolic calculations, nonlinear programming, dynamic relaxation, and group theory, (ii) selects configurations of minimal elastic potential energy, as well as (iii) reduces the knowledge required in the design process to $+1/-1$ depending on whether the member is in tension or compression. Previous and new structures are therefore easily handled with the proposed numerical procedure.

Outlook and future work

So far, the form-finding of tensegrities has plenty of methods that require specific knowledge of the final structure. This introduces extra constraints to the user and hinders uncompromised designs. As a result of the two investigations, previous and new tensegrity structures can easily be calculated and effectively opens the door to novel designs. It is expected that these investigations will help to discover new structures and provide starting points for future developments in the form-finding of statically indeterminate structures.

There are however a number of issues that have not been exhaustively studied. It is important to study, for instance, the sensitivity of the numerical form-finding procedure to random entries in the vector of prototypes. It is possible to set random entries in $\mathbf{q}^0$, preserving the signs according to tension and compression, and calculate valid tensegrity structures. The comparison between solutions with and without random entries in $\mathbf{q}^0$ is regarded as an interesting research direction.

In a more general setting, a designer might not be able to provide a signed vector of prototypes. Here, a topology optimisation approach will enhance the versatility of the proposed form-finding procedure. The design variables could be the number of tension and compression elements, which in turn leave the topology optimisation algorithms sample the $2^{\mathtt{b}}$ possible assignments of $+1$ and -1 in a vector of length $\mathtt{b}$.

Finally, in general terms, the basis of the numerical form-finding method could help other researchers in diverse fields. The numerical procedure searches for a geometry and tension coefficients that self-equilibrate a closed system subject to pointwise attractions and repulsions. Basic equations like the force density matrix, equilibrium matrix, and rank conditions are present in a variety of fields. It is therefore expected that the research presented here sheds light on numerical procedures devised for similar problems in other fields, such as rigidity percolation, molecular conformation, protein flexibility, or the determination of filament forces in cellular tensegrity models.

Zusammenfassung

Die Untersuchung statisch unbestimmter Strukturen erfordert die Berechnung von Anfangsgleichgewichtsgeometrien. Tensegrity Strukturen sind statisch unbestimmte Strukturen, mit der Zusatzbedingung, dass sie eine Gleichgewichtskonfiguration mit Hilfe innere Kräfte aufbauen, das heißt ohne Lager oder äußere Kräfte. Der sich im Gleichgewicht befindliche Eigenspannungszustand wird nur durch Zug- und Druckelemente aufrechterhalten. Das Verfahren zur Bestimmung der dreidimensionalen Gleichgewichtsform wird üblicherweise Formfindung genannt.

Bei der Formfindung von Tensegrity Strukturen werden linear elastische, mit reiblosen Gelenken verbundenen Strukturelemente definiert. Im Gegensatz zu anderen Verfahren berücksichtigt die Tensegrity Formfindung nicht das Eigengewicht der Strukturelemente. Deswegen ist jede in dieser Dissertation betrachtete Gleichgewichtsgeometrie durch das Zusammenspiel ihrer Strukturelemente definiert und somit werden nur allein stehende Tensegrity Strukturen behandelt. Totlasten und andere Belastungsarten können aufbauend auf den in dieser Dissertation berechneten Gleichgewichtsgeometrien mit anderen Techniken berücksichtigt werden. Streng genommen ist die idealisierte Annahme von reib- und masselosen Verbindungen niemals erfüllt, jedoch erleichtert diese Vereinfachung die Rechung und gibt sinnvolle Ausgangspunke. Die Elemente, entweder auf Zug oder auf Druck belastet, sind aus linear elastischem Material. Das Knicken der Druckstäbe sowie Stabausfall wird nicht berücksichtigt. Weiterhin werden Schwerkraft und Temperatureinflüsse auf die Tensegrity Struktur vernachlässigt.

Der Schlüssel im Tensegrity Konzept, das heißt das Ausgleichen von kontinuierlichem Zug und diskontinuierlichem Druck kann durch eine Auswahl physikalischer Modelle beschrieben werden. Im allgemeinen Fall können Zug und Druck durch Anziehung und Abstoßung beschrieben werden. Tensegrity Strukturen und verwandte Gebiete wie Steifigkeit haben Anwendungen im Leichtbau und für die Konstruktion faltbarer Strukturen, im Dombau und Mastbau, für Modelle des Zytoskelett, des Muskelskelettsystem, der Proteinflexibilität und der Molekularen-Konformation. Die Berechnung der Gestalt und der Kräfte mit Hilfe von Formfindungsverfahren ist ein wesentlicher Schritt für die Konstruktion dieser vorgespannten Strukturen.

Die Dissertation stellt zwei Untersuchungen über die Formfindung von Tensegrity Strukturen vor. Beide Untersuchungen, die eine analytische und die andere numerisch, ergänzen sich einander. Die wichtigsten Ergebnisse dieser Untersuchungen wurden in [77, 78, 79, 80] publiziert. Die analytische Formfindung wird zunächst für eine Klasse von

sehr symmetrischen Strukturen zylindrischer Form beschrieben.

Ein numerisches Formfindungsverfahren für allgemeine Strukturen wird im zweiten Teil vorgestellt. Das numerische Verfahren kann die Ergebnisse aus anderen Formfindungsmethoden äußerst exakt reproduzieren. Trotzdem wird die Vielseitigkeit dieser neuartigen, numerischen Formfindungsmethode nicht nur anhand von zylindrischen sondern auch anhand von kugelförmigen Tensegrity Strukturen demonstriert. Die Einzelheiten beider Untersuchungen sind unten aufgelistet.

Analytische Untersuchung

Eine sorgfältige Untersuchung von Tensegrity Strukturen, z.B. der Dreifach- und der Vierfachstruktur, wird in analytischer Form dargestellt. Das Triplex, auch als 3-Stab Tensegrity Modul oder Simplex [142], ist in Abbildung 6.4a dargestellt. Der Begriff n-plex wird im Folgenden für Tensegrity höherer Ordnung benutzt. Tensegrity Zylinder sind umfangreich in verschiedenen Gebieten der Mathematik und des Ingenieurwesens untersucht worden, z.B. [195, 196, 157, 174, 185, 146, 145, 51, 191].

Viele Lösungen des zur Formfindung dieser Strukturen sind bekannt und im wesentlichen gleichwertig aber als Winkel, Stab zu Seil Längenverhältnis oder Zugkoeffizienten ausgedrückt. Jedoch gibt es keine Lösung in Form von Zugkoeffizienten für Zylinder mit nicht gleichen Kreisflächen. Der Formalismus der Zugkoeffizienten ist hilfreich für den Einblick, zum Beispiel beim Zählen und Numerierung von gleichwertigen Lösungen, sowie zum Auswerten von Unterschieden zwischen den Lösungen. Das vorgeschlagene Verfahren der Formfindung macht sich die Symmetrie von Tensegrity Strukturen zu Nutze, siehe Abbildung 6.4b für die geometrische Konstruktion zur Herleitung der Gleichgewichtsgleichungen.

Die Formfindung ist mit Hilfe von Zugkoeffizienten für allgemeine, große n-plex formuliert. Im Verlauf der Forschung wurde für bestimmte Tensegrity Strukturen mehr als eine mögliche geometrische Konfiguration für dieselbe Konnektivität der Knotenpunkte gefunden. Diese werden gleichwertige oder strukturell identische Konfigurationen genannt. Abbildungen 6.4c-d zeigen zwei mögliche Konfigurationen für ein 5-plex, mit j=1 und j=2, mit $1 \leq j < n/2$ als ganzzahlige Parameter, die das grundlegende Aspektverhältnis des Zylinders definieren.

Die geschlossene Lösung des statischen Gleichgewichts für eine allgemeine zylindrische Struktur der Ordnung n, Abb. 6.4b, mit Radien r_1 und r_2 ergibt:

$$\left.\begin{array}{rcl} q_{c_1} & = & 1 \\ q_{c_2} & = & \frac{{r_1}^2}{{r_2}^2} \\ q_b & = & 2\,\frac{r_1}{r_2}\,\sin\left(\frac{\pi\,j}{n}\right) \\ q_s & = & -2\,\frac{r_1}{r_2}\,\sin\left(\frac{\pi\,j}{n}\right) \end{array}\right\} \text{ für } 1 \leq j < n/2 \text{ wie } GCD(n,j) \equiv 1. \qquad (6.2)$$

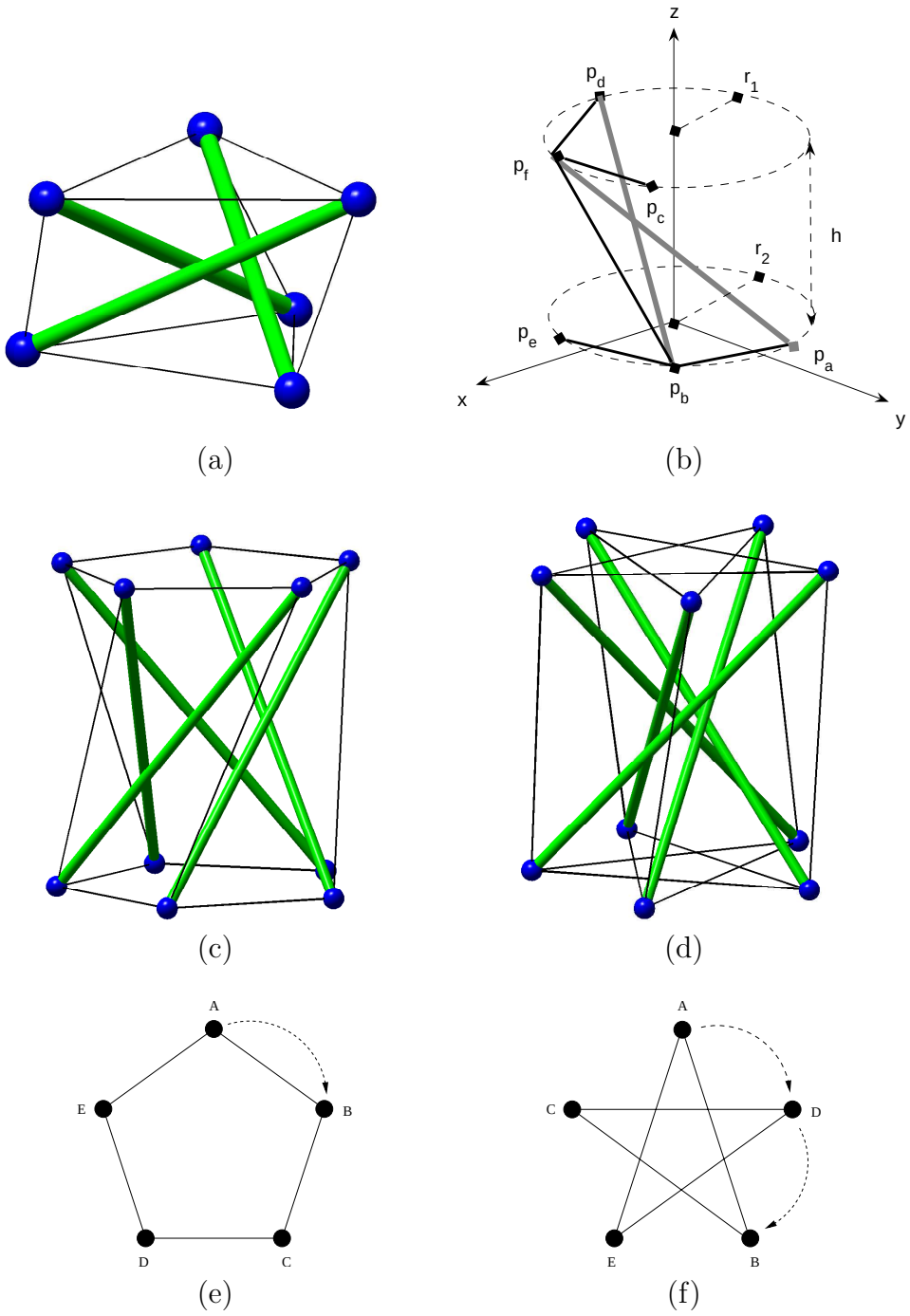

Fig. 6.4: Analytische Untersuchung : (a) das 3-plex im Selbst-Gleichgewicht; (b) zylindrisches Modell für die geometrische Konstruktion zur Herleitung mit Radien r_1 und r_2; (c) erste Gleichgewichtskonfiguration für das 5-plex mit $j = 1$; (d) zweite Gleichgewichtskonfiguration für das 5-plex mit $j = 2$; (e) Polygon mit 5 Punkten und $j = 1$; (f) Polygon mit 5 Punkten und $j = 2$; starke grüne Linien sind Druckelemente.

mit den Zugkoeffizienten der Zugelemente q_{c_1} und q_{c_2} (z.B. $\overline{p_f p_c}$ und $\overline{p_a p_b}$), die n auf dem Umfang der Kreise mit Radien r_1 bzw. r_2 liegende Knoten verbinden; q_b ist der

Zugkoeffizient, der jedem der n Spannseile zugeordnet (z.B. $\overline{p_f p_b}$) ist, die die Kreisflächen verbinden; q_s ist der Zugkoeffizient, der jedem der n Stäbe (z.B. $\overline{p_f p_a}$) zugeordnet ist, die die Kreisflächen auseinander halten. Die geschlossene Lösung, Gleichung 6.2, stimmt mit früheren Arbeiten mit über gleichen Kreisflächen überein, z.B. $r_1 = r_2$. Zum Beispiel, das Triplex in Abbildung 6.1b hat die kritische Zugkoeffizienten $q_b = -q_s = 2\sin(\pi/3)$, effektiv $\sqrt{3}$, wie in der Literatur berichtet, z.B. [142, 191, 195].

Die Zugelemente sind als einzelne geschlossene, sich nicht selbst schneidende Kurven auf zwei Dimensionen projiziert. Man erhält Polygone, die mit $n(j-1)$ Querverbindungen dargestellt werden. Mit $j = 1$ ergibt sich die konvexe Form. Dieser geometrische Unterschied kann an den konstitutiven Polygonen des 5-plex Abb. 6.4e-f mit j=1 und j=2 festgestellt werden. Zum Beispiel zeigt Abb. 6.4f ein Sternpolygon, mit j=2 und 5 Querelementen: $n(j-1) = 5(2-1) = 5$.

Als Besonderheit ist anzumerken, dass die Höhe h des Zylinders in den Zugkoeffizienten entälten ist, da sie als Elementkraft geteilt durch Länge definiert ist. Es gibt eine offensichtliche Einschränkung, wie die Seile auf den Kreisflächen angeordnet werden können. Die Anordnung der Seile einer jeden Kreisfläche muss ein voll besetztes Netzwerk ergeben. Dies kann einfach über den größten gemeinsamen Teiler (GCD) von n und j getestet werden: GCD(n,j)=1, für $1 \leq j < n/2$.

Die gleichwertigen Konfigurationen sind zuvor nicht gezählt oder charakterisiert worden. Die Zahl gleichwertiger Konfigurationen ist $\phi(n)/2$, mit der eulerschen ϕ-Funktion. Die Funktion zählt die Zahl der positiven reellen Wurzel der oben genannten trigonometrischen Funktion $\sin(\pi/n)$ aus Gleichung 6.2. Die anderen Wurzeln, z.B. negative, entgegengesetzt dem Vorzeichen der Spannseile und der Stäbe, die trotz ihrer gültigen Lösung unzulässige mit dem ursprünglichen Aufbau, der den Spannseilen Zug und den Stäben Druck zuordnet. Die Untersuchungen ergeben, dass es lediglich 3 zylindrische Tensegrity Strukturen mit nicht äquivalenten Konfigurationen gibt. Diese sind $n = 3, 4, 6$.

Für $n = 5$ und $n > 6$ gibt es eine Zahl unterschiedlicher Konfigurationen und es ist nicht eindeutig, welche andere Eigenschaften sie haben abgesehen von ihrer Geometrie haben. Ein energetisches Argument wurde herangezogen, um die Reihe geometrischer Konfigurationen zu analysieren. Die elastische Verzerrungsenergie wird jeder der $\phi(n)/2$ Konfigurationen mit gleichem n zugeordnet. Der Zustand der geringsten Energie wird nach Prinzipien wie Castigliano's Theorem der geringsten Arbeit aus der Mechanik oder nach Rayleigh's Prinzip aus der Schwingungslehre analiziert. Die elastische Verzerrungsenergie einer jeden n-plex Konfiguration ist

$$U^{n,j} \approx 4\pi^2 j^2 \frac{{r_1}^2}{n{r_2}^2}\left(3\,{r_1}^2 + 3\,{r_2}^2 + 2\,h^2\right) + O\left(\frac{1}{n^2}\right).$$

Der Vergleich von $\phi(n)/2$ äquivalenten Tensegrity Strukturen aus demselben n-plex mit denselben Radien und Höhen führt auf j=1 als den Zustand der geringsten Energie. Das heißt, die Verzerrungsenergie $U^{n,j}$ eines n-plex in der Konfguration $1 \leq j < n/2$ steigt mit j: $U^{n,1} < U^{n,2} < \ldots < U^{n,n/2-1}$.

Interessanterweise wurde von anderen Autoren [51] für Tensegrity Zylinder unter Annahme mathematischer Rigidität ein ähnliches Ergebnis gefunden. Tensegrity Strukturen wurden für j=1 als ,,global" steif bezeichnet [51]. Jedoch wurde zu diesem Ergebnis keine physikalische Interpretation geliefert. Der 5-plex zum Beispiel mit j=1 aus Abbildung 6.4c ist global steif und energetisch günstiger als der sternförmige Zylinder aus Abbildung 6.4d mit j=2.

Aus der Verbindung zwischen mathematischer Rigidität und elastischer Verzerrungsenergie folgt, dass globale Rigidität selbst ein spezieller Fall des Prinzips der geringsten Wirkung ist, bei dem eine Konfiguration minimaler Verzerrungsenergie angenommen wird. Somit ähnelt das Konzept der globalen Rigidität Castigliano's Theorem der geringsten Arbeit und Rayleigh's Prinzip aus der Schwingungslehre.

Numerische Untersuchung

Analytische Lösungen für die Formfindung von Tensegrity Strukturen sind nur für kleinere Systeme möglich und nicht einfach auf vielparametrige Strukturen übertragbar. Die analytische Lösung von zylindrischen Strukturen hat eine entscheidende Annahme: sie beinhaltet zwei Gruppen von Zugkoeffizienten. Die erste Gruppe ergibt sich aus den horizontalen Elementen ($q_{c_1} = 1$ und $q_{c_2} = r_1^2/r_2^2$) und die zweite aus den vertikalen Elementen ($q = q_b = -q_s$). Diese Vereinfachung in dem geometrischen Modell mit inbegriffen, das den Eigenspannungszustand beschreibt. Als einzige Unbekannte ist q zu bestimmen. Deswegen ist der Vektor des Zugkoeffizienten für die zylindrische Tensegrity Struktur im Selbst-Gleichgewicht:

$$\mathbf{t} = [\underbrace{1, 1, \ldots, 1, q_{c_2}, q_{c_2}, \ldots, q_{c_2}}_{\text{für horizontale Seil}}, \underbrace{q, q, \ldots, q, -q, -q, \ldots, -q}_{\text{für Spannseile und Stäbe}}].$$

Sei für einen Moment angenommen, dass anstelle von nur zwei Gruppen von Zugkoeffizienten unser Zylinder drei oder vier Gruppen aufweist. In diesem Extremfall sind für alle Zugkoeffizienten verschiedene Zugkoeffizienten denkbar

$$\mathbf{t} = [q_1 \neq q_2 \neq \ldots \neq q_{4n}].$$

Die inhärente Symmetrie unseres Modells, Abb. 6.4b ist nicht länger gültig. Das geometrische Modell, aus dem die analytische Formfindung entwickelt worden ist, ist nicht für diese Anzahl von Extragruppen von Zugkoeffizienten geeignet. Aufgrund der Zunahme der Komplexität betrachten alle vorherigen Arbeiten über Tensegrity Strukturen nur zwei Gruppen. Die Literatur der Formfindungsmethoden von Tensegrity Strukturen ist voll von solchen Vereinfachungen, die wichtige Teile der Struktur betreffen, siehe z.B. [142, 191] für einen Überblick.

Jede Formfindungsmethode, analytisch oder numerisch, hat nennenswerte Beschränkungen. Deswegen funktionieren Formfindungsmethode nur unter bestimmten Annahmen oder mit Kenntnissen des Lösungsraums. Dies hindert die Anwendbarkeit von Formfindungsmethoden auf Strukturen, die nur teilweise bekannt sind. Im Allgemeinen ist es nicht möglich, die unterschiedlichen Zugkoeffizienten oder die Elementlängen zu entscheiden.

In der zweiten Untersuchung wird eine Formfindungsmethode vorgeschlagen, die viele traditionelle Annahmen vereinfacht. Da exakte, analytische Lösungen für komplexere Strukturen unhandlich sind, wurde entschieden, eine numerische Lösung zu entwickeln: Zunächst wurde das Fehlen von Information festgestellt und durch die Entwicklung einer nicht-konventionellen Formfindungsmethode umgangen. Diese benötigt lediglich: der Häufigkeitsmatrix (das heißt Knotenverbindung) und das Vorzeichen der einzelnen Zug- oder Druckelemente, z.B.

$$\mathbf{q}^0 = [\underbrace{+1 \quad +1 \quad +1 \quad \ldots}_{\text{Zug}} \quad \underbrace{-1 \quad -1 \quad -1 \quad \ldots}_{\text{Druck}}].$$

Tensegrity Strukturen werden also durch das Entwickeln von Vektoren von *Prototypen* $\mathbf{q}^0$ berechnet und diese Entscheidung beeinflusst die Konvergenz. Andere Werte, z.B. positive Zufallseinträge in $\mathbf{q}^0$ beeinträchtigen die Konvergenz und das numerische Verfahren kann möglicherweise überhaupt nicht konvergieren. Ein Konstrukteur hat die Verantwortung für die Auswahl eines sinnvollen Vektors $\mathbf{q}^0$ von Prototypen. Abbildung 6.5 zeigt den Pseudocode für das vorgeschlagene Formfindungsverfahren.

$\mathbf{q}^0 = [+1, +1, \ldots, +1, -1, -1, \ldots, -1]$
$\mathbf{t} = \mathbf{q}^0$
$\mathtt{s} = 0$
do
  $\mathcal{U}\mathcal{V}\mathcal{U}^T = \mathcal{C}^T \mathrm{diag}(\mathbf{t})\mathcal{C}$
  $[\mathbf{x}\,,\,\mathbf{y}\,,\,\mathbf{z}] = \mathrm{select\_coordinates}(\mathcal{U})$
  $\mathcal{A} = \begin{pmatrix} \mathcal{C}^T\ \mathrm{diag}(\mathcal{C}\mathbf{x}) \\ \mathcal{C}^T\ \mathrm{diag}(\mathcal{C}\mathbf{y}) \\ \mathcal{C}^T\ \mathrm{diag}(\mathcal{C}\mathbf{z}) \end{pmatrix}$
  $\mathcal{U}\mathcal{V}\mathcal{W}^T = \mathcal{A}$
  $\mathbf{t} = \mathrm{select\_tension\_coefficients}(\mathcal{W}\,,\,\mathbf{q}^0)$
  $\mathtt{s} = \mathrm{count\_states\_selfstress}(\mathcal{V})$
while $\mathtt{s} = 0$

Fig. 6.5: Pseudocode : das numerische Formfindungsverfahren nähert die Gleichgewichtskoordinaten des aktuellen Vektors der Zugkoeffizienten (initialisiert als Prototypen $\mathbf{q}^0$) an und approximiert die Zugkoeffizienten mit den genäherten Koordinaten.

Das numerische Verfahren, Abb. 6.5, berechnet eine Reihe von Knotenkoordinaten, die die Gleichgewichtskonfiguration annähern. Die angenäherten Koordinaten werden dann für die Berechnung der Zugkoeffizienten benutzt, die die gespannte Tensegrity Struktur approximieren. Das numerische Verfahren ist deterministisch und hat für eine Struktur mit $\mathtt{n}$ Knoten und $\mathtt{b}$ Elementen den Aufwand $O(3\mathtt{n}\mathtt{b}^2)$ pro Iteration.

Die Zahl der Iterationen variiert stark mit dem Tensegrity Typ. Eine Lösung für eine beliebige Tensegrity Struktur wird in nur einem Iterationsschritt gefunden, jedoch brauch es $O(\log \mathtt{b})$ Iterationen für kugelförmige Tensegrities.

Die Hauptkomponente von Abb. 6.5 wird wie folgt beschrieben. Ein Prototyp von Zugkoeffizienten $\mathbf{q}^0$ wird als Design Variable verwendet. Das numerische Verfahren berechnet eine Nährung der Knotenkoordinaten vom den Zugkoeffizienten, die mit $\mathbf{q}^0$ initialisiert sind. Die Berechnung beinhaltet die Schur-Zerlegung der aktuellen Kraftdichte-Matrix und ein Auswahlverfahren, das den $\mathbf{1}$-Vektor und linear unabhängige Koordinaten eliminiert.

Die Koordinaten werden dann für die Berechnung einer Näherung der Zugkoeffizienten verwendet, mit denen sich die Struktur im Gleichgewicht befindet. Dieses geschieht durch die Berechnung des rechten Nullraums der Gleichgewichtsmatrix mit einer Singulärwertzerlegung. Ein Vektor von Zugkoeffizienten wird ausgewählt, für den die Lösung am besten mit den Vorzeichen übereinstimmt. Das Verfahren iteriert solange, bis ein Eigenspannung Zustand gefunden ist, $\mathtt{s} \neq 0$.

Zylindrische und kugelförmige Tensegrity Strukturen können mit der neuen Formfindungsmethode genauso berechnet werden wie andere drei- oder zweidimensionale Tensegrity Strukturen. Abbildung 6.6a zeigt eine zweidimensionale Struktur während Abb. 6.6b-f eine dreidimensionale Tensegrity Struktur zeigt.

Ohne Nebenbedingungen konvergiert das numerische Formfindungsverfahren also zu Strukturen, die mit $r_1 = r_2$ erzeugt werden können. Zum Beispiel zeigt Abb. 6.6b einen berechneten 50-plex mit $r_1 = r_2$. Des Weiteren wurden Gleichgewichtsgeometrien für zylindrische Tensegrity mit uneingeschränkter Anzahl von verschiedenen Zugelementen berechnet. Das numerische Ergebnis zeigt, dass alle Zugkoeffizienten unterschiedlich gesetzt werden können. Darüber hinaus gibt die Abweichung von der analytischen Lösung (mit zwei Gruppen) interessantes Wissen über Toleranz, Empfindlichkeit gegenüber Fehlern und Zugkoeffizienten in zylindrischen Tensegrity Strukturen. Abbildung 6.6c zeigt einen 3-plex, in dem alle Zugkoeffizienten unterschiedliche absolute Werte erlaubt waren.

Der abgeschnittene Tetraeder in Abbildung 6.6d ist eine kugelförmige Tensegrity Struktur, die seit Ende 1970 untersucht werden. Die grundlegende Annahme dieser Untersuchungen besagt, dass alle Seile dieselbe Länge haben und dass es eine Länge für alle Stäbe gibt, z.B. [191, 157, 140, 142]. Die beiden Nebenbedingungen für die Elementlängen sind von vornherein auferlegt. Da jedoch in unserer Formfindung die Elementlängen mitberechnet wurden, wurde der abgeschnittene Tetraeder gerechnet, um die Annahmen zu bestätigen oder zu verwerfen. Die Untersuchungen ergab eine Lösung mit zwei unter-

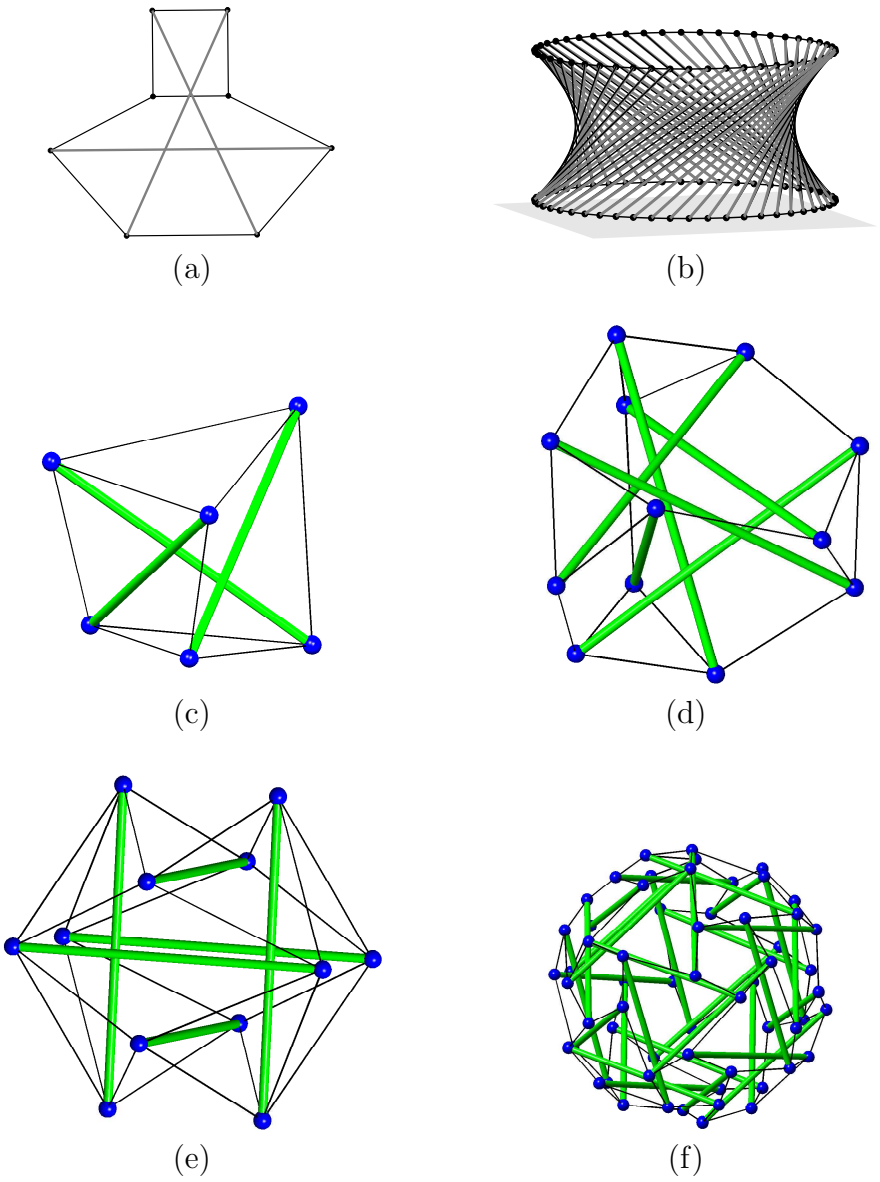

Fig. 6.6: Analytische Untersuchung : (a) zweidimensionale Tensegrity Strukture; (b) das 50-plex im Selbst-Gleichgewicht; (c) unsymmetrische 3-plex mit alle Zugkoeffizienten unterschiedlich gesetzt; (d) stabiles Selbst-Gleichgewichtsgeometrien für der abgeschnittene Tetraeder; (e) stabiles Selbst-Gleichgewichtsgeometrien für der erweiterte Oktaeder; (f) stabiles Selbst-Gleichgewichtsgeometrien für der abgeschnittene Ikosaeder; starke grüne Linien sind Druckelemente.

schiedlichen Kabellängen und einer Stablänge. Das gleiche energetische Argument wurde verwendet, um zwischen zwei gültigen Konfigurationen zu unterscheiden. Es kann gezeigt werden, dass die durch unsere Methode berechnete Struktur eine geringere Verzerrungsenergie ausweist als die Struktur mit nur einer Stablänge. Aufgrund dieser energetischen Überlegung sollte die mit der Formfindung numerisch gefundene Struktur mit zwei Kabellängen der mit nur einer Kabellänge bevorzugt werden. Das entwickelte neue Verfahren erfordert keine Angaben von Knotenkoordinaten und Symmetrie der Elemente oder von

Zugkoeffizienten. Das Fehlen dieser Annahmen macht diese Methode zu einem vielseitigen Formfindungsverfahren zur Berechnung von:

- zweidimensionale Tensegrity Strukturen, z.B. Abb. 6.6a;
- zylindrische Tensegrity Strukturen ohne Annahme von Seillängen oder Anzahl unterschiedlicher Zugkoeffizienten, z.B. Abb. 6.6b;
- unsymmetrische, zylindrische Tensegrity Strukturen, z.B. unsymmetrische 3-plex Abb. 6.6c;
- das abgeschnittene Tetraeder ohne Annahme von Kabellängen, z.B. Abb. 6.6d;
- der erweiterte Oktaeder ohne Annahme von unterschiedlichen Zugkoeffizienten, z.B. Abb. 6.6e;
- der abgeschnittene Ikosaeder ohne Annahme einer globalen Symmetrie, z.B. Abb. 6.6f.

Das numerische Verfahren ermöglicht die Berechnung neuer Konfigurationen in drei Dimensionen sowie zweidimensionaler Strukturen. Abschließend sei hier angemerkt werden, dass das numerische Formfindungsverfahren: (i) Lösungen reproduziert, die mit symbolischen Berechnungstechniken, nichtlinearer Optimierung, dynamischer Relaxation und Gruppentheorie erhalten werden, (ii) wählt Konfigurationen minimaler elastischer, potentieller Energie aus sowie (iii) verringert das für das Gestaltungsverfahren notwendige Wissen auf $+1/-1$ abhängig davon, ob das Element unter Zug oder Druck steht.

Ausblick und zukünftige Arbeiten

Frühere und neue Strukturen können mit dem vorgeschlagenen numerischen Verfahren einfach bearbeitet werden. Es gibt jedoch eine Anzahl von Fragen, die noch nicht genügend untersucht worden sind. Es wäre zum Beispiel interessant zu untersuchen, wie die die Empfindlichkeit des numerischen Formfindungsverfahren auf Zufallseinträge im Vektor des *Prototypen*.

Es ist möglich zufällige Einträge in $\mathbf{q}^0$ unter Beibehaltung der Vorzeichen entsprechend den Zug- und Druckelementen zu wählen und so gültige Tensegrity Strukturen zu berechnen. Der Vergleich zwischen Lösungen mit und ohne Zufallseinträge in $\mathbf{q}^0$ wird als interessante Fragestellung angesehen. Im allgemeinen Fall kann ein Konstrukteur möglicherweise keine vorzeichenbehaftet Vektor für Prototypen liefern. Hier würde eine Topologieoptimierung die Vielseitigkeit des vorgestellten Formfindungsverfahrens erhöhen. Als Konstruktionsvariabeln könnte die Anzahl der Druck- und Zugelemente dienen, die ein Sample aus der Topologieoptimierung mit $2^{\mathtt{b}}$ möglichen Zuordnungen von $+1$ und -1 in einem Vektor der Länge $\mathtt{b}$ liefern würde.

Résumé

Research interests: biostatistics and mathematical biology, attribute selection, colour and signal processing, theory of pre-stressed pin-jointed structures, mathematical modelling of discrete systems.
EMail: giovani.estrada@googlemail.com

I Education and research experience

2007- : Research fellow. Royal College of Surgeons in Ireland, Dublin.

2004-2006: Doctoral research at the Max-Planck-Institut für Metallforschung (MPI-MF) and Universität Stuttgart.

2002-2004 : Research staff at the MPI-MF.

2001-2002 : Research assistant. Monterrey Tech., ITESM, Division of Engineering Science, Mexico.

2000-2001 : Visiting scholar. Swiss Federal Institute of Technology, ETH-Zürich, Dept. of Electrical Engineering.

1997-1999: Master of Science in Computer Science. Monterrey Tech., ITESM, Division of Engineering Science, Mexico; and at the Center for Mathematical Research, CIMAT, Mexico. Thesis: Probabilistic estimation of local scale.

1992-1996: Bachelor of Science in Computer Engineering. Monterrey Tech., ITESM, Division of Engineering Science, Mexico.

II Publications under the affiliation of MPI (other than [77, 78, 79, 80])

1. F. Tian, H. Hosseinkhani, M. Hosseinkhani, A. Khademhosseini, Y. Yokoyama, *G. G. Estrada*, H. Kobayashi; Quantitative analysis of cell adhesion on aligned micro- and nanofibers. Journal of Biomedical Materials Research Part A (in press).

2. F. Tian, H. Hossinkhani, Y. Yokoyama, *G. G. Estrada*, H. Kobayashi; The effect of diameter of electronspun PGA scaffold for biological behaviour of human umbilical vein endothelial cells. Key Engineering Materials, vol. 342-343: 237-240, 2007.

3. F. Tian, *G. G. Estrada*, H. Kobayashi; Quantitative method for the analysis of cell attachment using aligned scaffold structures. Journal of Physics: Conference Series, 61: 587-590, 2007.

4. F. Tian, *G. G. Estrada*, H. Kobayashi; Quantitative method for the analysis of cell attachment using aligned scaffold structures. International Conference on Nanoscience and Technology. Section: Nano-implants and protheses. Basel, Jul/Aug 2006.

5. F. Tian, D. Cui, H. Schwarz, *G. G. Estrada*; Cytotoxicity of Single Wall Carbon Nanotubes on Human Fibroblasts. Toxicology in Vitro, 20(7): 1202-1212, Oct. 2006.

6. D. Cui, L. Zhang, X. Yan, L. Zhang, J. Xu, Y. Guo, G. Jin, *G. G. Estrada*, D. Li, J. Zhao, F. Han, J. Zhang, J. Hu, D. Fan, H. Gao; A microarray-based gastric carcinoma prewarning system. World Journal of Gastroenterology, 11(9): 1273-1282; March, 2005.

7. R. Kemkemer, *G. G. Estrada*, D. Kaufmann, D. Ulrich, H. Gruler; Feature Extraction of Non-stained Melanocyte Cells. Proc. of the Int. Conf. on Image Processing, vol. 3, pp. 605-608, Genova, Sep. 2005. Section: Biomedical Imaging and Processing. IEEE Signal Processing Society.

8. F. Tian, D. Cui, H. Schwarz, *G. G. Estrada*; Effect of Carbon Materials of Different Sizes on Human Fibroblast Cells. 4th World Congress of Cellular and Molecular Biology. Section: Nano-biotechnology and bio-safety. Abstracts book, pp. 101, Poitiers, France. Oct. 2005.

9. D. Cui, G. Jin, T. Gao, T. Sun, F. Tian, *G. G. Estrada*, H. Gao, A. Sarai; Characterization of BRCAA1 and its novel antigen epitope identification. Cancer Epidemiology, Biomarker & Prevention, vol. 13, pp. 1136-1145, July 2004.

10. *G. G. Estrada*, E. Morales; How does the Hue contribute to construct better colour features?. Proc. of the MICAI 2004, Springer-Verlag: Lecture Notes in Computer Science, vol. 2972, pp. 602-611, Apr. 2004.

11. *G. G. Estrada*; A note on designing logical circuits using SAT. Proc. of the ICES, Springer-Verlag: Lecture Notes in Computer Science, vol. 2606, pp. 410-421, Trondheim, Mar. 2003. Section: Logic Design.

Acknowledgements

This dissertation completes the period 2002-2006 in which I worked for the Max-Planck-Institut für Metallforschung, Stuttgart.

I would like to express my sincere gratitude to Hans-Joachim Bungartz, my supervisor, for his tireless support and endless patience bestowed upon me. His direction helped me retain focus on a broadly defined research project, and his support remained high throughout the ups and downs of the research. I wish to thank Huajian Gao for the continuous support provided me during my stage at the Max-Planck-Institut. His help was decisive for my research. I shall always keep good memories of the inspiring, enjoyable atmosphere of the department under his direction. Hans and Huajian are the persons without whom this dissertation would never have been possible.

The results in this dissertation would likely not have matured without the criticism and contributions of many people. I would especially like to thank a number of them that directly or indirectly contributed to focus my attention to interesting details or gave useful advice that improved the overall quality of this research work: Bin Liu, Ekkehard Ramm, Gunnar Tibert, Ken'ichi Kawaguchi, Klaus Linkwitz, Rene Motro, Simon Guest and Thomas Huckle. Special thanks go to Camilla Mohrdieck who drew my attention to tensegrity structures and spent a lot of time guiding my first steps into the field.

This research could hardly exist without appropriate financial support. I received a fellowship as well as funds for conferences, software and books; therefore, I would like to take this opportunity to thank the generosity of: CONACyT, Max-Planck-Institut für Metallforschung and Universität Stuttgart.

Last but not least, I want to thank Furong, Guadalupe, Rosa and my friends, for their ceaseless encouragement through these years. Finally, I am in debt to Silvia Casanova for her copious administrative help; Nils Brödling, Martin Bernreuther and Yong Kong for their help with the German summary; and Eduard Arzt for his support.

Index